The role of the platelet pannexin 1 channel in thrombosis, hemostasis and the development of abdominal aortic aneurysms

Inaugural-Dissertation

zur Erlangung des Doktorgrades

der Mathematisch-Naturwissenschaftlichen Fakultät

der Heinrich-Heine-Universität Düsseldorf

vorgelegt von

Lisa Maria Metz

aus Aachen

Düsseldorf, Juni 2022

Aus der Arbeitsgruppe Experimentelle Vaskuläre Medizin
der Klinik für Gefäß- und Endovaskularchirurgie
des Universitätsklinikums der Heinrich-Heine-Universität Düsseldorf

Gedruckt mit der Genehmigung der
Mathematisch-Naturwissenschaftlichen Fakultät der
Heinrich-Heine-Universität Düsseldorf

Berichterstatter:
1. Prof. Dr. Christoph Fahlke
2. Prof. Dr. Margitta Elvers

Tag der mündlichen Prüfung: 11.01.2023

Table of Content

Abbreviations

A	AA	Arachidonic acid
	AAA	Abdominal aortic aneurysm
	ADP	Adenosine diphosphate
	Akti1/2	Akt 1/2-inhibitor
	Ang II	Angiotensin II
	ANOVA	Analysis of variation of means
	AOD	Athero-occlusive diseases
	ApoE	Apolipoprotein E
	ATP	Adenosintriphosphat
B	BB	Brilliant Blue FCF
	BF	Bright field
	BM	Bone marrow
	BSA	Bovine serum albumin
C	Ca^{2+}	Calcium
	Cbx	Carbenoxolone
	CD40L	CD40 ligand
	CH_3OH	Methanol
	COX 1/2	Cyclooxygenase 1/2
	CRP	Collagen related peptide
	CNS	Central nervous system
	Cryo-EM	Cryogenic electron microscopy
	CVD	Cardiovascular diseases
	CT	Computed tomography
	Cvx	Convulxin
	CXCL	CXC chemokine ligand
D	d	Day
	DAPI	4′,6-Diamidine-2′-phenylindole dihydrochloride
	dH_2O	Distilled water
	DIC	Differential Interference Contrast
	DTT	Dithiothreitol
E	EC	Endothelial cell
	ECL	Electrochemiluminescence
	ECM	Extracellular matrix
	EDTA	Ethylenediaminetetraacetic acid
	EGF	Epidermal growth factor
	e.g.	Lat: *exempli gratia*, Eng: For example
	ELISA	Enzyme linked immunosorbent assay
	eNOS	Endothelial NO-Synthethase
	ER	Endoplasmic reticulum
	ERK	Extracellular-signal regulated kinase
	EtOH	Ethanol
	EVAR	Endovascular aortic repair
	ePPE	External periadventitial elastase application
F	FACS	Fluorescence activated cell sorting
	FcR	Fc receptor
	$FeCl_3$	Ferric chloride
	Fig.	Figure

	FITC	Fluorescein-Isothiocyanat
	FSC	Forward scatter
G	g	Gramm
	GAPDH	Glyceraldehyde 3-phosphate dehydrogenase
	GP	Glycoprotein
	GPCR	G-coupled protein receptor
H	H	hours
	HCl	Hydrochloric acid
	HMGB1	High-Mobility Group Box 1
	HRP	Horse Radish Peroxidase
	HSC	Hematopoeitic stemm cell
I	ICAM-1	Intercellular adhesion molecule-1
	IF	Immunofluorescence
	IgG	Immunoglobulin G
	IL-6	Interleukin-6
	IL-8	Interleukin-8
	IL-1β	Interleukin-1β
	IL-17	Interleukin-17
	ILT	Intraluminal thrombus
	ITAM	Immunoreceptor tyrosine-based activation motif
	IP_3	Inositol 1,4,5-trisphosphate
K	KCl	Potassium chloride
	kDa	Kilodalton
	KO	Knock-out
L	L	Liter
	LTA	Light Transmission Aggregometry
	LN_2	Liquid nitrogen
M	mAb	Monoclonal antibody
	MCP-1	Monocyte chemoattractant protein-1
	MEK	Mitogen-activated protein kinase-kinase
	Mfq	Mefloquine
	MFI	Mean fluorescence intensity
	mg	Milligram
	$MgCl_2$	Magnesium chloride
	MHEC5-T	Mouse heart endothelial cell clone 5-transformed
	MK	Megakaryocyte
	MM	Master mix
	MMP	Matrix metalloproteinase
	mol	Molarity
	MPV	Mean platelet volume
	MP	Microparticle
	MRI	Magnetic resonance imaging
N	Na_3OV_4	Sodiumorthovanadate
	NaCl	Sodium chloride
	NaH_2PO_4	Monosodium phosphate
	$NaHCO_3$	Sodium bicarbonate
	NaOH	Sodium hydrate
	NCX	Na^+/Ca^{2+} exchanger
	NETs	Neutrophil extracellular traps
	NMDAR	N-Methyl-D-Aspartat receptor

	NO	Nitric Oxid
P	PAI-1	Plasminogen activator inhibitor 1
	PANX1	Pannexin 1
	Panx1	Pannexin 1
	^{10}Panx peptide	Pannexin 1mimetic inhibitory peptide
	PANX2	Pannexin 2
	PANX3	Pannexin 3
	PAP-complex	Plasmin-antiplasmin complex
	PAR1	Protease activated receptor 1
	PAR4	Protease activated receptor 4
	PAR4 peptide	Protease activated receptor 4 peptide
	PBS	Phosphate buffered saline
	PCR	Polymerase chain reaction
	PE	Phycoerythrin
	PECA	Plasma membrane Ca^{2+} ATPase
	PF4	Platelet factor 4
	PGE_1	Prostaglandin E1
	PGI_2	Prostacyclin I2
	pH	*Potentia hydrogenii*
	PKB	Protein Kinase B
	PKC	Protein Kinase C
	PLCγ2	Phospholipase Cγ2
	Plt	Platelet
	PMP	Platelet-derived microparticle
	PET	Positron emission tomography
	PP2	3-(4-chlorophenyl) 1-(1,1-dimethylethyl)-1*H*-pyrazolo[3,4-*d*]pyrimidin-4-amine
	PP3	1-Phenyl-1*H*-pyrazolo[3,4-*d*]pyrimidin-4-amine
	PPE	Porcine Pancreatic Elastase
	PRP	Platelet rich plasma
	Prb	Probenecid
	PS	Phosphatidyl serine
	PSGL-1	P-selectin glycoprotein ligand-1
O	OAR	Open aneurysm repair
	OD	Optical density
R	RBC	Red blood cell
	RIPA	Radioimmunoprecipitation assay
	RO	Ro-31-8220
	ROC	Receptor-operated calcium
	ROS	Reactive oxygen species
	RT	Room temperature
S	SDF-1a	Stem cell derived factor alpha
	SDS	Sodium dodecyl sulfate
	SEM	Standard error of mean
	Ser	Serine
	SERCA	Sarcoplasmic/endoplasmic reticulum Ca^{2+} ATPase
	SFK	Src family kinase
	SOCE	Store-operated calcium entry
	SPF	Specific pathogen free
	SSC	Sideward scatter

	STIM1	Stromal interaction molecule 1
T	TEMED	N, N, N′, N′-Tetramethylethylendiamin
	TF	Tissue factor
	TGF-β	Transforming growth factor-β
	Thr	Thrombin
	TLR	Toll-like receptor
	TNFα	Tumor necrosis factor α
	TIMP-2	Tissue inhibitor of metalloproteinase 2
	t-PA	Tissue plasminogen activator
	TxA_2	Thromboxane A_2
	Tyr	Tyrosine
U	U46	U46619 (Thromboxane A_2 analogue)
	U/mL	Unites per milliliter
	µL	Microliter
	µM	Micromolar
	uPA	urokinase-type plasminogen activator
V	VCAM-1	Vascular cell adhesion molecule-1
	VSMCs	Vascular smooth muscle cells
	VTE	Venous thromboembolism
	vWF	von Willebrand Factor
W	WBC	White blood cell
	WT	Wild type

List of Tables

List of Figures

Zusammenfassung

Die durch Thrombozyten vermittelte primäre Hämostase ist ein wichtiger Prozess, da unkontrollierte Thrombusbildung zu einem Gefäßverschluss und damit zu kardiovaskulären Ereignissen wie z. B. einer Thrombose, führen kann. Pannexin 1 (PANX1) ist ein transmembranes Protein, welches ubiquitär in Säugetieren exprimiert wird, unter anderem auf humanen und murinen Thrombozyten. Strukturell sind PANX1 Kanäle aus vier Transmembran-Domänen aufgebaut, welche als Hexamer auf der Plasmamembran funktionsfähige Ionenkanäle mit einer hohen Leitfähigkeit für Adenosintriphosphat (ATP) Moleküle aufweisen, die wichtige Signalmoleküle in der Thrombozytenaktivierung darstellen.

In der vorliegenden Arbeit konnte gezeigt werden, dass der ITAM gekoppelte Signalweg durch Kollagenrezeptor Glykoprotein (GP)VI eine essenzielle Rolle in der PANX1 Aktivierung spielt. Pharmakologische Inhibition des humanen PANX1 Kanals mittels Probenecid als auch Analyse von PANX1 defizienten murinen Thrombozyten zeigten eine verminderte ATP Freisetzung und eine verringerte Thrombozytenaggregation nach Stimulation des GPVI vermittelten Signalweges. In einem *ex vivo* Flusskammerversuch unter dynamischen arteriellen Bedingungen führte eine thrombozyten-spezifische PANX1 Deletion als auch eine Inhibierung von PANX1 mittels Probenecid und Carbenoxolone zu einer verringerten Thrombusbildung bei geringen und intermediären arteriellen Scherraten auf einer mit Kollagen beschichteten Matrix. Detaillierte Untersuchungen zu Aktivierungsmechanismen des PANX1 Kanals mittels Western Blot Analysen demonstrieren, dass eine Stimulation mit klassischen Agonisten zu einer erhöhten Phosphorylierung von PANX1 an Tyr^{198} führte, welche nach Inhibierung der Src-Kinase-Familie (SFK) verringert war. Dabei wurde mit Hilfe von GPVI defizienten Thrombozyten dieser als zentraler Rezeptor für die Kollagen-induzierte PANX1 Tyr^{198} Phosphorylierung identifiziert. Interessanterweise führte eine Thrombozyten Aktivierung über purinerge Rezeptoren nicht zu einer Phosphorylierung von PANX1 an Tyr^{198}, sondern an Tyr^{308}, einer weiteren bekannten zur PANX1 Aktivierung beitragenden Phosphorylierungsstelle. Inhibierung von SFK zeigte, dass diese nur an der GPVI –vermittelten Phosphorylierung von PANX1 Tyr^{308} beteiligt sind, was auf weitere Aktivierungsmechanismen der PANX1 Kanäle hinweist. Inhibierungsversuche der Kinasen PKC und PKB lassen auf eine untergeordnete Rolle dieser in der PANX1 Aktivierung schließen.

Des Weiteren wurde in dieser Arbeit die Rolle des PANX1 Kanals in der Entstehung und Entwicklung abdominaler Aortenaneurysmen (AAA) untersucht. Patienten mit AAA zeigten einen erhöhten PANX1 Plasmaspiegel als auch eine verringerte Phosphorylierung des thrombozytären PANX1 Kanals an Tyr^{198} nach Stimulation des GPVI Signalweges. Um die Rolle des

thrombozytären PANX1 Kanals in dem Krankheitsbild des AAA detaillierter analysieren zu können, wurden Mäuse mit (*Panx1 fl/fl PF4-Cre*$^{+}$) und ohne (*Panx1 fl/fl PF4-Cre*$^{-}$) einer PANX1 Deletion auf Thrombozyten in einem wissenschaftlich anerkannten *in vivo* Mausmodell der Aneurysmainduktion mit „Porciner Pankreas-Elastase“ (PPE) 3, 7, 14 und 28 Tage nach PPE Operation untersucht. Eine Deletion des PANX1 Kanals veränderte den Aortendiameter auch 28 Tage nach PPE Operation nicht, allerdings zeigte sich nach 14 Tagen eine verringerte Anzahl zirkulierender Thrombozyten und Erythrozyten. Dies ging mit einer verminderten Aktivierung sowie prokoagulanten Oberfläche der Thrombozyten einher, während die Oberflächenexpression der untersuchten Glykoproteine 3, 7, 14 und 28 Tage nach PPE Operation unverändert blieb. Außerdem führte eine PANX1 Deletion auf Thrombozyten zu einer verringerten Bildung zirkulierender Thrombozyten-Neutrophilen Aggregaten sowie einer verringerten Anzahl migrierter Thrombozyten und Neutrophilen in das Aortengewebe ausschließlich 14 Tage nach PPE Operation.

Zusammenfassend zeigen die Ergebnisse dieser Dissertation, dass PANX1 Kanäle als ATP Freisetzungskanäle in Thrombozyten fungieren, die durch Veränderung der Thrombozytenfunktion in der Bildung arterieller Thromben eine entscheidende Rolle spielen. Die Aktivierung von PANX1 wird durch Phosphorylierung an Tyr^{198} und Tyr^{308} reguliert, wobei der GPVI-Src Signalweg eine zentrale Rolle spielt. Darüber hinaus deuten die Ergebnisse auf eine wichtige Rolle des PANX1 Kanals bei der Zell-Zell-Interaktion mit Neutrophilen in der AAA Progression hin.

Abstract

Platelet-mediated primary hemostasis is an important process because uncontrolled thrombus formation can lead to vascular occlusion and consequent cardiovascular events such as thrombosis. Pannexin 1 (PANX1) is a transmembrane protein that is ubiquitously expressed in mammals, including on human and murine platelets. Structurally, PANX1 channels are composed of four transmembrane domains, which build functional ion channels as hexamers on the plasma membrane with a high conductance for adenosine triphosphate (ATP), which is an important signaling molecule in platelet activation.

In the present work, the ITAM-coupled signaling pathway through collagen receptor glycoprotein (GP)VI was shown to play an essential role in PANX1 activation. Pharmacological inhibition of the human PANX1 channel by probenecid as well as analysis of PANX1 deficient murine platelets showed decreased ATP release and platelet aggregation after stimulation of the GPVI-mediated signaling pathway. In a thrombus formation assay *ex vivo*, platelet specific PANX1 deletion as well as inhibition of PANX1 using probenecid and carbenoxolone resulted in decreased thrombus formation at low and intermediate arterial shear rates on a collagen coated matrix. Detailed studies of PANX1 channel activation mechanisms by Western blot analysis demonstrate that stimulation with classical agonists resulted in increased phosphorylation of PANX1 at Tyr^{198}, which was decreased after inhibition of Src kinase family (SFK). Thereby, GPVI was identified as a central receptor for collagen induced PANX1 Tyr^{198} phosphorylation using platelets from *Gp6*$^{-/-}$ mice. Interestingly, platelet activation via purinergic receptors did not result in phosphorylation of PANX1 at Tyr^{198} but at Tyr^{308}, another known phosphorylation site contributing to PANX1 activation. Inhibition of SFK showed that they are only involved in GPVI mediated phosphorylation of PANX1 Tyr^{308}, suggesting further activation mechanisms of PANX1 channels in platelets. Inhibition experiments of the kinases PKC and PKB suggested a minor role of these in PANX1 activation displayed by Western blots analysis.

Furthermore, the role of PANX1 channel in the formation and development of abdominal aortic aneurysms (AAA) was investigated in this work. Patients with AAA showed increased plasma PANX1 levels as well as decreased phosphorylation of the platelet PANX1 channel at Tyr^{198} after stimulation of the GPVI signaling pathway. To analyze in more detail the role of the platelet PANX1 channel in the clinical picture of AAA, mice with (*Panx1 fl/fl PF4-Cre*$^{+}$) and without (*Panx1 fl/fl PF4-Cre*$^{-}$) a PANX1 deletion on platelets were studied in a scientific approved *in vivo* mouse model of aneurysm induction with "Porcine Pancreatic Elastase" (PPE) at 3, 7, 14, and 28 days after PPE surgery. Deletion of platelet PANX1 channels did not alter the aortic

diameter 28 days after PPE surgery; however, at 14 days, the number of circulating platelets and erythrocytes was decreased. This was associated with reduced activation and procoagulant surface of platelets, whereas surface expression of the analyzed glycoproteins remained unchanged 3, 7, 14 and 28 after PPE surgery. Furthermore, PANX1 deletion on platelets resulted in decreased formation of circulating platelet-neutrophil aggregates as well as decreased numbers of migrated platelets and neutrophils into aortic tissue exclusively 14 days after PPE surgery.

In summary, the results of this dissertation demonstrate that PANX1 channels function as ATP release channels in platelets that play a critical role in arterial thrombus formation by altering platelet functions. Activation of PANX1 is regulated by phosphorylation at Tyr^{198} and Tyr^{308}, with the GPVI-Src signaling pathway playing a central role. Furthermore, the results suggest an important role of the PANX1 channel in cell-cell interaction with neutrophils in the progression of AAA.

1 Introduction

1.1 Platelets in thrombosis and hemostasis

1.1.1 Platelet physiology

Platelets are the smallest cells in the blood flow with a diameter of 2.0 – 4.0 µm and a volume of approximately 10 fL [1]. The human system consists of around 1.5 – 3.5 x 10^5 platelets per µL blood. Murine platelets are smaller in size (2.0 µm) and the system consists of 1.0 – 1.5 x 10^6 platelets per µL blood [2]. These anucleate cells with a discoid shape are partially able to synthesize proteins due to storage of mRNA in their granules [3]. Proplatelets are produced in the bone marrow and in the lung by fragmentation of megakaryocytes (MK) [4, 5]. In rodents, they can additionally be formed in the spleen [2]. Platelet formation ends when the proplatelets are shed into the blood stream where they develop platelet typical properties like a high content of α- and δ (dense)-granules, lysosomes as well as an open intracanalicular system [6]. Since platelets lose their RNA content during maturation, they are only partially capable of protein synthesis [7]. Human platelets circulate in blood vessels for about 8 – 10 days, while murine platelets have a lifespan of 3 – 4 days [2, 8]. Clearance of aged platelets out of the vascular system occurs by macrophages in the liver and spleen through scavenger receptors [9]. Beside their essential role in the regulation of hemostasis and thrombosis, platelets also contribute to many other biological processes as angiogenesis, inflammation, immunity and tumour metastasis [10, 11]

1.1.2 Primary and secondary hemostasis

1.1.2.1 Platelet regulation in the vascular system

In the physiological state, platelets circulate in an inactive state (resting) through the vasculature. Platelet activation induced by shear stress from the blood flow is inhibited by anti-platelet factors and anti-thrombotic molecules expressed on the surface of the endothelial matrix. In detail, ectonucleotidases as the human CD39 (apyrase) are expressed on various tissues inhibiting the degradation from adenosintriphosphat (ATP) to adenosindiphosphat (ADP) [12, 13]. Thrombin generation is regulated and inhibited by the enzyme thrombomodulin [14]. Additionally, intracellular signaling cascades are inhibited by prostaglandin I_2 [or prostacyclin (PGI_2)] and nitric oxide (NO). PGI_2 is produced by the prostacyclin synthase from its progenitor prostaglandin H_2 in the endoplasmic reticulum (ER) of endothelial cells (ECs) [15], while NO is produced in platelets and ECs by the endothelial NO-synthase (eNOS) [14, 16].

1.1.2.2 Platelet activation in primary hemostasis

Platelets are the key players in primary hemostasis as they are responsible for forming a primary thrombus to prevent massive blood loss. This process is tightly regulated because uncontrolled thrombus formation can lead to vessel occlusion leading to cardiovascular events e.g. ischemia or infarction [17]. At sites of vascular injury, extracellular matrix proteins as collagen, laminin or vitronectin are exposed from the subendothelial extracellular matrix (ECM) leading to platelet adhesion mediated by the platelet receptors glycoprotein (GP) Ib-IX-V, integrin $\alpha_2\beta_1$ (GPIa-IIa) and glycoprotein (GP)VI [17]. The initial step of platelet adhesion is mediated by the interaction of platelet GPIb-IX-V receptor complex with the subendothelial matrix protein von Willebrand factor (vWF), which is secreted by endothelial Weibel-Palade bodies [18]. This interaction is essential to the induction of an unstable transient adhesion (tethering) of platelets to the vessel wall even under high shear rates above $1700s^{-1}$. Tethering of platelets leads to the recruitment of further platelets, which "roll" to the side of injury (Figure 1). Direct interaction between collagen and the GPVI receptor uniquely expressed on platelets leads to further platelet activation by intracellular signalling cascades resulting in influx of cytosolic Ca^{2+}. High $[Ca^{2+}]_{int}$ concentrations activate integrin receptors such as $\alpha_2\beta_1$ and $\alpha_{IIb}\beta_3$ on the platelet surface via inside-out signalling amplifying platelet granule secretion.

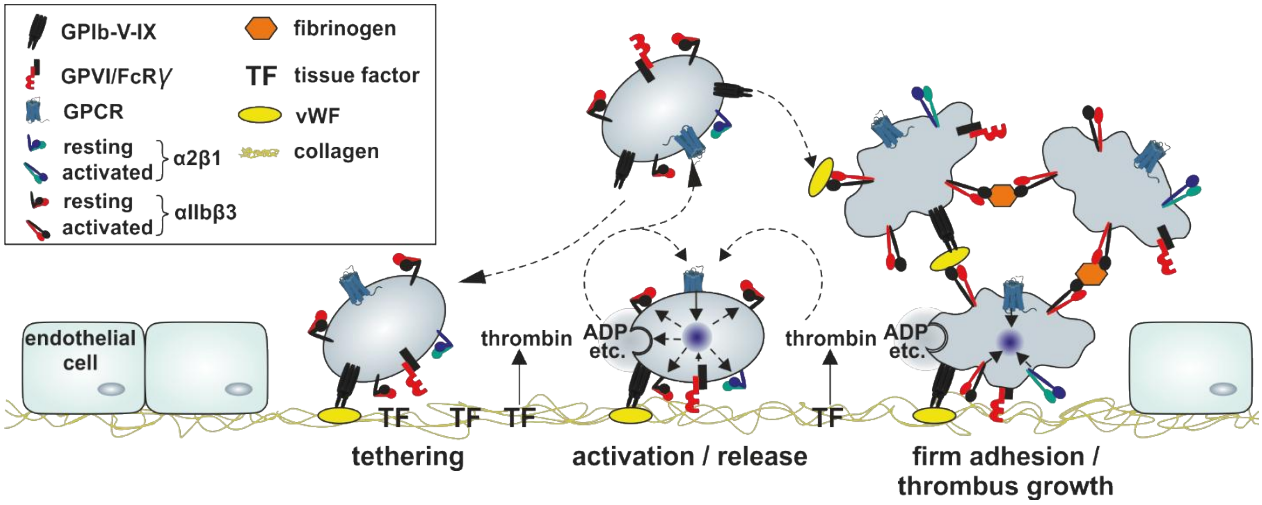

Figure 1: Steps of primary hemostasis after vascular injury. The initial adhesion to the subendothelum is mediated by the interaction of platelet GPIb-IX-V receptor complex and von Willebrand factor (vWF) from the extracellular matrix (ECM). Tethering of platelets leads to binding of GPVI to collagen inducing platelet activation and granule release of e.g. ADP. Additionally, the subendothelum synthesized tissue factor (TF), which leads to thrombin generation promoting further recruitment of platelets from circulation in the blood stream to the site of injury mediated by activation of platelet G-protein coupled receptors (GPCR). Platelet activation is controlled by the GPIb-V-IX-complex, GPVI and GPCR promoting integrin $\alpha_2\beta_1$ and $\alpha_{IIb}\beta_3$ activation from the resting state by conformational changes. Crosslinking of platelets through fibrinogen-bridges is mainly mediated by integrin $\alpha_{IIb}\beta_3$, promoting thrombus growth [Figure modified from Varga-Szabo, Pleines, Nieswandt, ATVB 2000].

1.1.2.3 The major collagen receptor GPVI

GPVI is a type I transmembrane receptor with a size of 62 kDa uniquely expressed on platelets and megakaryocytes [19]. It is associated with the Fc receptor (FcR) γ-chai, therefore its activation leading to autophosphorylation of the immunoreceptor tyrosine-based activation motif (ITAM) [20]. Binding of the SH2-domane from Src family kinases (Fyn and Lyn) at the prolin-rich motif at the cytosolic tail of GPVI leads to ITAM phosphorylation. Syk is activated by the binding of the SH2-domane from GPVI, leading to phosphorylation of phospholipase Cγ2 (PLCγ2). PLCγ2 induces the generation of 1,2-diacylglycerin (DAG) and inositol-1,4,5-Trisphosphat (IP3), which is important for activation of protein kinase C (PKC). The GPVI mediated intracellular signalling cascade results in influx of cytosolic Ca^{2+}, leading to integrin activation and the release of α- and δ-granules [21-23].

1.1.2.4 Integrin outside-in and inside-out signaling

Integrins are transmembrane α/β heterodimers, which contribute to various cell-matrix and cell-cell interactions. They consist of different numbers of integrin α- and β subunits and the resulting heterodimers are classified into groups due to their identity of their β subunit. Platelets express three different integrins of the β_1 subfamily ($\alpha_{II}\beta_1$, $\alpha_v\beta_1$, and $\alpha_{vI}\beta_1$) and both members of β_3 subfamily ($\alpha_v\beta_3$ and $\alpha_{IIb}\beta_3$) on their surface [24]. Stable platelet adhesion to the ECM proteins as collagen, fibronectin and laminin is mainly mediated by integrins, while the fibrinogen receptor integrin $\alpha_{IIb}\beta_3$ (GPIIb/IIIa) is the highest abundancy. Integrin $\alpha_{IIb}\beta_3$ (GPIIb/IIIa) is a glycoprotein complex with about 80,000 copies on the platelet surface and plays a central role in platelet activation [25] . In a resting state, integrin $\alpha_{IIb}\beta_3$ is in a conformation with low affinity to its ligand fibrinogen, which changes immediately upon platelet activation [26]. During platelet secretion, integrins $\alpha_{IIb}\beta_3$ are translocated to the platelet surface which can be measured as platelet activation marker [27]. The initial conformational change is mediated by ligand-induced binding to the extracellular part of integrin $\alpha_{IIb}\beta_3$ (“inside-out signaling”). Intracellular conformational changes lead to trans-phosphorylation of the cytoplasmic tail and further activation of downstream signaling cascades. This process is known as integrin “outside-in signaling” [28, 29]. Integrin outside-in signaling mediates platelet activation, shape change and aggregation [30, 31]. Externalization of integrin $\alpha_{IIb}\beta_3$ is also mediated via GPVI signaling by the release of α- and δ-granules upon platelet activation. Platelet granules contain e.g. second wave mediators as thromboxane (TxA_2) and ADP inducing integrin activation via autocrine signaling [29].

1.1.2.5 Platelet shape change and second wave mediators

ADP and TxA_2 are second wave mediators, which are released during degranulation and contribute to platelet activation by stimulation of various platelet receptors. Binding of ADP to platelet receptors P_2Y_1 or P_2Y_{12} leads to platelet shape change, calcium mobilization and finally platelet aggregation [32]. In detail, P_2Y_1 is responsible for shape change and calcium mobilization, while P_2Y_{12} inhibits the adenylyl cyclase, stabilizes platelet aggregation and leads to integrin $\alpha_{IIb}\beta_3$ activation [33]. In platelets, active phospholipase A2 cleaves fatty acids, which lead to the release of arachidonic acid (AA). Cyclooxygenase 1/2 (COX 1/2) converts AA into prostaglandin H_2 (PGH_2) [34]. The TxA_2 synthetase builds TxA_2, which is stored in platelet granules and released upon platelet activation. Released TxA_2 elevates platelet activation by binding the G-protein coupled thromboxane A_2 receptors, TPα and TPβ (T-prostanoid receptor; TP-receptor). The activation of this signaling cascade leads to $\alpha_{IIb}\beta_3$ integrin activation, calcium mobilization and shape change of platelets [18, 35]. Figure 2 provides an overview of the most important signaling cascades in platelet activation.

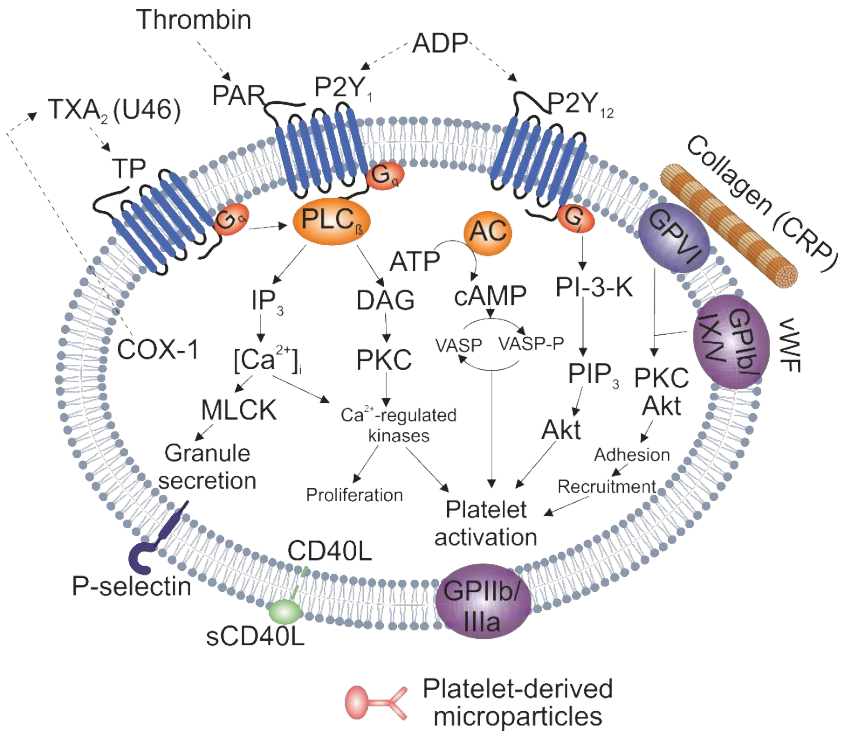

Figure 2: A brief overview of the main initial platelet activation signaling pathways. Platelets can be activated via different platelet agonists, which bind to different platelet receptors inducing various signaling events. Binding of collagen (or CRP) to the GPVI receptor leads to activation of the ITAM coupled receptor pathway leading to platelet activation. Platelet activation induced by vWF is mediated via the platelet GPIb-IX-V receptor complex. Platelet activation can be measured by the upregulation of integrin $\alpha_{IIb}\beta_3$ (GPIIb/IIIa), which serves as an activation marker of platelets. Thrombin acts on PAR1 and PAR4 receptors, while ADP binds to the platelet receptors P_2Y_1 or P_2Y_{12}. The second wave mediator TxA_2 or its analogue U46 amplifies TP receptor signaling leading to platelet activation and degranulation. During platelet degranulation, P-selectin is expressed as a component of α-granules on the platelet surface, which serves as a degranulation marker for platelets. Moreover, during platelet activation soluble mediators e.g. sCD40L and microparticles are released from platelets. ADP = Adenosine diphosphate, ATP = Adenosintriphosphat, TxA_2 = thromboxane A_2, vWF = von Willebrand factor, U46619 (U46) = Thromboxane A_2 analog, CRP = Collagen-related peptide, COX 1 = Cyclooxygenase 1, CD40L = CD40 ligand, cAMP = Cyclic adenosine monophosphate, PLC = Phospholipase C, PIP_3 = Phosphatidylinositol 4,5-trisphosphate, MLCK = Myosin light chain kinase, PI-3-K = Phosphatidylinositol 3-kinase, PKC = Protein kinase C, IP_3 = Inositol 1,4,5-trisphosphate [Figure modified from Tesfamariam, Pharmacol. 2016].

1.1.2.6 Calcium mobilization

The mobilization of intracellular calcium is essential for proper platelet aggregation [36]. Increased cytosolic Ca^{2+} levels are mediated by various agonists and signaling pathways, leading to reorganization of the cytoskeleton (shape change) as displayed in Figure 3 [37, 38]. In platelets, Ca^{2+} can be released either from major intracellular Ca^{2+} stores such as the dense tubular system and granules or by Ca^{2+} influx through the plasma membrane [36]. Platelet activation induced by various agonists leads to activation of phospholipase C (PLC) isoforms, while PLCγ2 and PLCβ2/3 are the most important isoforms in mouse platelets [39, 40]. The second messengers inositol 1,4,5-trisphosphate (IP_3) and 1,2-diacylglycerol (DAG) are hydrolyzed from

phosphatidylinositol 4,5-trisphosphate (PIP_2) by PLCβ isoforms, leading to the release of Ca^{2+} from intracellular stores, activation of protein kinase C (PKC) and stromal interaction molecule 1 (STIM1). STIM1 leads to opening of Orai1 channels at the platelet plasma membrane. This process is called store-operated calcium entry (SOCE) [41]. Beside SOCE, increased cytosolic Ca^{2+} levels through the plasma membrane also occur by the receptor-operated calcium (ROC) channel, $P2X_1$ and the Na^+/Ca^{2+} exchanger (NCX) [36, 42]. The regulation of the cytosolic calcium level is mediated by the sarcoplasmic/endoplasmic reticulum Ca^{2+} ATPase (SERCA) and the plasma membrane Ca^{2+} ATPase (PECA), which fill up intracellular calcium stores in platelets or pump Ca^{2+} out of the cell through the plasma membrane. SERCA activity can be blocked by the non-competitive compound tapsigargin, which is essential to study defects in fulfilling Ca^{2+} into the sarcoplasmic and endoplasmic reticulum [43].

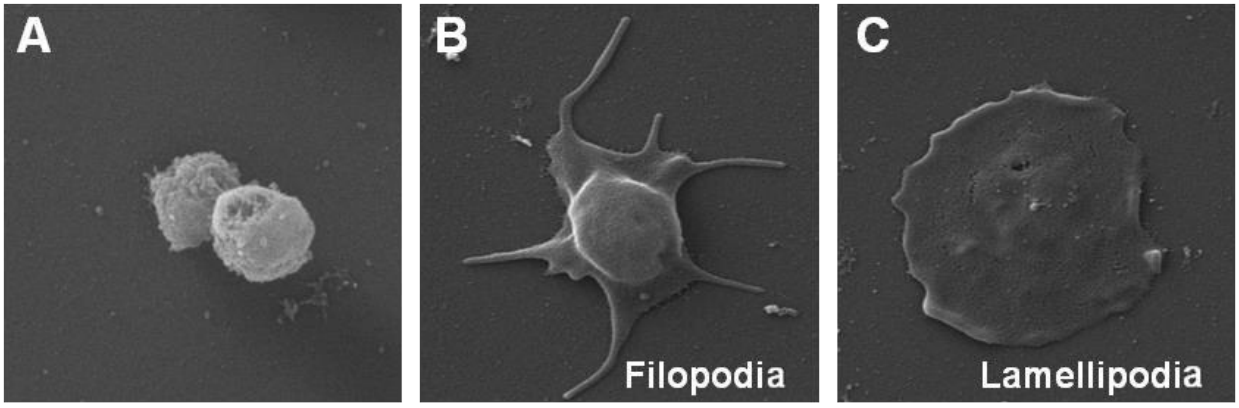

Figure 3: Platelet shape change after platelet activation visualized via electron microscopy. Platelets are shown (A) in an inactive state (resting) with a discoid morphology, after platelet activation and the formation of (B) filopodia and (C) lamellipodia [Figure from Prof. Dr. Margitta Elvers; Research group: Exp. Vascular Medicine; unpublished data].

1.1.2.7 Platelets and their role in secondary hemostasis

After primary plug formation, platelets are connected via fibrinogen bridges between cross-linked $\alpha_{IIb}\beta_3$ integrins [44]. Secondary hemostasis is essential for the formation of an insoluble fibrin-rich plug by activated coagulation factors, leading to thrombin generation and the formation of a fibrin net. Thrombin (Factor IIa) is the central serine protease from the coagulation system and is activated from its inactive precursor form prothrombin by enzymatic cleavage [45, 46]. One main procoagulant function of thrombin is cleavage of fibrinogen into soluble fibrin monomers, which are further inserted into a fibrin-rich plug. Platelet activation via thrombin occurs by cleavage of the human platelet PAR1 and PAR4 [47] and murine platelet PAR3 and PAR4 receptor [48]. Procoagulant platelets expose negative charged phosphatidyl serine (PS) at their surface [49]. The intrinsic prothrombinase complex (FXa, FVa, phospholipids and Ca^{2+}) is formed on

procoagulant platelets increasing the amounts of thrombin generation. Moreover, PS-exposure on the platelet surface lead to coated platelets by their released proteins after degranulation (e.g. vWF, fibrinogen, fibronectin) [50, 51]. Beside clot stabilization by fibrin insertion of crosslinked platelets, other blood cells e.g. erythrocytes are recruited in the thrombus [52].

The downregulation of the coagulation cascade occurs by binding of thrombin to thrombomodulin on ECs, which activates protein C. In the addition with protein S, factor V and the negatively charged platelet membrane, this complex inactivates factor VIIIa and factor Va. Serine protease inhibitors also inhibit the coagulation cascade. Thrombin is inhibited by antithrombin, FXa, FIXa and FXIa in the presence of heparin or heparan sulphate [45]. During wound healing, the process of fibrinolysis starts by the serine protease plasmin. Blood-circulating plasmin is activated by tissue-type plasminogen activator (tPA) and urokinase-type plasminogen activator (uPA) [53]. Plasmin cleaves fibrin, which leads to the degradation of the clot [54].

1.1.3 Platelets in inflammation

Under inflammatory conditions, leukocytes are recruited at sides of vascular injury. This initial adhesion process is mainly mediated by endothelial P-selectin, which is stored in the Weibel-Palade bodies of ECs [55, 56]. Together with endothelial E-selectin, vWF and vascular cell adhesion molecule-1 (VCAM-1), these molecules mediate leukocyte rolling over the inflamed endothelium. Beside leukocytes, platelets are also involved in inflammatory processes [57]. Endothelial E-selectin build a loose connection to platelets. Platelet GPIb-IX-V complex as well as P-selectin glycoproteinligand-1 (PSGL-1) induce binding of endothelial P-selectin leading to a loose adhesion to the inflamed endothelium. Stable platelet adhesion is mediated by platelet integrin $\alpha_{IIb}\beta_3$ and integrin $\alpha_V\beta_3$ on the endothelium. This interaction enables transcellular communication via soluble mediators as released growth factors, chemokines and cytokine-like factors. Especially interleukin-1β (IL-1β), released by platelets, displays one major mediator in EC activation. The release of IL-1β leads to the secretion of IL-6, IL-8 and monocyte chemoattractant protein-1 (MCP-1) from ECs, while MCP-1 leads to the recruitment of monocytes to the sides of inflammation [58, 59]. Additionally, the released IL-1β activates the transcription factor NF-κB, which in turn leads to the expression of the endothelial adhesion molecules integrin $\alpha_V\beta_3$ and intercellular adhesion molecule-1 (ICAM-1) [60]. The upregulation of these endothelial adhesion molecules further recruits neutrophils and monocytes to the inflamed tissue. Another platelet cytokine, CD40 ligand (CD40L/CD154), is involved in inflammatory cell responses. After platelet activation, CD40L is expressed on the platelet surface and directly binds endothelial

CD40 receptor [61]. This interaction enables the release of endothelial chemokines IL-8 (only in human [62]) and MCP-1, as well as the expression of adhesion molecules (E-selectin, ICAM-1 and VCAM-1). Leukocyte-platelet interactions via of PSGL-1/P-selectin signaling are also required for rolling and adhesion of leukocytes to sides of inflammation [63]. Moreover, platelet-leukocyte aggregates promote the release of pro-inflammatory mediators, phagocytoses and the release of neutrophil extracellular traps (NETs) from leukocytes [64, 65]. The fundamental immune cell-platelet interactions during inflammatory processes are summarized in Figure 4.

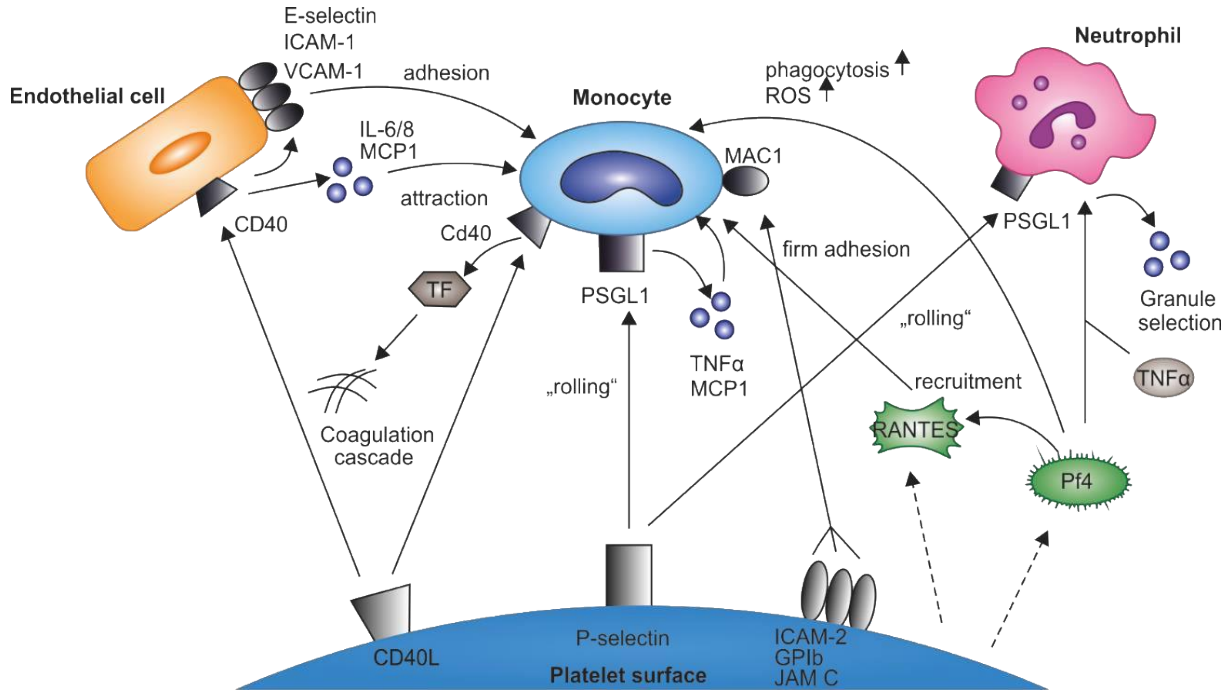

Figure 4: Immune cell-platelet interactions modulate inflammatory processes. The release of platelet cytokines, chemokines and other immune-modulating mediators attract immune cells as endothelial cells (ECs), monocytes and neutrophils. These interactions regulate inflammatory processes by the activation of various receptor-dependent signaling cascades. (ICAM-1: Intercellular adhesion molecule 1; IL 6/8: Interleukin 6/8; MCP1: Monocyte chemotactic protein 1; TF: Tissue factor; JAM C: Junctional adhesion molecule C; PF4: Platelet factor 4; PSGL-1: P-selectin glycoprotein ligand-1; RANTES: Chemokine ligand 5 (CCL5); TNF α: Tumor necrosis factor α; VCAM-1, vascular cell adhesion molecule 1) [Figure modified from Eisinger, Patzelt, Langer, Front.Med. 2018].

1.2 Function of pannexin channels

Pannexins build a group of transmembrane proteins consisting of three isoforms named pannexin 1 (PANX1), pannexin 2 (PANX2) and p annexin 3 (PANX3). In the mammalian genome, pannexins were first discovered in 2000 by Panchin and colleagues [66] due to their sequence homology to gap junction proteins called innexins from invertebrates [67]. Within this family, expression patterns between PANX1, PANX2 and PANX3 differ from each other. While PANX1 is ubiquitously expressed, PANX2 is mainly found in the brain and central nervous system (CNS) and PANX3 is found in bone and skin [68]. Moreover, PANX1 and PANX3 are located on human chromosome 11 and PANX2 is located on chromosome 22 [69].

1.2.1 Structure and functional properties of pannexin 1 channels

PANX1 is a single membrane channel, which functions as an ion channel for small molecules up to 1 kDa in size [70]. The channel consists of a hexameric structure of single membrane channels at the plasma membrane (Figure 5). Cryo-EM (Cryogenic electron microscopy) analysis showed that each channel consists of four transmembrane domains with two extracellular loops and an intracellular N- and C-termini [71]. Glycosylation at Asn^{254} of the second extracellular loop is essential for correct plasma membrane insertion, preventing PANX1 from the formation of gap junctions instead of channels [72-74]. PANX1 channels open in response to various mechanisms: Oxygen-glucose deprivation, caspase cleavage, mechanical stimulation, phosphorylation of Src family kinases (SFKs) and elevation of $[Ca^{2+}]_{int}$ [3, 70, 75]. Functionally, PANX1 are anion-selective channels with a high conductance for ATP and other small molecules. They display an important role in non-vesicular ATP release and intercellular communication by amplification of paracrine signaling in cells [70]. ATP release due to PANX1 channels leads to activation of P2 receptors by degrading ATP to ADP by ectonucleotidases (e.g. CD39) [76-78]. Overall, PANX1 channels play a major role in various physiological functions as normal development of skin and bones, synaptic plasticity and the regulation of blood pressure [79].

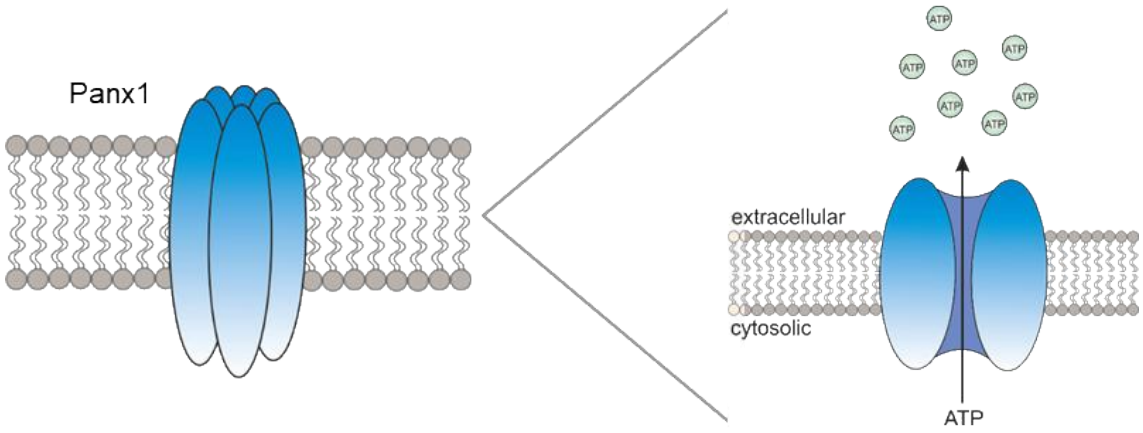

Figure 5: Pannexin 1 (PANX1) channels function as ion channels with a high conductance for ATP. (Left) PANX1 is formed of a hexameric structure of single membrane channels at the plasma membrane. (Right) During PANX1 activation, ATP or other small molecules are released from the cytosol to the extracellular space.

1.2.2 The role of pannexin 1 channels on platelets

Recent studies demonstrated that human and murine platelets express functional PANX1 channels on their plasma membrane [80, 81]. It was shown that PANX1 is expressed at similar mRNA levels as the ATP-gated cation channel P2X1 [81]. PANX1 channels on platelets were shown to function as ATP release channels, which was first demonstrated by inhibition of PANX1 channels by two non-specific inhibitors named Probenecid (Prb) and Carbenoxolone (Cbx). Reduced ATP release upon platelet stimulation with low concentrations of thrombin, collagen or the TxA_2 analogue U46619 resulted in reduced platelet aggregation as well as Ca^{2+} influx [81]. Moreover, similar results in terms of ATP release measurements and aggregation studies were obtained by Mollica and colleagues which were confirmed in *Panx1*$^{-/-}$ mice [80]. Here, it was shown that the classical platelet agonists ADP and AA do not amplify PANX1 activation in platelets.

It is assumed that GPVI mediated activation via collagen leads to phosphorylation and activation of SFKs, which leads to ATP release via PANX1 in the extracellular space, finally amplifying $P2X_1$ receptors for calcium mobilization and platelet aggregation (Figure 6) [80]. Physically, PANX1 receptors and P2X1 receptors were shown to interact in human platelets [80]. The inhibition of SFKs resulted in reduced platelet aggregation and intracellular phosphorylation of PANX1 Tyr^{308}, the Src kinase phosphorylation site on PANX1 channels [82]. In platelets, SFKs are proposed to be key regulators in PANX1 activation [82].

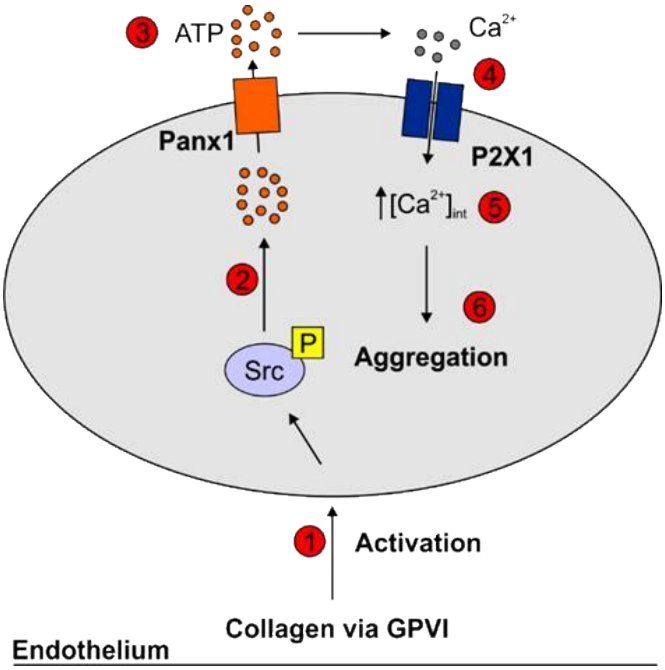

Figure 6: Activation of PANX1 channels leads to Ca^{2+} influx. Platelet activation induces the opening of PANX1 channels on platelets thereby amplifying Ca^{2+} influx, ATP release and platelet aggregation by co-activation of P2X1 channels [Figure modified from Molica, et al. JTH 2015].

Until now, many inhibitors for the analysis PANX1 channels as Prb, Cbx, mefloquine (Mfq) and Brilliant Blue FCF (BB) are identified. These non-specific inhibiting compounds were shown to inhibit PANX1 dependent currents after application to various mammalian cells via patch-clamp technique [83-86]. Recently, a specific inhibiting peptide ^{10}PANX1 peptide (WRQAAFVDSY) against the first extracellular loop was developed, which was shown to be selective against PANX1 channels [80]. Nevertheless, Prb and Cbx are the most common used PANX1 inhibitors, which inhibit the first extracellular loop in a concentration-dependent manner [87]. However, Cbx has been shown to inhibit connexins exceeding concentrations over 50 µM [88].

Mice targeting a global deletion and a platelet specific deletion of PANX1 were used to analyze the influence of PANX1 in thrombosis and hemostasis *in vivo*. Ubiquitous PANX1 deletion results in decreased hemostasis by increased tail bleeding time in about 2.5-fold times. Platelet specific Panx-1 deletion results in 2.0-fold time to arrest tail bleeding. Moreover, these mice showed reduced venous thromboembolism (VTE) after the injection of collagen/epinephrine in the jugular vein and reduced $FeCl_3$-induced thrombosis in mesenteric arteries concluding a functional role of platelet PANX1 channels on thrombosis and hemostasis [82].

1.2.3 The relevance of pannexin 1 channels on inflammation

Extracellular ATP is an important molecule involved in many inflammatory processes by e.g. activation of the inflammasome or increased immune cell infiltration [89, 90]. Recent studies demonstrate that controlled ATP release due to PANX1 channels supports intercellular communication [91]. For example, during acute inflammation the emigration of leukocytes is mediated by endothelial PANX1 and ATP release from apoptotic cells served as a find-me signal for phagocytes [92, 93]. Moreover, PANX1 dependent NLRP3 inflammasome activation results in IL1β and IL18 production, leading to toll-like receptor (TLR) signaling and the stimulation of purinergic receptors by high extracellular ATP concentrations [94]. In a mice model of multiple sclerosis, PANX1 deficient mice showed no upregulation of IL1β [95]. PANX1 deficient neutrophils do not release IL1β resulting in reduced neutrophil extracellular trap (NET) formation [96]. IL1β is identified as an important pro-inflammatory cytokine contributing to cardiovascular diseases (CVD) e.g. atherosclerosis [92]. Beside the production of IL1β, other cytokines are released during PANX1 dependent inflammasome activation as e.g., high mobility group box 1 (HMGB1) [97]. Myeloid PANX1 knockout mice displayed reduced levels of matrix metalloproteinase 9 (MMP-9) [98], an important collagenase also involved in the pathogenesis of abdominal aortic aneurysm (AAA) formation [99]. Beside the release of pro- and anti-inflammatory cytokines, activated NMDA receptors (NMDAR) can cross-activate PANX1 channels by phosphorylation of SFKs during neuroinflammation [100]. Inhibition of the NMDAR-Src-PANX1 complex showed protective effects in ischemia [101]. Overall, PANX1 channels contribute to inflammatory processes by various mechanisms in different cellular processes and systems.

1.3 Abdominal aortic aneurysms

Abdominal aortic aneurysm is the 12th to 15th leading cause of death in the western society including USA and Europe. Due to ultrasonographic screening programs the prevalence has decreased within the last two decades but the prevalence is estimated between 1-3% in men and 0.5-1% in women over 65 years of age [102, 103]. An aneurysm is defined as a permanent dilatation of an artery to 1.5 fold to its normal diameter. An AAA of the infrarenal aorta affects all three layers of the vascular tunica and is defined as aneurysmal starting from more than 3 cm in diameter dilatation in size [104, 105]. In the progression of the disease, the aortic wall becomes thinner due to proteolytic degradation of the ECM proteins elastin and collagen over time. Beside elastin fragmentation of the aortic wall, AAA development is characterized by death of vascular smooth muscle cells (VSMCs), immune cell infiltration, increased oxidative stress in the aortic wall

and the formation of an intraluminal thrombus (ILT) (Figure 7) [106]. In the past, AAAs were considered because of atherosclerosis. The view on the diseases changed during the last years of research because studies revealed differences between the pathogenesis of aneurysms and athero-occlusive diseases (AOD) [107]. Studies indicate lower expression levels of physiological inhibitors of proteases as tissue inhibitor of metalloproteinase 2 (TIMP-2) and plasminogen activator inhibitor 1 (PAI-1), but higher levels of the circulating inflammatory cytokines IL-1β and IL-6 in plasma of patients with AAA compared to AOD [107, 108]. These results show that proteolysis of the aortic wall is more essential in the development of AAA than AOD. During the process of remodeling the aortic wall, especially matrix metalloproteinases (MMPs) as MMP-9 and the transforming growth factor (TGF)-β pathway play a critical role [99, 109, 110].

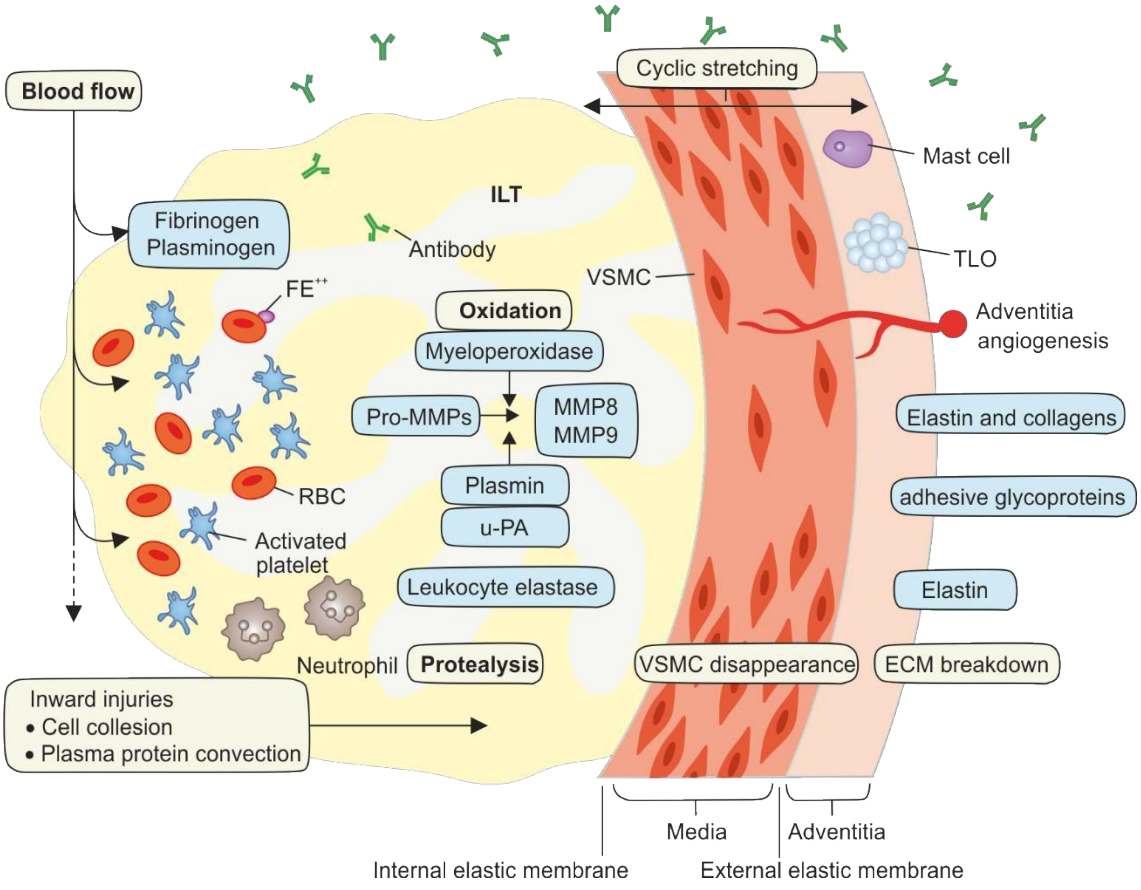

Figure 7: The progression of abdominal aortic aneurysm (AAA) occurs via different mechanisms. The development of AAA often occurs with the formation of an intraluminal thrombus (ILT), which constantly faces the blood circulation. Platelet activation causes the release of pro-inflammatory cytokines and mediators, leading to the recruitment of further immune cells, e.g. neutrophils. The release of proteases as matrix metalloproteinases (MMPs) and leukocyte elastase from immune cells lead to the degradation of elastin and collagens, while plasmin led to the degradation of adhesive glycoproteins. Oxidative stress is enhanced by redox active iron, which is released by red blood cells (RBCs). Active MMPs, enhanced reactive oxygen species (ROS) production and cyclic stretching lead to the detachment and apoptosis of vascular smooth muscle cells (VSMCs). Additionally, new blood vessels are developed (Neoangiogensis) into the media [Figure modified from Sakalihasan, Natzi, et al. 2018, Nat. Rev. Dis. Primers].

Rupture of the aortic wall by mechanical stress of the blood flow leads to a massive intra-abdominal haemorrhage and leads to 65-85% of the cases to death. The risk of aortic rupture increases with the increased aortic diameter [106]. AAAs are in most of the cases asymptomatic and are only detected by systemic screening of risk groups from people older than 65 years [111]. Due to the fact that AAA development is often asymptomatic, several risk factors are associated with this disease. Until now, tobacco smoking, age over 65 years, hypertension, chronic obstructive pulmonary disease, hyperlipidaemia, genetic susceptibility and male sex are considered as potential risk factors. Due to the fact that smoking prevalence trends towards equal between the genders, male sex might not be a risk factor in future [103]. One of the main avoidable risk factors in AAA development is smoking. It was shown that a life-time male smoker has a 2.5-fold increased risk to develop AAA compared to a male non-smoker [112]. Smoking degrades the elastic tissue in the aortic wall via the inhibition of α1-antitrypsin from elastase activity [113].

As already mentioned, AAAs are often asymptomatic and mostly treated by the insertion of a vascular graft after diagnosis. In case the diameter of the abdominal aorta has increased by more than 10 mm per year, is greater than 5 cm in women and 5.5 cm in men, a surgical repair is necessary [114, 115]. Modern imaging techniques as positron emission tomography (PET), computed tomography (CT) and magnetic resonance imaging (MRI) help to monitor the growth of aortic aneurysms. If a surgery is necessary, people underwent an elective repair of AAA with open surgery (Open aneurysm repair – OAR) or endovascular aortic repair (EVAR) to prevent rupture of the AAA [106, 116]. Generally, it is distinguished between two types of AAA named fusiform or saccular aneurysms. In case of a fusiform aneurysm the complete aortic vessel wall is dilated, while a saccular aneurysm describes the dilatation of only one aortic wall [117].

1.3.1 The intraluminal thrombus

In 70-80% cases of AAA patients the formation of an intraluminal thrombus (ILT) occurs. The ILT consists of an inhomogeneous thrombus structure; build out of a dense fibrin network including leukocytes and erythrocytes [118]. The three regions of a multi-layered ILT varied in thickness from millimeters to centimeters in size. The thrombus consists of a luminal layer, which is next to the blood, displays a red color and is rich in undegraded cross-linked fibrin fibers and aggregated erythrocytes. In contrast, the medial (middle) and abluminal layer (next to the aneurysmal wall) proteolysed layer consists of nucleated, cell-rich fibrin [119, 120]. Especially the medial layer is connected via a channel system named canaliculi. This system interconnects the medial layer and

increases the area from the luminal to the abluminal layer. Each ILT develops a unique structure, which must not be separated by three defined layers [121].

The ILT displays a biologically active structure, because of the expression of TF and phosphatidylserine (PS) at the luminar surface side, leading to aggregation and further recruitment of activated platelets and leukocytes, especially neutrophils in the ILT. The release of cytokines and microparticals (MPs) from platelets and leukocyte increase the biological activity of the ILT [122, 123]. Moreover, the ILT induces hypoxia, which weakened the aortic wall by increased vascular inflammatory processes. On the other side, mechanical stress induced by the vessel wall is reduced by ILT. The growth of AAA is related to the volume and thickness of the ILT, MMP levels, degradation of elastin fibers and apoptosis of SMC [124, 125].

1.3.2 The role of platelets in abdominal aortic aneurysm

Platelets contribute to inflammatory processes in cardiovascular diseases e.g. by the release of proinflammatory cytokines [105, 126]. The development of an ILT is a key element in most cases in the progression of AAA (1.3.1). Inhibition of ADP-induced platelet aggregation in a rat aneurysmal model *in vivo* showed a reduced aortic diameter, platelet CD41 expression and immune cell infiltration. Additionally, MMP-9 expression as well as elastic fiber degradation were reduced by inhibiting platelet aggregation with a compound named AZD6140 [127]. Another study in an angiotensin II (Ang II) -infused apolipoprotein E (ApoE)-knockout mice AAA model showed that treatment of the $P2Y_{12}$ receptor by clopidogel decreases the aortic diameter in size by about 47%. Additionally, ROS production and MMP activation in macrophages as well as the number of infiltrated inflammatory cells were reduced [128]. Until now, no anticoagulant therapy could be established for clinical trials because platelet treatment led to adverse clinical events e.g. rupture of the ILT [129, 130].

1.3.3 The influence of pannexin 1 channels in the progression of abdominal aortic aneurysms

Recent studies demonstrate that PANX1 channels contribute to AAA formation. Clinical studies of male patients showed increased PANX1 expression levels in aortic tissue [131]. The analysis of an AAA mice model (Porcine Pancreatic Elastase (PPE) Perfusion Model) investigating the role of endothelial cell specific PANX1 deficiency resulted in reduced AAA formation compared to respective WT mice [131, 132]. The same study detected reduced acute phase cytokines as

HMGB1, IL-17, MCP1 and TNFα in knockout (KO) mice compared to elastase-treated control mice. Additionally, a reduced number of infiltrating macrophages, neutrophils and CD3+ T cells were found in elastase-treated endothelial cell specific PANX1 deficient mice. These mice displayed decreased elastic fiber disruption compared to their respective controls. Application of Prb, an unspecific PANX1 inhibitor, to mice undergoing PPE surgery also annotated AAA formation. A smooth muscle cell specific PANX1 deficient mice undergoing PPE surgery do not alter AAA formation [131]. These studies display a functional role of PANX1 channels in the progression of AAA.

1.3.4 Porcine Pancreatic Elastase perfusion model

The Porcine Pancreatic Elastase (PPE) perfusion model enables to study the formation and progression of AAA in a mice model *in vivo* and was first described by Pyo et al, 2000 [133]. This elastase induced murine aneurysm model is performed by a short-term luminal perfusion of PPE to the infrarenal aorta, resulting in degradation of the ECM. After a time-period of around 8 weeks, the thickness of the aortic wall as well as the aortic diameter increase of about 170% [134]. In line with the remodeling of the vascular wall in the progression of AAA, cytokine expression, wall morphology and signaling mechanisms alter in the process from acute to chronic inflammation [110, 135]. In comparison to human AAA formation, many properties cover similarities to the murine PPE model. Nevertheless, not all features are similar between human and murine AAA progression, as e.g. fusiform shape of the aneurysm [135]. This is due to the reason that human AAAs are in most cases asymptomatic and only detected by systemic screening. In comparison to that, the formation of AAA in the murine model is mechanically induced by the perfusion of elastase and can be monitored overtime. Due to the current point of research, the murine PPE model is widely used to study the pathophysiology of AAA formation in mice to give mechanistic insights for a translational approach in progression of this disease in humans [131, 132].

1.4 Aim of the study

Since many years, it is well-known that platelets are key players in hemostasis and thrombosis. At sides of vascular injury, rapid platelet recruitment followed by their activation leads to primary plug formation. This process is rapidly and tightly regulated, mediated by a complex system of activating and inhibiting signaling events. On the other hand, CVDs as stroke or myocardial infarction are a result of misdirected platelet function, while arterial thrombosis is the major factor in the pathogenesis of CVDs. Therefore, antithrombotic targets are developed for an antiplatelet therapy, which either inhibit platelet receptors, block adhesion receptors or enhance inhibitory pathways. The development of antithrombotic targets faces problems regarding their efficacy and safety as for example bleeding risks for patients [136, 137]. Additionally, more than 5% of the patients suffering from CVD are resistant against the well-known drug aspirin [138]. Therefore, it is highly relevant that research investigates further details on platelet surface receptors in order to develop potential antiplatelet agents.

Previous studies demonstrate that PANX1 is involved in hemostatic responses by releasing extracellular ATP. Mice targeting a deletion of platelet PANX1 indicated reduced hemostatic responses *in vivo*, while bleeding time was moderate enhanced compared to their respective controls [82]. PANX1 may provide a potential target in intra- and intercellular communication regulating thrombotic responses without dramatic bleeding complications. As a result, the first aim of this thesis is to further analyze the impact of PANX1 on hemostasis and thrombosis. Nevertheless, the detailed activation mechanisms of PANX1 in platelets is poorly understood until today, what is the second objective of this work.

Platelets contribute to inflammatory processes in cardiovascular diseases e.g. by the release of pro-inflammatory molecules [105, 126]. Recently it was shown that platelets contribute to AAA formation [139]. Additionally, PANX1 channels are involved in the progression of this disease. One study demonstrated that PANX1 expression levels in aortic tissue are increased in male patients [131]. In line with that, an endothelial cell specific PANX1 deletion resulted in reduced AAA formation compared to respective WT mice in an AAA mice model. We hypothesized that platelet PANX1 may be involved in AAA pathology. To answer this hypothesis, platelet PANX1 deficient mice (*Panx1 fl/fl PF4-Cre*$^{+}$) and their respective controls (*Panx1 fl/fl PF4-Cre*$^{-}$) underwent the PPE perfusion model, which enables to study the formation and progression of AAA in a mice model *in vivo*. As a first translational approach, the analysis of platelets from patients suffering from AAA were investigated.

Overall, the aim of this thesis was to gain a deeper knowledge about the detailed function of PANX1 channels on platelets. To date it is clear that PANX1 channels have an impact on hemostasis and thrombosis but how is this phenotype regulated? Which agonist lead to PANX1 activation on the platelet side and what is the signaling mechanism behind this regulatory effect? Moreover, the influence of PANX1 in inflammatory processes is known but what is the impact of PANX1 in the progression of AAA? As a result, this study gives detailed insights in the understanding of PANX1 on platelets that might help by the development of new therapeutic approaches in the future.

2 Material

2.1 General devices and equipment

General laboratory materials as tubes, falcons, pipette tips and syringes were purchased from ErgoOne, Starlab, Sarstedt and Braun.

2.1.1 General devices

Equipment	Model	Company
Benchtop, pH-Meter	WTW pH526	Xylem Inc.
Bench scale	AE166	Mettler -Toledo
Bench scale	Practum®	Sartorius
Bench scale	Secura®	Sartorius
Centrifuge, cooling	5424-R	Eppendorf
Centrifuge, cooling	5804-R	Eppendorf
Centrifuge, mini	D-6020	neoLab
Centrifuge, tabletop	5415-C	Eppendorf
Centrifuge, tabletop	2-16	Sigma-Aldrich
Cell culture bottle (250 mL)	658175	Greiner Bio-One™
Laminar flow hood	BSB 3A	Gelaire Flow Laboratories
Magnetic stirrer	RET basic	IKA laboratory technology
Micropipettes	Research plus	Starlab & Eppendorf
Microwave	NN-E201WM	Panasonic
Multichannel pipette	Peqpette	Peqlab
Multipipette	Multipette® plus	Eppendorf
Parafilm	PM-996	Bemis®
Pipettor	Pipetboy acu	Integra Biosciences
Roll mixer	RM5	CAR
Thermo shaker	TS-100C	Biosan
Vortexer	444-0994	VWR
Waterbath 1000W	GFL 1052	GFL

2.1.2 Equipment for tissue preparation and histology

Equipment	Model	Company
Automatic microtome	Microm HM355	Thermo Fisher Scientific
Paraffin dispenser	Round model	Medax
Humidity chamber		Simpore Inc.
Paraffin section flotation bath	MH8517	Electrothermal
Precellys® 24 homogenizer	432-3750	Bertin Technologies

2.1.3 Equipment for gel electrophoresis, Western blot and imaging

Equipment	Model	Company
Chemiluminescence imager	Fusion-FX6-EDGE V.070	Vilber Lourmat
Double gel system	PerfectBlue™	Peqlab
Filter paper		Whatman
Horizontal agarose gel	PerfectBlue™ Wide Format Gel System	Peqlab
Microscope, inverse	Axio Observer D1	Zeiss
Microscope- color camera	Axiocam 503 color	Zeiss
Microscope	Axioskop	Zeiss
Microscope- color camera	Axiocam 105 color	Zeiss
Microscope- lamp module	HXP 120C	Zeiss
Nitrocellulose membrane		GE Healthcare
Semi-Dry blotsystem	PerfectBlue™	Peqlab
Universal power supply	PowerPac™	BioRad Laboratories

2.1.4 Equipment for sample analysis

Equipment	Model	Company
Dual-channel lumi-aggregometer	Model 700	Chrono-Log
Cuvettes for aggregometry		Chrono-Log
Flow chamber system		Maastrich Instruments
Flow cytometer	FACS Calibur	BD BioSciences
Hematology analyzer	KX-21N	Sysmex
Mikrotiter plate reader	GloMax® Multi+	Promega
PCR cycler	Mastercycler nexus gradient	Eppendorf
Reflotron®	Plus	Roche
Syringe pump	KDS100	KD Scientific Inc.

2.2 Special equipment for Porcine Pancreatic Elastase Perfusion Model

Equipment	Model	Company
Binokular	Mod.A1; s/n 250023	Optech Labcenter SpA
Clamps	13 cm	S&S Medizintechnik
Clipper	Isis Aescular GT420	Braun
Flowprobe	Transonic® Flowprobe	Transonic Systems Inc.
Forceps, surgical	11.5 cm, # BD555R	S&S Medizintechnik
Forceps, anatomical	11.5 cm, # BD043A	S&S Medizintechnik
Forceps, micro	07.61.82	Medicon eG
Forceps, tying	FD-281 R	Aesculap AG
Heating mat	ThermoLux®	Wiite + Sutor GmbH
Needle holder	15 cm, # 03E-022	S&S Medizintechnik
Scissors, cutticle	11.5 cm, # BC106R	S&S Medizintechnik
Scissors	14 cm, #BC242R	S&S Medizintechnik
Suture tie, vicryl 5-0	#V396H	Ethicon
Suture tie, mersilene 4-0	# EH7632H	Ethicon
Transparent polyurethane film	Opsite	Smith & Netphen
Ultrasound gel	Aquasonic 100 gel	Parker Laboratories
Ultrasound imaging	Vevo 2100® High-Resolution	VisualSonics

2.3 Chemicals and buffers

Bi-distilled water (ddH_20) was used for all solutions and buffers.

2.3.1 Chemicals

Chemical	Company
0.9% NaCl solution	Fresenius Kabi
4-2-Hydroxyethyl-piperazinyl-ethanesulfonic acid (HEPES)	Carl ROTH GmbH
4′,6-diamidino-2-phenylindole (DAPI)	Roche
Acetic acid (CH_3COOH)	Sigma-Aldrich

Acrylamide	Carl ROTH GmbH
Adenosine diphosphate (ADP)	Sigma-Aldrich
Agarose	Sigma-Aldrich
Akti-1/2 inhibitor	Tocris
Ammonium persulfate (APS 10%)	Sigma-Aldrich
Apyrase	Sigma-Aldrich
Bovine serum albumin	Sigma-Aldrich
Brilliant Blue (BB)	Sigma-Aldrich
Buprenorphine	Sigma-Aldrich
Calcium chloride (CaCl)	Sigma-Aldrich
Carbenoxolone (Cbx)	Sigma-Aldrich
Chloroform	Sigma-Aldrich
Citric acid ($C_6H_8O_7$)	Sigma-Aldrich
Convulxin (Cvx)	Santa Cruz Biotechnology
Collagen (Horm)	Takeda
Collagen related peptide (CRP)	University of Cambridge, UK
Dithiothreitol (DTT)	Sigma-Aldrich
DMEM (High glucose # 41965062)	Life Technologies
DMSO (Dimethylsulfatoxid)	Sigma-Aldrich
DNaseI recombinant RNAse - free	Roche
EDTA (ethylenediaminetetraacetate)	Sigma-Aldrich
Ethanol 100% (EtOH)	Merck Millipore
Fetal calf serum (FCS)	Life technologies
Ferric (III) chloride (Fe_3Cl)	Sigma-Aldrich
Fibrinogen	Sigma-Aldrich
Glucose	Carl ROTH GmbH
Glycine	Carl ROTH GmbH
Goat serum	Bio & Sell
Heparin-Natrium-25000	Braun
IGEPAL® CA-630	Sigma-Aldrich
Isoflurane	Piramal critical care
L-glutamine	Life technologies
Lipopolysaccharide (LPS)	Sigma-Aldrich
Magnesium chloride (MgCl)	Carl ROTH GmbH
Methanol 100% (MeOH)	Merck Millipore
MidoriGreen	Biozym
Mounting medium #S3023	Dako
PAR4 peptide	Tocris Bioscience
Paraffin	Carl ROTH GmbH
Paraformaldehyde 4%	Carl ROTH GmbH
Penicillin/Streptomycin	Life technologies
Phosphate buffered saline (PBS)	Sigma-Aldrich
Ponceau S solution	Sigma-Aldrich

Porcine Pancreatic Elastase (PPE)	Sigma- Aldrich
Potassium perrmanganate ($KMnO_4$)	Merck Millipore
Powdered skim milk	Frema Reform
PP2	Tocris
PP3	Tocris
Precision Plus Protein Dual Color Standards	BioRad Laboratories
Probenecid (water-soluble)	Sigma-Aldrich
Prostaglandin	Merck Millipore
Proteinase-inhibitor (cOmplete Tablets Mini Easypack)	Roche
Protein blocking solution #X0909	Dako
RNAse-1	Thermo Fisher Scientific
Ro-31-8220 (RO)	Calbiochem
Roti Histokitt	Carl ROTH GmbH
Roti Histol	Carl ROTH GmbH
Roti Quant 40%	Carl ROTH GmbH
Roti®Histol	Carl ROTH GmbH
Sodium chloride (NaCl)	Sigma-Aldrich
Sodium orthovanadate (Na_3VO_4)	Sigma-Aldrich
Sodium nitroprussid (SNP)	Merck Millipore
Sodium phosphate dibasic (Na_2HPO_4)	Carl ROTH GmbH
Sodium dihydrogenphosphate(NaH_2PO_4)	Carl ROTH GmbH
Sodium acid (NaN_3)	Carl ROTH GmbH
Sodium hydrogencarbonate ($NaHCO_3$)	Merck Millipore
Tetramethylethylenediamine (TEMED)	Carl ROTH GmbH
Thrombin 20U	Roche
Tumor necrosis factor (TNF-α)	Peprotech
Trisodium citrate	Carl ROTH GmbH
Triton™ X-100	Sigma-Aldrich
Trizma®-base	Sigma-Aldrich
Trizma®-HCl	Sigma-Aldrich
Trypsin-EDTA	Life technologies
TRIzol®	Sigma-Aldrich
Tween20	Merck Millipore
U46619 (U46)	Tocris Bioscience
β-mercaptoethanole	Carl ROTH GmbH
ε-aminocaproic acid ($C_6H_{13}NO_2$)	Sigma-Aldrich

2.3.2 Buffers and solutions

Buffer/Solution	Recipe
Annexin V binding buffer	10 mM Hepes (pH 7.4) 140 mM NaCl 2.5 mM $CaCl_2$
Blot buffer A	36.3 g Trizma-base 200 mL MeOH 800 mL ddH_2O pH 10.4
Blot buffer B	3.03 g Trizma-Base 200 mL MeOH 800 mL ddH_2O pH 10.4
Blot buffer C	5.2 g ε-aminocaproic acid 200 mL MeOH 800 mL ddH_2O
Citrate buffer	41 mL 0.1 M trisodium citrate 9 mL 0.1 M citrate acid 450 mL ddH_2O pH 6.0
Decalcification buffer	10% EDTA PBS pH 8.0
Heparin-solution (20 U/mL)	40 µL heparin natrium 5000 I.E 10 ml PBS
Human Tyrode's buffer	137 mM NaCl 12 mM $NaHCO_3$ 2.8 mM KCl 0.4 mM NaH_2PO_4 5.5 mM glucose pH 7.4
IP-buffer (5x stock solution)	15 mM Tris-HCl 155 mM NaCl 1 mM EDTA 0.005% NaN_3 *ad* 1 L ddH_2O

Laemmli (6x)	0.93 g DTT 1 g SDS 7 mL 4x stacking gel buffer 3 mL glycerine 0.02% bromphenol blue
Lysis buffer (human) (5x stock solution)	145 mM NaCl, 20 mM Tris-HCl, 5 mM EDTA, 0.5% sodium deoxycholat, 1% Triton™ X-100 1x Proteaseinhibitor cOmplete plus Roche
Lysis buffer (murine) (5x stock solution)	5 x IP-Puffer (2mL) 5% IGPAL 5 mM Na_3VO_4 1x Proteaseinhibitor cOmplete plus Roche
Murine Tyrode's buffer	134 mM NaCl 12 mM $NaHCO_3$ 2.9 mM KCl 0.34 mM Na_2HPO_4 20 mM HEPES 10 mM $MgCl_2$ 5 mM glucose 0.2 mM $CaCl_2$ pH 7.35
RIPA buffer	150 mM NaCl 50 mM Tris 0.1% SDS 0.5% sodium deoxycholate 1% TritonX-100 1 mM Na_3VO_4 1x Proteaseinhibitor cOmplete plus Roche pH 8.0
SDS-PAGE-running buffer (5x stock solution)	15.1 g Trizma-base 72 g glycine 5 g SDS *ad* 1 L ddH_2O pH 8.3

SDS-PAGE stacking gel buffer (4x stock solution)	6.05 g Trizma-base 80 mL dH_2O pH 6.8 *ad* 100 mL ddH_2O 0.4 g SDS
SDS-PAGE running gel buffer (4x stock solution)	91 g Trizma-Base 400 mL dH_2O pH 8.8 *ad* 500 mL ddH_2O
Tris buffered saline (TBS, 5x stock solution)	15.8 g Trizma-HCl 45 g NaCl *ad* 1 L ddH_2O pH 7.6
TBS-T	100 mL 5x TBS-Puffer 500 µL Tween 400 mL ddH_2O
Tris acetate EDTA (TAE)-buffer	242 g Trisma-base 57.1 ml acetic acid 100 ml 0.5% EDTA pH = 8.0

2.4 Antibodies and peptides

2.4.1 Primary antibodies used for Western blotting

Antigen	**Host species**	**Clonality**	**Dilution**	**Company**
β-Actin #4979	rabbit	monoclonal	1:1000	Cell Signaling
Akt #9272S	rabbit	polyclonal	1:1000	Cell Signaling
phosphoAkt Ser^{473} #9271S	rabbit	polyclonal	1:1000	Cell Signaling
Fibrinogen #A0080	human	polyclonal	1:2500	Dako
GAPDH #2118S	rabbit	monoclonal	1:1000	Cell Signaling
Src #2108	rabbit	monoclonal	1:1000	Cell Signaling
Pannexin 1 #91137	rabbit	monoclonal	1:1000	Cell Signaling
phosphoSrc Tyr^{416} #9271S	rabbit	polyclonal	1:1000	Cell Signaling
phosphoPanx1 Tyr^{198} #ABN1681	rabbit	polyclonal	1:1000	Merck
phosphoPanx1 Tyr^{308} #ABN1680	rabbit	polyclonal	1:500	Merck
phosphoTyr 4G10 #96215	mouse	monoclonal	1:1000	Cell Signaling

2.4.2 Primary antibodies used for IF

Antigen	Host species	Clonality	Dilution	Company
GPIbα #M042-0	rat	monoclonal	1:50	emfret
Ly6G #551459	Rat	monoclonal	1:50	BD Biosciences

2.4.3 Secondary antibodies

Antigen	Species	Clonality	Conjugate	Dilution	Company
Anti-rabbit	goat	polyclonal	horseradish-peroxidase	1:10000	Invitrogen
Anti-mouse	goat	polyclonal	horseradish-peroxidase	1:10000	Invitrogen

2.4.4 Antibodies for flow cytometry

Antigen	Term/Clone	Species	Company
Mouse CD62P	P-selectin/Wug.E9	rat	Emfret analytics
Mouse CD41/CD61	JON/A	rat	Emfret analytics
Mouse CD61	Luc.H11	rat	Emfret analytics
Mouse GPVI	JAQ1	rat	Emfret analytics
Mouse CD49e	Tap.A12	rat	Emfret analytics
Mouse CD42b	Xia.G5	rat	Emfret analytics
Mouse Ly6g	1A8	rat	BioLegend
Mouse CD45	2D1	mouse	In vitrogen
Human CD41/CD61	PAC-1	mouse	BD BioSciences
Human CD62P	P-Selectin	mouse	BD BioSciences

2.4.5 Peptides and dyes

Peptide/Dye	Conjugate	Dilution/Concentration	Company
Annexin V #559934	Cy5	1:10	BD BioSciences
4′,6-Diamidine-2′-phenylindole dihydrochloride (DAPI) #10236276001	-	1:3000	Dako
2′,7′-Dichlorofluorescindiacetat (DCF-DA) #287810	-	10 µM	Sigma
DyLight488 conjugated anti - mouse GPIbβ derivative antibody #35503	488	0.3 µg/mL	Emfret
Mepacrine hydrochloride salt #Q3251	-	10 µM	Sigma

Strepetavidin eFluorTM #50-4317-80	660	1:20	Thermo Fisher Scientific

2.4.6 Oligonucleotides

All used oligonucleotides were synthesized and purchased from Eurofins Scientific.

Target gene	**Direction**	**Primer sequence**
GluN1 WT	forward reverse	5-'GTGAGCTGCACTTCCAGAAG-3' 5-'GACTTTCGGCATGTGAAATG-3'
GluN1 KO	forward reverse	5-'CTTGGGTGGAGAGGCTATTC-3' 5-'AGGTGAGATGACAGGAGATC-3'
Panx1 (KO fl/fl)	forward reverse (common)	5-'AGATGGCGCAACGCAATTAATGA-3' 5-'TGGCTCTCATAATTCTTGCCCTGG-3'
Panx1 (WT fl/fl)	forward reverse (common)	5-'CCGTAGCTTGCTTGCTTTGATCT-3' 5-'TGGCTCTCATAATTCTTGCCCTGG-3'
Panx1 (WT global)	forward reverse	5-'GGAAAGTCAACAGAGGTACCC-3' 5-'GTCCCTCTCACCACTTTTCTTACC-3'
Panx1 (KO global)	forward reverse	5-' GGAAAGTCAACAGAGGTACCC-3' 5-' GGCCACGGAGTATGTGTT-3'
PF4-cre	forward reverse	5-'CCCATACAGCACACCTTTTG-3' 5-'TGCACAGTCAGCAGGTT-3'

2.4.7 Kits

Kit	**Catalog No.**	**Company**
ATP Bioluminescence Assay Kit HS II	11699709001	Roche
Chrono-log luciferase + ATP standard	P/N 395	Chrono-log
Fast Sybr Green Master Mix	4385610	Life Technologies
G-LISA Kit (Precision Red Protein Assay Reagent)	GL50	Cytoskeleton
ImmobilonTM Western Chemiluminescent HRP substrate solution	1705061	BioRad
KAPA-Mouse-Genotyping Hot Start Kit	07-KK7352-01	Peqlab
Mouse IL - 6 DuoSet ELISA	DY406	R&D Systems
Mouse IL-1 beta/IL-1F2 DuoSet ELISA	DY401	R&D Systems

Mouse Total MMP-9 Quantikine ELISA Kit	MMPT90	R&D Systems
Mouse TGF-β DuoSet ELISA	DY1679	R&D Systems
Human Panx1 ELISA	39097	Signalway Antibody
Precellys® Lysing Kit	P000918-LYSK0-A	Bertin Technologies

2.5 Software

Software	**Company**
CorelDRAW X8	Corel
Microsoft Office 2010	Microsoft Corporation
Graph Pad Prism 8.0.2	GraphPad Software
Fiji Is Just ImageJ	NIH Image
FlowJo Single Cell Analysis v10	FlowJo LLC
ViiA™ 7 Software	Thermo Fisher Scientific
ZEN 2012 (blue)	Zeiss
LabChart Reader 8.1.6 Windows	ADInstruments

2.6 Animals

Pathogen-free *Panx1 fl/fl* mice were kindly provided by Dr. Brant Isakson (University of Virginia, Charlottesville, VA, USA) and crossed to *PF4-Cre* mice, which were purchased from the Jackson Laboratory (C57BL/6-*Tg* [*PF4-Cre*] *Q3Rsko/J*) resulting in mice with a platelet specific deletion of *Panx1* (WT: *Panx1 fl/fl PF4-Cre*$^{-}$; KO: *Panx1 fl/fl PF4-Cre*$^{+}$*).*

Prof. Dr. C. Schmidt (Hospital clinic of the University Heidelberg, Germany) kindly provided mice with target a global deletion of *Panx1* (WT: *Panx1*$^{+/+}$; KO: *Panx1*$^{-/-}$).

Mice targeted a deletion in the exon 11-10 from the Grin1-Gen coding for the *GluN1* subunit of NMDA receptors were kindly provided by Prof. Dr. E. Lammert (Heinrich-Heine University Duesseldorf, Germany). These mice *B6.129S4-Grin1tmStl/J* (*Grin1loxP/loxP*) were crossed to *PF4-Cre* mice, which were purchased from the Jackson Laboratory (C57BL/6-*Tg* [*PF4-Cre*] *Q3Rsko/J*) to obtain platelet specific *GluN1* WT (*NMDAR fl/fl PF4-Cre*$^{-}$) and *GluN1* KO mice (*NMDAR fl/fl PF4-Cre*$^{+}$).

Mice with targeted deletion of GPVI were kindly provided by J.Ware (University of Arkansas for Medical Sciences) and backcrossed to C57BL/6 mice (Jackson Laboratory). For the generation of homozygous WT and *Gp6*$^{-/-}$ mice, heterozygous breeding partners were mated. *Gp6*$^{-/-}$ and WT mice were phenotyped using murine GPVI (FITC) conjugated antibody by FACS.

All experiments were performed with male and female mice aged 2–4 months. The animals were maintained in an environmentally controlled room at 22 ± 1 °C with a 12 h day-night cycle. Mice were housed in Macrolon cages type III with *ad libitum* access to food (standard chow diet) and water. All animal experiments were conducted according the Declaration of Helsinki and approved by the Ethics Committee of the State Ministry of Agriculture, Nutrition and Forestry State of North Rhine-Westphalia, Germany (Reference number: AZ 84-02.05.40.16.073; AZ 81-02.4.2018.A409).

2.7 Human blood samples

2.7.1 Ethics votes

Fresh ACD-anticoagulated blood (BD-Vacutainer®; Becton, Dickinson and Company) was obtained from healthy volunteers aged between 18 to 70 years and abdominal aortic aneurysm (AAA) patients. Samples from AAA patients were compared to age-matched controls (AMCs, older than 60 years). Participants provided their written informed consent to participate in this study according to the Ethics Committee of the University Clinic of Duesseldorf, Germany (2018-140-kFogU, study number: 2018064710; biobank study number: 2018-222_1 and MELENA study: 2018-248-FmB, study number: 2018114854). The Ethics Committee of the University Clinic of Duesseldorf, Germany approved the consent procedure and specifically this study according to the Declaration of Helsinki.

3 Methods

3.1 Porcine Pancreatic Elastase Perfusion Model (PPE)

The porcine pancreatic elastase perfusion model is a murine *in vivo* model to mimic AAA by infusion of porcine pancreatic elastase (PPE) into an abdominal aortic segment. Mice were anesthetized with 2% isoflurane and the depth of anesthesia was constantly monitored. Above the iliac bifurcation, an aortotomy was induced by the ligation of the proximal and distal infrarenal part of the aorta. At the distal end of the aortotomy a catheter was inserted. Perfusion of the aorta occurred with sterile isotonic saline containing type I Porcine Pancreatic Elastase (2.5 U/mL or 3 U/mL, dependent on activity monitored by dilution curve, Sigma- Aldrich) for 5 min at 120 mm Hg. After perfusion of the aortotomy the catheter was removed and the aortotomy repaired (Figure 8). The abdomen was closed and after surgery, all animals immediately received local Bupivacaine [0.1 mg/kg] and 1% Buprenorphine subcutaneous every 6–12 h for up two days or continuously through the drinking water (0.009 mg /mL buprenorphine in H_2O). Mice were weighed to enable the determination of weight losses or gains on following days. At post-surgery day 28 mice were euthanized by retro bulbar blood sampling under deep isoflurane anesthesia. Afterwards the circulatory system was flushed with cooled heparin solution (20 U/mL) and organs were collected for further preparations (more detailed description in 3.1.2.) All PPE surgeries were performed by Dr. med. Joscha Udo Nikolaus Mulorz (Clinic for Vascular- and Endovascular surgery, Hospital Clinic of the Heinrich-Heine University, Duesseldorf) and Julia Pauli (Division of Cardiology, Pulmonology and Vascular Medicine, Hospital Clinic of the Heinrich-Heine University, Duesseldorf – S1 Project of the TRR259 Aortic Disease).

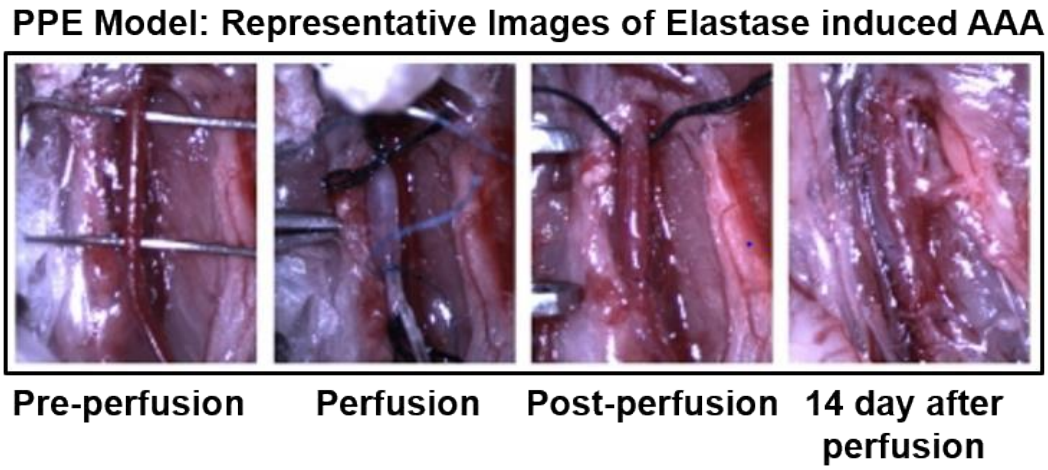

Figure 8: Overview of the Porcine Pancreatic Elastase Perfusion Model (PPE) inducing aortic aneurysm formation in mice. (From left to right) Anesthetized mice underwent an aortotomy by the ligation of the proximal and distal infrarenal part of the aorta. A catheter was inserted at the distal end of the aorta and the perfusion of the aorta with sterile isotonic saline containing type I Porcine Pancreatic Elastase (2.5 U/mL) occurred for 5 min at 120 mm Hg. The catheter was removed and the aortotomy repaired. After surgery the abdomen was closed and dilatation of the aortic wall was monitored via ultrasound imaging [Figure modified from Azuma J, et al. 2009, J Vis Exp.].

3.1.1 Ultrasound imaging

To monitor the dilatation of the aortic wall, maximal aortic diameters at the aneurysm site were measured. Ultrasound imaging was performed at baseline (day 0) and on days 3, 7, 14, 21 and 28 after PPE surgery. For imaging mice were anaesthetized with 2% isoflurane, placed on a 37 °C heated plate and ultrasound imaging was performed using a Vevo 2100® High-Resolution In Vivo Micro-Imaging System (VisualSonics). During the systolic phase inner diameter-measurements were obtained following a standardized imaging algorithm with longitudinal B-Mode images.

3.1.2 Preparation of murine tissues

Murine organs were embedded in paraffin to perform histological analysis of mice. Mice were kept under deep isoflurane anesthesia; the thorax was opened, and the heart was flushed with cooled heparin solution (20 U/mL) to prevent blood clotting. Therefore, the butterfly cannula was placed into the apex cordis of the left ventricle of the heart, while the right atrium was incised to ensure by a systemic flush of approximal 20 mL of heparin solution (20 U/mL). Organs were removed and directly fixed in 4% paraformaldehyde (PFA) for at least 24 h at 4 °C for immunohistochemistry and histological analysis or directly transferred part in LN_2 and stored at -70°C for protein analysis.

3.1.3 Paraffin fixation

After fixation, organs were transferred in organ cartridges and washed with tap water. Since melted paraffin is hydrophobic, most of the water from the tissues must be removed by an ascending ethanol row (stepwise from 100% to 70%) and further incubated in Roti®Histol (Carl Roth) for 12 h at RT. Tissues were neutralized in melted paraffin for 4-6 h (Roth) and embedded. Samples were stored at RT until further use.

3.2 Cell biological methods

3.2.1 Human platelet and plasma preparation

Fresh ACD-anticoagulated blood was obtained from healthy volunteers (Ages from 18-50 years). Participants provided their written informed consent to participate in this study according to the Ethic Committee and the Declaration of Helsinki (study number 2018-140-KFogU). Collected blood was centrifuged at 200 x g for 10 min at RT. The supernatant (Platelet-rich plasma; PRP) was added to phosphate buffered saline (PBS pH 6.5, apyrase: 2.5 U/ml and 1 µM PGI_2 in 1:1 A/V and centrifuged at 1000 x g for 6 min. Platelets were resuspended in Tyrode´s-buffer solution (140 mM NaCl; 2.8 mM KCl; 12 mM $NaHCO_3$; 0.5 mM Na_2HPO_4; 5.5 mM Glucose pH 7.4). The cell count was determined by a hematology analyzer (Sysmex - KX21N, Norderstedt, Germany) and adjusted according for each experiment. Plasma was collected by centrifugation of the ACD-anticoagulated blood for 10 min at 1500 x g and 4 °C. The supernatant (Platelet free plasma) was stored at -70 °C until use.

3.2.2 Human platelet lysates and releasates

Platelets (40×10^6) were stimulated with 0.1, 1 or 5 µg/mL CRP; 70 or 200 µM PAR4 peptide, 1 or 3 µM U46 or 5 or 10 µM ADP in Tyrode's buffer (pH 7.4) for 2, 5 or 10 min (agonist dependent) at 37 °C. When indicated, pretreatment with a SFK inhibitor PP2 (Tocris) or the negative control PP3 (Tocris) were performed for 20 min at 37 °C. Same procedure was performed for pretreatment with a PKC inhibitor RO (Ro-31-8220 – Calbiochem) or Akti-1/2 inhibitor (Tocris). Platelet activation was stopped by centrifugation at 800 x g at 4 °C for 5 min or by direct cell lysis using 5× human lysis buffer. When the reaction was stopped via centrifugation, the platelet releasate was collected and stored at -70°C until use for Western blot or ELISA. Platelet pellets were lysed

for 15 min on ice with 1× human lysis buffer. 6x Laemmli buffer was added to the lysates, denatured at 95 °C for 5 min and stored at -20 °C until use.

3.2.3 Human red blood cell (RBC) isolation

Fresh ACD-anticoagulated blood was obtained from healthy volunteers (Age from 18-50 years). Participants provided their written informed consent to participate in this study according to the Ethic Committee and the Declaration of Helsinki (Study number 2018-140-KFogU). Collected blood was centrifuged at 231 x g for 10 min at RT. The PRP was separated, and the remaining blood was transferred to a closed syringe and centrifuged at 800 x g for additional 15 min at RT. Leukocytes and RBCs were separated by centrifugation within the syringe, while the upper layer consists of the buffy coat (Including leukocytes) and the lower layer consists of RBCs. The syringe was opened, and RBCs were transferred in a new reaction tube and washed 3 times with 5 times volume of ice cold saline solution [154 mM]. The cell count was determined by a hematology analyzer (Sysmex - KX21N, Norderstedt, Germany) and adjusted according for each experiment.

3.2.4 Murine platelet and plasma preparation

Murine blood was acquired by retro bulbar puncture and collected in 20 U/mL Heparin-Natrium (Braun). Blood was centrifuged at 250 x g for 5 min. After collection of the supernantent, samples were further centrifuged at 50 x g for 6 min to obtain platelet rich plasma (PRP). PRP was washed two times (650 x g for 5 min at RT), before resuspension of the pellet in Tyrode's buffer [136 mM NaCl, 0.4 mM Na_2HPO_4, 2.7 mM KCl, 12 mM $NaHCO_3$, 0.1% glucose, 0.35% bovine serum albumin (pH 7.4)] supplemented with prostacyclin (0.5 µM) and apyrase (0.02 U/ml). Before use, platelets were resuspended in the same buffer supplemented with 1 mM $CaCl_2$. The cell count was determined by a hematology analyzer (Sysmex - KX21N, Norderstedt, Germany) and adjusted according for each experiment. Plasma was collected by centrifugation of the heparinized blood for 10 min at 8000 x g and 4 °C. The supernatant (platelet free plasma) was stored at -70°C until use.

3.2.5 Murine platelet lysates

Platelets (40×10^6) were stimulated with CRP [0.1, 1 or 5 µg/mL]; PAR4 peptide [70 or 200 µM], U46 [1 or 3 µM] or ADP [5 or 10 µM] in Tyrode's buffer (pH 7.4) for 2, 5 or 10 min at 37 °C and 250 rpm respectively. Platelet activation was stopped by centrifugation at 800 x g at 4 °C for 5 min or by direct cell lysis using 5× IP buffer. When the reaction was stopped via centrifugation platelet pellets were lysed for 15 min on ice with 1× IP buffer. Laemmli buffer (6x) was added to the lysates, denatured at 95 °C for 5 min and stored at -20 °C until use.

3.2.6 Adhesion experiments

Adhesion experiments enable to study the adhesion of cells on different extracellular matrix proteins. Cover slips (24 x 60 mm) were coated with type I collagen [200 µg/mL] at a defined area (10 x 10 mm) at 4 °C overnight. To reduce unspecific binding of platelets, coverslips were washed for three times with PBS and blocked with 1% BSA in PBS for 60 min. Isolated human platelets (4×10^4) were when indicated preincubated with Probenecid for 20 min at RT and then added to the collagen matrices for 20 min at RT. Coverslips were carefully washed for two times with PBS to remove non-adherent platelets and fixed with 4% PFA at 4 °C for 10 min. Coverslips were covered with Aquatex to analyze platelet adhesion with an Axio ObserverD1 microscope. At least five pictures per visual field for each sample were analyzed by using the ImageJ-win64 software.

3.2.7 Light Transmission Aggregometry (LTA) with ATP release

Light transmission aggregometry is a method to analyze the platelet function induced by various agonists. Human or murine isolated platelets were adjusted to a concentration of 50×10^6 cells with Tyrode's buffer in a glass cuvette with stirrer. When inducated, pre-treatment with Prb, Cbx or Brilliant Blue (BB) occurred for 20 min at 37 °C. Aggregation responses to various concentrations of indicated agonists with 0.1, 1 or 5 µg/mL CRP and 70 or 200 µM PAR4 peptide were measured as percentage light transmission compared to Tyrode's buffer using a Chrono-Log dual-channel lumi-aggregometer (Model 700) at 37 °C and stirring conditions (1000 rpm). ATP release was measured using a luciferin/luciferase bioluminescent assay. Luciferase (Chrono-Log) was added in a concentration of 1:10 before platelet activation. Final ATP release was calculated using an ATP standard protocol from Chrono-Log, followed by the manufacturer's instructions.

3.2.8 ATP release measurements (Bioluminescence Assay Kit)

To measure ATP via ELISA, 40×10^6 murine or human platelets were activated with 0.1, 1 or 5 µg/mL CRP; 70 or 200 µM PAR4 peptide, 1 or 3 µM U46 or 5 or 10 µM ADP in Tyrode's buffer (pH 7.4) for 2, 5 or 10 min (agonist dependent) at 37 °C. When inducated, pre-treatment with Prb occurred for 20 min at 37 °C. After platelet activation, samples were fixed with an ATP fixation solution (0.1% PFA and 3 mM EDTA in ddH_2O) for 1.5 h at RT. After centrifugation for 1 min at 13,000 rpm, platelet supernatants (= ATP release) were supplemented with 100% EtOH in a ratio of 1:1. Samples were stored at -20 °C until use. ATP release was measured using an ATP Bioluminescence Assay Kit HS II (Roche) followed by the manufacturer's instructions.

3.2.9 Thrombus formation assay (Flow chamber)

The flow chamber method is used to study thrombus formation by the involvement of dynamic forces in the blood flow. Rectangular coverslips (24 × 60 mm) were coated with 0.2 mg/mL fibrillar type I collagen (Nycomed) overnight at 4 °C and blocked with 1% BSA in PBS at RT. Fresh ACD-anticoagulated blood from human doners were labeled with 10 µM meparcine (Sigma) and heparinized blood from mice were labeled with Dylight-488 (Emfret) at 0.3 µg/mL for 10 min at 37 °C. When indicated, pre-treatment of human whole blood with Prb or Cbx occurred for 20 min at 37 °C. When only human RBCs were treated with Prb, platelets, RBCs, and plasma were isolated separately from each donor. RBC treatment with Prb occurred for 20 min at 37 °C. The cell counts of the human samples were adjusted to 2×10^5 platelets/µL and 4×10^6 RBCs/µL using previously isolated plasma from each donor.

Blood was perfused through the flow chamber system over a collagen coated surface at a shear rate of $450s^{-1}$, $1000s^{-1}$ and $1{,}700\ s^{-1}$ using a pulse-free electric pump which mimics the blood flow in vessels (Figure 9). The blood perfusion was stopped after a defined time period of three minutes and the system was perfused with 1.8 mL PBS at a shear rate of either $450s^{-1}$ or $1000s^{-1}$. In total, 5-7 images per flow chamber run were taken at 400x magnification (Axio Observer.D1, Carl Zeiss). Thrombus formation were analyzed as the mean percentage of the total area (Surface coverage) and the three-dimension structure of the covered thrombi measured by the mean fluorescence intensity (MFI) using ImageJ (GNU General Public License).

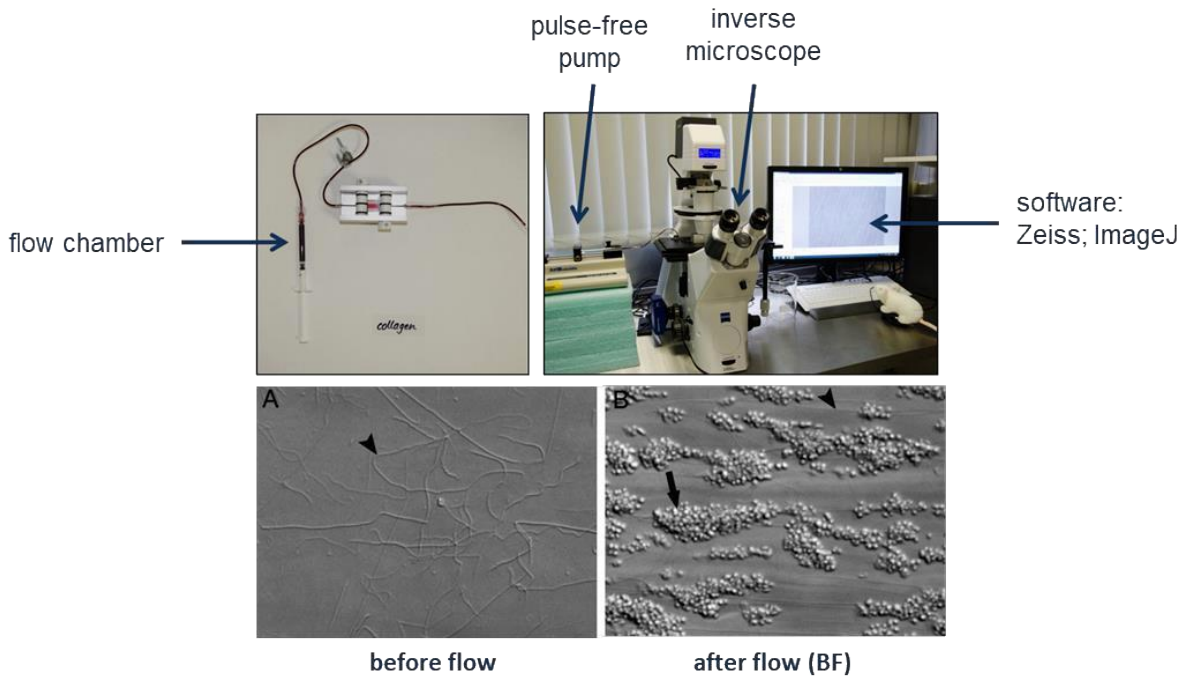

Figure 9: Flow chamber is a method to measure platelet activation and thrombus formation in whole blood at defined shear rates *ex vivo*. A pulse-free pump perfused whole blood over through the flow chamber over a collagen coated matrix recorded by an inverse microscope. Representative images are shown of (A) a collagen coated matrix and (B) after thrombus formation after blood perfusion (Figure was modified from Research group: Exp. Vascular Medicine).

3.2.10 Flow cytometry

Flow cytometry is a method used to study the expression of mainly cell surface, but also intracellular molecules. The method based on the specific analysis of cells regarding their size (Forward scatter, FCS) and granularity (Side scatter, SSC). Cell suspensions pass through a flow cell of a defined size and in a defined speed that a laser beam can detect single cells to measure their specific FSC/SSC profile displayed in a dot graph. This technique allows distinguishing between different cell types and subpopulations within a cell population as for example platelets from RBCs. Cells that are fluorescently labeled by conjugated antibodies or fluorescent dyes can be measured and analyzed by the mean fluorescence intensity (MFI). In this thesis, flow cytometric analysis of human or murine whole blood as well as isolated platelets were performed using FACSCalibur flow cytometer (BD Biosciences). Data was processed using CELLQuest Analysis v10 Software (BD Biosciences).

3.2.10.1 Flow cytometric analysis of human samples

Human whole blood was diluted 1:10 Tyrode's buffer. Analysis of isolated human platelets were performed with a concentration of 40 × 10^3 cells/µL. To measure platelet activation, cells were stimulated with indicated agonist and labeled with fluorophore-conjugated antibodies for P-selectin expression for degranulation (P-selectin-FITC) and the active form of $\alpha_{IIb}\beta_3$ integrin (PAC-1-PE) in a ratio of 1:10 for 15 min at 37 °C. Reaction was stopped using 400 µL PBS and samples were analyzed.

3.2.10.2 Flow cytometric analysis of murine samples

Heparinized murine blood was washed three times with 500 µL Tyrode's buffer at 650 x g. Washed samples were diluted in Tyrode´s buffer supplemented with 1 mM $CaCl_2$. Analysis of isolated murine platelets were performed with a concentration of 40 × 10^3 cells/µL.

To measure platelet activation, cells were stimulated with indicated agonist and labeled with fluorophore-conjugated antibodies for P-selectin expression for degranulation (Wug.E9-FITC) and the active form of $\alpha_{IIb}\beta_3$ integrin (JON/A-PE) in a ratio of 1:10 for 15 min at 37 °C. Reactions were stopped using 400 µL PBS.

For the expression of glycoproteins on the platelet surface, washed blood was incubated with the following antibodies in a ratio of 1:10 (GPVI, JAQ1-FITC; GPIb/CD42, Xia.G5 – PE; Integrin α5/CD49e, Tap.A12 – FITC) and incubated for 15 min at RT. Up-regulation of CD61 was determined after platelet activation with indicated concentrations of CRP using an antibody against the integrin β_3 chain (Luc.H11-FITC). Reactions were stopped using 400 µL PBS.

Mepacrine release experiments were performed to analyze the degranulation of platelet dense granules. The fluorescent dye mepacrine (10 µM) was loaded to 40 × 10^3 platelets for 15 min at 37 °C. After platelet activation with PAR4 peptide and thrombin, reactions were stopped using 400 µL PBS. Mepacrine release was analyzed by the reduction of the MFI measured in the FITC channel ($\lambda_{em\ max}$ 525 nm).

Measurements of the generation of reactive oxygen species (ROS) was determined by the cell-permeable dye 2′,7′-Dichlorofluorescindiacetat (DCF-DA). DCF-DA can enter the plasma membrane via diffusion. Within the cytosol, DCF-DA is deacetylated by intracellular esterases to form 2′,7′-dichlorodihydrofluorescein (H_2DCF). H_2DCF is rapidly oxidized to 2′,7′-dichlorofluorescein (DCF) in the presence of ROS. DCF is a highly fluorescent dye with an excitation and emission wavelengths of 498 and 522 nm, respectively. Platelets were loaded with

10 µM DCF-DA and stimulated with indicated agonist for 15 min at 37 °C. Reactions were stopped using 400 µL PBS. ROS-generation was measured in the FITC channel ($\lambda_{em\ max}$ 526 nm).

For murine Annexin V measurements, a high dose Ca^{2+} binding buffer (10 µM HEPES (pH 7.4), 140 µM NaCl, 2.5 mM $CaCl_2$) was used instead of Tyrode's buffer and PBS. Cells were stimulated with indicated agonist and labeled with a Cy™5 -conjugated antibody against Annexin V (BD Bioscience) and CD42 (GPIb-PE) in a ratio of 1:10. Reactions were stopped using 400 µL high dose Ca^{2+} binding buffer. Samples were measured and percent of gated PS-positive cells analyzed.

To measure platelet-neutrophil aggregates, cells were stimulated with indicated agonist or kept under resting conditions and labeled with fluorophore-conjugated antibodies for CD42 (GPIb-PE) as a platelet marker (ratio 1:10) and Ly6g-APC (Clone 1A8, BioLegend) as a marker to label neutrophil (ratio 1:30). Reactions were stopped using 400 µL PBS. Samples were measured and percent of gated GPIb/Ly6g-positive cells analyzed.

3.2.11 Endothelial cell culture (MHEC5-T)

In all experiments the mouse heart endothelial cell line MHEC5-T (Mouse heart endothelial cell clone 5 obtained from H. Langer, University clinic Tübingen, Germany) was used, cultured in DMEM high glucose medium (Gibco, #41965062) supplemented with 10% fetal calf serum (FCS; Life technologies); 100X penicillin-streptomycin (Penicillin [10,000 U/ml]; Streptomycin [10,000 µg/ml]; Life technologies) and 200 mM L-glutamine (Life technologies) at 37 °C in a humidified atmosphere with 5% CO_2. Cells were separated every 3 – 4 days using 0.05% trypsin-EDTA (Life technologies). If not stated differently, cells were seeded on sterile 48-well plates (125,000 cells/mL).

3.2.11.1 Co-culture of platelets and MHEC5-T cells

Platelets (30×10^6 cells) from whole blood taken from Panx1 fl/fl Cre^- or Panx1 fl/fl Cre^+ mice were isolated as described previously (3.2.4) and co-incubated with mouse heart endothelial cell clone 5-transformed (MHEC5-T) cells (125,000 cells/mL) in Tyrode's buffer for 3.5 h at 37 °C in a humidified atmosphere with 5% CO_2. When indicated, platelets were activated with classical platelet agonist. MHEC5-T cells stimulated with indicated agonists served as negative controls, TNFα [100 ng/mL] served as a positive control. After 3.5 h of platelet-MHEC5-T co-incubation, supernatants were harvested into reaction tubes. Cell remains were removed by centrifugation at

800 x g for 5 min. Supernatants were transferred into new reaction tubes and stored at -70 °C for cytokine analysis via ELISA technique (IL-6).

3.3 Protein biochemical methods

3.3.1 Organ lysates and determination of protein concentrations

Murine organs (3.1.2) were transferred from -80 °C into Precellys® reaction tubes (Precellys® Lysing Kit) with 500 µL RIPA buffer. Reaction tubes were placed in the Precellys® 24 homogenizer (432-3750) and organs were homogenized at 4 °C following the manufactures instructions (Bertin Technologies). After homogenization, tubes were spun for 20 min at 14,000 x g at 4 °C to pellet tissue leftovers and the beads of the Precellys® Lysing Kit. The supernatants were transferred into new reaction tubes and protein concentrations were determined using the quick protein concentration method from G-LISA Kit following the manufactures instructions (Cytoskeleton). Murine brain lysates were adjusted to a protein concentration of 50 µg/µL per lysate.

3.3.2 SDS-PAGE

Sodium dodecyl sulfate polyacrylamide gel electrophoresis (SDS-PAGE) is used to separate proteins of 5 to 250 kDa due to their molecular weight and charge in an electrical field. The method based on molecular properties of SDS, which binds the hydrophobic areas of a protein leading to negative charged proteins. Proteins are additionally denaturated by β-mercaptoethanol, which cleaves disulfide bridges leading to a linearized protein structure. Due to their negative charge, proteins migrate towards the anode in an electrical field. At first, the stacking gel (4% of acrylamide) is used to concentrate all the proteins in one band that they start migrating in the separting gel all at the same time. The separating gel (12% of acrylamide) consists of a small-pored structure where negatively charged proteins are separated according to their molecular weight. To determine the proteins of interest on the gel, the Precision Plus Protein™ Dual Color Standards (BioRad) was used to estimate the size of the proteins. Each electrophoresis was performed at 25 mA per gel using running buffer. After 180 min, the gel was directly used for Western blot analysis to transfer the size-separated proteins onto suitable nitrocellulose membranes.

3.3.3 Western blot

Semi-dry Western blot analysis were performed to transfer the separated proteins from the gel-electrophoresis (3.3.2) on nitrocellulose membranes. To perform Western blots, a specific buffer system was used to equilibrate the Whatman filter papers (GE Healthcare), the nitrocellulose membrane (GE Healthcare) and the gel. The blotting chamber was constructed according to the following scheme: Cathode: Six Whatman filter papers in buffer C, nitrocellulose membrane in buffer B, polyacrylamide gel and six Whatman filter papers in buffer A, anode. The transfer occurred at 0.75 mA/cm^2 gel (in total 75 mA/gel) for 1h. A Ponceau S staining using 0.1% Ponceau S solution verified a successful transfer. Membrane was blocked with 5 % (w/v) powdered skim milk in TBS-T (TBS buffer supplemented with 0.1% Tween 20) for 60 min at RT and incubated with the indicated primary antibody overnight. The membrane was washed with TBS-T (3 × 5 min at RT) and incubated with horseradish peroxidase (HRP)-conjugated secondary anti-rabbit IgG antibodies in 5% powdered skim milk in TBS-T (GE Healthcare, NA9340, 1:2500) for 1 h at RT. Protein bands on the nitrocellulose membrane were visualized using ImmobilonTM Western Chemiluminescent HRP substrate solution (BioRad). The chemiluminescence signal was recorded with the Fusion-FX6-EDGE V.070 imaging system (Vilber Lourmat). Band intensities (Optical density, OD) were quantified using the Bio 1d FUSION-FX7 software (Version 18.02; Vilber Lourmat). Relative protein amounts were normalized to indicated housekeeping genes (= Loading controls: GAPDH; β-Actin) or each gel.

3.3.4 ELISA

To determine a quantitative analysis of soluble substances as for example cytokines within the plasma of human or murine samples, cell culture supernatants and platelet releasates, enzyme-linked immunosorbent assays (ELISA) were performed. All ELISA analysis were performed according to the manufacturer's instructions. In short, the sandwich ELISA technique based on an immobilized primary antibody which is coated on a multititer plate. The antigen of the sample specifically binds to the immobilized primary antibody. The antibody-antigen-antibody complex (= sandwich) is formed, when the biotin-coupled secondary antibody specifically binds to the antigen of the sample. A substrate containing a streptavidin-coupled horseradish-peroxidase (HRP) is added, leading to an enzymatic color reaction. The reaction was stopped by adding 2N sulfuric acid (H_2S0_4). Photometrical analyses were recorded at 450 nm using the GloMax microplate reader (Promega).

3.4 Immunohistochemistry

3.4.1 Immunofluorescence staining from mouse aortae

In murine AAA, immune cells and platelets were visualized using IF stainings. Following the embedding of murine aortas in paraffin, 5 µM large sections were prepared using an automatic microtome (#Microm HM355, Thermo Fisher Scientific). The tissue sections were transferred into citrate buffer (pH 6.0) and boiled in the microwave at 300 W for 10 min. This was followed by cooling of the sections cooked in the citrate buffer for 30 min and washed once with PBS. To prevent drying of the tissue sections, samples were transferred to a humidity chamber. The sections were blocked with protein blocking solution (#X0909, Dako) for 1h at RT, followed by washing with PBS and incubation with the primary antibody at 4°C overnight. Staining of platelets were performed by use of the platelet specific GPIb α antibody (CD42b #M042-0, emfret, 1:50) and neutrophils were stained with Ly6G (#551459, BD Biosciences, 1:50). Either specific IgG primary antibodies or PBS only were used as controls for staining of the tissue sections. Next day, slices were washed 3× with PBS and incubated for 1h at RT with anti-rat Biotin (#BA-9400, Vector, 1:200). Afterwards strepetavidin eFluorTM 660 conjugate (#50-4317-80, Thermo Fisher Scientific, 1:20) was applied to the sections for detection of the target antigen of the primary antibody. Sections were washed for 3× with PBS and cell nuclei were stained with 4′,6-Diamidine-2′-phenylindole dihydrochloride (DAPI, #10236276001, Roche, 1:3000) for 5 min at RT. Slides were carefully rinsed with PBS before embedding the tissue sections with mounting medium (#S3023, Dako) and stored at 4°C in the dark before further use.

3.5 Molecular biological methods

3.5.1 Animal genotyping

Animal genotyping was performed using the obtained protocol from the KAPA - Mouse - Genotyping Hot Start Kit (PeqLab). Biopsies (Ear punches) from each mice were used for genotyping. In short, DNA was extracted by lysing ear punches for 10 min at 75 °C in extraction buffer (PeqLab). Reaction was stopped by heat-inactivation of the enzymes at 95 °C for 10 min. Tissue remains were removed by centrifugation at 14,000 x g for 90 sec. Supernatants with extracted DNA were transferred into new reaction tubes and directly used for PCR reactions.

Table 1: Composition of the PCR reaction mixture using for mice genotyping

Mastermix	**Volume [µL]**
KAPA Mix	12.5
Forward primer	1.25
Reverse primer	1.25
HPLC H_20	9
DNA	1

The PCR was prepared followed by the protocol listed in Table 1 and performed as listed in Table 2.

Table 2: PCR reaction steps for murine genotyping

	Temperature (°C)	**Time (s)**	**Cycles**
Initial denaturation	95	180	1
Denaturation	95	15	40
Annealing	58	20	40
Elongation	72	15	40
Final elongation	72	180	1

A gel electrophoresis (1.5% agarose) containing Midori Green (Biozym) in 1 × Tris acetate EDTA (TAE) buffer was performed to visualize PCR products using the Fusion-FX6-EDGE V.070 system (Vilber Lourmat).

3.6 Statistical analysis

Data is provided by arithmetic means or individual values ± SEM (Standard error of the mean). The number of analyzed individuals is indicated as n. Significant differences were calculated using an ordinary one-way ANOVA or two-way ANOVA with multiple-comparison analysis (post-hoc test, Sidak's multiple comparison test) or student's t-test as indicated in the figure legends. The survival analysis was performed by Kaplan-Meier plotting. All statistics were performed using Graph Pad Prism version 8.0.2. Significant outliers were identified with the Grubbs' test and excluded from the evaluation of mean values as mentioned in the figure legends. Asterisks indicate the level of significance (***, $p < 0.001$; **, $p < 0.01$; *, $p < 0.05$).

4 Results

To investigate the role of the platelet PANX1 channel, two different genetically modified mouse models were used within this thesis: Mice targeting a *Panx1* deletion (*Panx1 fl/fl*) that have been crossed to platelet factor 4-Cre recombinase transgenic mice (PF4-Cre) to generate a specific deletion of PANX1 channels on the platelet surface (Figure 10, wild-type (WT): *Panx1 fl/fl PF4-Cre*$^{-}$ and knock-out (KO): *Panx1 fl/fl PF4-Cre*$^{+}$) and mice with a constutive *Panx1* deletion (Figure 11, WT: *Panx1*$^{+/+}$ and KO: *Panx1*$^{-/-}$).

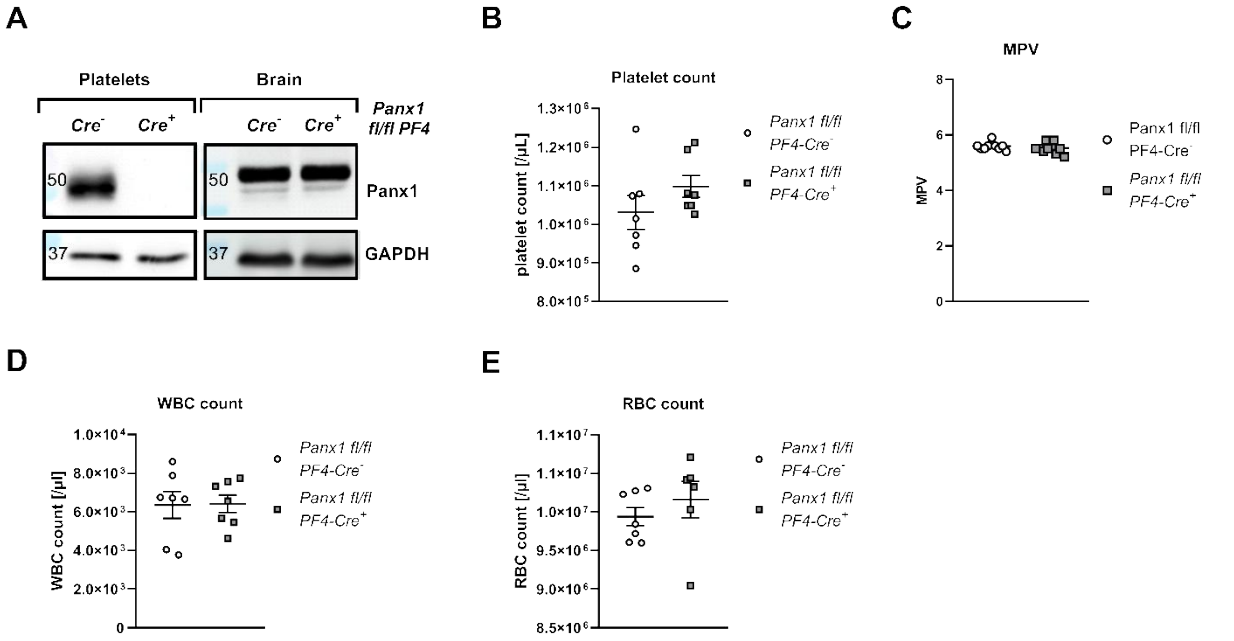

Figure 10: *Panx1 fl/fl PF4-Cre* mice display no alterations in blood cell counts and MPV. (A) *Panx1 fl/fl PF4-Cre*$^{+}$ mice do not express PANX1 protein in platelets but in the brain compared to *Panx1 fl/fl PF4-Cre*$^{-}$ mice as shown by Western blot analysis (n = 3). No alterations in cell counts of (B) platelets, (D) WBCs and (E) RBCs were observed in *Panx1 fl/fl PF4-Cre*$^{-}$ mice compared to *Panx1 fl/fl PF4-Cre*$^{+}$ mice (n (WT) = 7, n (KO) = 6-7). (C) MPV is not changed between *Panx1 fl/fl PF4-Cre*$^{-}$ mice and *Panx1 fl/fl PF4-Cre*$^{+}$ mice (n (WT) = 10, n (KO) = 11). Statistical analyses were performed using an unpaired student's t-test. Bar graphs indicate mean values ± SEM, WBC = White Blood Cell, RBC = Red Blood Cell, MPV = Mean Platelet Volume, Panx1 = Pannexin 1 [Figure from Metz, Elvers, IJMS 2022].

Figure 10 A indicates that *Panx1 fl/fl PF4-Cre*$^{-}$ mice but not *Panx1 fl/fl PF4-Cre*$^{+}$ express PANX1 protein in platelets, while the PANX1 expression in brain was similar within both genotypes. Moreover, no alterations concerning blood cell counts of platelets (Figure 10 B), white blood cells (WBCs) (Figure 10 D) and red blood cells (RBCs) (Figure 10 E) were observed between *Panx1 fl/fl PF4-Cre*$^{+}$ and *Panx1 fl/fl PF4-Cre*$^{-}$ mice. Additionally, the mean platelet volume (MPV) does not differ between platelets from *Panx1 fl/fl PF4-Cre*$^{-}$ and *Panx1 fl/fl PF4-Cre*$^{+}$ mice (Figure 10 C).

Constitutive *Panx1*$^{-/-}$ mice do not express PANX1 protein, neither in platelets nor in the brain as shown by Figure 11 A. Moreover, no alterations of platelet counts (Figure 11 B), WBC counts (Figure 11 D) and RBC counts (Figure 11 E) were detected in constitutive *Panx1* knock-out compared to controls. No alteration of the MPV was observed between platelets from *Panx1*$^{+/+}$ mice and *Panx1*$^{-/-}$ mice (Figure 11 C).

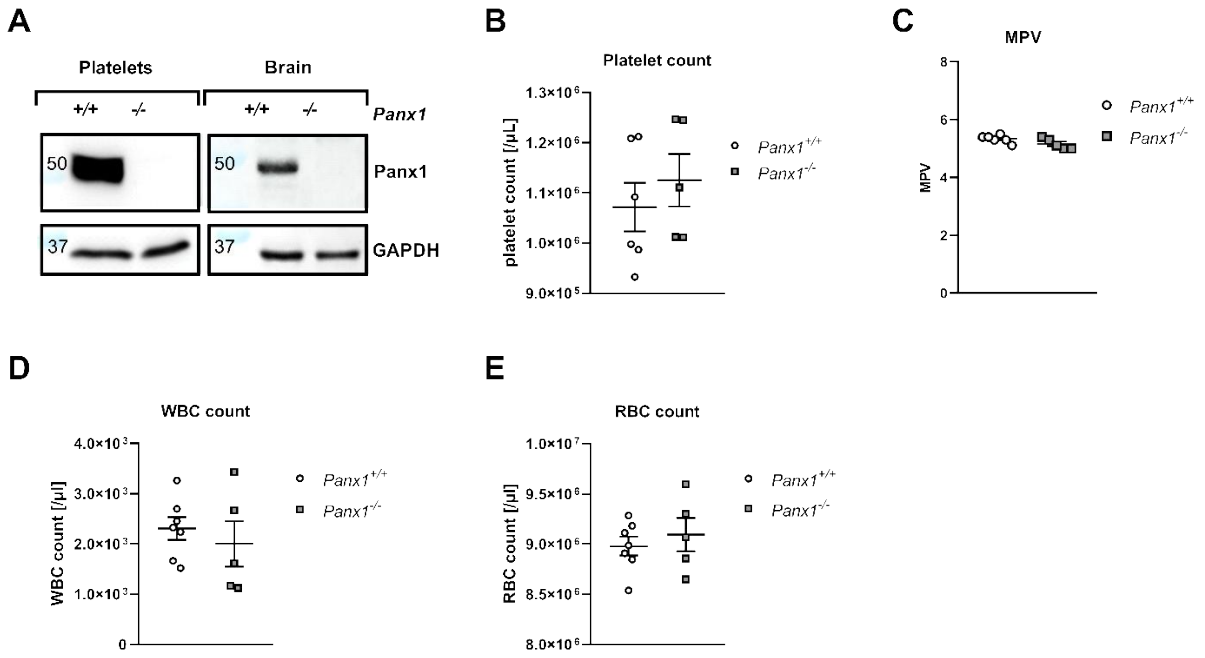

Figure 11: A global deletion of PANX1 in mice does not change blood cell counts and MPV. (A) *Panx1*$^{-/-}$ mice do not express PANX1 protein in platelets and brain compared to *Panx1*$^{+/+}$ mice shown by Western blot analysis (n = 3). No alterations in cell counts of (B) Platelets, (C) WBCs and (E) RBCs were observed in *Panx1*$^{-/-}$ mice compared to *Panx1*$^{+/+}$ mice (n (WT) = 6-7, n (KO) = 5). (C) MPV is not changed between *Panx1*$^{-/-}$ mice compared to *Panx1*$^{+/+}$ mice (n (WT) = 6, n (KO) = 5). Statistical analyses were performed using an unpaired student's t-test. Bar graphs indicate mean values ± SEM. WBC = White Blood Cell, RBC = Red Blood Cell, MPV = Mean Platelet Volume, Panx1 = Pannexin 1.

Figure 10 and Figure 11 display that in both mouse models platelet PANX1 protein is not expressed in the knock-out mouse strain (*Panx1 fl/fl PF4-Cre*$^{+}$ and *Panx1*$^{-/-}$) compared to the control mouse strain (*Panx1 fl/fl PF4-Cre*$^{-}$ and *Panx1*$^{+/+}$), respectively. Within both genotypes of genetically modified mice, no alterations concerning blood cell counts and MPV were observed (Figure 10, Figure 11), which are essential parameters influencing hemostatic responses.

4.1 Platelet pannexin 1 channel function as ion channels for small molecules like ATP

As already mentioned in chapter 1.2.2, PANX1 channels act as ATP release channels in response to platelet activation with low concentrations of collagen, thrombin and the TxA_2 analogue U46619 in human platelets as shown by inhibitory experiments using pharmacological compounds [81]. We aim to investigate, if the ATP release is diminished in platelets of mice with a platelet specific PANX1 deletion (*Panx1 fl/fl PF4-Cre*$^+$) compared to platelets from *Panx1 fl/fl PF4-Cre*$^-$ animals (Figure 12).

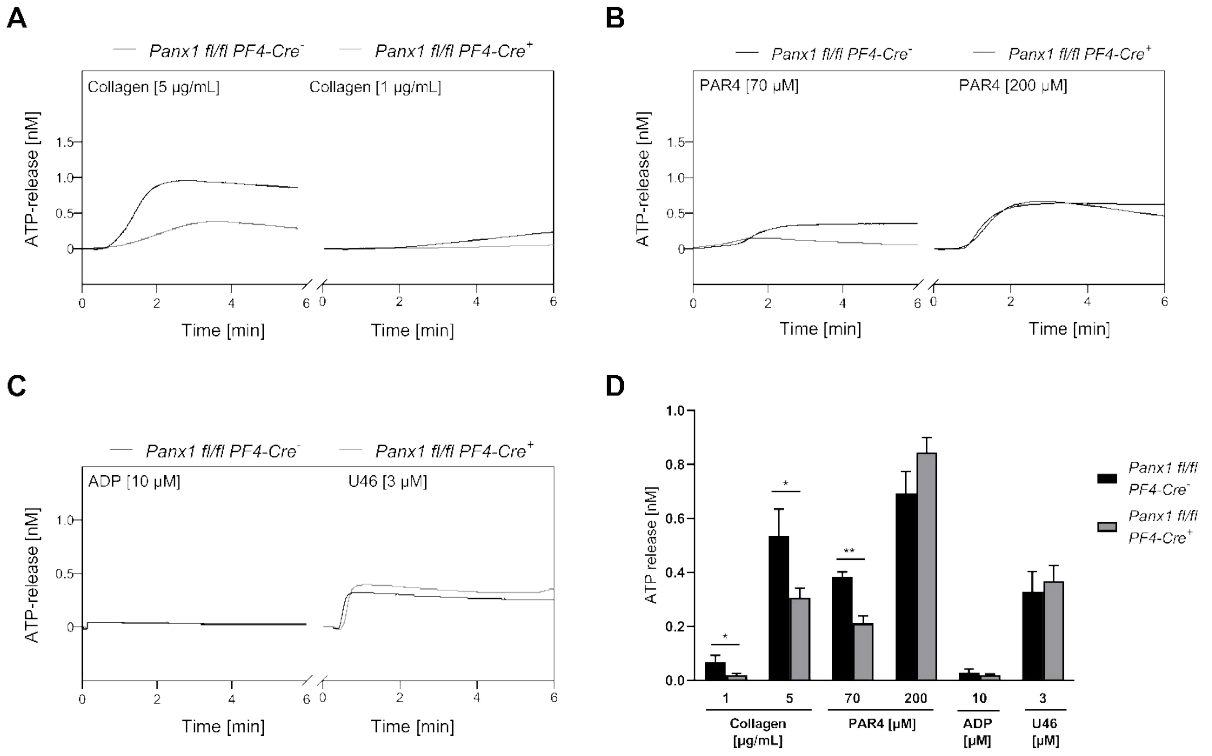

Figure 12: ATP release is reduced in PANX1 deficient platelets in response to platelet activation with collagen and low doses of PAR4 peptide compared to respective control platelets. Isolated platelets from *Panx1 fl/fl PF4-Cre*$^-$ and *Panx1 fl/fl PF4-Cre*$^+$ mice were stimulated with depicted agonists and ATP release was measured under apyrase (0.04 U/mL) by a luciferin/luciferase bioluminescent assay for 6 min. Representative curves of ATP release of platelet activation with (A) 5 µg/mL (n (WT) = 6; n (KO) = 9) and 1 µg/mL collagen (n (WT) = 4; n (KO) = 6), (B) 70 µM (n (WT) = 4; n (KO) = 8) and 200 µM PAR4 peptide (n (WT) = 6; n (KO) = 8) and (C) 10 µM ADP (n (WT) = 3; n (KO) = 6) and 3 µM U46 (n (WT) = 5; n (KO) = 9) from platelets from *Panx1 fl/fl PF4-Cre*$^-$ and *Panx1 fl/fl PF4-Cre*$^+$ mice. (D) The graph displays the results of the maximal ATP release measurements for all tested agonists. Statistical analyses were performed using an unpaired multiple students t-test. Bar graphs indicate mean values ± SEM, *p < 0.05: **p < 0.01. PAR4 peptide = Protease-activated receptor 4 peptide, ADP = Adenosine diphosphate, U46 (U46619) = Thromboxane A_2 analogue, WT = Wild type, KO = Knock-out, Panx1 = Pannexin 1. Experiments were performed in cooperation with M.Sc. Larissa De Biasi, Research group: Exp. Vascular Medicine [Figure from Metz, Elvers, IJMS 2022].

Where indicated, a collagen mimetic peptide containing 10 repeats of the Gly-Pro-Hyp sequence of collagen (CRP) was used as a GPVI receptor agonist [140]. For activation of the GPCR signaling pathway induced by PAR4 receptor signaling, a hexapeptide (Gly-Tyr-Pro-Gly-Gln-Val) consisting of the N-terminal fragment of the PAR4 receptor was used as a platelet agonist (PAR4 peptide) [141]. In the present work, the TxA_2 signaling pathway mediated by TP receptors was activated by the TxA_2 analogue U46619.

Collagen induced platelet activation resulted in reduced ATP release in PANX1 deficient platelets in response to both concentrations tested. In detail, ATP release is diminished about 0.23 nM in PANX1 deficient platelets (0.31 ± 0.05 nM (SEM)) compared to platelets from *Panx1 fl/fl PF4-Cre*$^-$ mice (0.54 ± 0.1 nM (SEM)) in response to platelet activation with 5 µg/mL collagen (Figure 12 A, D, $p = 0.025$). Similar results of ATP release were obtained when platelets were activated with 1 µg/mL collagen (Figure 12 A, D, WT: 0.07 ± 0.02 nM (SEM); KO: 0.02 ± 0.01 nM (SEM), $p = 0.041$). Low dose platelet activation with PAR4 peptide (70 µM) resulted in reduced ATP release in PANX1 deficient platelets (0.21 ± 0.03 nM (SEM)) compared to controls (0.39 ± 0.02 nM (SEM) $p = 0.002$), while ATP release was not altered between both genotypes in response to platelet activation with 200 µM PAR4 peptide (Figure 12 B, D, WT: 0.7 ± 0.08 nM (SEM); KO: 0.85 ± 0.05 nM (SEM). No differences in ATP release were observed for platelet activation with 10 µM ADP between both genotypes (Figure 12 C, D, WT: 0.03 ± 0.01 nM (SEM); KO: 0.02 ± 0.01 nM (SEM)). Additionally, ATP release with the TxA_2 analogue U46619 is not altered between platelets from *Panx1 fl/fl PF4-Cre*$^-$ and *Panx1 fl/fl PF4-Cre*$^+$ mice (Figure 12 C, D, WT: 0.33 ± 0.08 nM (SEM); KO: 0.37 ± 0.06 nM (SEM)). These results demonstrate that PANX1 is responsible for ATP release via the ITAM coupled GPVI receptor pathway activated by low and high doses of collagen as well as after low dose stimulation of GPCR signaling by 70 µM PAR4 peptide (Figure 12). Murine platelet activation with 200 µM PAR4 peptide, 10 µM ADP and with 3 µM of U46619 did not alter ATP release between platelets from *Panx1 fl/fl PF4-Cre*$^-$ and *Panx1 fl/fl PF4-Cre*$^+$ mice (Figure 12).

As a first translational approach, ATP release measurements were performed by inhibition of human platelet PANX1 channels with Probenecid (Prb) as displayed in Figure 13. In detail, human platelets were preincubated with or without 100 µM Prb and ATP release was measured either by a luciferin/luciferase bioluminescent assay at 37°C under stirring conditions at 1000 rpm or via a bioluminescence assay (ELISA). All experiments were performed in Tyrode's buffer containing apyrase (0.04 U/mL).

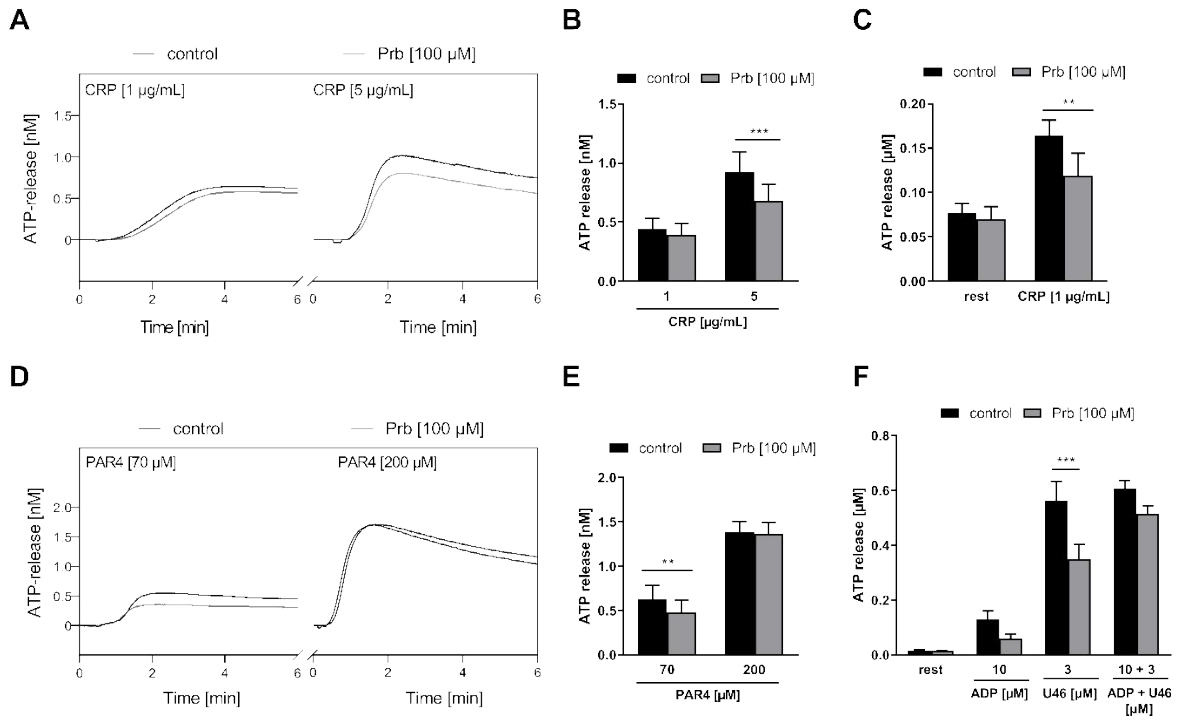

Figure 13: Inhibition of PANX1 by Probenecid reduces ATP release upon platelet activation with collagen-related peptide (CRP), low dose PAR4 peptide and U44619. Isolated platelets were preincubated with or without 100 µM Prb and stimulated with depicted agonists and ATP release was measured under apyrase (0.04 U/mL) by either a luciferin/luciferase bioluminescent assay for 6 min or by ATP ELISA. (A) Representative curves of ATP release of platelet activation with 1 and 5 µg/mL CRP and (B) results of the maximal ATP release measurements for 1 and 5 µg/mL CRP with or without 100 µM Prb (n (control) = 4, n (Prb) = 6). (C) ATP ELISA of platelets preincubated with or without 100 µM Prb under resting conditions and stimulated with 1 µg/mL CRP (n (control) = 6, n (Prb) = 6) (D) Representative curves of ATP release of platelet activation with 70 and 200 µM PAR4 peptide and (E) the results of the maximal ATP release measurements for 70 and 200 µM PAR4 peptide with or without 100 µM Prb (70 µM: n (control) = 6, n (Prb) = 6; 200 µM: n (control) = 4, n (Prb) = 4). (F) ATP ELISA of platelets preincubated with or without 100 µM Prb under resting conditions and stimulated with 10 µM ADP, 3 µM U46 and 10 µM ADP + 3 µM U46 (n (control) = 5, n (Prb) = 5). Statistical analyses were performed using a two-way ANOVA followed by a Sidak's multiple comparisons post-hoc test. Bar graphs indicate mean values ± SEM, **p < 0.01 and ***p < 0.001. Rest = Resting, CRP = Collagen-related peptide, PAR4 peptide = Protease-activated receptor 4 peptide, ADP = Adenosine diphosphate, U46 (U46619) = Thromboxane A_2 analogue, Prb = Probenecid, PANX1 = Pannexin 1 [Figure from Metz, Elvers, IJMS 2022].

Inhibition of human PANX1 channels with Prb resulted in reduced ATP release upon platelet activation with collagen-related peptide CRP, an agonist for the platelet collagen receptor GPVI (Figure 13 A-C). In detail, ATP release was decreased up to 35% after platelet activation with 5 µg/mL CRP in Prb treated human platelets compared to control platelets (Figure 13 A, B). These results were measured by a luciferin/luciferase bioluminescent assay at 37°C under stirring conditions (Control: 0.92 ± 0.17 nM (SEM); Prb: 0.68 ± 0.14 nM (SEM), p = 0.0001). For low dose CRP concentration of 1 µg/mL, ATP release was reduced only by trend in Prb treated human platelets compared to control platelets using the indicated method (Figure 13 A, B, control: 0.44 ± 0.09 nM (SEM); Prb: 0.39 ± 0.09 nM (SEM); p = 0.06). Therefore, ATP ELISA experiments were performed, because ATP measurements by ELISA technique revealed a higher sensitivity regarding detection limits. Detection of ATP release by ELISA displayed a significant

reduction when PANX1 channels are inhibited by Prb (Figure 13 C, control: 0.16 ± 0.02 nM (SEM); Prb: 0.12 ± 0.03 nM (SEM), p = 0.003). Similar to the obtained results of PANX1 deficient platelets in Figure 12, application of Prb lead to diminished ATP release in response to 70 µM PAR4 peptide compared to control platelets (Control: 0.63 ± 0.16 nM (SEM); Prb: 0.48 ± 0.13 nM (SEM), p = 0.0019), but not 200 µM PAR4 peptide (Control: 1.38 ± 0.12 nM (SEM); Prb: 1.4 ± 0.13 nM (SEM)) in human platelet (Figure 13 D, E). Moreover, the data obtained in murine platelets correspond to the results obtained for platelet activation with 10 µM ADP in human platelets, because Prb application does not alter ATP release compared to control platelets (Figure 13 F, control: 0.13 ± 0.03 nM (SEM); Prb: 0.06 ± 0.02 nM (SEM)). However, application of Prb to human platelets led to reduced ATP release in response to 3 µM U46619 compared to control platelets (Figure 13 F, p = 0.0008), which was not observed in PANX1 deficient platelets compared to controls (Figure 12).

These results confirm that PANX1 acts as an ATP release channel in human and mouse platelets after activation of the ITAM coupled GPVI receptor pathway with low and high doses of collagen or CRP (Figure 12, Figure 13). PANX1 dependent ATP release was obtained after low dose stimulation of the GPCR signaling pathway by 70 µM PAR4 peptide and the second wave mediator ADP (Figure 12, Figure 13). In addition, differences in ATP release in response to platelet activation with U46619 by PANX1 inhibition with Prb were detected in human platelets, which platelets from mice mice with a platelet specific PANX1 deletion did not indicate (Figure 12, Figure 13).

4.2 The role of platelet pannexin 1 channels in thrombosis and hemostasis

The results in chapter 4.1 display that PANX1 alters ATP release in response to all concentrations of collagen induced and mild concentration of PAR4 peptide. Previous studies already revealed that PANX1 inhibition by pharmacological compounds alters platelet function especially in collagen induced platelet activation as shown by aggregation or reduced Ca^{2+} influx [80, 81]. Additionally, mice with a platelet specific and a global deletion of PANX1 indicate reduced hemostatic responses *in vivo* [82]. Until now, the mechanisms leading to reduced hemostatic responses are unclear and further analysis were performed investigating the functional role of PANX1 in thrombosis and hemostasis.

4.2.1 Unaltered glycoprotein expression, but minor alterations in platelet activation either in genetically modified pannexin 1 mice or by pharmacological inhibition of pannexin 1 channels

Following the characterization of the *Panx1 fl/fl PF4-Cre* and the constitutive *Panx1* knock-out mouse stains, we aim to understand if a PANX1 deletion in platelets leads to altered glycoprotein expression at the platelet surface. Differences in the intensity of expressed glycoproteins on platelets are potential reasons for altered platelet activation. The most abundant glycoproteins GPVI, α_5-integrin, β_3-integrin and GPIb on the platelet surface were measured via flow cytometric analysis in washed murine whole blood and were not altered within *Panx1 fl/fl PF4-Cre* and constitutive *Panx1* knock-out mouse stains as shown in Figure 14. In platelets of *Panx1*$^{-/-}$ mice, platelet GPIb expression was only reduced by trend (Figure 14 B, p = 0.057).

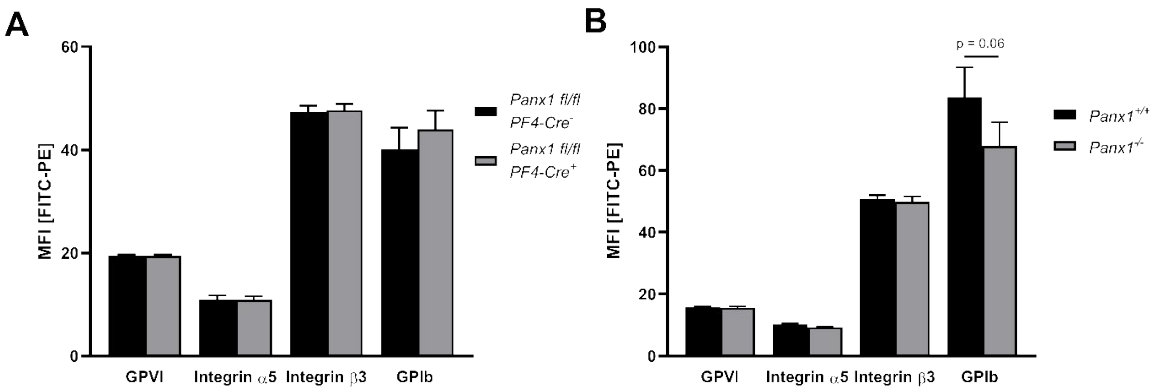

Figure 14: No alterations in glycoprotein expression on the platelet surface within genetic modified PANX1 deficient mouse models compared to respective control mice. Mice targeting a platelet specific deletion of PANX1 channels (WT: *Panx1 fl/fl PF4-Cre*$^{-}$, KO: *Panx1 fl/fl PF4-Cre*$^{+}$) and a global deletion of PANX1 channels (WT: *Panx1*$^{+/+}$, KO: *Panx1*$^{-/-}$) were analyzed regarding to glycoprotein expression of GPVI, α_5-integrin, β_3-integrin and GPIb. (A) Platelet specific deletion of PANX1 does not alter glycoprotein expression in unstimulated platelets (n (WT) = 10, n (KO) = 10). (B) A global deletion of PANX1 does not lead to alterations of analyzed glycoproteins in unstimulated platelets (n (WT) = 6, n (KO) = 6). Statistical analyses were performed using a two-way ANOVA followed by a Sidak's multiple comparisons post-hoc test. Bar graphs indicate mean values ± SEM, MFI = Mean fluorescence intensity, WT = Wild type, KO = Knock-out, Panx1 = Pannexin 1.

Platelet PANX1 channels act as ATP release channels in response to collagen induced as well as mild PAR4 (70 µM) induced stimulation (4.1). To investigate, if platelet specific PANX1 deletion alters platelet activation, flow cytometric analysis was performed after stimulation with different platelet receptor agonists. Therefore, expression of active integrin $\alpha_{IIb}\beta_3$ (fibrinogen receptor) and P-selectin, as marker for platelet degranulation, were analyzed.

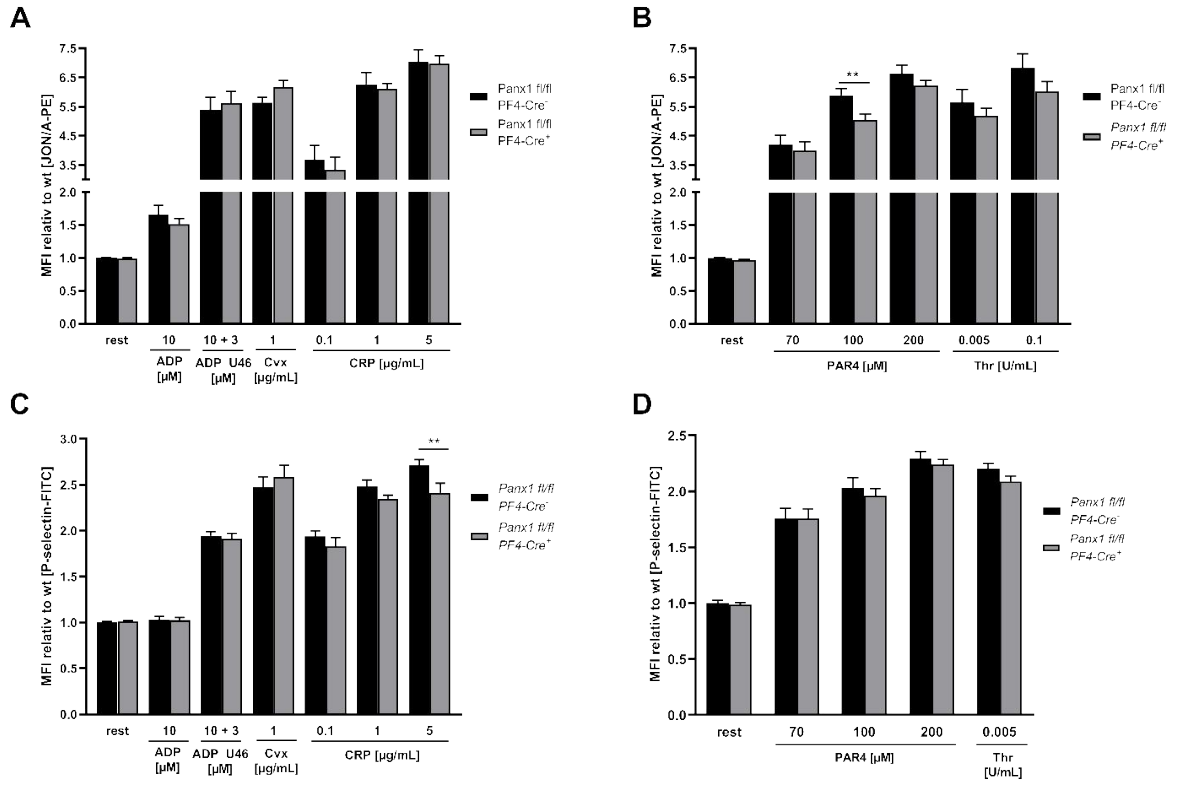

Figure 15: Minor changes in platelet activation between platelets from *Panx1 fl/fl PF4-Cre*$^-$ and *Panx1 fl/fl PF4-Cre*$^+$ mice. Platelets from *Panx1 fl/fl PF4-Cre*$^-$ and *Panx1 fl/fl PF4-Cre*$^+$ mice were analyzed regarding to their activation profile for integrin $\alpha_{IIb}\beta_3$ (JON/A-PE) and P-selectin (FITC) via flow cytometric analysis. (A and B) Integrin $\alpha_{IIb}\beta_3$ activation is decreased only upon intermedium (100 µM) PAR4 stimulation (n (WT) = 9-20, n (KO) = 8-19). (C and D) Degranulation (P-selectin) is altered upon platelet activation with 5 µg/mL CRP (n (WT) = 9-20, n (KO) = 9-20). Statistical analyses were performed using a mixed-effect analysis followed by a Sidak's multiple comparisons post-hoc test. Bar graphs indicate mean values ± SEM; **p < 0.01. Rest = resting, ADP = Adenosine diphosphate, U46619 (U46) = Thromboxane A_2 analogue, CRP = Collagen-related peptide, Cvx = Convulxin, PAR4 peptide = Protease-activated receptor 4 peptide, Thr = Thrombin, MFI = Mean fluorescence intensity, WT = Wild type (*Panx1 fl/fl PF4-Cre*$^-$), KO = Knock-out (*Panx1 fl/fl PF4-Cre*$^+$), Panx1 = Pannexin 1 [Figure from Metz, Elvers, IJMS 2022].

Flow cytometric analysis showed that integrin $\alpha_{IIb}\beta_3$ activation is only reduced upon platelet activation with 100 µM PAR4 peptide (Figure 15 B, p = 0.046). No alterations were observed for all other tested agonists as displayed in Figure 15 A, B. P-selectin, a marker for degranulation of platelet α-granules, is reduced upon high dose CRP (5 µg/mL) stimulation in platelets from *Panx1 fl/fl PF4-Cre*$^+$ mice compared to platelets from *Panx1 fl/fl PF4-Cre*$^-$ mice (Figure 15 C, p = 0.03). Platelet activation due to GPCRs by either thrombin, PAR4 peptide, ADP or the TxA_2 analogue U46619 displayed no differences upon P-selectin exposure between both genotypes (Figure 15 C, D).

Recent studies from our group demonstrated a major role for RBCs and platelet interaction leading to thrombin generation and thus contributing to thrombus formation [142]. Since other blood cells in the vasculature, e.g. RBCs [70] and leukocytes [143] also express PANX1 channels, potential

inhibiting compounds might also face other cells contributing to potential bleeding disorders. Therefore, mice targeting a global deletion of PANX1 channels were analyzed regarding their platelet specific activation profiles to avoid unexpected PANX1 inhibiting site effects in further human translational approaches (Figure 16).

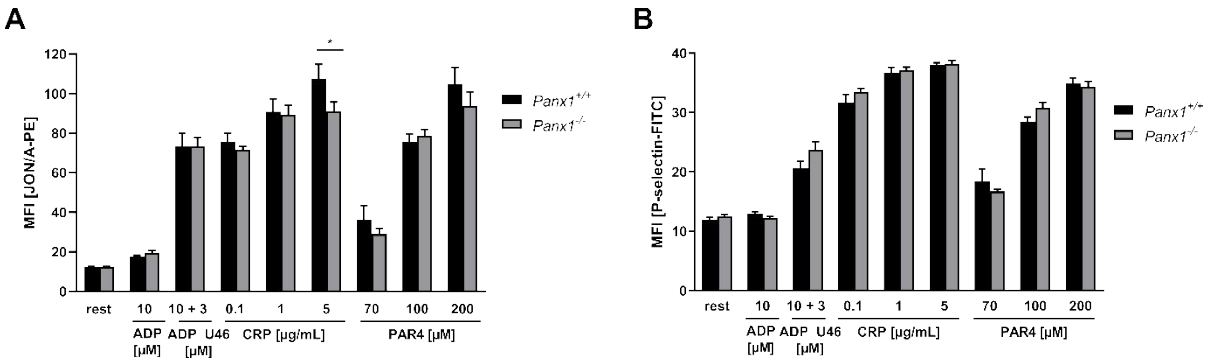

Figure 16: Constutive PANX1 deletion in murine whole blood leads to reduced platelet integrin $\alpha_{IIb}\beta_3$ activation upon high dose CRP stimulation. Washed whole blood of mice targeting a global deletion of PANX1 channels were analyzed regarding platelet integrin $\alpha_{IIb}\beta_3$ (JON/A-PE) and P-selectin (FITC) exposure via flow cytometric analysis. (A) Integrin $\alpha_{IIb}\beta_3$ activation is decreased only upon CRP stimulation with 5 µg/mL (n (*Panx1*$^{+/+}$) = 4-6, n (*Panx1*$^{-/-}$) = 4-6). (B) Degranulation (P-selectin) is not altered between *Panx1*$^{+/+}$ and *Panx1*$^{-/-}$ mice (n (*Panx1*$^{+/+}$) = 4-6, n (*Panx1*$^{-/-}$) = 3-6). Statistical analyses were performed using an unpaired multiple students t-test. Bar graphs indicate mean values ± SEM, *p < 0.05. Rest = resting, ADP = Adenosine diphosphate, U46619 (U46) = Thromboxane A_2 analogue, CRP = Collagen-related peptide, PAR4 peptide = Protease-activated receptor 4 peptide, MFI = Mean fluorescence intensity, PANX1 = Pannexin 1.

Analysis of platelet activation profiles in washed whole blood of mice targeting a global deletion of *Panx1* (*Panx1*$^{-/-}$) compared to their respective controls (*Panx1*$^{+/+}$) showed significant reduced integrin $\alpha_{IIb}\beta_3$ activation upon platelet activation with 5 µg/mL CRP (Figure 16 A, p = 0.046). Integrin $\alpha_{IIb}\beta_3$ activation due to other concentrations of CRP as well as other agonists did not differ between both genotypes (Figure 16 A). Platelet degranulation, measured by P-selectin, does not change in platelets from global deleted PANX1 mice compared to control platelets (Figure 16 B).

As a translational approach, PANX1 channels were blocked either with Prb or Carbenoxolone (Cbx) in human platelets and activation profiles were measured via flow cytometric analysis. According to the above described analysis of murine platelets, integrin $\alpha_{IIb}\beta_3$ activation was determined via PAC-1, an antibody specific for activated integrin $\alpha_{IIb}\beta_3$, and degranulation was measured by P-selectin exposure at the platelet surface (Figure 17).

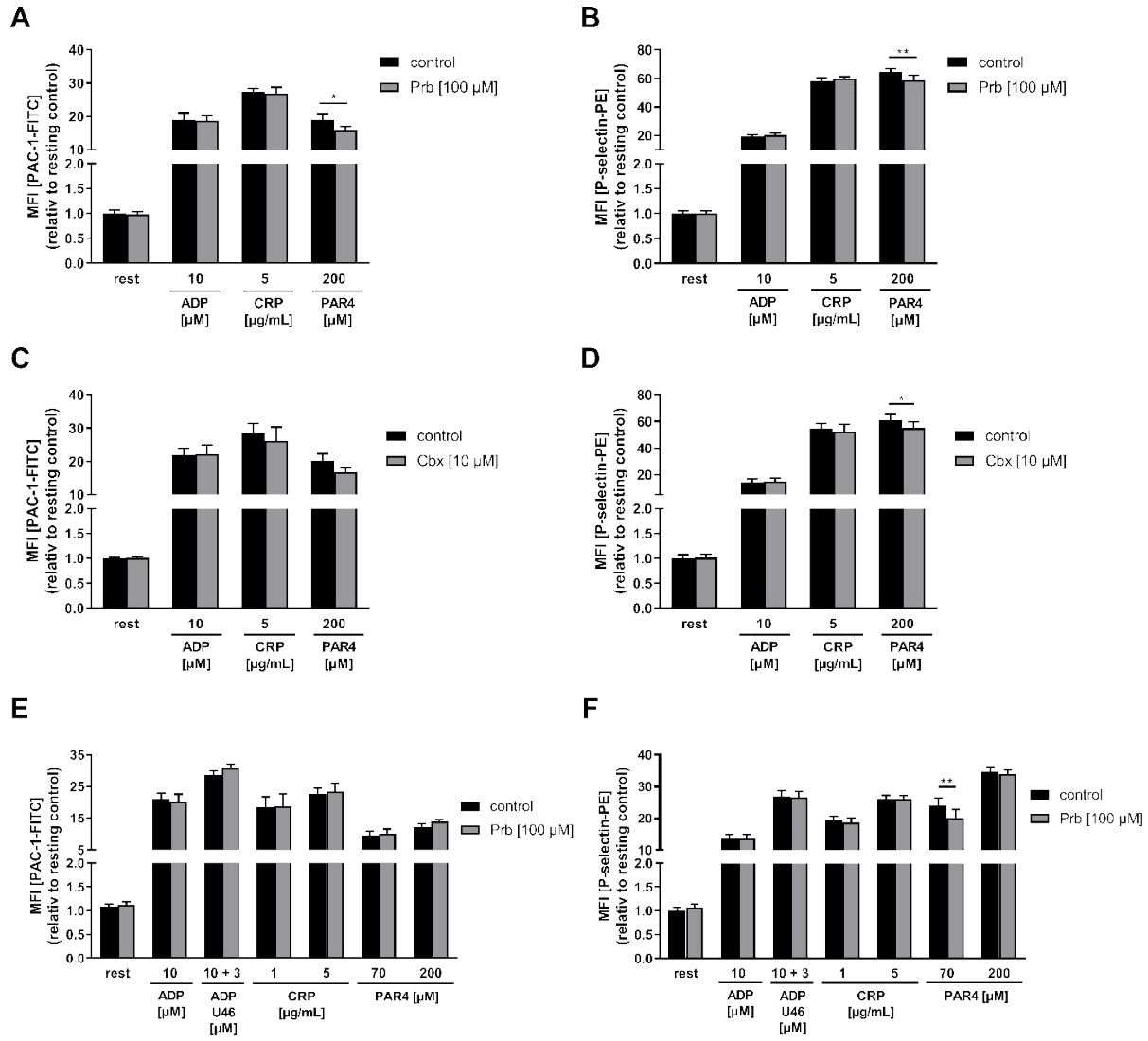

Figure 17: Pharmacological inhibition of PANX1 by either Probenecid or Carbenoxolone alters degranulation upon platelet activation with PAR4 peptide. Diluted human whole blood (A-D) or isolated human platelets (E + F) were either pre-treated with or without 100 µM Prb (A,B,D,F) or 10 µM Cbx (C + D) and analyzed in response to integrin $\alpha_{IIb}\beta_3$ (PAC-1/FITC) and P-selectin (PE) exposure via flow cytometric analysis. (A) Integrin $\alpha_{IIb}\beta_3$ activation is decreased only upon high PAR4 peptide (200 µM) stimulation after inhibition of PANX1 channels by Prb (n (control) = 7-11, n (Prb) = 7-11). (B) Degranulation (P-selectin) is altered upon platelet activation with 200 µM PAR4 peptide (n (control) = 7-11, n (Prb) = 7-11). (C) Inhibition of PANX1 by Cbx does not alter PAC-1 expression in diluted human whole blood (n (control) = 6, n (Cbx) = 6). (D) P-selection exposure is reduced upon high dose PAR4 peptide stimulation after application of 10 µM Cbx (n (control) = 6, n (Cbx) = 6). (E) Integrin $\alpha_{IIb}\beta_3$ activation is not altered in human isolated platelets with or without 100 µM Prb (n (control) = 10-11, n (Prb) = 8). (F) Degranulation (P-selectin) is altered upon platelet activation with 70 µM PAR4 peptide Prb (n (control) = 11-14, n (Prb) = 12-14). Statistical analyses were performed using (A, C, D) a two-way ANOVA or (B, E, F) a multiple-comparison analysis followed by a Sidak's multiple comparisons post-hoc test. Bar graphs indicate mean values ± SEM, *p < 0.05: **p < 0.01. Rest = resting, ADP = Adenosine diphosphate, U46 (U46619) = Thromboxane A_2 analogue, CRP = Collagen-related peptide, PAR4 peptide = Protease-activated receptor 4 peptide, Prb = Probenecid, Cbx = Carbenoxolone, MFI = Mean fluorescence intensity. [Figure from Metz, Elvers, IJMS 2022].

Application of Prb to human whole blood resulted in reduced integrin $\alpha_{IIb}\beta_3$ activation ($p = 0.046$) as well as degranulation ($p = 0.008$) only after platelet activation with 200 µM PAR4 peptide (Figure 17 A, B). Reduced degranulation upon high PAR4 peptide stimulation correspond to the results obtained after application of 10 µM Cbx to human platelets compared to control platelets (Figure 17 D, $p = 0.018$). Cbx does not change integrin $\alpha_{IIb}\beta_3$ activation on human platelets as shown in Figure 17 C. Treatment of human isolated platelets with 100 µM Prb resulted in reduced degranulation upon mild PAR4 peptide (70 µM) stimulation ($p = 0.006$), while integrin $\alpha_{IIb}\beta_3$ activation is not altered (Figure 17 E, F).

Overall, the results revealed only minor changes in activation markers between platelets from *Panx1 fl/fl PF4-Cre*$^-$ and *Panx1 fl/fl PF4-Cre*$^+$ mice. In detail, integrin $\alpha_{IIb}\beta_3$ activation is reduced upon platelet activation with 100 µM PAR4 peptide (Figure 15 B) and P-selectin is reduced upon high dose CRP (5 µg/mL) stimulation in platelets from *Panx1 fl/fl PF4-Cre*$^+$ mice compared to platelets from *Panx1 fl/fl PF4-Cre*$^-$ mice (Figure 15 C). Mice targeting a global deletion of PANX1 (*Panx1*$^{-/-}$) showed significant reduced integrin $\alpha_{IIb}\beta_3$ activation upon platelet activation with high doses of CRP (Figure 16 A), but no alterations in degranulation measured by P-selectin (Figure 16 B). Application of PANX1 inhibiting compounds (Prb and Cbx) to diluted human whole blood leads to reduced platelet degranulation after activation of the GPCR mediated signaling pathway by indicated concentrations of PAR4 peptide (Figure 17 B, D, F). Integrin $\alpha_{IIb}\beta_3$ activation is only reduced after pre-incubation of diluted human whole blood with Prb in response to a high dose PAR4 peptide stimulation (Figure 17 A).

Beside P-selectin, fibrinogen release was determined in isolated PANX1 deficient platelets compared to isolated control platelets as an additional marker for α-granule release (Figure 18 A). Moreover, δ-granule release via mepacrine release was determined by flow cytometric analysis in isolated murine platelets (Figure 18 B). The fluorescent dye meparcine was loaded to platelet dense granules, which is released after stimulation of the GPCR signaling pathway. Therefore, the reduction of the MFI measured in the FITC channel was determined. The upregulation of β_3-integrin (CD61) in response to CRP induced platelet activation was determined as an additional marker indicating alterations in platelet mediated activation between platelets from *Panx1 fl/fl PF4-Cre*$^-$ and *Panx1 fl/fl PF4-Cre*$^+$ mice (Figure 18 C).

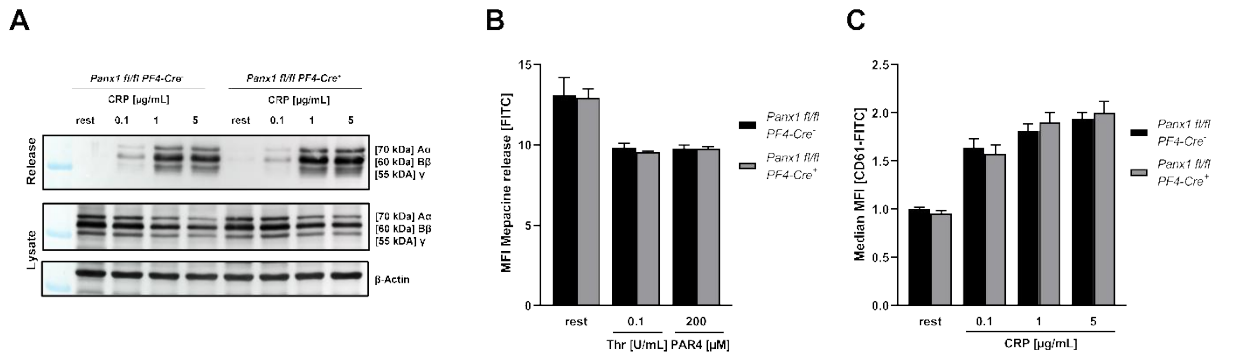

Figure 18: Deletion of PANX1 does not alter degranulation as well as CD61 exposure of platelets. (A) Fibrinogen release was analyzed using isolated platelets from *Panx1 fl/fl Pf4-Cre*$^+$ and *Panx1 fl/fl Pf4-Cre*$^-$ mice by Western blot analysis (n=3). (B) Mepacrine release was measured in isolated platelets from *Panx1 fl/fl Pf4-Cre*$^+$ and *Panx1 fl/fl Pf4-Cre*$^-$ mice by flow cytometric analysis (n (WT) = 5, n (KO) = 5). (C) Washed whole blood from *Panx1 fl/fl Pf4-Cre*$^+$ and *Panx1 fl/fl Pf4-Cre*$^-$ mice was incubated with different concentrations of CRP and CD61 exposure was determined (n (WT) = 10, n (KO) = 10). (B+C) Statistical analyses were performed using a two-way ANOVA followed by a Sidak's multiple comparisons post-hoc test. Bar graphs indicate mean values ± SEM. Rest = Resting, CRP = Collagen-related peptide, PAR4 peptide = Protease-activated receptor 4 peptide, Thr = Thrombin, MFI = Mean fluorescence intensity, PANX1 = Pannexin 1, WT = Wild type (*Panx1 fl/fl PF4-Cre*$^-$), KO = Knock-out (*Panx1 fl/fl PF4-Cre*$^+$) [Figure from Metz, Elvers, IJMS 2022].

As shown in Figure 18 A, the release of fibrinogen was not altered between platelets from *Panx1 fl/fl PF4-Cre*$^-$ and *Panx1 fl/fl PF4-Cre*$^+$ mice (Figure 18 A). In addition, δ-granule release as measured by mepacrine release in response to high doses of thrombin and PAR4 peptide is not changed between platelets from *Panx1 fl/fl Pf4-Cre*$^+$ *and Panx1 fl/fl Pf4-Cre*$^-$ mice (Figure 18 B). CD61 exposure on the platelet surface upon CRP induced platelet activation enhances in a dose-dependent manner, while no alterations were observed between the genotypes (Figure 18 C). These data concludes that degranulation of platelet α-granules as well as δ-granules is not altered in platelets from *Panx1 fl/fl PF4-Cre*$^+$ mice compared to platelets from *Panx1 fl/fl PF4-Cre*$^-$ mice under tested conditions (Figure 18).

Nevertheless, the data indicate that platelet PANX1 modulates platelet activation and degranulation after stimulation of the ITAM coupled signaling pathway and PAR4 receptor stimulation. In order to elucidate whether platelet PANX1 channels display alterations in intracellular signaling pathways in response to CRP or PAR4 peptide, Western blot analysis were performed to analyze tyrosine phosphorylation in platelets because tyrosine phosphorylation takes a key role in cellular signal transduction [144].

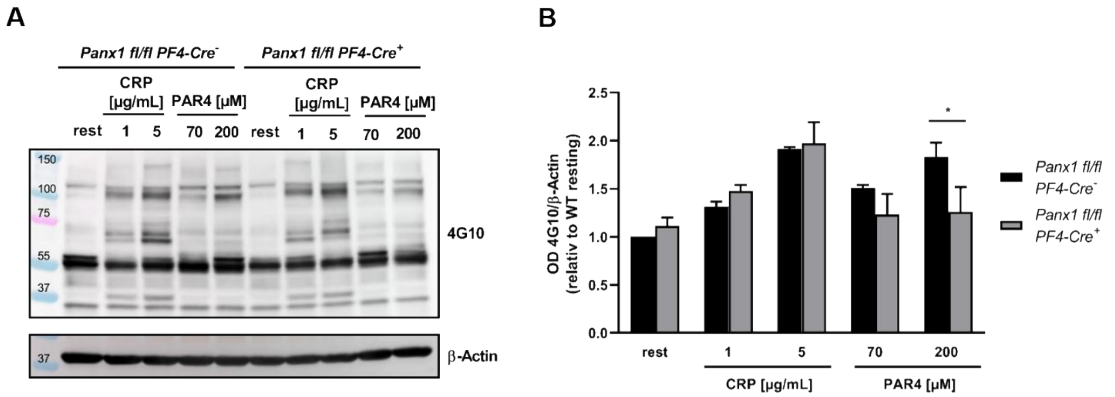

Figure 19: Tyrosine phosphorylation is altered in PANX1 deficient platelets in response to high GPCR stimulation. (A) Representative image and (B) quantification of tyrosine phosphorylation (4G10) via Western blot analysis from isolated platelets from *Panx1 fl/fl Pf4-Cre*$^{+}$ and *Panx1 fl/fl Pf4-Cre*$^{-}$ mice activated with 1 and 5 µg/mL CRP and 70 and 200 µM PAR4 peptide (n = 3). Statistical analyses were performed using a two-way ANOVA followed by a Sidak's multiple comparisons post-hoc test. Bar graphs indicate mean values ± SEM, *p < 0.05. Rest = Resting, CRP = Collagen-related peptide, PAR4 peptide = Protease-activated receptor 4 peptide, PANX1 = Pannexin 1, OD = Optical density.

As shown in Figure 19, platelet stimulation with 5 µg/mL CRP resulted in a rapid increase in tyrosine phosphorylation, but no alterations between platelets from *Panx1 fl/fl PF4-Cre*$^{-}$ and *Panx1 fl/fl PF4-Cre*$^{+}$ mice were observed (Figure 19 A). In contrast, activation of the GPCR signaling pathway by PAR4 peptide induces tyrosine phosphorylation in a dose-dependent manner, which was significantly decreased upon high dose PAR4 peptide (200 µM) in PANX1 deficient platelets compared to controls (Figure 19 B, p = 0.0491). The second wave mediators ADP and U46619 did not induce an increase in tyrosine phosphorylation (Figure 53).

4.2.2 Enhanced pro-coagulant activity only in global deleted mice compared to platelet specific pannexin 1 deletion upon collagen induced platelet activation

During platelet activation, platelets expose phosphatidylserine (PS) on their surface leading to the formation of a pro-coagulant surface [145]. PS exposure is crucial for thrombin generation leading to enhanced platelet activation and the formation of fibrin important for the stabilization of the thrombus [146]. Therefore, PS exposure was analyzed by Annexin V binding in platelets of the constitutive deleted *Panx1* and the platelet specific *Panx1 fl/fl PF4-Cre* mouse strain using washed whole blood (Figure 20). Platelet activation was induced by low and high doses of CRP, thrombin and a combination of both agonists together and assessed via flow cytometric analysis. [147].

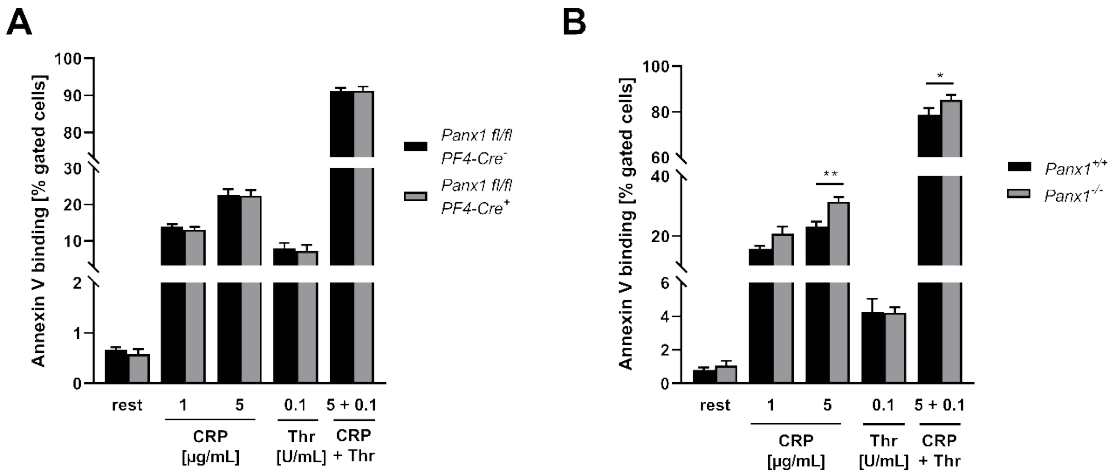

Figure 20: PS exposure is enhanced only upon high dose of ITAM coupled receptor signaling and coated platelet formation in platelets of constitutive deleted Panx1$^{-/-}$ mice compared to platelet specific *Panx1 fl/fl PF4-Cre*$^{+}$ mice. Blood of mice with (A) a platelet specific deletion of PANX1 channels (WT: *Panx1 fl/fl PF4-Cre*$^{-}$, KO: *Panx1 fl/fl PF4-Cre*$^{+}$) (n (WT) = 5-12, n (KO) = 5-10) and (B) a global deletion of PANX1 channels (WT: *Panx1*$^{+/+}$, KO: *Panx1*$^{-/-}$) (n (WT) = 5, n (KO) = 5) were analyzed regarding the PS exposure on the platelet surface upon platelet activation with indicated concentrations of collagen, thrombin and a combination of both agonists. PS exposure was assessed by the percentage of gated Annexin V positive platelets. Statistical analyses were performed using a two-way ANOVA followed by a Sidak's multiple comparisons post-hoc test. Bar graphs indicate mean values ± SEM; *p < 0.05, **p < 0.01 Rest = Resting, CRP = Collagen-related peptide, Thr = Thrombin, MFI = Mean fluorescence intensity, PS = Phospholipid phosphatidylserine, WT = Wild type, KO = Knock-out, PANX1 = Pannexin 1 [Figure 20 A from Metz, Elvers, IJMS 2022].

A platelet specific PANX1 deletion does not alter PS exposure on the platelet surface compared to platelets from *Panx1 fl/fl PF4-Cre*$^{-}$ controls in response to all tested agonists (Figure 20 A). Platelet activation with high dose CRP (5 µg/mL) leads to enhanced pro-coagulant activity only on the platelet surface of mice with a global deletion of PANX1 compared to respective controls (Figure 20 B, p = 0.003). PS exposure due to low dose CRP stimulation (1 µg/mL) and thrombin does not alter the percentage of Annexin V positive cells compared to *Panx1*$^{+/+}$ controls on the platelet surface of *Panx1*$^{-/-}$ mice (Figure 20 B). Additionally, coated platelet formation induced by CRP and thrombin together is enhanced when global PANX1 is not expressed (Figure 20 B, p = 0.0224). Overall, PANX1 deficient platelets from *Panx1*$^{-/-}$ mice do enhance the formation of a pro-coagulant surface only in response to high dose CRP (5 µg/mL) and CRP with thrombin together, which was not observed in platelets from mice with a platelet specific PANX1 deletion (Figure 20).

4.2.3 Pannexin 1 alters platelet function in response to collagen induced platelet activation

Light transmission aggregometry is a method to analyze platelet aggregation induced by various agonists. To determine functional effects between platelets from *Panx1 fl/fl PF4-Cre*$^-$ and *Panx1 fl/fl PF4-Cre*$^+$ mice, aggregometry experiments were performed in response to indicated concentrations of collagen, PAR4 peptide, and 10 µM ADP as well as 3 µM of the TxA_2 analogue U46619 at 37°C under stirring conditions at 1000 rpm (Figure 21). All experiments were performed with isolated platelets in Tyrode's buffer containing apyrase (0.04 U/mL).

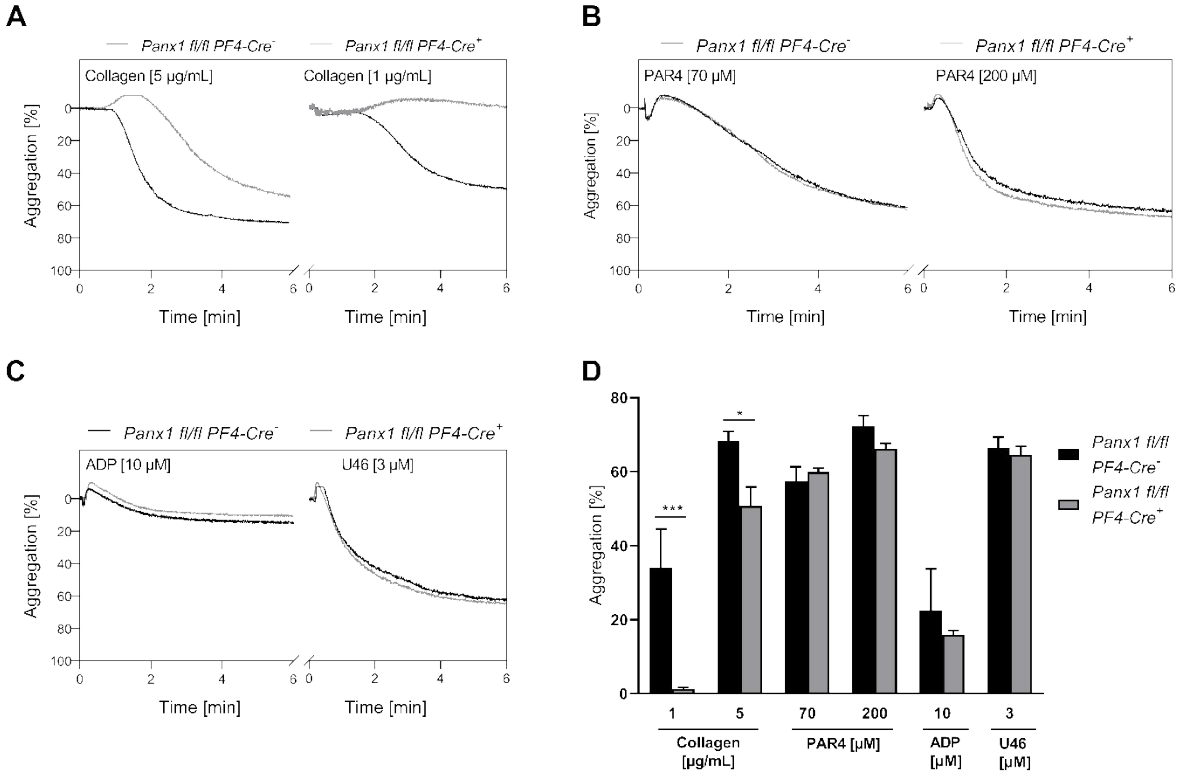

Figure 21: Aggregation is reduced in PANX1 deficient platelets in response to platelet activation with 1 and 5 µg/mL collagen compared to respective control platelets. Isolated platelets from *Panx1 fl/fl PF4-Cre*$^-$ and *Panx1 fl/fl PF4-Cre*$^+$ mice were stimulated with depicted agonists and aggregation responses were measured under apyrase (0.04 U/mL) by light transmission aggregometry for 6 min. Representative curves of aggregation-responses of platelet activation with (A) 5 µg/mL (n (WT) = 4, n (KO) = 9) and 1 µg/mL collagen (n (WT) = 4, n (KO) = 7), (B) 70 µM (n (WT) = 6, n (KO) = 10) and 200 µM PAR4 peptide (n (WT) = 6, n (KO) = 10) and (C) 10 µM ADP (n (WT) = 4, n (KO) = 6) and 3 µM U46 (n (WT) = 6, n (KO) = 10) from *Panx1 fl/fl PF4-Cre*$^-$ and *Panx1 fl/fl PF4-Cre*$^+$ platelets. (D) Graph displays results of the maximal detected aggregation responses for all tested agonists. Statistical analyses were performed using a two-way ANOVA followed by a Sidak's multiple comparisons post-hoc test. Bar graphs indicate mean values ± SEM; *p < 0.05, ***p < 0.001. Rest = Resting, CRP = Collagen-related peptide, PAR4 peptide = Protease-activated receptor 4 peptide, ADP = Adenosine diphosphate, U46 (U46619) = Thromboxane A_2 analogue, WT = Wild type (*Panx1 fl/fl PF4-Cre*$^-$), KO = Knock-out (*Panx1 fl/fl PF4-Cre*$^+$), PANX1 = Pannexin 1 [Figure from Metz, Elvers, IJMS 2022].

As indicated in Figure 21, platelet aggregation was altered only in response to collagen induced platelet activation (Figure 21 A, D). In detail, aggregation was diminished about 96% in platelets from *Panx1 fl/fl PF4-Cre*$^{+}$ mice (1.3 ± 0.42% (SEM)) compared to platelets from *Panx1 fl/fl PF4-Cre*$^{-}$ mice (34 ± 10.5% (SEM)) in response to 1 µg/mL collagen (Figure 21 A, D, $p < 0.0001$). High dose platelet activation with 5 µg/mL collagen reduces aggregation from PANX1 deficient platelets compared to respective controls (WT: 68.3 ± 2.66% (SEM); KO: 56 ± 3.36% (SEM), $p = 0.018$). Low and high dose platelet activation with PAR4 peptide (70 µM and 200 µM) does not alter aggregation responses between both genotypes (Figure 21 B, D, 70 µM: WT: 57.5 ± 3.84% (SEM), KO: 59.1 ± 1.46% (SEM); 200 µM: WT: 72.3 ± 2.87% (SEM), KO: 67.9 ± 1.64% (SEM). Figure 21 C and D show no differences between platelets from *Panx1 fl/fl PF4-Cre*$^{-}$ and *Panx1 fl/fl PF4-Cre*$^{+}$ mice in response to platelet activation with 10 µM ADP (WT: 22.5 ± 11.23% (SEM); KO: 15.8 ± 1.46% (SEM)) and 3 µM U46619 (WT: 66.5 ± 2.87% (SEM); KO: 63.7 ± 2.96% (SEM)). Taken together, PANX1 channels are involved in GPVI mediated aggregation upon collagen induced platelet stimulation (Figure 21 A, D). Activation of the other tested signaling pathways do not alter platelet aggregation (Figure 21 B, C, D).

4.2.4 Pannexin 1 is involved in thrombus formation under flow conditions *ex vivo* at arterial shear rates

Chapter 4.2.3 confirmed that platelet PANX1 channels have an impact on collagen induced platelet activation (Figure 21). Previous studies indicated that PANX1 channels are mechanosensitive in response to shear induced mechanical stretch as it is the case in the vasculature [148]. Therefore, we aim to study the role of PANX1 channels under dynamic conditions *ex vivo* by flow chamber experiments. This method enables analysis of thrombus formation including the involvement of dynamic forces in the blood flow by adjusting different arterial shear rates. Murine whole blood from both platelet specific *Panx1 fl/fl PF4-Cre*$^{-}$ and *Panx1 fl/fl PF4-Cre*$^{+}$ mice was collected and perfused over a collagen (200 µg/mL) coated matrix to analyze thrombus formation (Represented by surface coverage) and thrombus volume (Measured by the MFI) under flow conditions as displayed in Figure 22.

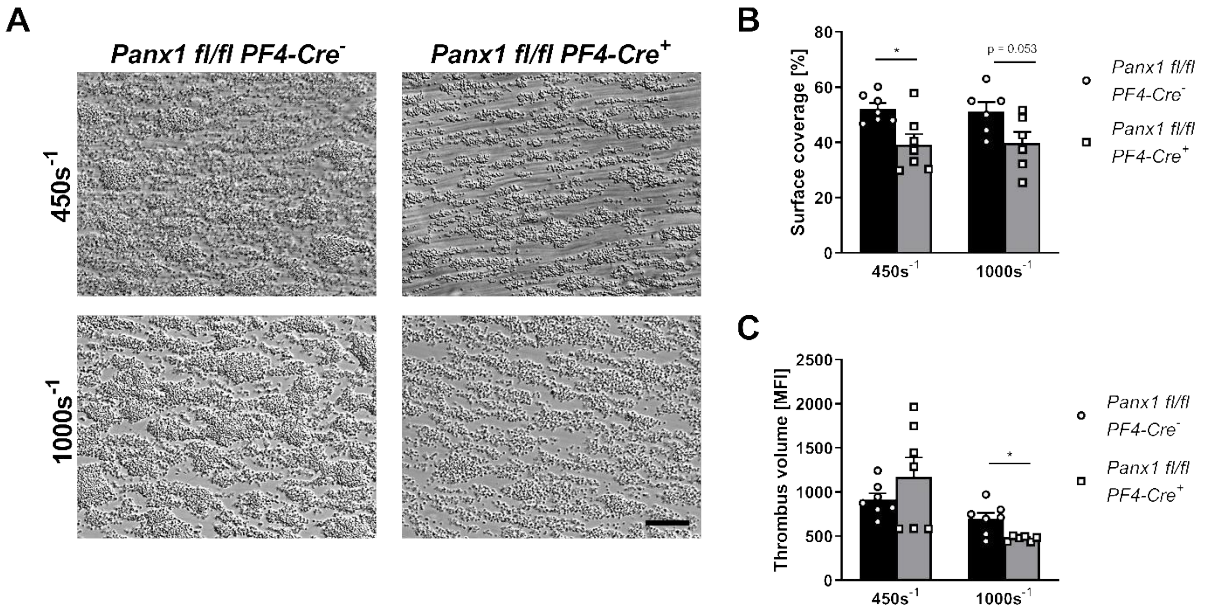

Figure 22: Whole blood from *Panx1 fl/fl PF4-Cre*$^{+}$ mice leads to impaired thrombus formation at a shear rate of 1,000s^{-1} and reduced thrombus volume at a shear rate of 450s^{-1}. (A) Representative BF images of thrombus formation with whole blood from *Panx1 fl/fl PF4-Cre*$^{-}$ and *Panx1 fl/fl PF4-Cre*$^{+}$ mice at 1,000s^{-1} and 450s^{-1} shear rates Scale bar represents 100 µm. (B) Thrombus formation, measured by the surface coverage in percent was determined at 450s^{-1} (n (WT) = 7, n (KO) = 7) and 1,000s^{-1} (n (WT) = 7, n (KO) = 6). (C) Thrombus volume was assessed by the MFI of the fluorescently labeled platelets at a shear rate of 1,000s^{-1} (n (WT) = 7, n (KO) = 7) and 450s^{-1} (n (WT) = 7, n (KO) = 6). Statistical analyses were performed using (B, C) an unpaired multiple student's t-test. Bar graphs indicate mean values ± SEM, *p < 0.05. MFI = Mean fluorescence intensity, WT = Wild type (*Panx1 fl/fl PF4-Cre*$^{-}$), KO = Knock-out (*Panx1 fl/fl PF4-Cre*$^{+}$), Panx1 = Pannexin 1, BF = Bright field [Figure from Metz, Elvers, IJMS 2022].

Analysis of flow chamber experiments at low arterial shear rates of 450s^{-1} displayed that thrombus formation is impaired with whole blood from platelet specific *Panx1 fl/fl PF4-Cre*$^{+}$ mice , which is shown by a reduction of the surface coverage compared to respective controls (Figure 22 B, p = 0.0127). In detail, the covered area with three-dimensional thrombi was 52.31 ± 1.94% (SEM) for *Panx1 fl/fl PF4-Cre*$^{-}$ mice and 39.25 ± 3.78% (SEM) for *Panx1 fl/fl PF4-Cre*$^{+}$ mice (Figure 22 B). At a shear rate of 450s^{-1}, no alterations between *Panx1 fl/fl PF4-Cre*$^{-}$ and *Panx1 fl/fl PF4-Cre*$^{+}$ mice were observed with regard to the three-dimensional structure of the thrombi as measured by the MFI of the thrombus volume (Figure 22 C). In contrast, the thrombus volume is reduced when whole blood from *Panx1 fl/fl PF4-Cre*$^{+}$ mice was perfused through the chamber using an intermediate arterial shear rate of 1,000s^{-1} compared to controls (Figure 22 C, p = 0.0102). At a shear rate of 1,000s^{-1}, the surface coverage was only altered by trend between the indicated groups (Figure 22 B, WT: 48.7 ± 3.83% (SEM), KO: 38.76 ± 4.09% (SEM), p = 0.089). Together, these results display a functional role of platelet PANX1 channels in thrombus formation at low- and intermediate arterial shear rates (Figure 22).

As a translational approach, PANX1 channels were inhibited by either 100 µM Prb or 10 µM Cbx in human whole blood. Like previous experiments, thrombus formation and thrombus volume were analyzed after perfusion of human whole blood with or without pre-treatment of PANX1 inhibitors. Flow chamber experiments with human whole blood pretreated with 100 µM Prb resulted in reduced thrombus formation as measured by the surface coverage at both conditions (Figure 22). At a shear rate of $450s^{-1}$, surface coverage was 12.8 ± 1.36% (SEM), which was reduced up to 9.4 ± 0.5% (SEM) when PANX1 was inhibited by Prb (Figure 23 B, p = 0.0073). At an intermediate arterial shear rate ($1000s^{-1}$), PANX1 inhibition resulted in a thrombus covered area of 17.7 ± 0.99% (SEM), while the surface coverage of controls was increased (Figure 23 B, C, 21.3 ± 0.76% (SEM), p = 0.0017). A significant reduction in thrombus volume was observed at $1,000s^{-1}$ (p = 0.0092), while the three-dimensional structure of the thrombi was altered at low ($450s^{-1}$) arterial shear rates only by trend (Figure 23 C, B, p = 0.0572).

Similar results were obtained after pretreatment of human whole blood with 10 µM Cbx compared to controls. In detail, surface coverage was reduced up to 13.8 ± 1.39% (SEM) after pretreatment with Cbx in comparison to controls (16.6 ± 1.56% (SEM)) at low arterial shear rates of $450s^{-1}$ (Figure 23 E, p = 0.0127). Moreover, thrombus volume was reduced only by trend after PANX1 inhibition with Cbx (p = 0.0774) at $450s^{-1}$ (Figure 23 F). At an arterial shear rate of $1,000s^{-1}$, surface coverage was 18.3 ± 0.74% (SEM) for control conditions, while Cbx application reduces the percentage of covered surface to 16.1 ± 0.96% (SEM) (Figure 23 E, p = 0.0488). Moreover, the application of Cbx reduces thrombus volume significantly at a shear rate of $1000s^{-1}$ (Figure 23 F, p = 0.0488).

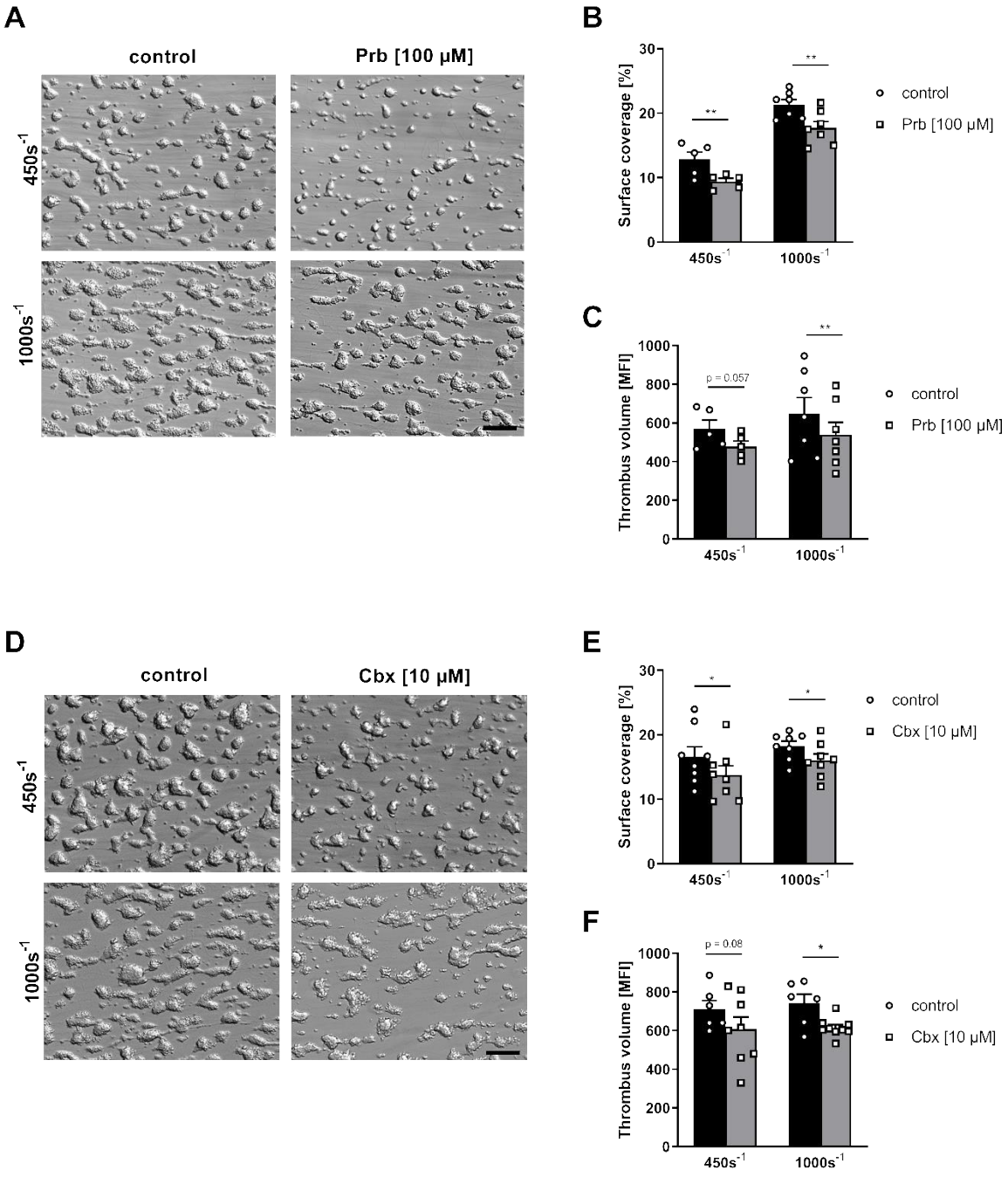

Figure 23: Pharmacological inhibition of PANX1 leads to reduced thrombus formation at arterial shear rates *ex vivo*. Human whole blood was perfused over a collagen (200 µg/mL) coated matrix with or without pretreatment with (A-C) 100 µM Prb at 450s^{-1} (n (control) = 5, n (Prb) = 5) or 1,000s^{-1} (n (control) = 7, n (Prb) = 7) and (D-E) 10 µM Cbx at 450s^{-1} (n (control) = 7-8, n (Prb) = 8) or 1,000s^{-1} (n (control) = 8-9, n (Prb) = 8-9). (A, D) Representative BF images of whole blood pretreated with Prb or Cbx perfused at either 450s^{-1} or 1,000s^{-1} over collagen coated matrices *ex vivo*. Scale bar represents 100 µm. (B, E) Analysis of surface coverage [%] and (C, F) thrombus formation [MFI]. Statistical analyses were performed using a two-way ANOVA followed by a Sidak's multiple comparisons post-hoc test. Bar graphs indicate mean values ± SEM, *p < 0.05: **p < 0.01. Prb = Probenecid, Cbx = Carbenoxolone, MFI = Mean fluorescence intensity, BF = Bright field, PANX1 = Pannexin 1 [Figure from Metz, Elvers, IJMS 2022].

Taken together these results demonstrate that PANX1 channels have an impact on thrombus formation at low ($450s^{-1}$) and intermediate ($1{,}000s^{-1}$) arterial shear rates. In mice, platelet PANX1 deletion resulted in reduced surface coverage at $450s^{-1}$ and reduced thrombus volume at $1{,}000s^{-1}$ (Figure 22). Using human platelets, application of the PANX1 inhibiting compounds Prb and Cbx resulted in reduced surface coverage at both shear rates, while thrombus volume was only altered at a shear rate of $1{,}000s^{-1}$ (Figure 23). At a shear rate of $450s^{-1}$, thrombus volume was diminished only by trend after PANX1 inhibition with Prb or Cbx (Figure 23).

Overall, the results display a functional role for platelet PANX1 channels in thrombosis and hemostasis as seen by reduced ATP release, reduced aggregation and thrombus formation especially in response to ITAM-coupled mediated signaling. So far, it is not known how platelets regulate the activation of PANX1 channels. Therefore, PANX1 dependent signaling in platelets was investigated as shown in the following paragraph.

4.3 The platelet pannexin 1 channel is phosphorylated after platelet activation

The regulation of ion channel activity is partially mediated via post-translational modifications. It was shown that PANX1 consists of several phosphorylation sites [149-151]. Until now, two phosphorylation sites at tyrosine (Tyr) residues for PANX1 channels are known, Tyr^{198} and Tyr^{308}, respectively. Phosphorylation at these tyrosine residues activate PANX1 channels, as demonstrated in various cell types of the vasculature [148, 151]. Immunofluorescence (IF) staining in human platelets indicated that phosphorylation at PANX1 Tyr^{308} is increased after collagen dependent platelet activation [82]. To date, the regulation of PANX1 activation by Tyr^{198} phosphorylation in platelets is not known. Since platelet activation is mediated by various platelet receptors activating different intracellular signaling pathways, phosphorylation studies via Western blot analysis of PANX1 Tyr^{198} and PANX1 Tyr^{308} in human platelets in response to classical platelet agonists were performed (Figure 24).

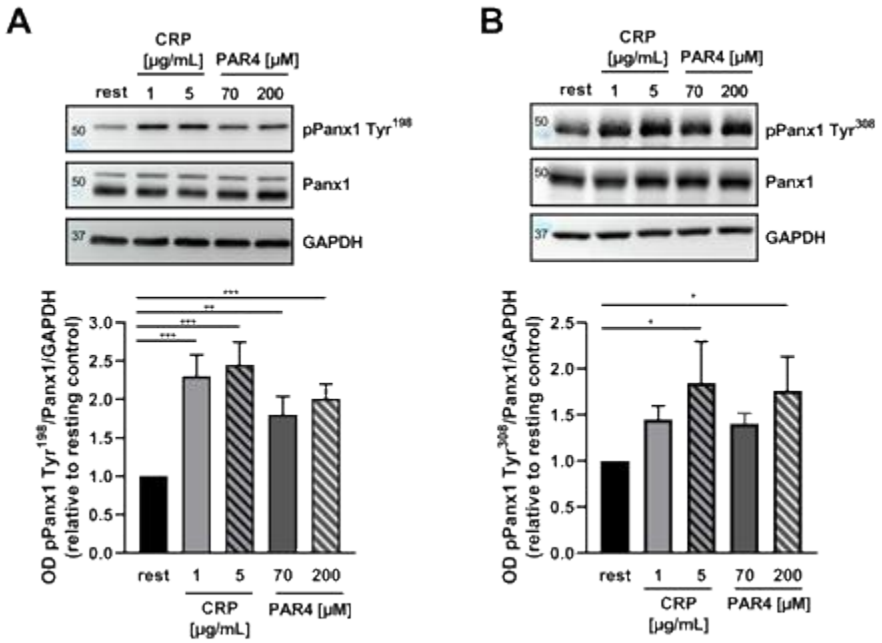

Figure 24: PANX1 is phosphorylated at Tyr^{198} and Tyr^{308} after platelet activation with CRP and PAR4 peptide. Western blot analysis and quantification of (A) PANX1 Tyr^{198} (n = 9) and (B) PANX1 Tyr^{308} (n = 4) after platelet activation with 1 and 5 µg/mL CRP and 70 and 200 µM PAR4 peptide. Statistical analyses were performed using a one-way ANOVA (compared to resting) followed by a Sidak's multiple comparisons post-hoc test. Bar graphs indicate mean values ± SEM, *p < 0.05: **p < 0.01 and ***p < 0.001. Rest = Resting, CRP = Collagen-related peptide, PAR4 peptide = Protease-activated receptor 4 peptide [Figure from Metz, Elvers, IJMS 2022].

Platelet activation with CRP (Collagen-related peptide) as well as PAR4 peptide resulted in an increase in PANX1 Tyr^{198} phosphorylation compared to unstimulated platelets (= platelet resting control, Figure 24 A). In detail, platelet activation with 1 µg/mL CRP leads to a 2.3 ± 0.28 (SEM; $p < 0.0001$) fold increase in phosphorylation levels, while high dose stimulation resulted in 2.45 ± 0.3 (SEM; $p < 0.0001$) fold increase compared to unstimulated platelets (Figure 24 A). Phosphorylation levels at PANX1 Tyr^{198} in response to low (70 µM) and high dose (200 µM) PAR4 peptide stimulation resulted in a 1.80 ± 0.24 (SEM; $p < 0.0001$) and 2.01 ± 0.19 (SEM; $p < 0.0001$) fold increase compared to unstimulated platelets, respectively (Figure 24 A).

PANX1 Tyr^{308} phosphorylation is increased after high dose CRP stimulation compared to platelet resting (1.85 ± 0.45 (SEM); $p = 0.04$) in contrast to low dose platelet activation with CRP, which did not induce a significant increase in phosphorylation of PANX1 Tyr^{308} (Figure 24 B, 1.45 ± 0.15 (SEM)). The same result regarding PANX1 Tyr^{308} phosphorylation was obtained after low and high dose PAR4 stimulation (70 µM: 1.4 ± 0.11 (SEM); 200 µM: 1.76 ± 0.37 (SEM)) as shown by Figure 24 B.

To evaluate if platelet second wave mediators ADP and TxA_2 also lead to PANX1 phosphorylation at either Tyr^{198} or Tyr^{308}, corresponding experiments were performed. For platelet activation with TxA_2, the analogue U46619 (U46) was used for all experiments (Figure 25).

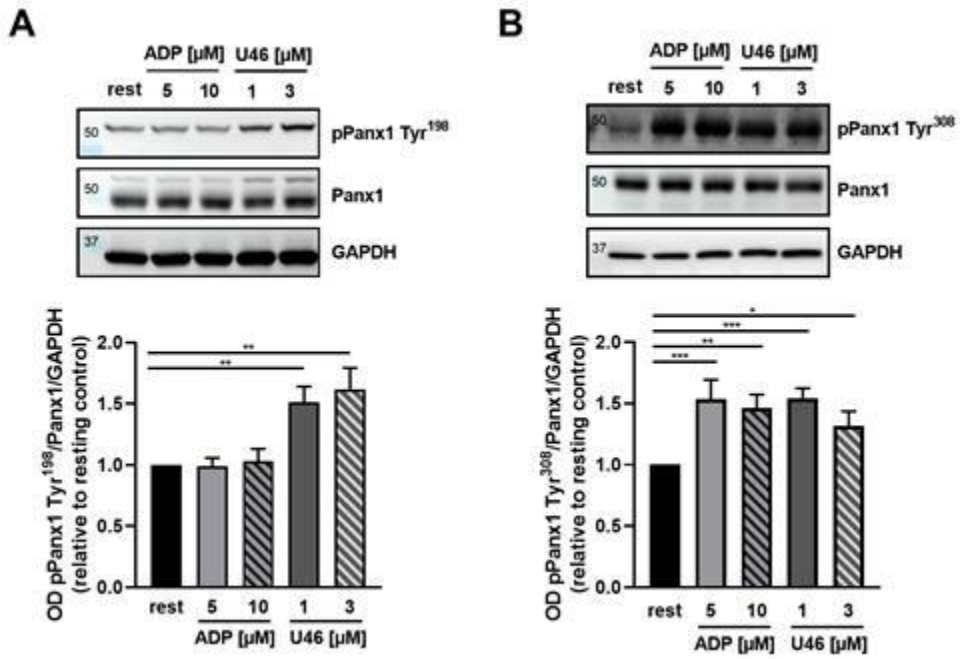

Figure 25: Second wave mediators are also involved in platelet PANX1 phosphorylation. Western blot analysis and quantification of (A) PANX1 Tyr^{198} (n = 7) and (B) PANX1 Tyr^{308} (n = 8) after platelet activation with 5 and 10 µM ADP and 1 and 3 µM U46. Statistical analyzes were performed using a one-way ANOVA (compared to resting) followed by a Sidak's multiple comparisons post-hoc test. Bar graphs indicate mean values ± SEM, *p < 0.05: **p < 0.01 and ***p < 0.001. Rest = Resting, ADP = Adenosine diphosphate, U46 (U46619) = Thromboxane A_2 analogue [Figure from Metz, Elvers, IJMS 2022].

Phosphorylation of PANX1 at Tyr^{198} was only increased after low (1 µM: 1.51 ± 0.13 (SEM) p = 0.009) and high dose (3 µM: 1.62 ± 0.17 (SEM) p = 0.002) U46619 stimulation, while no increase in phosphorylation was observed after low and high dose ADP stimulation compared to unstimulated platelets (5 µM: 0.99 ± 0.07 (SEM); 10 µM: 1.03 ± 0.10 (SEM)) as shown in Figure 25 A. In comparison to the previous results, phosphorylation of PANX1 at Tyr^{308} is also increased after low (1 µM: 1.54 ± 0.09 (SEM) p = 0.0004) and high dose U46619 stimulation (3 µM: 1.32 ± 0.12 (SEM) p = 0.043) when compared to resting platelets (Figure 25 B). Platelet activation with ADP also lead to enhanced phosphorylation levels of PANX1 Tyr^{308} (Figure *25* B) in response to 5 µM (1.54 ± 0.16 (SEM) p = 0.0005) and 10 µM ADP (1.47 ± 0.11 (SEM) p = 0.002) in comparison to unstimulated platelets. Overall, these results display that PANX1 is phosphorylated at Tyr^{198} and Tyr^{308} after platelet activation with different concentrations of classical platelet agonists. In detail, G-protein coupled receptors (GPCR) activation by low (70 µM) and high doses (200 µM) of PAR4 peptide and ITAM coupled receptor signaling induced by 1 and 5 µg/mL CRP led to phosphorylated of PANX1 Tyr^{198}, while only high doses induce

PANX1 Tyr^{308} phosphorylation (Figure 24). The second wave mediators U46619 and ADP lead to phosphorylation of PANX1 Tyr^{308}, but only low (1 µM) and high doses (3 µM) of U46619 induce PANX1 Tyr^{198} phosphorylation (Figure 25).

4.3.1 Collagen-depended pannexin 1 Tyr^{198} phosphorylation is mediated by the GPVI signaling pathway

The results in chapter 4.3 indicate that GPVI mediated platelet activation via CRP induces maximum increase in PANX1 Tyr^{198} phosphorylation compared to all tested platelet receptor agonists. Since GPVI receptors are the physiological receptors for collagen induced platelet activation during vascular injury [21], we aim to understand if PANX1 Tyr^{198} phosphorylation is diminished when GPVI receptors are not expressed on platelets. To investigate the impact of GPVI in this process, platelets from *Gp6*$^{-/-}$ mice and WT control mice were activated with indicated concentrations of CRP, ADP and PAR4 peptide and phosphorylation of PANX1 at Tyr^{198} was investigated (Figure 26).

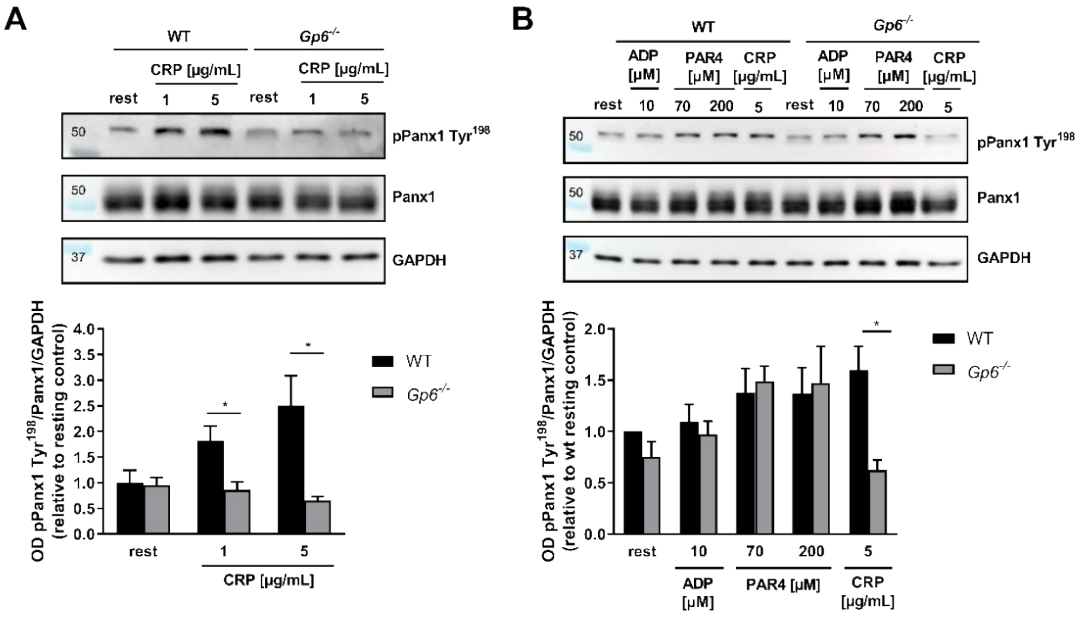

Figure 26: Phosphorylation of PANX1 Tyr^{198} is diminished to levels of resting platelets upon CRP stimulation of GPVI deficient platelets. GPVI WT vs. GPVI deficient platelets were activated with indicated agonists and phosphorylation studies of PANX1 Tyr^{198} were performed. Graphs show representative Western blot image and quantification of PANX1 Tyr^{198} phosphorylation (A) in response to indicated concentrations of CRP (n = 4) and (B) in response to 10 µM ADP as well as 70 µM and 200 µM PAR4 peptide (CRP served as a positive control, n = 3). Statistical analyses were performed using (A) a two-way ANOVA followed by a Sidak's multiple comparisons post-hoc test. Bar graphs indicate mean values ± SEM, *p < 0.05. Rest = Resting, CRP = Collagen-related peptide, PAR4 peptide = Protease-activated receptor 4 peptide, ADP = Adenosine diphosphate, PANX1 = Pannexin 1 [Figure 26 A from Metz, Elvers, IJMS 2022].

Figure 26 A displays the analysis of phosphorylation of PANX1 at Tyr^{198} in GPVI deficient platelets. The results indicate that phosphorylation of PANX1 Tyr^{198} is diminished to phosphorylation levels of unstimulated platelets compared to their respective controls in response to 1 µg/mL CRP ($p = 0.028$) and 5 µg/mL CRP ($p = 0.019$). In contrast, platelet activation with ADP and PAR4 peptide did not alter PANX1 Tyr^{198} phosphorylation in platelets from *Gp6*$^{-/-}$ compared to control mice (Figure 26 B). Overall, these results confirm that collagen induced PANX1 Tyr^{198} phosphorylation is diminished in platelets from *Gp6*$^{-/-}$ mice (Figure 26 A). A genetic deletion of *Gp6*$^{-/-}$ in platelets does not lead to altered PANX1 Tyr^{198} phosphorylation after platelet activation with ADP and PAR4 peptide (Figure 26 B).

A previous study indicated, that Src family kinases (SFKs) are key regulators of PANX1 Tyr^{198} phosphorylation during vasoconstriction [151], we aim to understand if and how Src phosphorylation is altered when platelet PANX1 is not expressed. Src is regulated by tyrosine phosphorylation at two distinct sites, Tyr^{416} and Tyr^{527}, while phosphorylation at Src Tyr^{416} displays the active state of Src [152]. For this reason, the activating phosphorylation site was selected for further analysis. Alterations in Src phosphorylation at Tyr^{416} were investigated using PANX1 deficient and control mouse platelets in response to CRP (Figure 27).

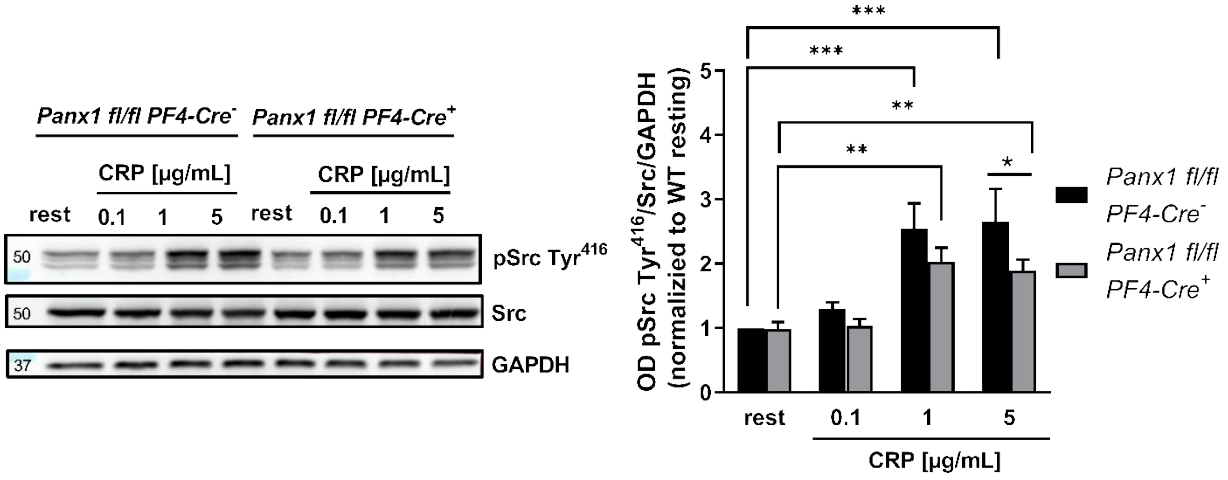

Figure 27: A genetic deletion of PANX1 in platelets leads to reduced Src phosphorylation at Tyr^{416} upon 5 µg/mL CRP stimulation. (A) Representative Western blot of platelets of *Panx1 fl/fl PF4-Cre*$^{-}$ and *Panx1 fl/fl PF4-Cre*$^{+}$ mice after stimulation with 0.1, 1 and 5 µg/mL CRP. (B) Quantification of Src Tyr^{416} phosphorylation from *Pan1 fl/fl PF4-Cre*$^{-}$ and *Panx1 fl/fl PF4-Cre*$^{+}$ mice upon 0.1, 1 and 5 µg/mL CRP stimulation (n = 4). Statistical analyses were performed using a two-way ANOVA followed by a Sidak's multiple comparisons post-hoc test (Compared to unstimulated platelets within each genotype and between genotypes). Bar graphs indicate mean values ± SEM, *$p < 0.05$: **$p < 0.01$ and ***$p < 0.001$. Rest = Resting, CRP = Collagen-related peptide, PANX1 = Pannexin 1.

Figure 27 displays that Src phosphorylation at Tyr^{416} increases upon stimulation with 1 and 5 µg/mL CRP in platelets from *Panx1 fl/fl PF4-Cre*$^{-}$ (1 µg/mL: $p < 0.001$; 5 µg/mL: $p < 0.001$) and *Panx1 fl/fl PF4-Cre*$^{+}$ mice (1µg/mL: $p = 0.002$); 5 µg/mL: $p = 0.007$) compared to unstimulated

platelets (Figure 27). A genetic deletion of PANX1 in platelets led to significantly reduced Src phosphorylation at Tyr^{416} upon high dose CRP (5 µg/mL) stimulation compared to platelets from control mice (Figure 27 B, p = 0.015). Taken together, a genetic deletion of platelet PANX1 channels in mice led to alterations of Src activation as shown by reduced phosphorylation at Src Tyr^{416} in response to platelet high ITAM coupled receptor activation (Figure 27).

4.4 Src Family Kinases are the major regulators of pannexin 1 phosphorylation at Tyr^{198}

In different cells it was demonstrated that PANX1 phosphorylation depends on SFKs, Protein Kinase A (PKA) and Protein Kinase C (PKC) [149-151]. PANX1 Tyr^{308} phosphorylation in platelets was shown to be dependent on SFKs after collagen-dependent platelet activation [82]. To investigate, if PANX1 Tyr^{198} phosphorylation also rely on SFKs in platelets, human platelets were preincubated with 20 µM of the SFK inhibiting compound PP2 and activated with different platelet receptor agonists. The inactive analogue PP3 served as a negative control (Figure 28).

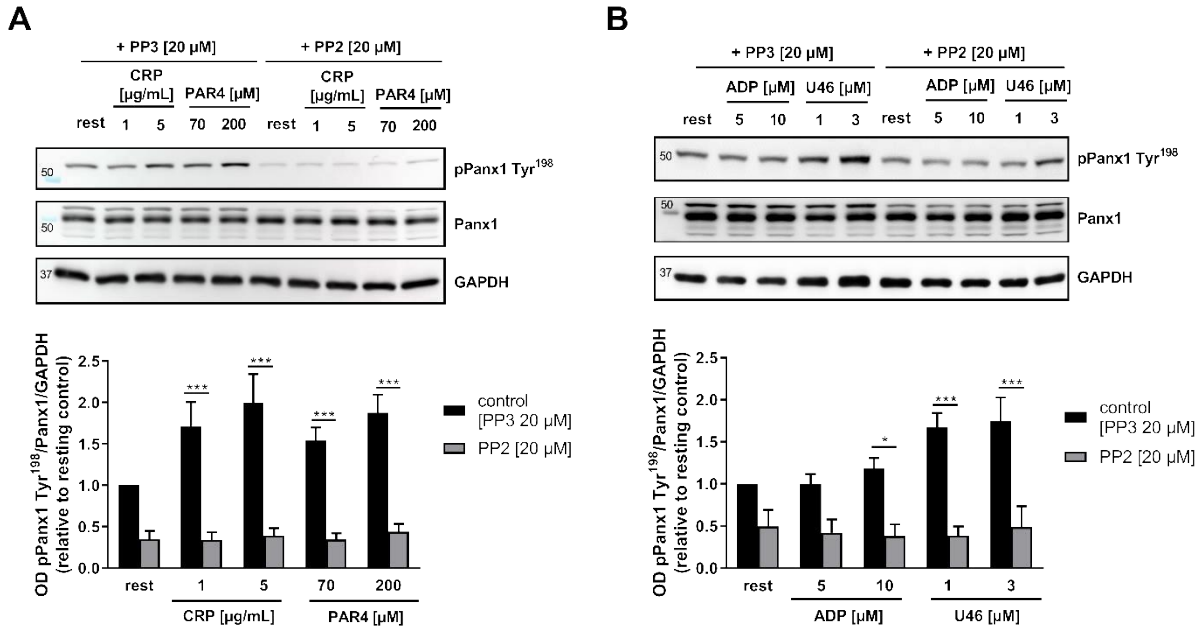

Figure 28: PANX1 Tyr^{198} phosphorylation completely depends on SFKs. Representative images and quantification of Western blot analysis from human isolated platelets with or without pre-incubation with the SFK inhibiting compound PP2 or PP3 (negative control). (A) Isolated platelets were activated with 1 and 5 µg/mL CRP and 70 and 200 µM PAR4 peptide (n = 6). (B) Isolated platelets were activated with 5 and 10 µM ADP and 1 and 3 µM U46 (n = 4). Statistical analyses were performed using a two-way ANOVA followed by a Sidak's multiple comparisons post-hoc test. Bar graphs indicate mean values ± SEM, *p < 0.05: ***p < 0.001. Rest = Resting, CRP = Collagen-related peptide, PAR4 peptide = Protease-activated receptor 4 peptide, ADP = Adenosine diphosphate, U46 (U46619) = Thromboxane A_2 analogue, SFK = Src Family Kinases, PANX1 = Pannexin 1 [Figure from Metz, Elvers, IJMS 2022].

The results in Figure 28 A show that platelet pre-incubation with the SFK inhibiting compound PP2 abolished PANX1 Tyr^{198} phosphorylation in response to all tested concentrations of CRP ($p < 0.0001$) and PAR4 peptide ($p < 0.0001$). The same results were obtained after platelet activation with the second wave mediator U46619 (Figure 28 B, 1 µM: $p = 0.0001$; 3 µM: $p = 0.0001$). Additionally, a high dose ADP stimulation (10 µM) also leads to a significant decrease in PANX1 Tyr^{198} phosphorylation when SFKs are inhibited by PP2 (Figure 28 B, $p = 0.01$). Inhibition of SFKs decreases PANX1 Tyr^{198} phosphorylation only by trend in unstimulated resting platelets (Figure 28 A, $p = 0.06$). Taken together, no increase in PANX1 Tyr^{198} phosphorylation was observed after inhibition of SFKs with PP2 to control platelets indicating that activation of SFKs is crucial for PANX1 phosphorylation at Tyr^{198}.

4.4.1 Pannexin 1 phosphorylation at Tyr^{308} depends on SFKs only upon high dose CRP stimulation

The results from chapter 4.3.1 confirm that PANX1 Tyr^{198} phosphorylation is fully dependent on SFKs. A previous study displayed that PANX1 Tyr^{308} phosphorylation is abolished in collagen activated platelets after application of the SFK inhibiting compound PP2 shown by IF stainings [82]. To identify if SFKs are also key players in the regulation of PANX1 Tyr^{308} phosphorylation in response to PAR4 peptide, U46 and ADP, human platelets were preincubated with the SFK inhibiting compound PP2 and activated with indicated agonists. The inactive analogue PP3 served as a negative control and phosphorylation studies of PANX1 Tyr^{308} were performed via Western blot analysis (Figure 29).

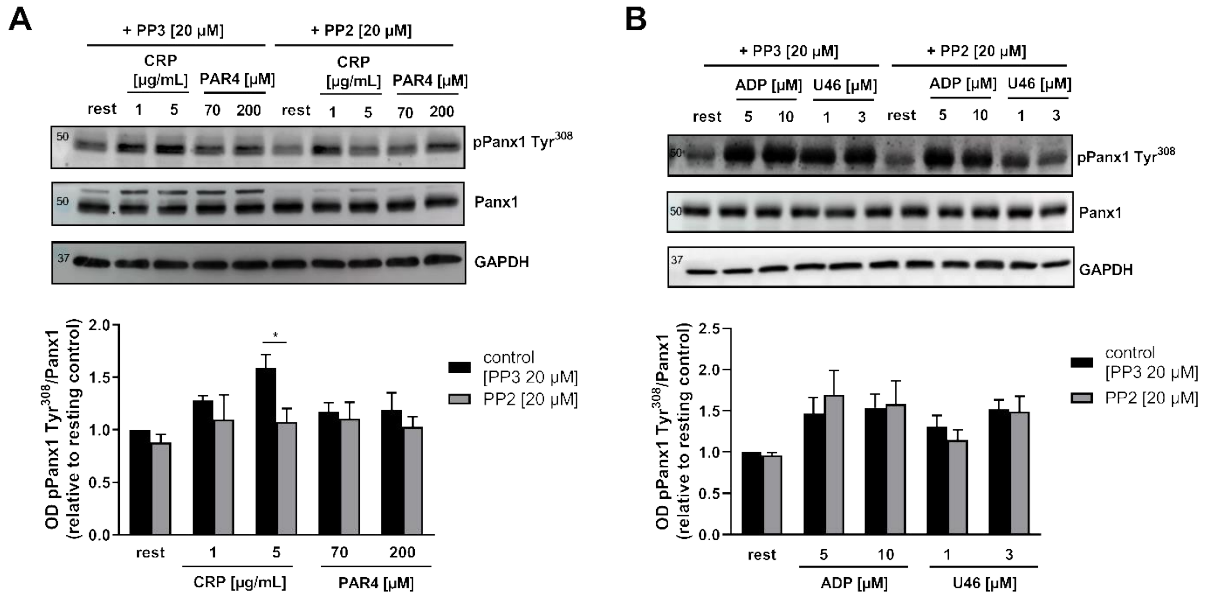

Figure 29: SFKs are responsible for PANX1 Tyr^{308} phosphorylation in human platelets only after high dose CRP stimulation. Representative Western blot image and quantification of phosphorylation of PANX1 Tyr^{308} after inhibition of Src family kinases by pre-incubation of platelets with PP2; PP3 served as a negative control. (A) Platelets were activated with 1 and 5 µg/mL CRP and 70 and 200 µM PAR4 peptide (n = 4). (B) Platelets were activated with 5 and 10 µM ADP and 1 and 3 µM U46 (n = 9). Statistical analyses were performed using a two-way ANOVA followed by a Sidak's multiple comparisons post-hoc test. Bar graphs indicate mean values ± SEM, *p < 0.05. Rest = Resting, CRP = Collagen-related peptide, PAR4 peptide = Protease-activated receptor 4 peptide, ADP = Adenosine diphosphate, U46 (U46619) = Thromboxane A_2 analogue, SFKs = Src Family Kinases, PANX1 = Pannexin 1 [Figure from Metz, Elvers, IJMS 2022].

The results demonstrate that PANX1 phosphorylation at Tyr^{308} is decreased on SFKs only upon platelet activation with 5 µg/mL CRP (Figure 29 A, p = 0.037). PANX1 Tyr^{308} phosphorylation was not significantly reduced after platelet activation with low or high dose stimulation of PAR4 peptide (Figure 29 A), ADP and U46 under the application of PP2 (Figure 29 B). These results show that PANX1 Tyr^{308} phosphorylation is not only dependent on SFKs, indicating that other kinases might be involved in the regulation of PANX1 Tyr^{308}.

4.4.2 PKC is partially involved in pannexin 1 phosphorylation at Tyr^{198} and Tyr^{308}

Beside SFKs, it was shown that PANX1 phosphorylation is partially regulated by PKC and PKA [149-151]. In platelets, GPVI mediated signaling results in Ca^{2+} influx in platelets by activation of the downstream signaling cascade thus samplifying PKC activation (1.1.2.3). To further evaluate the intracellular signaling mechanisms inducing PANX1 phosphorylation at either Tyr^{198} or Tyr^{308}, PKC was inhibited by Ro-31-8220 (RO) and phosphorylation analyses were performed. In detail, human platelets were preincubated with 20 µM RO and activated with indicated agonists. DMSO served as a negative control (Figure 30).

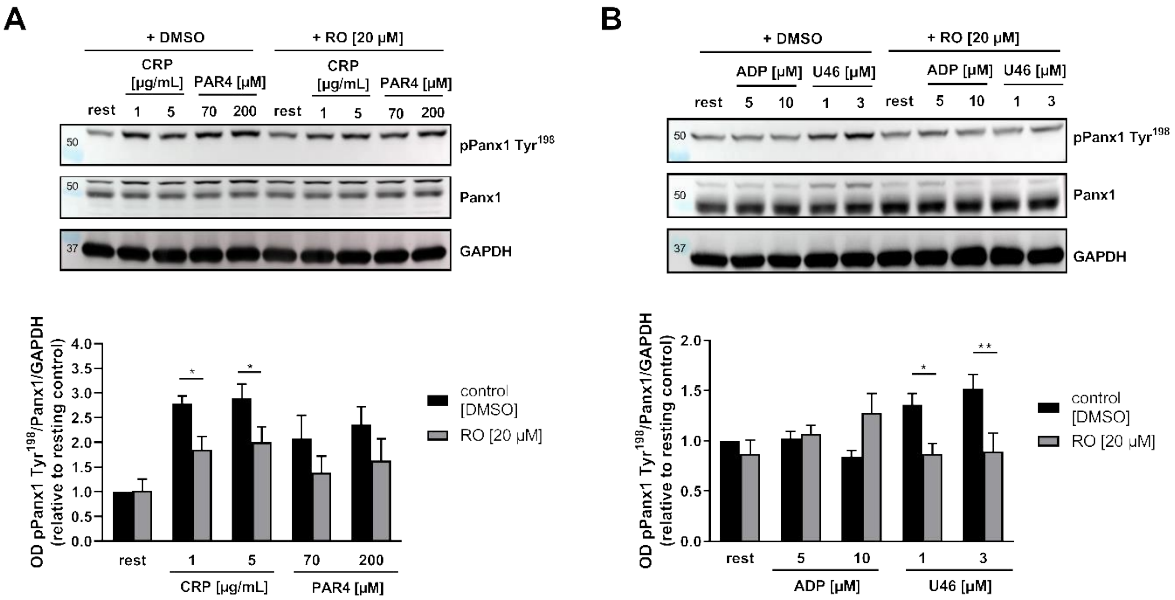

Figure 30: PKC is partially involved in PANX1 Tyr^{198} phosphorylation in response to platelet activation with low dose CRP and PAR4 peptide as well as both concentrations of U46619. Representative Western blot image and quantification of phosphorylation of PANX1 Tyr^{198} after inhibition of PKC by pre-incubation of platelets with Ro-31-8220 (RO) or DMSO as a negative control. (A) Platelets were activated with 1 and 5 µg/mL CRP and 70 and 200 µM PAR4 peptide (n = 3). (B) Platelets were activated with 5 and 10 µM ADP and 1 and 3 µM U46 (n = 4). Statistical analyses were performed using a two-way ANOVA followed by a Sidak's multiple comparisons post-hoc test. Bar graphs indicate mean values ± SEM, *p < 0.05: **p < 0.01 and ***p < 0.001. Rest = Resting, CRP = Collagen-related peptide, PAR4 peptide = Protease-activated receptor 4 peptide, ADP = Adenosine diphosphate, U46 (U46619) = Thromboxane A_2 analogue, PKC = Protein Kinase C, DMSO = Dimethyl sulfoxide [Figure from Metz, Elvers, IJMS 2022].

As shown in Figure 30 A the inhibition of PKC by RO led to a significantly decrease demonstrated by PANX1 phosphorylation at Tyr^{198} following low dose CRP (1 µg/mL, p = 0.034) and high dose CRP stimulation (5 µg/mL, p = 0.049). Platelet activation induced by low and high doses of PAR4 peptide (70 µM and 200 µM) did not alter PANX1 Tyr^{198} phosphorylation when PKC was inhibited by RO treatment (Figure 30 A). Both tested concentrations of U46 (1 µM and 3 µM) led to decreased PANX1 Tyr^{198} phosphorylation (Figure 30 B). Comparison of the statistical power of different U46619 concentrations indicates that high doses of U46619 lead to a stronger increase in phosphorylation levels (3 µM: p = 0.005) compared to the low dose concentration of U46619 (1 µM: p = 0.037). However, both tested concentrations lead to decreased PANX1 phosphorylation at Tyr^{198} (Figure 30 B). ADP did not alter PANX1 Tyr^{198} phosphorylation levels as described in 4.3, which is also not altered after PKC inhibition (Figure 30 B). These experiments confirm that PKC plays an important role in GPVI and TxA_2 receptor mediated PANX1 phosphorylation at Tyr^{198} in platelets (Figure 30). Similar experiments were performed to analyze if PKC is involved in PANX1 Tyr^{308} phosphorylation (Figure 31).

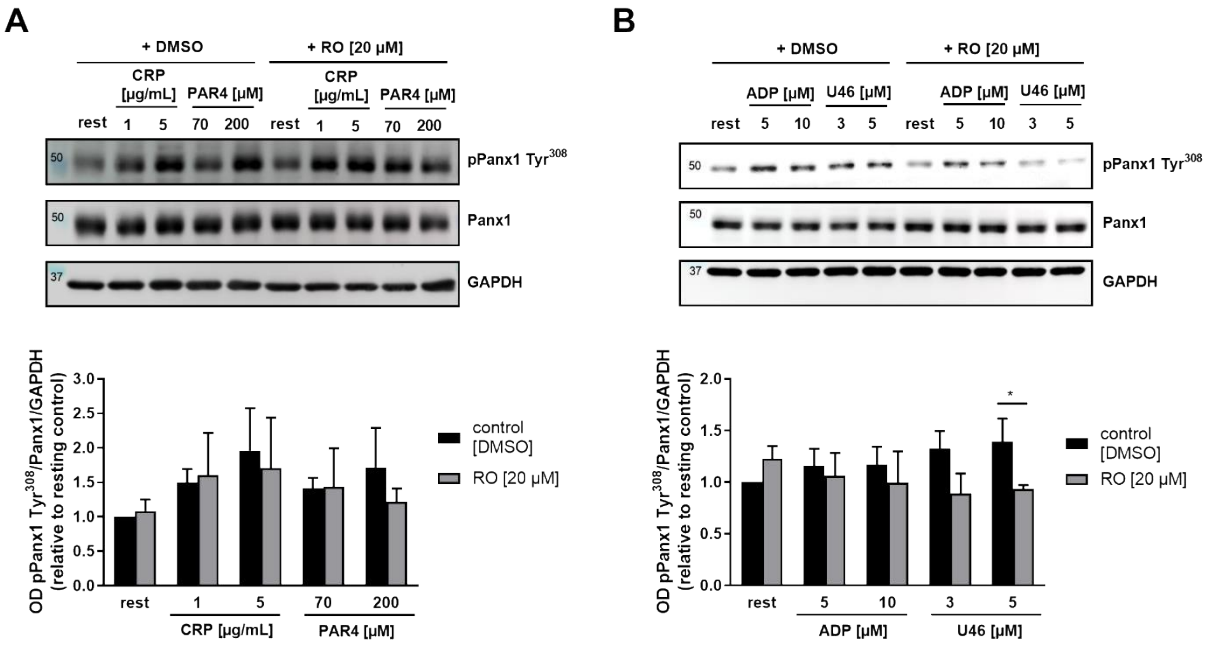

Figure 31: PANX1 Tyr^{308} phosphorylation is decreased only after platelet activation with 3 µM U46619. Representative Western blot image and quantification of phosphorylation of PANX1 Tyr^{308} after inhibition of PKC by pre-incubation of platelets with Ro-31-8220 (RO) or DMSO as a negative control. (A) Platelets were activated with 1 and 5 µg/mL CRP and 70 and 200 µM PAR4 peptide (n = 3). (B) Platelets were activated with 5 and 10 µM ADP and 1 and 3 µM U46 (n = 3). Statistical analyses were performed using a two-way ANOVA followed by a Sidak's multiple comparisons post-hoc test. Bar graphs indicate mean values ± SEM, *p < 0.05: **p < 0.01 and ***p < 0.001. Rest = Resting, CRP = Collagen-related peptide, PAR4 peptide = Protease-activated receptor 4 peptide, ADP = Adenosine diphosphate, U46 (U46619) = Thromboxane A_2 analogue, PKC = Protein Kinase C; DMSO = Dimethyl sulfoxide [Figure from Metz, Elvers, IJMS 2022].

Inhibition of PKC by RO leads to decreased phosphorylation of PANX1 at Tyr^{308} only upon platelet activation with a high dose of U46619 (Figure 31 B, 3 µM; p = 0.048). PANX1 Tyr^{308} phosphorylation is not altered in response to all tested concentrations of CRP, PAR4 peptide and ADP when PKC was inhibited by RO (Figure 31). Additionally, a low dose platelet activation with U46619 does not alter PANX1 Tyr^{308} phosphorylation (Figure 31 B), which was the case for PANX1 Tyr^{198} phosphorylation (Figure 30 B). These results demonstrate that PKC is important only for enhanced U46619 mediated PANX1 phosphorylation at Tyr^{308} via the TxA_2 receptor signaling pathway (Figure 31 B). In contrast, PKC is important for the regulation of PANX1 Tyr^{198} in response to GPVI receptor and TxA_2 receptor mediated signaling by CRP and U46619, respectively (Figure 30).

4.4.3 Involvement of Akt in pannexin 1 phosphorylation

Akt is a serine–threonine kinase, also known as protein kinase B (PKB), which contributes to signaling mechanisms leading to platelet activation. The two known isoforms Akt1 and Akt2 are expressed in human platelets and inhibition of those alter proper platelet functions e.g. aggregation responses or calcium influx [153]. As shown above, PANX1 Tyr^{308} phosphorylation is not fully dependent on neither SFKs (4.4.1) nor PKC (4.4.2) following platelet activation with low-doses of CRP, low and high doses of PAR4 peptide and all tested concentrations of ADP. Therefore, Akt displays a potential candidate in the regulation of the predicted tyrosine phosphorylation site (PANX1 at Tyr^{308}). Since PKC was shown to be also partially involved in PANX1 Tyr^{198} phosphorylation, the involvement of Akt on PANX1 Tyr^{198} phosphorylation was analyzed. To this end, platelet lysates were prepared with or without pre-incubation of human platelets with the Akti1/2 (Akt 1/2-inhibitor) inhibiting compound, DMSO served as a negative control. PANX1 Tyr^{198} phosphorylation was analyzed in response to classical platelet agonists as shown in Figure 32.

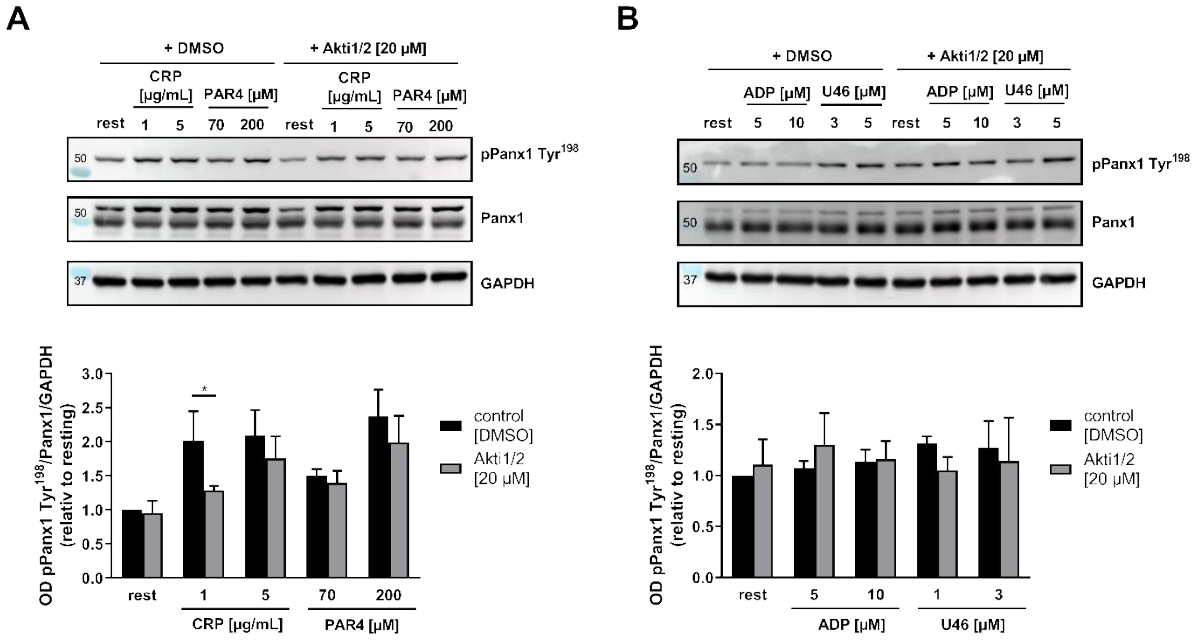

Figure 32: Inhibition of Akt leads to reduced PANX1 Tyr^{198} phosphorylation only in response to platelet activation with 1 µg/mL CRP. Representative Western blot image and quantification of phosphorylation of PANX1 Tyr^{198} after inhibition of Akt by pre-incubation of platelets with 20 µM Akti1/2 or DMSO as a negative control. (A) Platelets were activated with 1 and 5 µg/mL CRP and 70 and 200 µM PAR4 peptide (n = 4). (B) Platelets were activated with 5 and 10 µM ADP and 1 and 3 µM U46 (n = 3). Statistical analyses were performed using a two-way ANOVA followed by a Sidak's multiple comparisons post-hoc test. Bar graphs indicate mean values ± SEM, *p < 0.05: **p < 0.01 and ***p < 0.001. Rest = Resting, CRP = Collagen-related peptide, PAR4 peptide = Protease-activated receptor 4 peptide, ADP = Adenosine diphosphate, U46 (U46619) = Thromboxane A_2 analogue, DMSO = Dimethyl sulfoxide, Akti 1/2 = Akt-inhibitor 1/2. [Figure from Metz, Elvers, IJMS 2022].

Western blot analysis of PANX1 Tyr^{198} phosphorylation after application of Akti1/2 revealed that phosphorylation levels were decreased only after platelet activation with 1 µg/mL CRP (Figure 32 A, p = 0.041). Platelet activation with 5 µg/mL CRP, as well as all tested concentrations of PAR4 peptide, ADP or U46619 does not alter PANX1 Tyr^{198} phosphorylation after Akt 1/2 inhibition (Figure 32). Figure 33 displayed that PANX1 Tyr^{308} phosphorylation levels are not diminished when Akt is inhibited in response to all tested agonists, concluding that Akt is not involved in the regulation of PANX1 phosphorylation at Tyr^{308}.

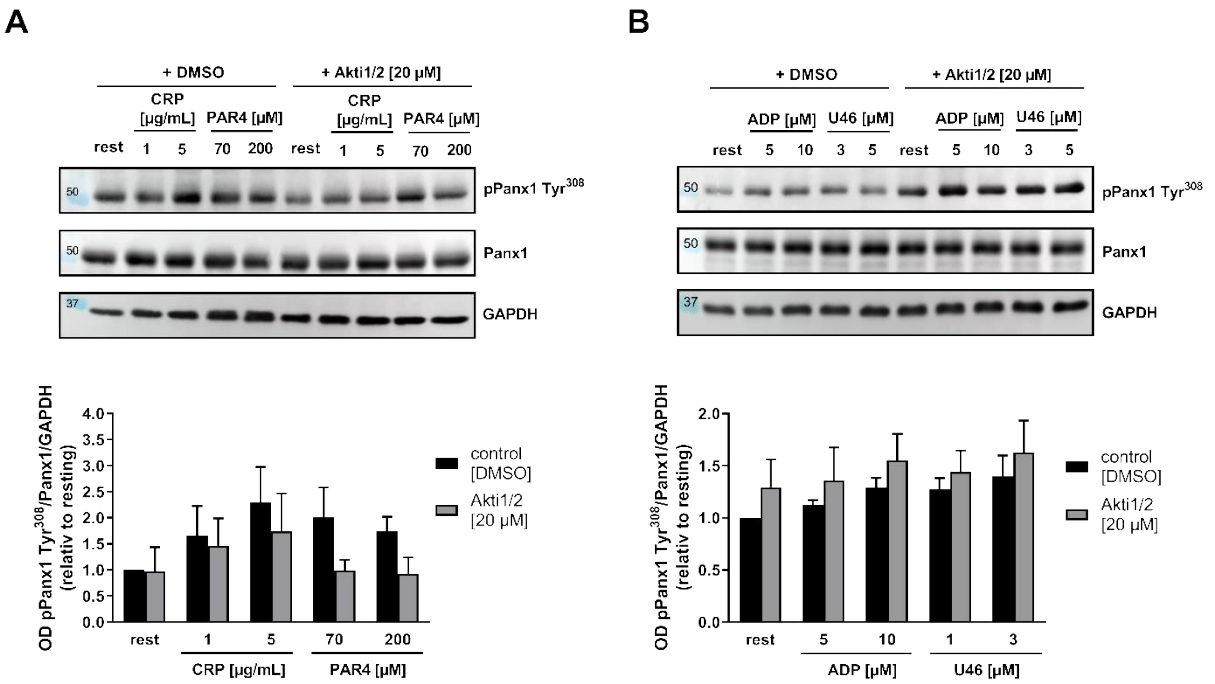

Figure 33: Inhibition of Akt does not alter PANX1 Tyr^{308} phosphorylation in response to all tested agonists. Representative Western blot image and quantification of phosphorylation of PANX1 Tyr^{308} after inhibition of Akt by pre-incubation of platelets with 20 µM Akti1/2 or DMSO as a negative control. (A) Platelets were activated with 1 and 5 µg/mL CRP and 70 and 200 µM PAR4 peptide (n = 3). (B) Platelets were activated with 5 and 10 µM ADP and 1 and 3 µM U46 (n = 5). Statistical analyses were performed using a two-way ANOVA followed by a Sidak's multiple comparisons post-hoc test. Bar graphs indicate mean values ± SEM, *p < 0.05: **p < 0.01 and ***p < 0.001. Rest = Resting, CRP = Collagen-related peptide, PAR4 peptide = Protease-activated receptor 4 peptide, ADP = Adenosine diphosphate, U46 (U46619) = Thromboxane A_2 analogue, DMSO = Dimethyl sulfoxide, Akti 1/2 = Akt-inhibitor 1/2 [Figure from Metz, Elvers, IJMS 2022].

Activation of Akt is mediated by binding of phospholipids and phosphorylation at Thr^{308} and Ser^{473} [154]. To investigate, if phosphorylation of Akt at Ser^{473} is altered when PANX1 is not expressed, Western blot analyses were performed. Therefore, platelets from *Panx1 fl/fl PF4-Cre*$^{-}$ and *Panx1 fl/fl PF4-Cre*$^{+}$ mice were stimulated with 1 and 5 µg/mL CRP and 70 and 200 µM PAR4 peptide and phosphorylation levels of Akt Ser^{473} were investigated by densiometric analysis (Figure 34).

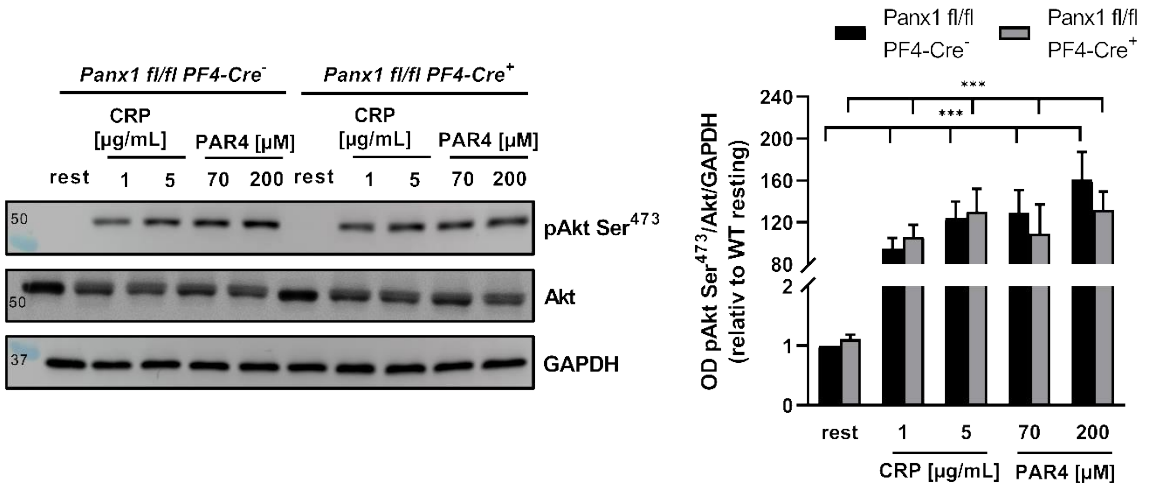

Figure 34: Akt phosphorylation at Ser^{473} is not altered in PANX1 deficient platelets. (A) Representative Western blot image and (B) quantification of phosphorylation of Akt Ser^{473} of platelets from *Panx1 fl/fl PF4-Cre*$^{-}$ and *Panx1 fl/fl PF4-Cre*$^{+}$ mice activated with 1 and 5 µg/mL CRP and 70 and 200 µM PAR4 peptide (n = 3). Statistical analyses were performed using a two-way ANOVA (compared to WT resting or KO resting) followed by a Sidak's multiple comparisons post-hoc test. Bar graphs indicate mean values ± SEM, *p < 0.05: **p < 0.01 and ***p < 0.001. Rest = Resting, CRP = Collagen-related peptide, PAR4 peptide = Protease-activated receptor 4 peptide, WT = Wild type, KO = Knock-out, Panx1 = Pannexin 1.

Western blot analysis showed an increase in phosphorylation of Akt at Ser^{473} following platelet activation with 1 and 5 µg/mL CRP and 70 and 200 µM PAR4 peptide compared to resting platelets from *Panx1 fl/fl PF4-Cre*$^{-}$ and *Panx1 fl/fl PF4-Cre*$^{+}$ mice (Figure 34, $p < 0.001$). However, no alterations in Akt phosphorylation at Ser^{473} were detected between PANX1 deficient and control platelets (Figure 34). Overall, the results display that Akt does not play a major role in mediating PANX1 activation via phosphorylation, neither at Tyr^{198} nor at Tyr^{308} of PANX1 in human platelets (Figure 32, Figure 33). Moreover, a genetic deletion of PANX1 in murine platelets does not change phosphorylation of Akt at Ser^{473} (Figure 34).

Since collagen induced platelet activation is a key mechanism in PANX1 activation, human platelets were activated with 1 and 5 µg/mL CRP with or without inhibition of SFKs and PKC to analyze Akt phosphorylation at Ser^{473}. These experiments were performed to investigate the downstream signaling cascade between SFKs, PKC and Akt. Platelet activation with 70 and 200 µM PAR4 peptide served as an additional control because platelet activation due to PAR4 peptide also increases PANX1 phosphorylation at Tyr^{198} and at Tyr^{308} (Figure 35).

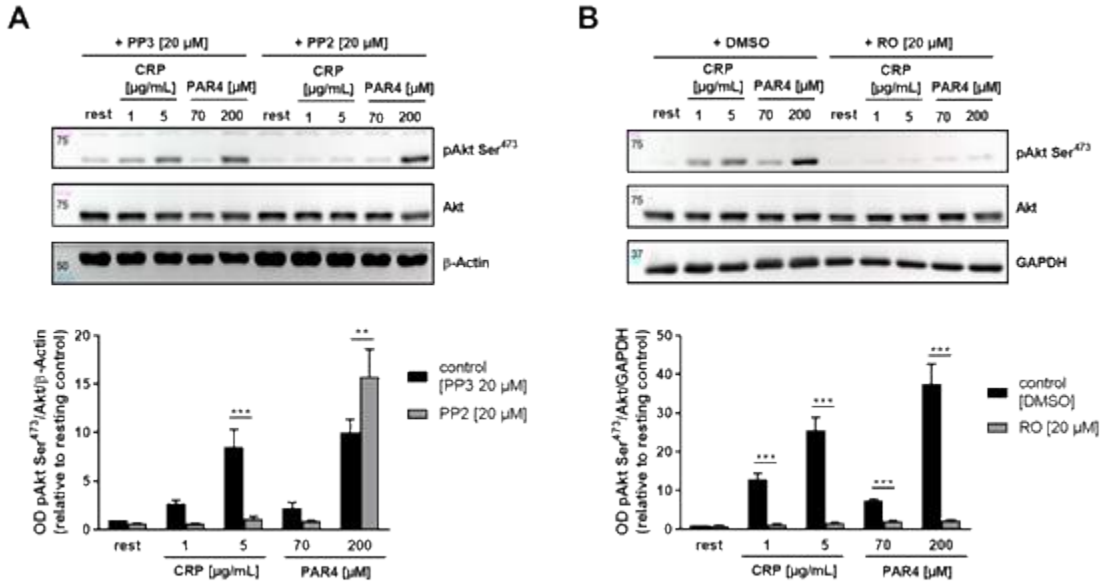

Figure 35: Phosphorylation of Akt Ser^{473} depends on PKC and partially on SFKs. Representative Western blot images and quantification of phosphorylation of Akt Ser^{473} after inhibition of (A) SFKs by pre-incubation of platelets with 20 µM PP2 or PP3 as a negative control (n = 4) or (B) PKC by pre-incubation of platelets with 20 µM Ro-31-8220 (RO) or DMSO as a negative control (n = 3). Platelets were activated with 1 and 5 µg/mL CRP and 70 and 200 µM PAR4 peptide. Statistical analyses were performed using a two-way ANOVA followed by a Sidak's multiple comparisons post-hoc test. Bar graphs indicate mean values ± SEM, *p < 0.05: **p < 0.01 and ***p < 0.001. Rest = Resting, CRP = Collagen-related peptide, PAR4 peptide = Protease-activated receptor 4 peptide, SFKs = Src Family Kinases, PKC = Protein Kinase C, DMSO = Dimethyl sulfoxide [Figure from Metz, Elvers, IJMS 2022].

Analysis of Akt phosphorylation at Ser^{473} in the presence of the SFK inhibitor PP2 demonstrated that phosphorylation is significantly decreased upon platelet activation with high dose CRP (5 µg/mL; p = 0.0005) and enhanced upon platelet stimulation with 200 µM PAR4 peptide (Figure 35 A, p = 0.0085). In comparison, inhibition of PKC by RO led to diminished phosphorylation of Akt Ser^{473} comparable to the slight auto phosphorylation signal already obtained in resting platelets without inhibitor (Figure 35 B, CRP: 1 µg/mL p = 0.002; 5 µg/mL p = 0.002; PAR4: 70 µM p = 0.0002, 200 µM p = 0.002). It is conclusive that phosphorylation of Akt at Ser^{473} in response to CRP as well as PAR4 peptide is highly dependent on PKC (Figure 35 B). SFKs are dependent on Akt Ser^{473} phosphorylation only after high dose CRP (5 µg/mL) stimulation, however high doses of PAR4 peptide led to enhanced Akt phosphorylation at Ser^{473} after SFK inhibition (Figure 35 A).

4.4.4 Platelet pannexin 1 is released upon platelet activation

Beside post-translational modifications, further analysis of platelet receptor shedding revealed that PANX1 is proteolytically cleaved after platelet activation as it is detectable in platelet releasates (Figure 36 A). Platelet activation via ADP stimulation does not lead to PANX1 Tyr^{198} phosphorylation (Figure 25 A), however an increase of PANX1 protein was found in the respective platelet releasate (Figure 36 A, p = 0.003). The increase in optical density (OD) regarding PANX1 in platelet releasates compared to the endogenous control (GAPDH was used as reference protein from platelet lysate) variates between each donor between a range of 1.03 and 4.25 × fold compared to unstimulated platelets and for platelet activation with 10 µM ADP (Figure 36 C). After stimulation of platelets with low dose CRP (1 µg/mL), PANX1 levels in platelet releasates variate between 0.15 × and 1.74 × fold compared to resting controls (Figure 36 C). PANX1 protein was not detected in platelet releasates from all donors following platelet activation with high dose of CRP (5 µg/mL) or PAR4 peptide (200 µM) (Figure 36 A, C). PANX1 phosphorylation at Tyr^{198} in platelet cell lysates was increased with CRP and PAR4 peptide (Figure 24 A). Additionally, cleaved PANX1 protein with a predicted size of 19 kDa was detected after platelet activation with 10 µM ADP (Figure 36 A).

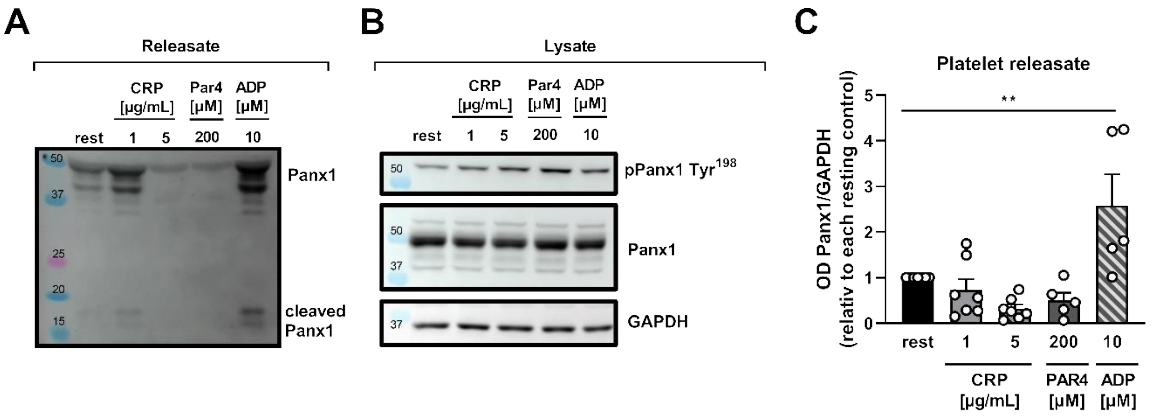

Figure 36: PANX1 is proteolytically cleaved after platelet activation with 10 µM ADP. (A) Western blot analyses were performed using human isolated platelets activated with 1 and 5 µg/mL CRP, 200 µM PAR4 peptide and 10 µM ADP. (A) Analysis of platelet releasate showed that PANX1 protein is found in platelet releastes from unstimulated platelets as well as upon platelet activation with 10 µM ADP and after 1 µg/mL CRP stimulation (dependent on each doner for 1 µg/mL CRP). (B) Western blot image of cell lysate investigating PANX1 Tyr^{198} phosphorylation with indicated agonists. (C) Quantification by densitometric analysis of platelets releasates in comparison to their respective endogenous control (GAPDH) from cell lysate (n = 5-7). Statistical analyses were performed using an ordinary one-way ANOVA followed by a Sidak's multiple comparisons post-hoc test (compared to normalized resting control). Bar graphs indicate mean values ± SEM, **p < 0.01. Rest = Resting, CRP = Collagen-related peptide, PAR4 peptide = Protease-activated receptor 4 peptide, ADP = Adenosine diphosphate.

4.4.5 The impact of pannexin 1 phosphorylation on platelet NMDA receptors

Recent studies in the neuronal system of mammals demonstrate that N-methyl-D-aspartate receptors (NMDARs) cross-activate PANX1 channels via SFKs [149]. The results presented here confirm that SFKs are central mediators of PANX1 activation in platelets (4.3.1). THerfore, the activation of SFKs by phosphorylation of Tyr^{416} in NMDAR deficient platelets compared to their respective WT controls were analyzed (Figure 36 A). In order to assess the impact of NMDARs on PANX1 phosphorylation at Tyr^{198} in platelets, Western blot analyses of murine cell lysates of NMDAR deficient and control platelets were performed (Figure 36 B). In both experimental setups, low and high doses of CRP and PAR4 peptide were used as platelet agonists (Figure 36).

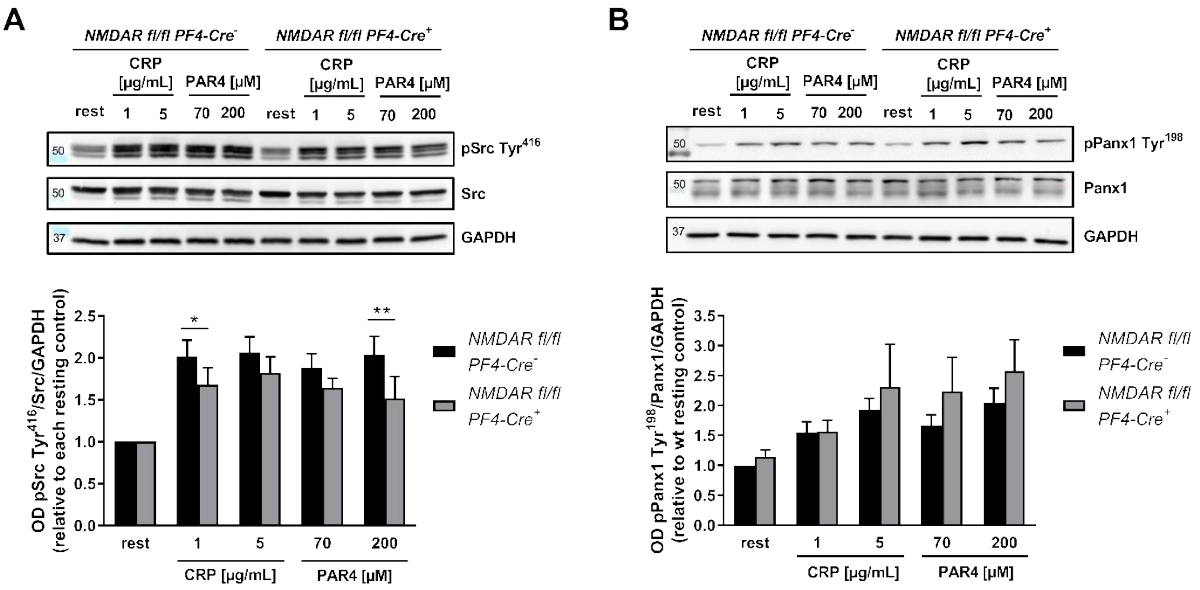

Figure 36: NMDAR deficient platelets display reduced Src phosphorylation at Tyr^{416}, but no alteration was observed regarding PANX1 phosphorylation at Tyr^{198} compared to their respective control platelets. Representative Western blot images and quantification of phosphorylation of (A) Src Tyr^{416} (n = 4) and (B) PANX1 Tyr^{198} (n (WT) = 4; n (KO) = 4). NMDAR WT control and NMDAR deficient platelets were activated with 1 and 5 µg/mL CRP and 70 and 200 µM PAR4 peptide. Statistical analyses were performed using a two-way ANOVA followed by a Sidak's multiple comparisons post-hoc test. Bar graphs indicate mean values ± SEM, *p < 0.05: **p < 0.01. Rest = Resting, CRP = Collagen-related peptide, PAR4 peptide = Protease-activated receptor 4 peptide, NMDAR = N-methyl-D-aspartate receptor, WT = Wild type, KO = Knock-out, PANX1 = Pannexin 1.

Western blot analysis of Src in NMDAR deficient platelets showed that the phosphorylation at Tyr^{416} is decreased in NMDAR deficient platelets in response to platelet activation with 1 µg/mL CRP ($p = 0.047$) and 200 µM PAR4 (Figure 36 A, $p = 0.002$). Platelet activation with 5 µg/mL CRP and 70 µM PAR4 peptide do not alter Src Tyr^{416} phosphorylation levels in NMDAR deficient platelets compared with WT control platelets (Figure 36 A). PANX1 phosphorylation at Tyr^{198} is not altered in NMDAR deficient platelets compared to control platelets in response to CRP and

PAR4 peptide (Figure 36B). These results indicate that SFK mediated signaling is altered when NMDAR is not expressed in murine platelets (Figure 36 A). Additionally, NMDAR deficient murine platelets did not reveal a difference in the activation of PANX1 via the phosphorylation of Tyr^{198} as shown by unaltered phosphorylation levels (Figure 36 B).

These results provide first insights into the regulation and function of PANX1 channels in platelets. Detailed studies of PANX1 channel activation mechanisms and signaling pathways show that platelet activation with classical agonists leads to increased phosphorylation of at PANX1 Tyr^{198}, which is completely dependent on SFKs. Here, GPVI was identified as a central receptor for collagen induced phosphorylation of PANX1 at Tyr^{198} via SFKs. The genetic deletion von NMDARs on platelets did not lead to altered PANX1 Tyr^{198} phosphorylation, although this receptor is also controlled by SFKs as shown in the neuronal system [101]. In addition to SFKs, PKC plays a minor role, while Akt does not contribute to the activation of PANX1 channels on platelets. In addition, the PANX1 Tyr^{308} phosphorylation site was shown to be controlled by the GPVI-Src signaling pathway only via CRP. Until now it is unclear, which signaling pathway leads to phosphorylation of PANX1 at Tyr^{308} in response to 200 µM PAR4 peptide, U46619 and ADP.

4.5 The influence of pannexin 1 in inflammation and progression of AAA

4.5.1 The role of pannexin 1 in inflammation and cell-cell interactions *in vitro*

In many inflammatory processes extracellular ATP plays an important role e.g. in the activation of the inflammasome or the increase of immune cell infiltration [89, 90]. Previous studies indicate that controlled ATP release via PANX1 channels supports intercellular communication [91]. To investigate, if platelet PANX1 channels are involved in intracellular communication in the vasculature, first experiments were performed investigating direct cell-cell interactions during inflammatory processes. In the following experiments, TNFα and Lipopolysaccharide (LPS) were used to mimic inflammatory stimuli *in vitro* (Figure 37).

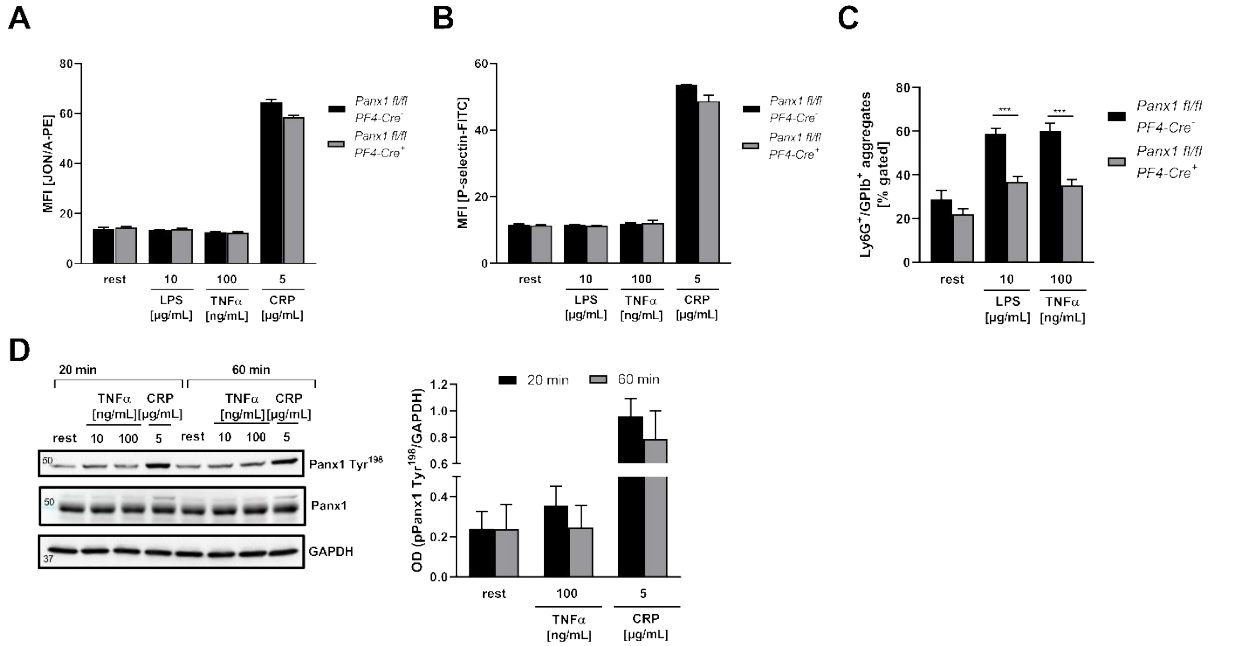

Figure 37: Inflammatory stimuli lead to reduced platelet-neutrophil aggregate formation in PANX1 deficient platelets. *Panx1 fl/fl PF4-Cre*$^-$ and *Panx1 fl/fl PF4-Cre*$^+$ mice were analyzed regarding platelet activation for (A) integrin $\alpha_{IIb}\beta_3$ (JON/A-PE) and (B) P-selectin (FITC) via flow cytometric analysis upon TNFα and LPS stimulation. CRP served as a positive control (n (WT) = 3, n (KO) = 3). (C) The percent of GPIb and Ly6G positive cells (platelet-neutrophil aggregates) were analyzed upon inflammatory stimuli in washed whole blood from *Panx1 fl/fl PF4-Cre-* and *Panx1 fl/fl PF4-Cre+*mice (n (WT) = 10, n (KO) = 10). (D) Representative Western blot and quantification of Panx1 Tyr^{198} phosphorylation in human whole cell lysates upon platelet stimulation with 100 ng/mL TNFα for 20 and 60 min respectively; 5 µg/mL CRP served as a positive control (n = 4). Statistical analyses were performed using a two-way ANOVA followed by a Sidak's multiple comparisons post-hoc test. Bar graphs indicate mean values ± SEM; ***p < 0.001. Rest = Resting, CRP = Collagen-related peptide, TNFα = Tumor necrosis factor alpha, LPS = Lipopolysaccharide, WT = Wild type (*Panx1 fl/fl PF4-Cre*$^-$), KO = Knock-out (*Panx1 fl/fl PF4-Cre*$^+$), PANX1 = Pannexin 1.

Figure 37 shows that the inflammatory stimuli TNFα and LPS do not induce platelet activation in platelets from *Panx1 fl/fl PF4-Cre*$^-$ and *Panx1 fl/fl PF4-Cre*$^+$ mice as measured by the standard platelet activation markers for activated integrin $\alpha_{IIb}\beta_3$ (JON/A) and P-selectin exposure. Moreover, Western blot analysis with indicated agonists did not lead to PANX1 Tyr^{198} phosphorylation in human platelets, indicating that TNFα does not activate platelet PANX1 channels (Figure 37 D). Interestingly, the number of formed platelet-neutrophil aggregates were significantly reduced in response to TNFα ($p < 0.0001$) and LPS ($p < 0.0001$) when platelet PANX1 is not expressed (Figure 37 C).

Beside the recruitment of neutrophils at sites of inflammation, platelet-endothelium interactions are essential in mediating stable platelet adhesion by integrin $\alpha_{IIb}\beta_3$ and integrin $\alpha_V\beta_3$ on the endothelium. This interaction enables transcellular communication via soluble mediators as released growth factors, chemokines, and cytokine-like factors [58, 59]. IL-6 is released from endothelial cells and displays an important cytokine during the first steps on inflammation [155].

Under physiological conditions, platelets do not store IL-6 [156]. Additionally, plasma levels of IL-6 were shown to be enhanced in patients suffering from AAA [107]. Therefore, the effect of PANX1 deficient and WT control platelets on endothelial IL-6 release under static conditions was investigated using a co-culture experiment *in vitro* (Figure 38).

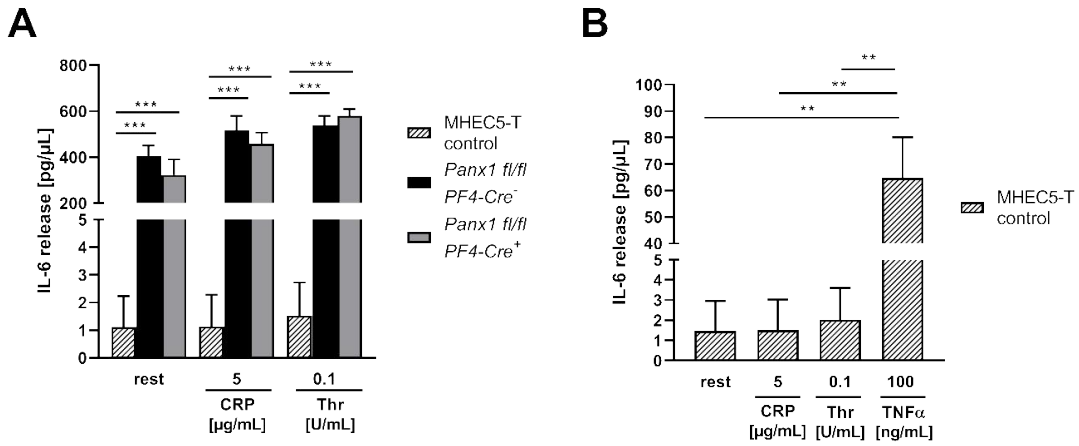

Figure 38: Platelets induce IL-6 release from endothelial cells, which is not altered between platelets from *Panx1 fl/fl PF4-Cre*$^-$ and *Panx1 fl/fl PF4-Cre*$^+$ mice. (A) Platelets from *Panx1 fl/fl PF4-Cre*$^-$ and *Panx1 fl/fl PF4-Cre*$^+$ mice were co-cultured with MHEC5-T cells (125,000 cells/mL) in Tyrode's buffer for 3.5 h at 37°C in a humidified atmosphere with 5% CO_2. After 3.5 h of platelet-MHEC5-T co-incubation, supernatants were harvested and IL-6 ELISA was performed (n (WT) = 6, n (KO) = 6-8). MHEC5-T cells only treated with platelet agonists served as negative controls (MHEC5-T control). (B) MHEC5-T cells stimulated with indicated agonists served as negative controls, TNFα [100 ng/mL] served as a positive control (n = 8-13). Statistical analyses were performed using (A) a two-way ANOVA between both genotypes and (B) an ordinary one-way ANOVA (compared to TNFα) followed by a Sidak's multiple comparisons post-hoc test. Bar graphs indicate mean values ± SEM, **p < 0.01 and ***p < 0.001. Rest = Resting, CRP = Collagen-related peptide, Thr = Thrombin, TNFα = Tumor necrosis factor alpha, WT = Wild type (*Panx1 fl/fl PF4-Cre*$^-$), KO = Knock-out (*Panx1 fl/fl PF4-Cre*$^+$), Panx1 = Pannexin 1.

Co-cultures of platelets with murine endothelial MHEC5-T cells displayed that platelets induce IL-6 release from ECs (Figure 38 A, rest: p <0.0001; CRP: p <0.0001; Thr: p <0.0001). However, no differences were observed between *Panx1 fl/fl PF4-Cre*$^-$ and *Panx1 fl/fl PF4-Cre*$^+$ platelets neither with unstimulated plateletsnor after platelet activation with CRP and thrombin (Figure 38 A). MHEC5-T cells stimulated with CRP and thrombin served as negative controls, while TNFα (positive control) significantly enhanced endothelial IL-6 release compared to unstimulated, CRP or thrombin stimulated MHEC5-T cells (Figure 38 B, rest: p = 0.004; CRP: p = 0.004; Thr: p = 0.004). Under these experimental conditions, platelet PANX1 channels do not influence endothelial IL-6 release in response to high doses of CRP and thrombin or without platelet activation (Figure 38 A).

4.5.2 Increased plasma levels of pannexin 1 in AAA patients, but reduced phosphorylation of platelet pannexin 1 at Tyr^{198}

Beside the involvement of PANX1 in acute inflammatory responses, PANX1 is also associated with chronic inflammatory diseases [157]. Since platelets are key players in inflammation by the release of pro-inflammatory cytokines and mediators [57], the role of platelet PANX1 was further investigated. PANX1 channels play a role in the pathogenesis of AAA [131, 132]. In detail, endothelium specific *Panx1 fl/fl PF4-Cre*$^{+}$ mice displayed a reduced aortic diameter compared to control animals in the AAA experimental mouse model of porcine pancreatic elastase (PPE) [132]. Moreover, PANX1 levels in aortic tissue are upregulated in male patients suffering from AAA compared to aged-matched controls [131]. As a first translational approach, patients suffering from AAA were analyzed regarding their PANX1 protein levels in plasma, the phosphorylation of platelet PANX1 at Tyr^{198} and the respective platelet releasate PANX1 levels (Figure 39).

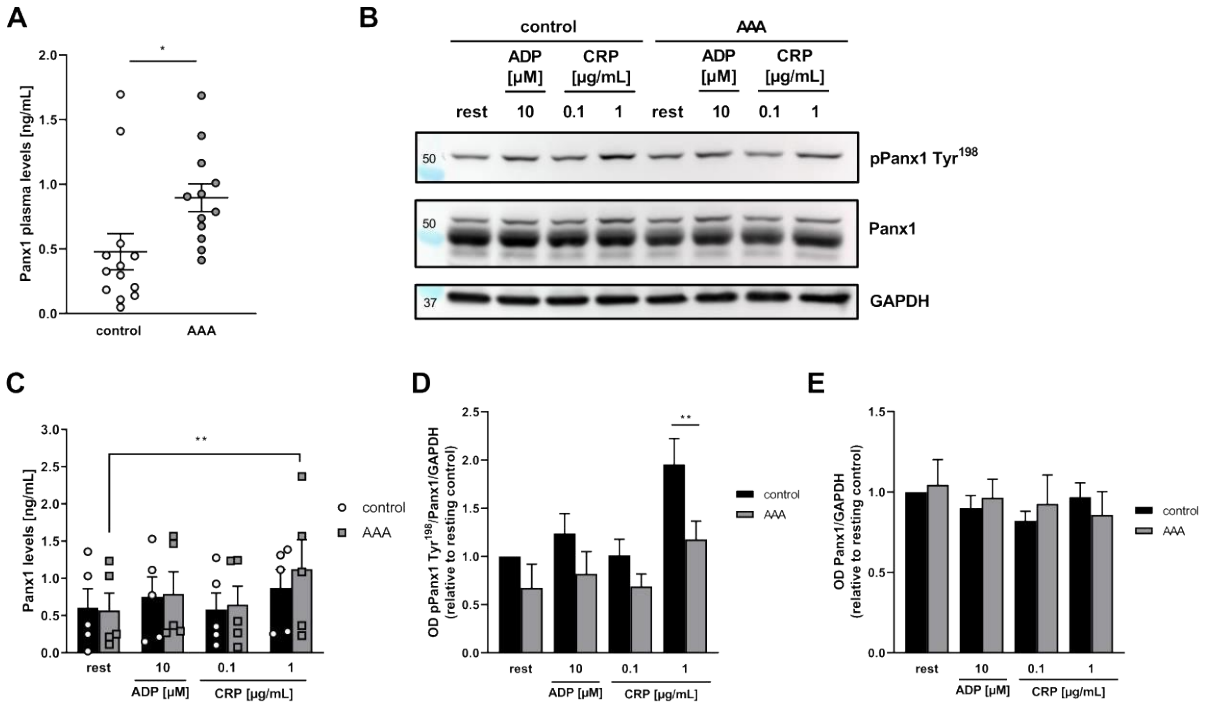

Figure 39: Enhanced PANX1 protein in plasma, but reduced phosphorylation of PANX1 at Tyr^{198} in patients suffering from AAA compared to aged-matched controls. (A) PANX1 proteins plasma levels in AAA patients compared to aged-matched controls were determined via ELISA (n (control) = 13, n (AAA) = 12). (B) Isolated platelets from patients suffering from AAA and aged-matched controls were stimulated with indicated agonists and Western blot analyses were performed. The Western blot displayed a representative image (n = 4). (C) Platelet releasates were analyzed via ELISA from isolated platelets from AAA patients and aged-matched controls stimulated with indicated agonists (n (control) = 5, n (AAA) = 5). (D + E) Quantification of Western blot analysis from patients suffering from AAA and aged-matched controls regarding (D) PANX1 Tyr^{198} (n = 4) and (E) PANX1 (n = 3). Statistical analyses were performed using a two-way ANOVA followed by a Sidak's multiple comparisons post-hoc test. Bar graphs indicate mean values ± SEM, *p < 0.05: **p < 0.01. Rest = Resting, CRP = Collagen-related peptide, ADP = Adenosine diphosphate, AAA = Abdominal aortic aneurysm, PANX1 = Pannexin 1.

Patients suffering from AAA displayed enhanced PANX1 protein in the plasma compared to aged-matched controls (Figure 39 A, p = 0.028). Since PANX1 is ubiquitously expressed in the vasculature, the source of PANX1 might be endothelial cells, leukocytes, red blood cells and/or platelets. Therefore, the analysis of isolated platelets from AAA patients compared to controls were performed to verify if platelets are responsible for enhanced PANX1 plasma levels. Western blot analysis of whole platelet lysates showed that AAA patients display reduced phosphorylation of PANX1 at Tyr^{198} following platelet activation with 1 µg/mL CRP compared to aged-matched controls (Figure 39 B, D, p = 0.002). Platelet activation with 10 µM ADP, 0.1 µg/mL CRP as well as resting platelets did not show any alterations in Tyr^{198} phosphorylation between both groups (Figure 39 B, D). Control experiments showed that the expression levels of PANX1 proteins in platelets do not differ between AAA patients and aged-matched controls (Figure 39 E). Platelet releasates using isolated platelets from AAA patients indicated enhanced PANX1 levels only upon platelet activation with 1 µg/mL CRP compared to resting controls but no differences between both groups (Figure 39 C, p = 0.003). These data indicates that platelet PANX1 channels differ from AAA patients compared to aged-matched controls confirming the involvement of PANX1 channels in the pathogenesis of AAA.

4.5.3 The role of platelet pannexin 1 channels in the Porcine Pancreatic Elastase Perfusion Model

To further analyze the role of platelet PANX1 in the development of AAA, *Panx1 fl/fl PF4-Cre*- and *Panx1 fl/fl PF4-Cre*$^{+}$ mice underwent Porcine Pancreatic Elastase Perfusion (PPE) surgery. The PPE model is a murine *in vivo* model to mimic AAA by infusion of PPE into an abdominal aortic segment, which leads to AAA formation in mice (Method description in chapter 3.1). Within this study, the dilatation of the aortic wall was monitored over 28 days via ultrasonic imaging (Figure 40) and blood cell counts, the expression of surface molecules at the platelet membrane as well as platelet interactions with immune cells were analyzed at different time points after surgery.

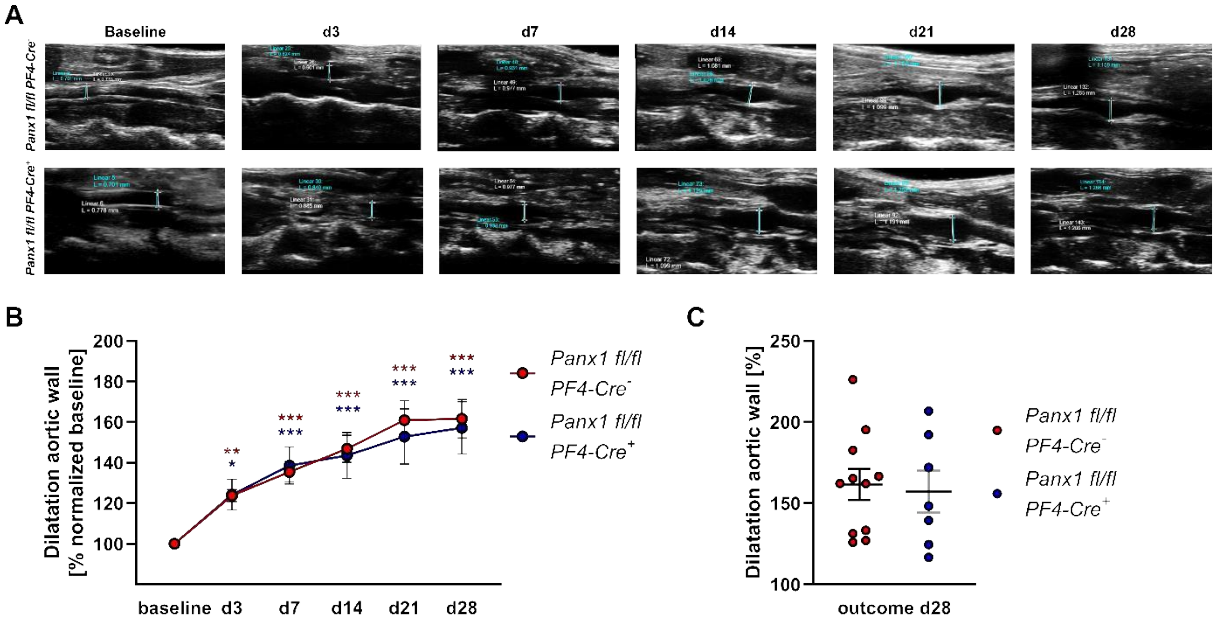

Figure 40: The dilatation of the aortic wall 28 days post-PPE surgery is not altered between *Panx1 fl/fl PF4-Cre*$^-$ and *Panx1 fl/fl PF4-Cre*$^+$ mice. (A) Representative images of ultrasonic imaging of the abdominal aorta at baseline conditions and at day 3, 7, 14, 21 and 28 post-PPE surgery from *Panx1 fl/fl PF4-Cre*$^-$ and *Panx1 fl/fl PF4-Cre*$^+$ mice. (B) The growth of the dilatation from the abdominal aorta is represented at day 3, 7, 14, 21 and 28 post-PPE surgery from *Panx1 fl/fl PF4-Cre*$^-$ and *Panx1 fl/fl PF4-Cre*$^+$ mice normalized to baseline conditions of each mouse. (C) Final outcome of the dilatation from the aortic wall at day 28 post-PPE surgery in percent. Statistical analyses were performed using (B) a two-way ANOVA (compared to WT baseline or KO baseline) followed by a Sidak's multiple comparisons post-hoc test and (C) an unpaired student's t-test. Bar graphs indicate mean values ± SEM; *p < 0.05, **p < 0.01, ***p < 0.001. Colored asterisks indicate statistical differences within one genotype (WT red asterisk; KO blue asterisk; listed in chapter *0.*) compared to their baseline control (n (WT) = 11, n (KO) = 7). D = Day, WT = Wild type (*Panx1 fl/fl PF4-Cre*$^-$), KO = Knock-out (*Panx1 fl/fl PF4-Cre*$^+$), Panx = Pannexin 1.

The dilatation of the aortic wall was monitored over time as shown in Figure 40 A and B. Analyzes of the dilatation of the abdominal aorta (Final outcome) at day 28 post-PPE surgery displayed no alterations between *Panx1 fl/fl PF4-Cre*$^-$ and *Panx1 fl/fl PF4-Cre*$^+$ mice (Figure 40 C). In detail, the dilatation of the abdominal aorta was 161.6 ± 9.5% (SEM, n = 11) for *Panx1 fl/fl PF4-Cre*$^-$ ($p < 0.001$) and 157.1 ± 12.9% (SEM, n = 7) for *Panx1 fl/fl PF4-Cre*$^+$ mice ($p < 0.001$) compared to baseline (100%).

In total, 14 *Panx1 fl/fl PF4-Cre*$^-$ and 16 *Panx1 fl/fl PF4-Cre*$^+$ mice underwent PPE surgery. However, 11 *Panx1 fl/fl PF4-Cre*$^-$ and 7 *Panx1 fl/fl PF4-Cre*$^+$ mice survived the procedure until day 28. To examine the association between the length of survival between *Panx1 fl/fl PF4-Cre*$^-$ and *Panx1 fl/fl PF4-Cre*$^+$ mice undergoing PPE surgery, a survival analysis by Kaplan-Meier plotting was performed as shown in Figure 41.

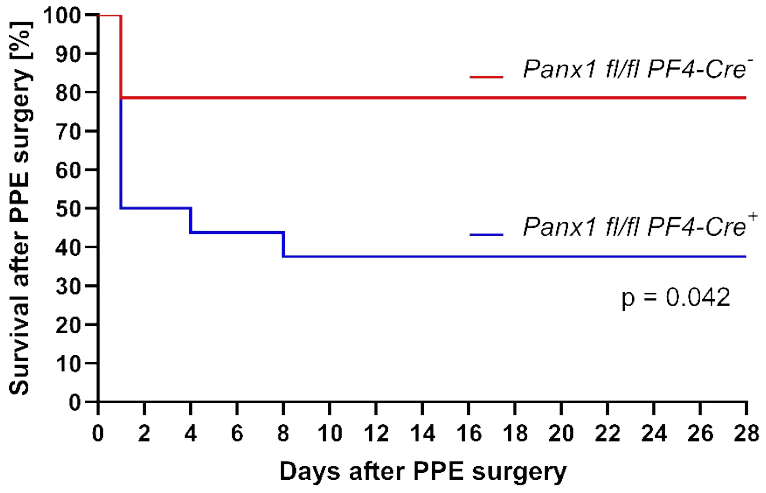

Figure 41: Platelet specific deletion of PANX1 decreases the percentage of mice surviving PPE surgery. This plot shows the survival curve by the proportion of individuals, which have survived until 28 days post-PPE surgery. The blue line indicates *Panx1 fl/fl PF4-Cre*$^{+}$ mice (n = 7) and the red line displays *Panx1 fl/fl PF4-Cre*$^{-}$ mice (n = 11). Statistical analysis was performed using a Log-rank (Mantel-Cox) test, *p < 0.05. WT = Wild type, KO = Knock-out, PPE = Porcine Pancreatic Elastase, PANX1 = Pannexin 1. Only mice with a final abdominal aortic dilatation ≥ 115% compared to baseline conditions (= 100%) are included.

The survival curve in Figure 41 displays that a gentic deletion of PANX1 in platelets (*Panx1 fl/fl PF4-Cre*$^{+}$) decreases the percentage of mice surviving PPE surgery compared to *Panx1 fl/fl PF4-Cre*$^{-}$ mice (Figure 41, p = 0.042). In detail, 50% of *Panx1 fl/fl PF4-Cre*$^{+}$ mice died 1 day after the PPE surgery. Compared to the group of *Panx1 fl/fl PF4-Cre*$^{-}$ mice, the survival rate 1 day post-PPE surgery was 80% and no additional mice died until a 28 days follow-up. As soon as the critical time point of 24 hours after surgery has been exceeded, no major alterations in the survival rate of *Panx1 fl/fl PF4-Cre*$^{-}$ mice compared to *Panx1 fl/fl PF4-Cre*$^{+}$ mice were observed. However, a minor group of mice within the *Panx1 fl/fl PF4-Cre*$^{+}$ group died within 8 days post-PPE surgery (Figure 41). Taken together, at day 28, 80% of all *Panx1 fl/fl PF4-Cre*$^{-}$ mice and 37.5% of all *Panx1 fl/fl PF4-Cre*$^{+}$ mice survived the PPE infusion/surgery with a dilatation of the abdominal part of the aorta ≥ 115% compared to baseline sizes (Figure 41).

Beside the determination of aortic dilatation, blood cell counts were measured at baseline conditions (day 0), as well as at day 3, 7, 14 and 28 days post-PPE surgery using a hematology analyzer. The number of WBCs was increased after PPE surgery within both groups (*Panx1 fl/fl PF4-Cre*$^{-}$ mice and *Panx1 fl/fl PF4-Cre*$^{+}$ mice) at day 3, 7, 14 and 28 days post-PPE surgery compared to day 0 (Figure 42 A, Table 4). No alterations in WBC counts were detected between *Panx1 fl/fl PF4-Cre*$^{-}$ mice and *Panx1 fl/fl PF4-Cre*$^{+}$ mice (Figure 42 A). The number of RBCs was reduced at day 14 post-PPE surgery in *Panx1 fl/fl PF4-Cre*$^{+}$ mice compared to *Panx1 fl/fl PF4-Cre*$^{-}$ mice (Figure 42 B, WT: 11.14 ± 0.45 SEM x 10^{6} /µL;

KO: 9.77 ± 0.25 SEM x 10^6 /µL; p = 0.04). Additionally, platelet counts were reduced in *Panx1 fl/fl PF4-Cre*$^+$ mice compared to *Panx1 fl/fl PF4-Cre*$^-$ mice at day 14 post-PPE surgery (Figure 42 C, WT: 1.32 ± 0.11 SEM x 10^6 /µL; KO: 0.94 ± 0.95 SEM x 10^6 /µL, p = 0.03). The platelet size was determined by the MPV, which is enhanced in platelets from *Panx1 fl/fl PF4-Cre*$^+$ mice compared to platelets from to *Panx1 fl/fl PF4-Cre*$^-$ mice 28 days after PPE surgery (Figure 42 D, WT: 5.2 ± 0.11 (SEM); KO: 5.6 ± 0.23 (SEM), p = 0.03). The levels of significances within both genotypes are listed in tables of chapter 7.1.6.

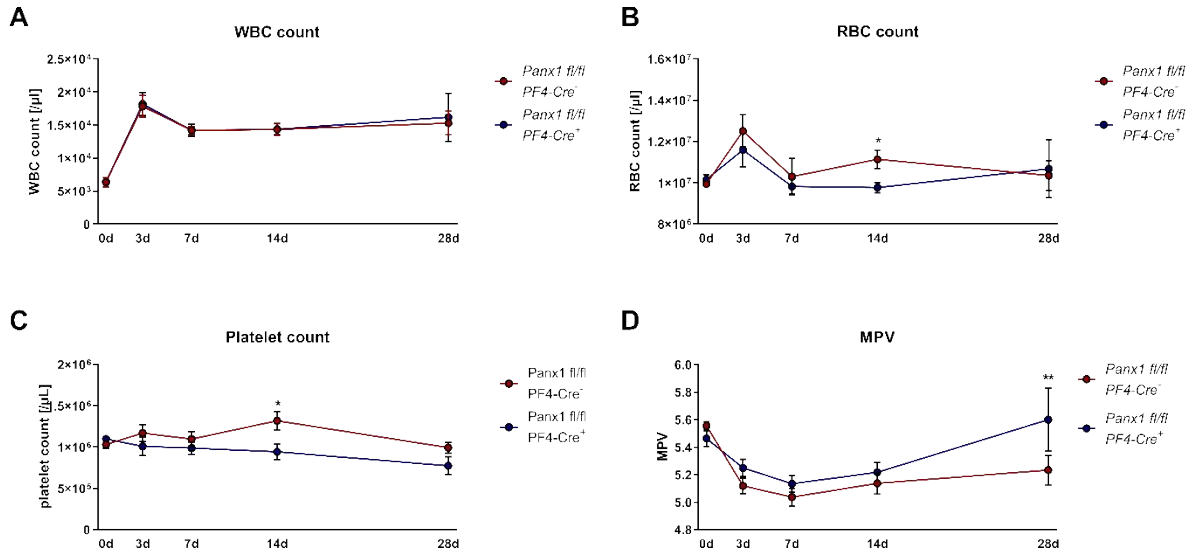

Figure 42: Alterations in blood cell counts and MPV after PPE surgery between *Panx1 fl/fl PF4-Cre*$^-$ and *Panx1 fl/fl PF4-Cre*$^+$ mice. Cell counts of (A) WBCs (n WBC (WT): 0d = 7, 3d = 11, 7d = 11, 14d = 11, 28d = 10 (KO) 0d = 7, 3d = 7, 7d = 7, 14d = 7, 28d = 6, (B) RBCs (n RBC (WT): 0d = 7, 3d = 11, 7d = 11, 14d = 9, 28d = 10 (KO) 0d = 6, 3d = 7, 7d = 7, 14d = 6, 28d = 6; n and (C) Platelets (n Plts (WT): 0d = 7, 3d = 11, 7d = 11, 14d = 9, 28d = 9 (KO) 0d = 7, 3d = 6, 7d = 6, 14d = 6, 28d = 6) were determined in native and at day 3, 7, 14, 21 and 28 post-PPE surgery from *Panx1 fl/fl PF4-Cre*$^-$ and *Panx1 fl/fl PF4-Cre*$^+$ mice using a hematology analyzer (Sysmex KN-X21). (D) MPV was measured in whole blood samples from native and 3, 7, 14, 21 and 28 post-PPE surgery in *Panx1 fl/fl PF4-Cre*$^-$ and *Panx1 fl/fl PF4-Cre*$^+$ mice (n (WT): 0d = 9, 3d = 11, 7d = 11, 14d = 11, 28d = 9, (KO) 0d = 8, 3d = 6, 7d = 6, 14d = 6, 28d = 6). Statistical analyses were performed using a two-way ANOVA followed by a Sidak's multiple comparisons post-hoc test. Bar graphs indicate mean values ± SEM, *p < 0.05: **p < 0.01 and ***p < 0.001. D = Day, WT = Wild type (Panx1 fl/fl PF4-Cre$^-$), KO = Knock-out (Panx1 fl/fl PF4-Cre$^+$), RBCs = Red Blood Cells, WBCs = White Blood Cells, Plts = Platelets, MPV = Mean Platelet Volume, Panx1 = Pannexin 1.

Three days after PPE-surgery, blood cell counts do not differ between *Panx1 fl/fl PF4-Cre*$^-$ and *Panx1 fl/fl PF4-Cre*$^+$ mice (Figure 42). However, the number of WBCs was increased within both genotypes compared to respective baseline cell counts (Figure 42 A, Table 4). To investigate, if the surgery-induced inflammation at day 3 accounts for defects regarding platelet activation or alterations in platelet receptor abundance, platelets from both genotypes were analyzed by flow cytometric analysis (Figure 43).

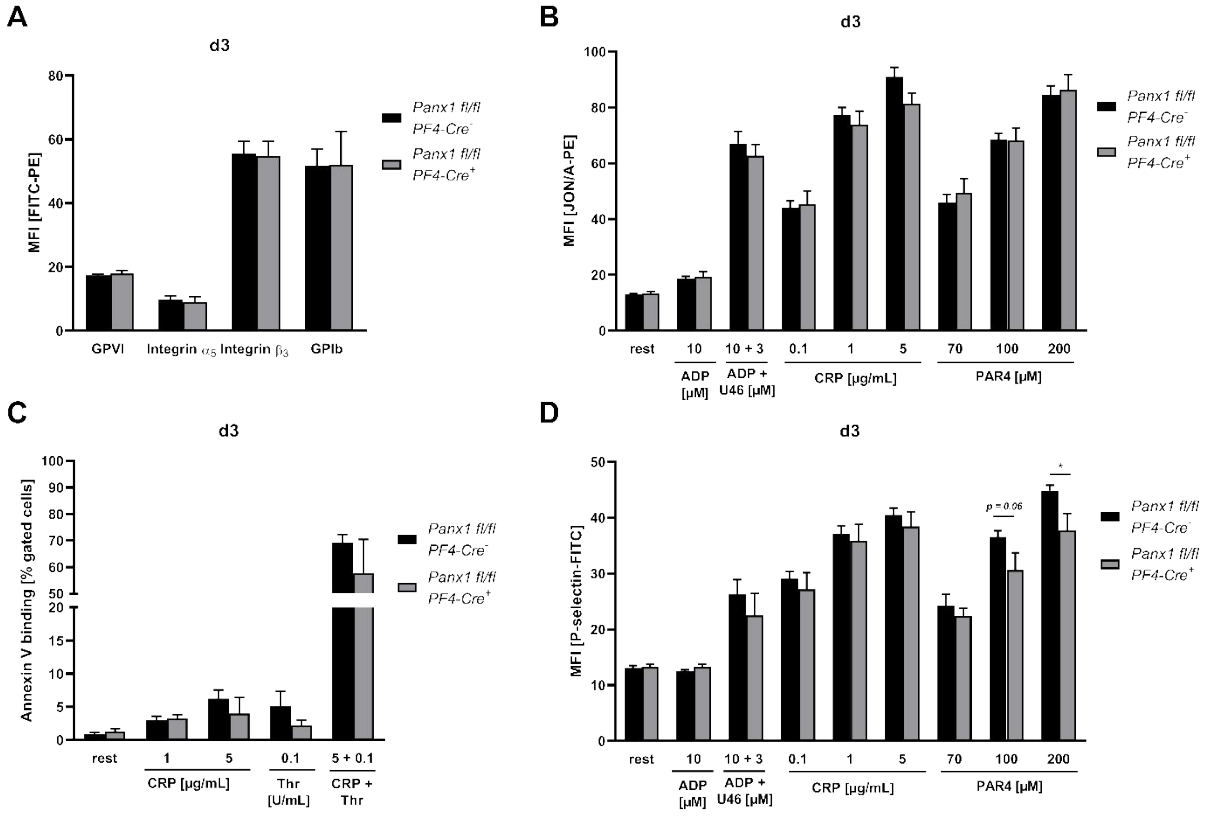

Figure 43: Platelet degranulation defects in response to PAR4 peptide 3 days after PPE surgery in platelets from *Panx1 fl/fl PF4-Cre*$^+$ mice compared to *Panx1 fl/fl PF4-Cre*$^-$ mice. Platelets from *Panx1 fl/fl PF4-Cre*$^-$ and *Panx1 fl/fl PF4-Cre*$^+$ mice were analyzed by flow cytometric analysis regarding their specific side scatter (SSC) and forward scatter (FSC) profile 3 days after PPE surgery. (A) Expression of indicated glycoproteins on the surface of platelets measured via the MFI (n (WT) = 11; n (KO) = 6). (B) Integrin $\alpha_{IIb}\beta_3$ activation is not altered between platelets from *Panx1 fl/fl PF4-Cre*$^-$ and *Panx1 fl/fl PF4-Cre*$^+$ mice (n (WT) = 11; n (KO) = 6). (C) PS exposure was assessed by the percentage of gated Annexin V positive platelets, which is not altered on the platelet surface from *Panx1 fl/fl PF4-Cre*$^-$ and *Panx1 fl/fl PF4-Cre*$^+$ mice (n (WT) = 6; n (KO) = 3). (D) Platelet degranulation marker (P-selectin) is reduced upon platelet activation with 100 and 200 µM PAR4 peptide in platelets from *Panx1 fl/fl PF4-Cre*$^+$ mice compared to *Panx1 fl/fl PF4-Cre*$^-$ mice (n (WT) = 7-11; n (KO) = 6). Statistical analyses were performed using an unpaired multiple students t-test. Bar graphs indicate mean values ± SEM, *p < 0.05. Rest = Resting, ADP = Adenosine diphosphate, U46619 (U46) = Thromboxane A_2 analogue, CRP = Collagen-related peptide, PAR4 peptide = Protease-activated receptor 4 peptide, Thr = Thrombin, MFI = Mean fluorescence intensity, WT = Wild type (*Panx1 fl/fl PF4-Cre*$^-$), KO = Knock-out (*Panx1 fl/fl PF4-Cre*$^+$), PPE = Porcine Pancreatic Elastase, Panx1 = Pannexin 1.

Analysis of platelets from *Panx1 fl/fl PF4-Cre*$^-$ and *Panx1 fl/fl PF4-Cre*$^+$ mice revealed no differences regarding glycoprotein expression at the surface of platelets 3 days after PPE surgery (Figure 43 A). Additionally, no differences regarding the PS-exposure on the platelet surface measured by Annexin V positive cells were obtained between platelets from *Panx1 fl/fl PF4-Cre*$^-$ and *Panx1 fl/fl PF4-Cre*$^+$ mice (Figure 43 C). Moreover, activation of integrin $\alpha_{IIb}\beta_3$ on the platelet surface is not different between groups at 3 days after PPE surgery (Figure 43 B). These results demonstrate that platelets from *Panx1 fl/fl PF4-Cre*$^+$ mice displayed degranulation defects following stimulation with intermediate (100 µM, p = 0.057) and high doses (200 µM, p = 0.025) of

PAR4 peptide compared to platelets from *Panx1 fl/fl PF4-Cre*$^-$ mice 3 days after PPE surgery (Figure 43 D). However, platelet activation of the ITAM coupled GPVI receptor pathway activated by CRP and platelet activation by the second wave mediators U46 and ADP did not change platelet degranulation responses between platelets from *Panx1 fl/fl PF4-Cre*$^-$ and *Panx1 fl/fl PF4-Cre*$^+$ mice at early time points after PPE infusion (Figure 43 D). Seven days after PPE surgery the number of WBCs decreased in comparison to 3 days post-PPE surgery (Figure 42 A). To analyze whether platelet degranulation defects persisted 7 days after surgery even when the acute inflammatory phase has been subsided, the same analyses were performed as on day 3 (Figure 44).

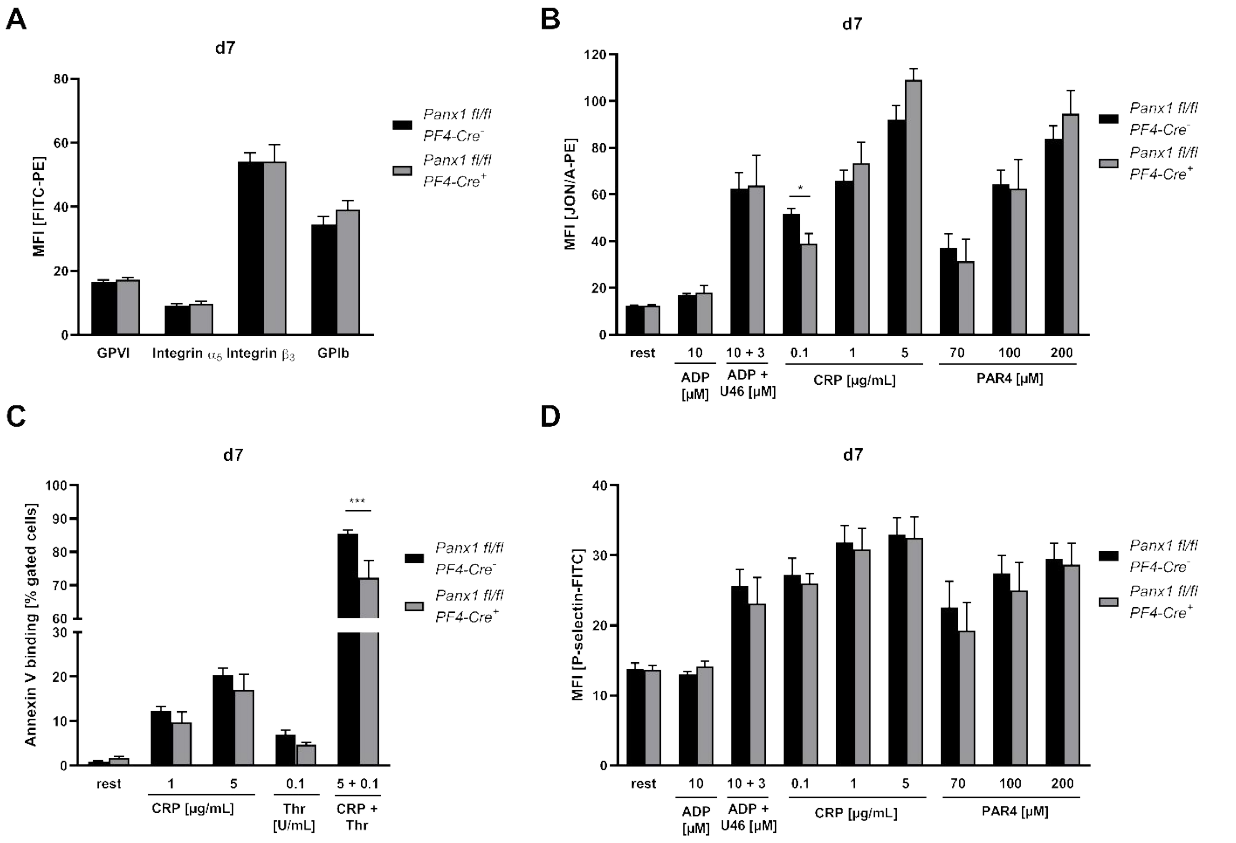

Figure 44: Mild platelet defects in *Panx1 fl/fl PF4-Cre*$^+$ mice compared to *Panx1 fl/fl PF4-Cre*$^-$ mice 7 days post-PPE surgery. Platelets from *Panx1 fl/fl PF4-Cre*$^-$ and *Panx1 fl/fl PF4-Cre*$^+$ mice were analyzed by flow cytometric analysis regarding their specific side scatter (SSC) and forward scatter (FSC) profile seven days after PPE surgery. (A) Expression of indicated glycoproteins on the surface of platelets measured via the MFI (n (WT) = 11; n (KO) = 6). (B) Integrin $\alpha_{IIb}\beta_3$ activation is only altered in platelets from *Panx1 fl/fl PF4-Cre*$^+$ mice compared to platelets from *Panx1 fl/fl PF4-Cre*$^-$ mice after platelet activation with 0.1 µg/mL CRP (n (WT) = 7-9; n (KO) = 4-6). (C) PS exposure was assessed by the percentage of gated Annexin V positive platelets, which is only altered on the platelet surface from *Panx1 fl/fl PF4-Cre*$^+$ mice compared to *Panx1 fl/fl PF4-Cre*$^-$ mice in response to 5 µg/mL CRP with 0.1 U/mL Thr (n = (WT) = 6; n (KO) = 5). (D) Degranulation (P-selectin) is not altered between platelets from *Panx1 fl/fl PF4-Cre*$^+$ mice compared to *Panx1 fl/fl PF4-Cre*$^-$ mice (n (WT) = 7-11; n (KO) = 6). Statistical analyses were performed using an unpaired multiple students t-test. Bar graphs indicate mean values ± SEM; *p < 0.05, ***p < 0.001. Rest = Resting, ADP = Adenosine diphosphate, U46619 (U46) = Thromboxane A_2 analogue, CRP = Collagen-related peptide, PAR4 peptide = Protease-activated receptor 4 peptide, Thr = Thrombin, MFI = Mean fluorescence intensity, WT = Wild type (*Panx1 fl/fl PF4-Cre*$^-$), KO = Knock-out (*Panx1 fl/fl PF4-Cre*$^+$), PPE = Porcine Pancreatic Elastase, Panx1 = Pannexin 1.

Flow cytometric analysis using platelets from *Panx1 fl/fl PF4-Cre*$^-$ and *Panx1 fl/fl PF4-Cre*$^+$ mice 7 days after PPE surgery showed no significant differences in glycoprotein expression (Figure 44 A). Moreover, exposure of activated integrin $\alpha_{IIb}\beta_3$ on the platelet surface was decreased on platelets from *Panx1 fl/fl PF4-Cre*$^+$ mice compared to platelets from *Panx1 fl/fl PF4-Cre*$^-$ mice only in response to 0.1 µg/mL CRP (Figure 44 B, $p = 0.011$). No alterations in platelet degranulation (P-selectin) were observed (Figure 44 D). Interestingly, Annexin V binding was reduced in platelets from *Panx1 fl/fl PF4-Cre*$^+$ mice compared to platelets from *Panx1 fl/fl PF4-Cre*$^-$ mice only in response to CRP and thrombin (Figure 44 C; $p = 0.0002$). Overall, minor alterations in platelet activation were observed in platelets from *Panx1 fl/fl PF4-Cre*$^+$ mice compared to platelets from *Panx1 fl/fl PF4-Cre*$^-$ mice 7 days post-PPE surgery (Figure 44).

The literature indicates that the remodeling of the aortic wall starts within the first 14 days post-PPE surgery, which leads to AAA formation up to 82 ± 15% increase in aortic size with 60% incidence in mice compared to respective baseline size [158]. The question rises, if platelet activation, glycoprotein expression and PS exposure is altered during the remodeling phase between platelets from *Panx1 fl/fl PF4-Cre*$^-$ and *Panx1 fl/fl PF4-Cre*$^+$ mice. Therefore, platelet activation was investigated after 14 days post PPE surgery. Flow cytometric analysis showed that glycoprotein expression is not altered between platelets from *Panx1 fl/fl PF4-Cre*$^-$ and *Panx1 fl/fl PF4-Cre*$^+$ mice 14 days post PPE surgery (Figure 45 A). Platelet activation, as measured by activated integrin $\alpha_{IIb}\beta_3$ exposure on the platelet surface revealed reduced integrin activation in platelets from *Panx1 fl/fl PF4-Cre*$^+$ mice compared to platelets from *Panx1 fl/fl PF4-Cre*$^-$ mice in response to high doses of CRP (5 µg/mL, $p = 0.015$) and PAR4 peptide (200 µM, $p = 0.012$) as shown in Figure 45 B. Additionally, platelets from *Panx1 fl/fl PF4-Cre*$^+$ mice displayed degranulation defects as measured by P-selectin exposure at the platelet surface following stimulation of platelets with 1 µg/mL CRP to activate the GPVI signaling pathway CRP (Figure 45 D, $p = 0.025$).

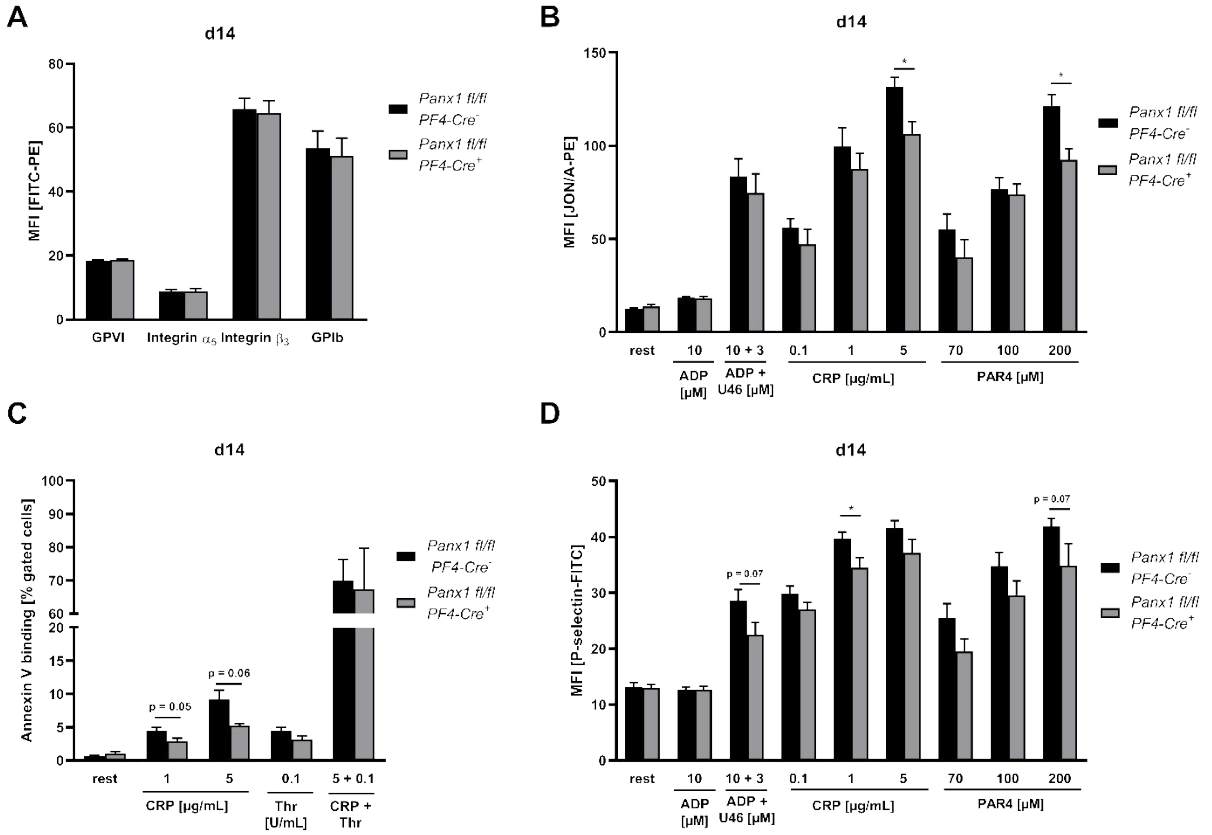

Figure 45: Platelet activation defects and reduced PS-exposure in platelets from *Panx1 fl/fl PF4-Cre*$^+$ mice compared to platelets from *Panx1 fl/fl PF4-Cre*$^-$ mice 14 days post-PPE surgery. Platelets from *Panx1 fl/fl PF4-Cre*$^-$ and *Panx1 fl/fl PF4-Cre*$^+$ mice were analyzed flow cytometric analysis regarding their specific side scatter (SSC) and forward scatter (FSC) profile 14 days after PPE surgery. (A) Expression of indicated glycoproteins on the surface of platelets measured via the MFI revealed no differences between platelets from *Panx1 fl/fl PF4-Cre*$^-$ and *Panx1 fl/fl PF4-Cre*$^+$ mice (n (WT) = 11; n (KO) = 6). (B) Integrin $\alpha_{IIb}\beta_3$ activation is reduced in platelets from *Panx1 fl/fl PF4-Cre*$^+$ mice compared to platelets from *Panx1 fl/fl PF4-Cre*$^-$ mice after platelet activation with 5 µg/mL CRP and 200 µM PAR4 peptide (n (WT) = 6-10; n (KO) = 4-6). (C) PS-exposure was assessed by the percentage of gated Annexin V positive platelets, which is altered on the platelet surface from *Panx1 fl/fl PF4-Cre*$^+$ mice compared to *Panx1 fl/fl PF4-Cre*$^-$ mice in response to 1 and 5 µg/mL CRP (n = (WT) = 4-6; n (KO) = 3-5). (D) Degranulation (P-selectin) is reduced in platelets from *Panx1 fl/fl PF4-Cre*$^+$ mice compared to *Panx1 fl/fl PF4-Cre*$^-$ mice in response to platelet activation1 µg/mL CRP and 200 µM PAR4 peptide (n (WT) = 10; n (KO) = 6). Statistical analyses were performed using an unpaired multiple students t-test. Bar graphs indicate mean values ± SEM, *p < 0.05: **p < 0.01 and ***p < 0.001. Rest = Resting, ADP = Adenosine diphosphate, U46619 (U46) = Thromboxane A_2 analogue, CRP = Collagen-related peptide, PAR4 peptide = Protease-activated receptor 4 peptide, Thr = Thrombin, MFI = Mean fluorescence intensity, WT = Wild type *(Panx1 fl/fl PF4-Cre*$^-$), KO = Knock-out (*Panx1 fl/fl PF4-Cre*$^+$), PPE = Porcine Pancreatic Elastase, Panx1 = Pannexin 1.

The dilatation of the aortic wall enhances from day 14 until day 28 post-PPE surgery (Figure 40). Therefore, further experiments were performed to investigate if platelet activation is altered at day 28 after PPE-surgery.

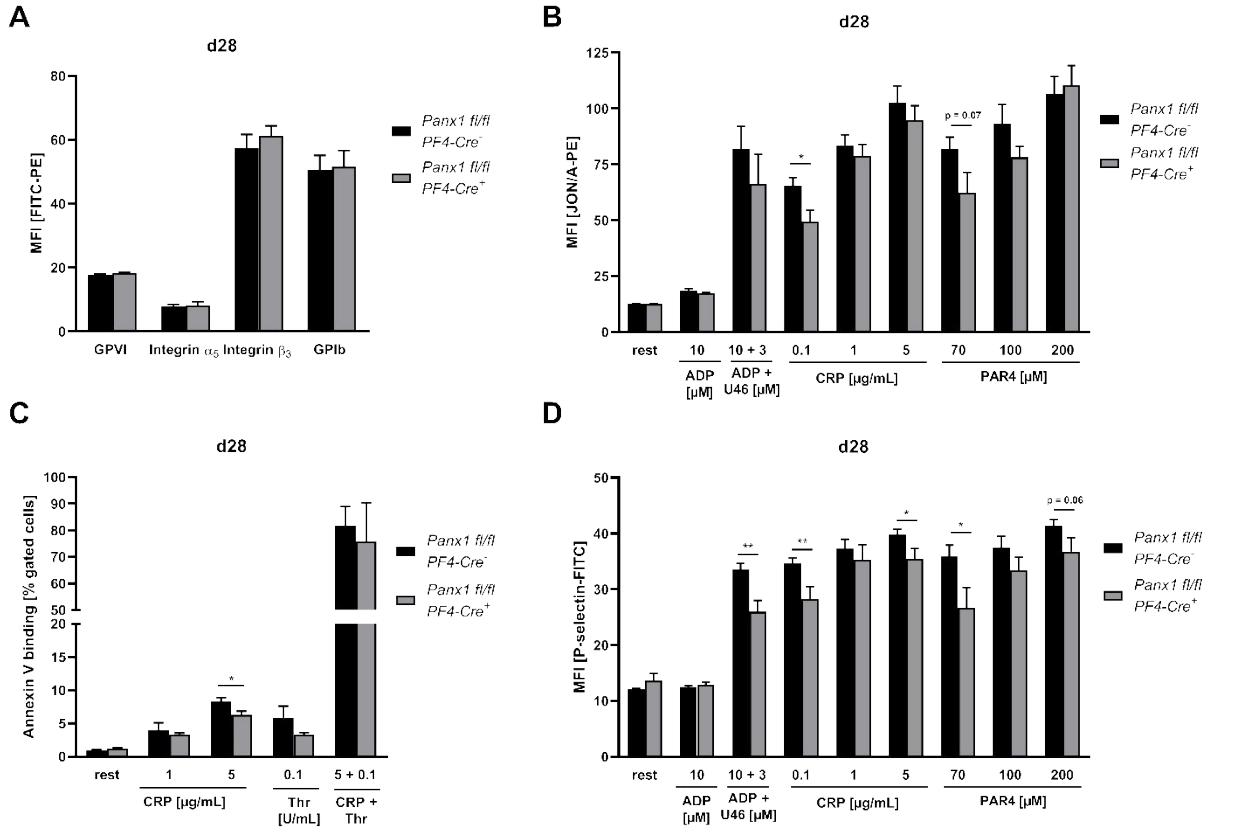

Figure 46: Platelet activation defects and reduced PS-exposure in platelets from *Panx1 fl/fl PF4-Cre*$^+$ mice compared to platelets from *Panx1 fl/fl PF4-Cre*$^-$ mice 28 days post-PPE surgery. Platelets from *Panx1 fl/fl PF4-Cre*$^-$ and *Panx1 fl/fl PF4-Cre*$^+$ mice were analyzed by flow cytometric analysis regarding their specific side scatter (SSC) and forward scatter (FSC) profile 28 days after PPE surgery. (A) Expression of indicated glycoproteins on the surface of platelets measured via the MFI indicated no differences between platelets from *Panx1 fl/fl PF4-Cre*$^-$ and *Panx1 fl/fl PF4-Cre*$^+$ mice (n (WT) = 11; n (KO) = 6). (B) Integrin $\alpha_{IIb}\beta_3$ activation is reduced in platelets from *Panx1 fl/fl PF4-Cre*$^+$ mice compared to platelets from *Panx1 fl/fl PF4-Cre*$^-$ mice after platelet activation with 0.1 µg/mL CRP and 70 µM PAR4 peptide (n (WT) = 6-10; n (KO) = 4-6). (C) PS-exposure was assessed by the percentage of gated Annexin V positive platelets, which is altered on the platelet surface from *Panx1 fl/fl PF4-Cre*$^+$ mice compared to *Panx1 fl/fl PF4-Cre*$^-$ mice in response to 5 µg/mL CRP (n = (WT) = 5-6; n (KO) = 3-4). (D) Degranulation (P-selectin) is reduced in platelets from *Panx1 fl/fl PF4-Cre*$^+$ mice compared to *Panx1 fl/fl PF4-Cre*$^-$ mice in response to platelet activation with 10 µM ADP + 3 µM U46, 0.1 µg/mL CRP and 70 and 200 µM PAR4 peptide (n (WT) = 6-10; n (KO) = 4-6). Statistical analyses were performed using an unpaired multiple students t-test. Bar graphs indicate mean values ± SEM, *$p < 0.05$; **$p < 0.01$. Rest = Resting, ADP = Adenosine diphosphate, U46619 (U46) = Thromboxane A_2 analogue, CRP = Collagen-related peptide, PAR4 peptide = Protease-activated receptor 4 peptide, Thr = Thrombin, MFI = Mean fluorescence intensity, WT = Wild type (*Panx1 fl/fl PF4-Cre*$^-$), KO = Knock-out (*Panx1 fl/fl PF4-Cre*$^+$), PPE = Porcine Pancreatic Elastase, Panx1 = Pannexin 1.

AAA formation was observed 28 days after surgery when the dilation of the aortic lumen exceeded 120% compared with basal aortic diameter before surgery. In all mice with stable AAA formation, FACS analyses revealed no differences in glycoprotein expression between platelets from *Panx1 fl/fl PF4-Cre*$^-$ and *Panx1 fl/fl PF4-Cre*$^+$ mice at 28 days post PPE surgery (Figure 46 A). PS exposure as measured by Annexin V binding was reduced in platelets from *Panx1 fl/fl PF4-Cre*$^+$ compared with platelets from *Panx1 fl/fl PF4-Cre*$^-$ mice only in response to 5 µg/mL CRP (Figure 46 C, $p = 0.026$). Integrin $\alpha_{IIb}\beta_3$ exposure on the platelet surface was

significantly reduced after platelet activation with low dose CRP (0.1 µg/mL, p = 0.019) and reduced only by trend with mild PAR4 peptide stimulation (p = 0.066) using platelets from *Panx1 fl/fl PF4-Cre*$^{+}$ mice compared to WT platelets as shown in Figure 46 B. Platelets from *Panx1 fl/fl PF4-Cre*$^{+}$ mice displayed reduced degranulation responses compared to the control group, which was measured by P-selectin exposure at the platelet membrane (Figure 46 D). In particular, platelet activation with mild (0.1 µg/mL, p = 0.008) and high (5 µg/mL, p = 0.033) doses of CRP led to reduced degranulation responses in platelets from *Panx1 fl/fl PF4-Cre*$^{+}$ mice compared to platelets from *Panx1 fl/fl PF4-Cre*$^{-}$ mice (Figure 46 D). GPCR activation by low (70 µM, p = 0.033) and high (200 µM, p = 0.065) doses of PAR4 peptide reduced platelet degranulation of platelets from *Panx1 fl/fl PF4-Cre*$^{+}$ mice compared to platelets from *Panx1 fl/fl PF4-Cre*$^{-}$ mice, respectively (Figure 46 D). Platelet activation induced by the second wave mediators U46619 and ADP together leads to reduced degranulation in platelets from *Panx1 fl/fl PF4-Cre*$^{+}$ mice compared to platelets from *Panx1 fl/fl PF4-Cre*$^{-}$ mice (Figure 46 D, p = 0.005). The results indicate that the genetic deletion of PANX1 in platelets leads to reduced platelet activation and PS exposure 28 days post PPE surgery, which correlates with ongoing aortic wall remodeling and enhanced AAA formation as shown in Figure 45 and Figure 46.

The release of inflammatory cytokines by platelets is a crucial mechanism of immune cell recruitment to sites of inflammation [57, 105, 126]. Previous studies report that neutrophils play a central role in the pathogenesis of AAA [159, 160]. Interplay of platelets and neutrophils were shown to promote the development of AAA [160]. Furthermore, we detected reduced platelet-neutrophil aggregates upon LPS and TNF-a stimulation *in vitro*. To investigate, if a genetic deletion of PANX1 in platelets also alters aggregate formation of platelets and neutrophils *in vivo*, flow cytometric analysis was performed. Therefore, cells were stimulated with or without CRP (5 µg/mL) or thrombin (0.1 U/mL) and labeled with fluorophore-conjugated antibodies for CD42 (GPIb-PE) as platelet marker and Ly6G-APC as marker for neutrophils. The percentage of double positive events for GPIb and Ly6G were analyzed before surgery (Baseline) and at day 3, 7, 14 and 28 days post PPE surgery (Figure 47).

The results indicate a reduced number of platelet-neutrophil aggregates 14 days post-PPE surgery in washed whole blood samples from *Panx1 fl/fl PF4-Cre*$^{+}$ mice compared to *Panx1 fl/fl PF4-Cre*$^{-}$ mice (Figure 47 A, p = 0.027). For all other time points no significant differences were observed between both genotypes. Platelet activation by CRP (Figure 47 B) and thrombin (Figure 47 C), respectively, induced elevated platelet-neutrophil aggregate formation compared to baseline conditions (day 0) at day 7, day 14 and day 28 after PPE surgery except for CRP stimulation at day 14 post-PPE surgery in the group of *Panx1 fl/fl PF4-Cre*$^{+}$ mice (7.1.7). However, no significant

differences were observed between both groups of *Panx1 fl/fl PF4-Cre* mouse stains at all measured time points (Figure 47 B, C). The levels of significances within both genotypes are listed in chapter 7.1.7.

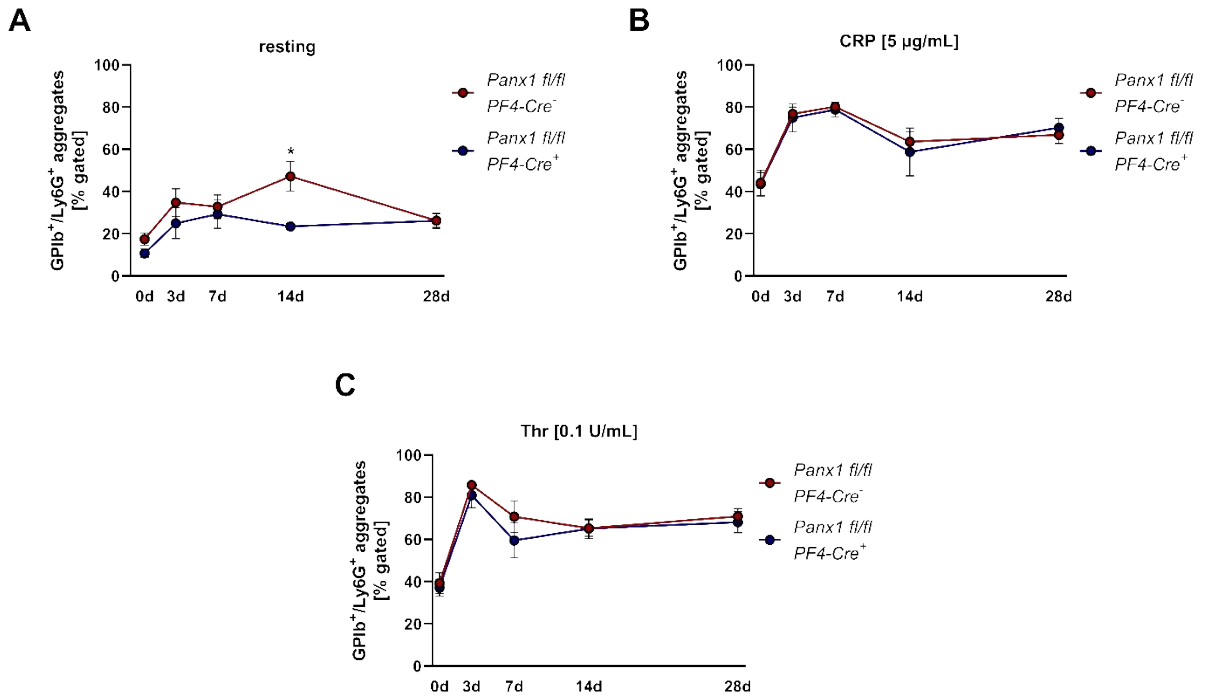

Figure 47: Reduced number of platelet-neutrophil aggregates at 14 days post-PPE surgery in blood samples of *Panx1 fl/fl PF4-Cre*$^{+}$ compared to *Panx1 fl/fl PF4-Cre*$^{-}$ mice. Platelet-neutrophil aggregates were measured (A) under resting conditions and after platelet activation with (B) 5 µg/mL CRP and (C) 0.1 U/mL Thr at different time points under native conditions (0d) and at day 3,7, 14 and 28 post-PPE surgery (n rest (WT): 0d = 6, 3d = 11, 7d = 11, 14d = 10, 28d = 11, (KO) 0d = 6, 3d = 6, 7d = 6, 14d = 6, 28d = 7; n CRP (WT): 0d = 6, 3d = 11, 7d = 11, 14d = 10, 28d = 11 (KO) 0d = 6, 3d = 6, 7d = 6, 14d = 6, 28d = 6; n Thr (WT): 0d = 6, 3d = 11, 7d = 11, 14d = 9, 28d = 11 (KO) 0d = 6, 3d = 6, 7d = 6, 14d = 6, 28d = 6). Aggregates were determined by the percent of gated double positive events for CD42 (GPIb-PE) as a platelet marker and Ly6g-APC as a marker to for neutrophils. Statistical analyses were performed using a two-way ANOVA followed by a Sidak's multiple comparisons post-hoc test. Bar graphs indicate mean values ± SEM, *p < 0.05. D = Day, Rest = Resting, CRP = Collagen-related peptide, Thr = Thrombin, WT = Wild type (*Panx1 fl/fl PF4-Cre*$^{-}$), KO = Knock-out (*Panx1 fl/fl PF4-Cre*$^{+}$), PPE = Porcine Pancreatic Elastase, Panx1 = Pannexin 1.

Furthermore, it has been described that higher levels of the circulating inflammatory cytokines IL-1β and IL-6 are found in the plasma of patients with AAA compared with patients with AOD [107, 108]. This is due to proteolysis of the aortic wall upon AAA development, where especially MMP-9 and TGF-β play a crucial role [99, 109, 110]. Therefore, the plasma of native and operated mice at day 14 and day 28 after PPE surgery was analyzed for levels of IL-1β, IL-6 IL1, MMP-9 and TGF-β by ELISA (Figure 48). Plasma analysis between of samples from *Panx1 fl/fl PF4-Cre*$^{-}$ and *Panx1 fl/fl PF4-Cre*$^{+}$ mice revealed altered IL-1β levels 14 days after surgery only by trend (Figure 48 A, p = 0.0588). Moreover 28 days after PPE surgery, both groups displayed a

downregulation of circulating TGF-β levels (Figure 48 B, WT p = 0.0129; KO p = 0.0388) which was not altered at 14 days after surgery compared to TGF-β plasma levels in native mice. On the other hand, MMP-9 plasma levels were significantly increased in the group of operated *Panx1 fl/fl PF4-Cre*$^{-}$ animals 28 after surgery, whereas in the group of *Panx1 fl/fl PF4-Cre*$^{+}$ animals MMP-9 only increased by trend compared to native mice, respectively (Figure 48 C, WT: p = 0.0032; KO: p = 0.0705). IL-6 was not detectable in the plasma of these mice (Data not shown).

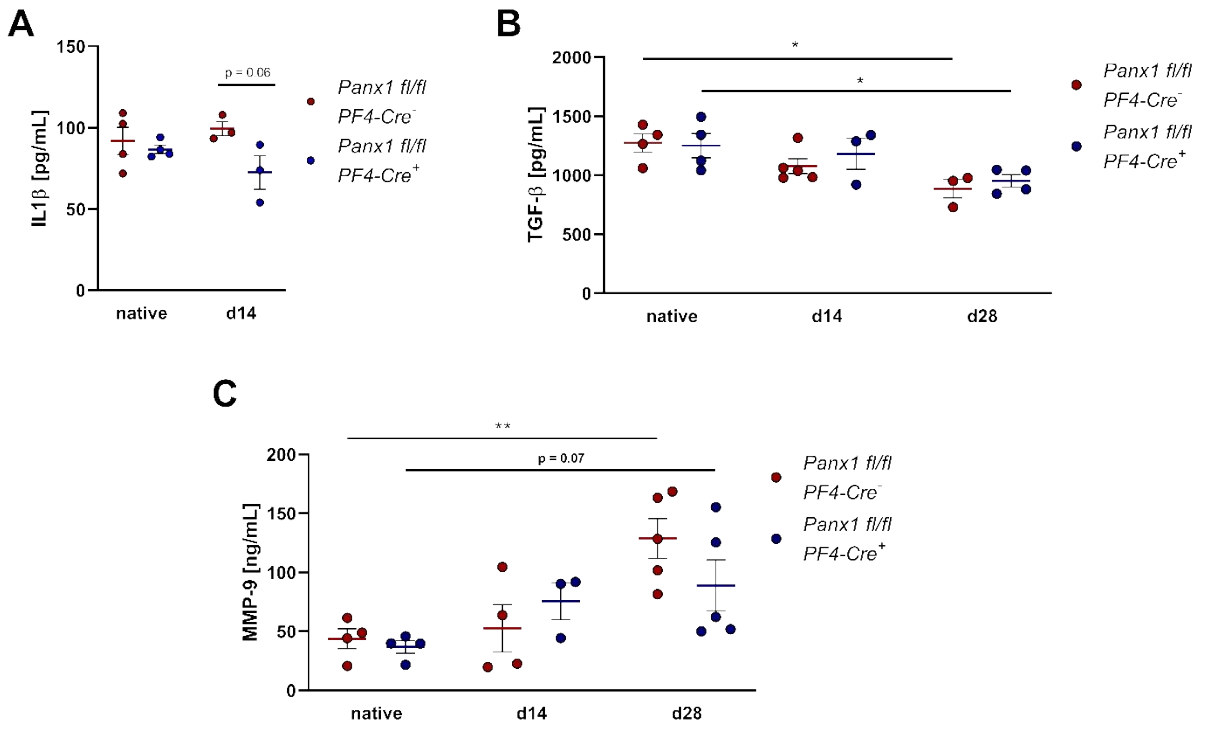

Figure 48: Minor changes between plasma analysis of IL-1β, MMP-9 and TGF-β between *Panx1 fl/fl PF4-Cre*$^{+}$ compared to *Panx1 fl/fl PF4-Cre*$^{-}$ *mice.* Plasma levels of (A) IL-1β (native n (WT) = 4, n (KO) = 4; 14d n (WT) = 3, n (KO) = 3) (B) TGF-β (native n (WT) = 4, n (KO) = 4; 14d n (WT) = 5, n (KO) = 3; 28d n (WT) = 3, n (KO) = 4) and (C) MMP-9 (native n (WT) = 4, n (KO) = 4; 14d n (WT) = 4, n (KO) = 3; 28d n (WT) = 5, n (KO) = 5) native mice and operated mice at day 14 and day 28 (only MMP-9 and TGF-β) after PPE surgery was measured by ELISA. Statistical analyses were performed using a two-way ANOVA followed by a Sidak's multiple comparisons post-hoc test. Bar graphs indicate mean values ± SEM, *p < 0.05, **p < 0.01. D = Day, WT = Wild type (*Panx1 fl/fl PF4-Cre*$^{-}$), KO = Knock-out (*Panx1 fl/fl PF4-Cre*$^{+}$), PPE = Porcine Pancreatic Elastase, Panx1 = Pannexin 1, IL-1β = Interleukin-1β, TGF-β = Transforming growth factor-β, MMP-9 = Matrix metalloproteinase-9, Panx1 = Pannexin 1.

Another characteristic feature in the progression of AAA is the migration of immune cells into the aortic tissue [161]. Initially, neutrophils inflame the tissue, followed by macrophages and lymphocytes 10-14 days after PPE surgery [162]. A platelet specific PANX1 deletion in mice leads to altered platelet activation (Figure 45), platelet-neurtophil aggregate formation (Figure 47) as well as circular plasma levels (Figure 48) 14 days after PPE surgery *in vivo*, we were interested whether these alterations affect the migration of immune cells into the aortic tissue. Therefore,

histological sections of the aorta from *Panx1 fl/fl PF4-Cre*$^{-}$ and *Panx1 fl/fl PF4-Cre*$^{+}$ mice were prepared, which were stained with IF. This method describes an important immunochemical procedure that allows the detection and localization of a variety of antigens in different tissue types such as the aorta. Initially, the focus was on neutrophils, as they showed reduced aggregate formation with platelets 14 days after surgery (Figure 47 A). Neutrophils were visualized using the neutrophil specific marker (Ly6G/Cy5 in red), while cell nuclei were stained with DAPI (blue). Neutrophil infiltration in the aorta is displayed in Figure 49.

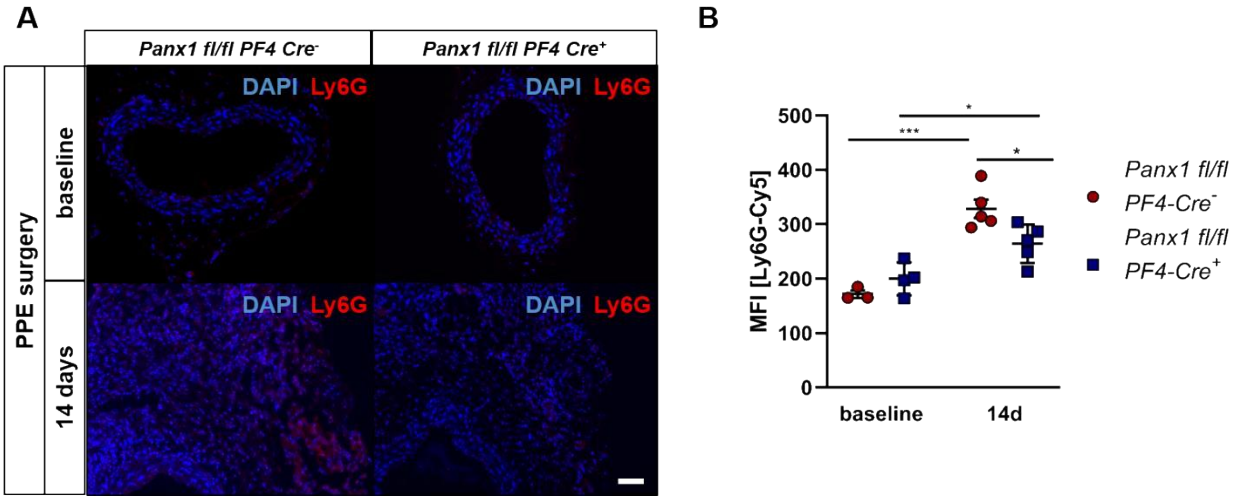

Figure 49: Reduced neutrophil infiltration in aortic tissue 14 days after PPE surgery in *Panx1 fl/fl PF4-Cre*$^{+}$ mice. Aortic sections from murine tissues from *Panx1 fl/fl PF4-Cre*$^{-}$ and *Panx1 fl/fl PF4-Cre*$^{+}$ mice were analyzed regarding neutrophil infiltration before (Baseline) and 14 after PPE surgery. (A) Neutrophils were visualized using the neutrophil specific marker (Ly6G/Cy5 in red), while cell nuclei were stained with DAPI (blue). Representative merged images of Ly6G and DAPI of both genotypes before (baseline) and 14 days after surgery. Scale bar represents 50 µM. Single channel images according to merged images and corresponding IgG controls are found in Figure 58 and Figure 59. (B) Neutrophil infiltration was quantified by the total Ly6G positive fluorescence area [IFLy6G/ µm²] of the aortic sections at indicated time points. Platelet specific deletion reduces neutrophil infiltration 14 days after PPE surgery, which was not altered before surgery. At 14 days after PPE surgery, the number of migrated neutrophils was increased only in *Panx1 fl/fl PF4-Cre*$^{-}$ mice (baseline n (WT) = 3, n (KO) = 4; 14d n (WT) = 5, n (KO) = 5). Statistical analyses were performed using a two-way ANOVA followed by a Sidak's multiple comparisons post-hoc test. Bar graphs indicate mean values ± SEM, *p < 0.05, ***p < 0.001. D = Day, WT = Wild type (*Panx1 fl/fl PF4-Cre*$^{-}$), KO = Knock-out (*Panx1 fl/fl PF4-Cre*$^{+}$), PPE = Porcine Pancreatic Elastase, Panx1 = Pannexin 1, MFI = Mean fluorescence intensity, d = Days.

At 14 days after PPE surgery, neutrophil migration was significantly increased compared to baseline conditions within both genotypes (Figure 49 B, WT: $p < 0.001$, KO: $p = 0.0218$). However, in *Panx1 fl/fl PF4-Cre*$^{+}$ mice the number of infiltrated neutrophils was reduced at 14 days after PPE surgery compared to *Panx1 fl/fl PF4-Cre*$^{-}$ controls (Figure 49 B, $p = 0.024$), while no alterations were detected before the surgery in these mice (Figure 49 B). To analyze the migration of platelets in PPE mice, aortic sections from *Panx1 fl/fl PF4-Cre*$^{-}$ and *Panx1 fl/fl PF4-Cre*$^{+}$ mice were labeled with the platelet specific marker GPIb (Cy5) and visualized

via IF staining. Although platelets do not have a cell nucleus, nuclei were stained with DAPI as a control to better visualize platelet localization (Figure 50).

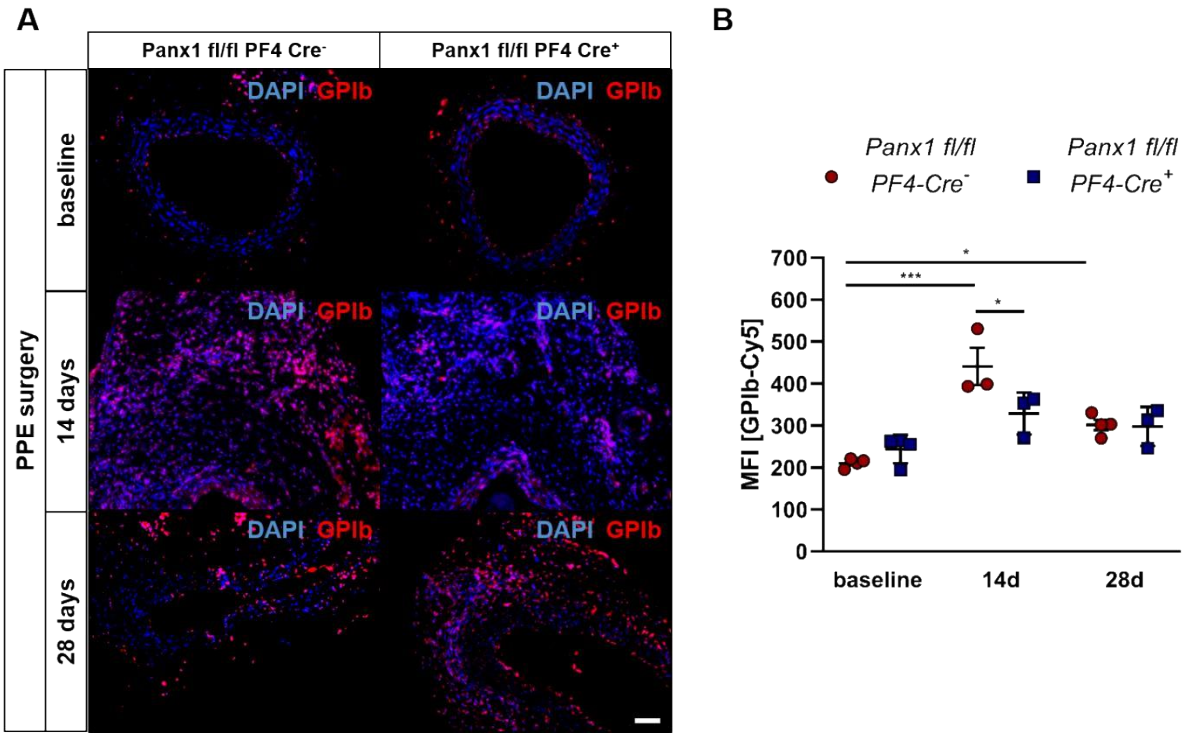

Figure 50: Reduced platelet migration in aortic tissue 14 days after PPE surgery in *Panx1 fl/fl PF4-Cre*$^+$ mice. Aortic sections from murine tissues from *Panx1 fl/fl PF4-Cre*$^-$ and *Panx1 fl/fl PF4-Cre*$^+$ mice were analyzed regarding platelet migration before (Baseline) and 14 and 28 days after PPE surgery. (A) Platelets were visualized using a platelet specific marker (GPIb/Cy5 in red), while cell nuclei were stained with DAPI (blue). Representative merged images of GPIb and DAPI of both genotypes at indicated time points. Scale bar represents 50 µM. Single channel images according to merged images and corresponding IgG controls are found in Figure 60 and Figure 61. (B) Platelet migration was quantified by the total GPIb positive fluorescence area [IFGPIb/ µm²] of the aortic sections at indicated time points. Platelet specific *Panx1* deletion in mice (*Panx1 fl/fl PF4-Cre*$^+$) leads to reduced platelet migration 14 days after PPE surgery, while platelet migration was not altered before and 28 days after surgery. Platelet migration increases over AAA progression only in *Panx1 fl/fl PF4-Cre*$^-$ mice (baseline n (WT) = 4, n (KO) = 4; 14d n (WT) = 3, n (KO) = 4; 28d n (WT) = 4, n (KO) = 3). Statistical analyses were performed using a two-way ANOVA followed by a Sidak's multiple comparisons post-hoc test. Bar graphs indicate mean values ± SEM, *p < 0.05, ***p < 0.001. D = Day, WT = Wild type (*Panx1 fl/fl PF4-Cre*$^-$), KO = Knock-out (*Panx1 fl/fl PF4-Cre*$^+$), PPE = Porcine Pancreatic Elastase, Panx1 = Pannexin 1, MFI = Mean fluorescence intensity, d = Days.

Analysis of platelet migration into the aortic wall after PPE surgery displays an increased number of migrated platelets in aortic sections of *Panx1 fl/fl PF4-Cre*$^-$ mice at day 14 ($p < 0.001$) and day 28 ($p = 0.039$) after surgery compared to baseline controls (Figure 50 B). The number of migrated platelets were increased in the group of *Panx1 fl/fl PF4-Cre*$^+$ mice at day 14 and day 28 after PPE surgery without reaching statistical significance (Figure 50 B, $p = 0.08$). In addition, *Panx1 fl/fl PF4-Cre*$^+$ mice revealed reduced platelet migration 14 days after PPE surgery compared to controls (Figure 50 B, $p = 0.0167$). Taken together, the results of the present work demonstrate that platelet PANX1 channels play a role in the activation and migration of neutrophils and thus modulate inflammatory processes during the development of AAA.

5 Discussion

Platelets are key players in primary hemostasis as they are responsible for the formation of a primary plug to prevent massive blood loss. Since platelet mediated primary hemostasis is a tightly regulated process, uncontrolled thrombus formation can lead to vessel occlusion resulting in cardiovascular events as stroke or myocardial infarction [17]. To reduce the probability of CVDs, antiplatelet therapies are developed which were shown to inhibit platelet receptors (e.g. $P2Y_{12}$ and $P2Y_1$ antagonists using clopidogel, prasugrel and ticagrelor), block adhesion receptors (e.g. Glycoprotein IIb/IIIa inhibiton with abciximab, eptifibatide and tirofiban) or enhance inhibitory pathways (e.g. COX-1 inhibiton by aspirin) [163-165]. However, the population is becoming increasingly resistant to classic antiplatelet agents such as aspirin [138]. As a result, the development of novel antithrombotic targets are relevant which do on the one hand not enhance bleeding risks and on the other hand are highly efficient against thrombotic events [136, 137]. Previous studies suggest that PANX1 channels play a crucial role in hemostasis and thrombosis [23, 80-82], however the regulation of PANX1 channels in platelets is poorly understood to date.

5.1 Pannexin 1 as an important channel mediating non-vesicular ATP release in platelets

The present study demonstrates a functional role of PANX1 in human and mouse platelets as an ATP release channel in response to ITAM coupled and GPCR mediated signaling. These data is in line with results from previous studies from others, because measurements in platelets indicate reduced ATP release in PANX1 deficient platelets or after pharmacological PANX1 inhibition in response to platelet stimulation with low concentrations of collagen [80, 81]. Beside collagen induced platelet activation, Taylor *et al.* observed reduced ATP release after pharmacological inhibition of PANX1 upon platelet activation with low doses of U46119 [81]. The present thesis demonstrates a reduction in ATP release in response to TP receptor stimulation only after pharmacological inhibition of PANX1 in human platelets, which confirms the observations from Taylor and colleagues [81]. However, the present results do not indicate a role for TP receptors in PANX1 activation in murine platelets. One reason might be that Prb as a PANX1 inhibitor is not specific for PANX1 but also blocks anion transporters [166]. The IC_{50} of Prb is ~150 µM and pharmacokinetic studies indicate that Prb reaches plasma concentrations in patients taking oral Prb of around 78 µM [166]. Therefore, the here used concentration of 100 µM Prb does not inhibit anion transporters and is suitable as well-tolerated potential medication for patients [167],

concluding that 100 µM of PANX1 inhibitor Prb should be sufficient for the performed experiments in this thesis. The observed differences in TP receptor mediated ATP release through PANX1 channels in platelets from genetically modified mice and pharmacological inhibition of human platelets may be due to species related differences between murine and human platelets [2]. It was shown that murine and human platelets consist of major mRNA expression differences of about 80% and the altered expression patterns of expressed surface receptors can alter signaling pathways between murine and human platelets [168]. Interestingly, the study revealed that especially Src as well as ADP receptor $P2Y_{12}$ is differentially regulated at mRNA as well as protein levels between human and murine platelets [168]. In particular, SFKs play a central role in platelet PANX1 activation [23]. Platelet activation with ADP does not alter ATP release after PANX1 inhibition in human platelets as well as in PANX1 deficient platelets from genetically modified mice, which was also observed in previous studies [80]. All results concerning ATP release measurements were performed under the application of apyrase. This enzyme is essential to reduce a part of the platelet second wave mediated activation, since apyrase scavenges released ATP from platelets [169]. Complete inhibition of platelet second wave activation would be possible by inhibition of the TxA_2 synthesis by indomethacin [170]. However, this is not required in the present experiments, since ATP release due to PANX1 directly amplifies P2 receptor signaling. Without application of apyrase, the role of PANX1 channels in non-vesicular ATP release cannot be examined since platelet degranulation covers the effects of PANX1 channels. PANX1 deficient platelets displayed reduced ATP release in resting conditions, which might be due to PANX1 autophosphorylation as discussed above in chapter 5.3. Since PANX1 deficient and respective control platelets contain similar ATP concentrations [82], PANX1 might be required for proper degranulation responses because ATP is stored in platelet dense granules and released upon platelet activation [171]. These results may suggest that the genetic loss of PANX1 channels alters the proper regulation of intracellular degranulation responses, hypothesizing a role for PANX1 in intracellular communication by balancing ATP hemostasis.

5.2 Platelet pannexin 1 is a fine-tuning regulator of hemostasis and involved in arterial thrombosis

In this thesis, two genetically modified mouse models as well as pharmacological inhibition of PANX1 channels by Prb and Cbx in human platelets as a first translational approach were used. The genetic loss of PANX1 either in platelets or as a constitutive *Panx1* knock-out does not change blood cell counts or MPV. Alterations within these parameters are important to analyze because

they can modulate hemostasis as known for patients suffering from platelet disorders [172]. Beside platelet disorders, the number of platelets can alter under pathological conditions as shown by an increase of platelets enhancing hemostatic responses as observed in pulmonary arterial hypertension [173]. Nevertheless, it is important to consider that genetically modified mouse models can present pitfalls. Mice with a global deletion of PANX1 showed increased levels of PANX3 even in tissues where this isoform is normally not located e.g. the endothelium [174]. Due to these reasons, it is important to investigate compensatory mechanisms in genetiallyc modified knock-out mouse models. A study from Molica *et al.* displayed no differences in constitutive *Panx1*$^{-/-}$ mice regarding platelet counts and the number of lymphocytes [82], which is in line with the here presented results. For the platelet specific *Panx1 fl/fl PF4-Cre*$^{+}$ mouse strain, no pitfalls regarding hemostasis were reported in the literature until today and the reported cell counts do not differ between genotypes [82] which is in line with the results of this thesis.

Flow cytometric analysis displays that integrin $\alpha_{IIb}\beta_3$ activation is only reduced upon platelet stimulation with PAR4 peptide. Since Src dependent ATP secretion is essential for proper integrin $\alpha_{IIb}\beta_3$ activation [175], reduced integrin $\alpha_{IIb}\beta_3$ activation in PANX1 deficient platelets might be due to reduced ATP release upon low dose PAR4 peptide stimulation. Additionally, PAR4 peptide induced platelet activation increases PANX1 Tyr^{198} phosphorylation, which is dependent on SFKs, supporting the hypothesis of reduced integrin $\alpha_{IIb}\beta_3$ activation after GPCR signaling. Reduced degranulation responses of platelet α-granules as measured by P-selectin exposure at the platelet membrane was observed upon high dose stimulation of CRP, which was not observed for low or intermediate concentrations of CRP. This is not surprising, since collagen induced platelet activation via GPVI signaling is the main regulator in PANX1 activation as shown by increased PANX1 Tyr^{198} phosphorylation and by collagen induced ATP release. However, the observed differences were not detected in response to threshold concentrations of CRP, which is unexpected because PANX1 dependent ATP release and aggregation were mediated especially in response to lower concentrations of CRP or collagen [23, 80, 81]. Additionally, the release of platelet δ-granules was measured via mepacrine release to investigate general defects in δ-granule release and upon PAR4 and thrombin stimulation, indicating that PANX1 channels do not alter degranulation responses of either platelet α-granules or δ-granules in response to platelet activation via PAR receptor signaling. However, the results from human platelets indicate reduced degranulation in response to GPCR signaling. Thus, the observed results do not completely correspond to the results from PANX1 deficient murine platelets concerning platelet activation. As already mentioned before, it must be considered that Cbx and Prb are non-specific inhibiting compounds of PANX1 channels, which were shown to mainly inhibit PANX1 dependent currents

but also other platelet receptors [83-86]. Additionally, the observed altered activation profiles after pharmacological PANX1 inhibition were performed in human platelets, which differ from murine platelets e.g. in platelet size, number, lifespan [2] and mRNA content [168] as discussed in chapter 5.1. Interestingly, whole blood analysis of constitutive *Panx1* knock-out mice displayed differences in platelet activation compared to the group of mice with a platelet specific PANX1 deletion. Whole blood analysis of *Panx1*$^{-/-}$ mice revealed significantly reduced integrin $\alpha_{IIb}\beta_3$ activation only upon high dose CRP stimulation, but not after PAR4 stimulation as it was detected in *Panx1 fl/fl PF4-Cre*$^{+}$ mice. Minor differences in platelet activation profiles between *Panx1 fl/fl PF4-Cre* mice and constitutive deleted *Panx1* mice might be because all measurements were performed in washed whole blood. Since RBCs [70] and leukocytes [143] also express PANX1 channels contributing to platelet activation [142, 176], these potential interaction mechanisms can explain altered activation profiles between both genotypes. Moreover, within both PANX1 deficient mouse models no significant differences in glycoprotein expression of GPVI, α_5-integrin, β_3-integrin and GPIb on the platelet surface were observed. Altered glycoprotein expression on the platelet surface can potentially account for altered platelet activation which was shown in *Bgn*$^{-/0}$ mice [177]. Those platelets displayed reduced expression of GPVI receptors on their surface compared to WT platelets which is indicative of reduced platelet activation of integrin $\alpha_{IIb}\beta_3$ and reduced degranulation as measured by P-selectin upon collagen induced platelet activation [177]. Up and downregulation of platelet glycoproteins in knock-out mouse models might also be due to compensatory mechanisms because of genetic modification of the genome, which was already displayed in constitutive *Panx1* knock-out mice [178].

Analysis of platelet activation confirms that platelet PANX1 channels contribute to platelet aggregation only in response to ITAM coupled receptors. The current results correspond to the findings from Molica and colleagues which already published decreased aggregation in PANX1 deficient platelets in response to platelet activation with low doses of collagen compared to respective control platelets in 2015 [80]. Moreover, within the same study no alterations in response to ADP induced platelet activation between platelets from *Panx1*$^{-/-}$ mice compared to control platelets were observed confirming the present findings. In line, human platelets preincubated with the PANX1 inhibiting compound Prb showed comparable results as observed in murine studies [80]. Here, concentrations of Prb of 2 mM were used which completely abolished platelet aggregation suggesting potentially inhibition of anion transporters by Prb as well [167]. Moreover, the results of this thesis do not reveal PANX1 dependent aggregation responses after platelet activation with either PAR4 peptide or U46619. It was assumed that reduced ATP release due to PANX1 channels potentially correlates with reduced aggregation responses because of

altered $P2X_1$ receptor stimulation [81]. However, this is not correct because platelet stimulation with low dose PAR4 peptide reduced ATP release but not aggregation responses in PANX1 deficient platelets compared to respective WT controls as shown in chapter 4.1 and 4.2.3.

PANX1 channels are well-known to be activated via mechanical stimulation [179], and are involved in many vascular processes such as the regulation of blood pressure. Therefore, a possible role of platelet PANX1 in hemostasis has been suggested. Under high arterial conditions, ATP receptor $P2X_1$ was shown to be activated by low concentrations of collagen concluding ATP as an important agonist at early stages of arterial vascular injury of the endothelium [180]. This was the reason why thrombus formation assays were carried out on a collagen coated matrix at arterial shear rates in an experimental approach *ex vivo*. Analysis of experiments at a low arterial shear of $450s^{-1}$ indicated a role of PANX1 in thrombus formation, which was shown by a reduction of the surface coverage in platelet specific *Panx1 fl/fl PF4-Cre*$^+$ mice compared to blood from respective control mice. However, the three-dimensional structure of the thrombi measured by the MFI of the thrombus volume was not altered at a shear rate of $450s^{-1}$ suggesting that the initial adhesion process is altered but not the recruitment of further platelets from the blood stream important for three-dimensional thrombus formation under flow. At an intermediate arterial shear rate of $1{,}000s^{-1}$, surface coverage was reduced by trend, but the thrombus volume was decreased in whole blood from *Panx1 fl/fl PF4-Cre*$^+$ mice compared to whole blood from *Panx1 fl/fl PF4-Cre*$^-$ mice. These results suggest that PANX1 displays different functional roles at different shear rates. It is well-known that PANX1 mediated ATP release is important for chemotaxis of e.g. neutrophils [77], hypothesizing that cell-cell interaction might be the reason for the observed results at different shear rates. To investigate the question, if platelet PANX1 channels are essential for the initial adhesion process, similar experiments supplemented with apyrase can give insights by inhibition of $P2X_1$ receptors scavenging ATP to mimic platelet second wave inhibition [180]. Nevertheless, the role of PANX1 in arterial thrombosis was already confirmed by $FeCl_3$-injured mesenteric arteries experiments *in vivo* [82]. Mice, targeting a platelet specific PANX1 deletion tend to increased initial thrombus formation and the time to arterial occlusion was prolonged *in vivo* underlining the role of PANX1 in both initial adhesion and thrombus formation at arterial shear rates [82].

Moreover, the results of thrombus formation using human blood are comparable with the experiments performed with murine blood. However, it must be taken into consideration that in human whole blood PANX1 channels on WBCs and RBCs are also inhibited by either Prb or Cbx, whereas the mouse carries a platelet specific PANX1 deletion. To exclude the side effect of Prb on RBCs, which have been shown to contribute significantly to thrombus formation [142], isolated

platelets were treated with Prb in a separate batch and reconstructed with isolated RBCs and plasma in physiological amounts. The results provided evidence that the PANX1 channel on RBCs had no effect on thrombus formation at a shear rate of 1,000s^{-1} (Appendix 7.1.4). In whole blood, thrombus volume was significantly reduced at 1,000s^{-1} with Prb, which correspond to the observations with murine blood. These results give cause for concern that PANX1 channels have an impact on thrombus formation probably by the reduced number of recruited blood cells by reduced ATP release. The same experimental approach indicates a role for human PANX1 channels in thrombus formation as measured by surface coverage at both tested shear rates. At a shear of 1,000s^{-1} the present results are in line with previous analysis from Taylor and colleagues [81]. In contrast to the results of the present study, Taylor *et al,* did not observe reduced thrombus formation but reduced thrombus volume at a shear rate of 1,000s^{-1} using Cbx to block PANX1 in human whole blood [167], however thrombus formation but reduced thrombus volume were reduced after Cbx application in the present thesis. The different results might be due to methodological differences. In the published study as well as in this work, self-coated matrices were used, but the flow chamber is from a different manufacturer. The chamber size can also change the flow geometry [181], which can lead to turbulence when the blood hits the collagen coated matrix. Overall, platelet PANX1 channels were shown to modulate hemostatic responses and offer a potential opportunity as a therapeutic target against arterial thrombosis which is discussed in chapter 5.5.

5.3 Pannexin 1 is activated and regulated by post-translational modifications

Platelet activation induces post-translational modifications of proteins such as the phosphorylation of platelet PANX1 at the tyrosine residues Tyr^{198} and Tyr^{308}. Beside phosphorylation events of serine or threonine residues, it is also well-known that tyrosine phosphorylation events serve as regulatory control mechanisms for ion channels in platelets [182]. Phosphorylation and dephosphorylating events change the electrophysiological properties of ion channels as shown in neuronal cells [183], leading to different physiological alterations as opening or closing of the channel [184] that might be also a mechanism for PANX1 channels in platelets. Phosphorylation of PANX1 at Tyr^{198} increases after platelet activation of ITAM-coupled, PAR and TP receptor signaling, but not after P2 receptor signaling. It is likely that the phosphorylation site at Tyr^{198} on PANX1 channels can function as an activation marker for PANX1 channels in human platelets, as it was shown for the endothelium [91]. The hypothesis of the phosphorylation of PANX1 at Tyr^{198}

might function as an activation marker is in agreement with the decreased ATP release mediated by PANX1 in response to ITAM-, GPCR-, and TP-receptor-mediated signaling (Summarized in Figure 51 and Figure 52).

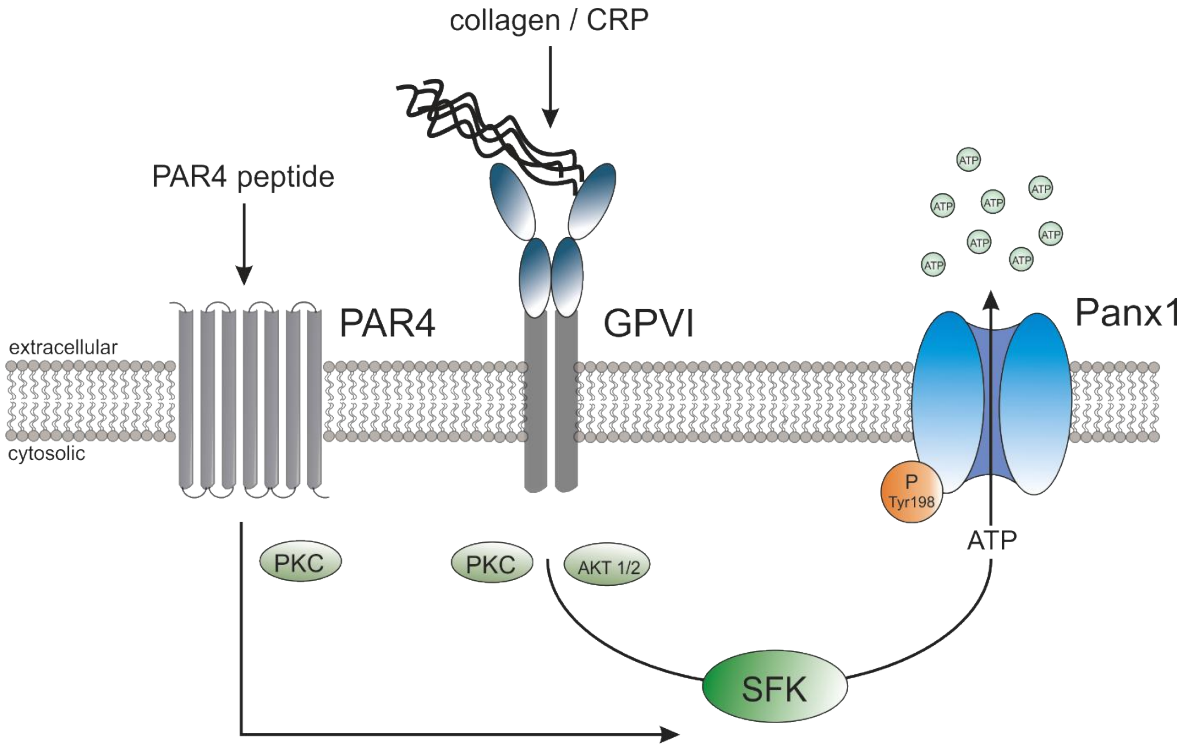

Figure 51: Increased PANX1 Tyr^{198} phosphorylation and PANX1 mediated ATP release after platelet activation with collagen/CRP and PAR4 peptide. Collagen/CRP induced platelet activation leads to phosphorylation of PANX1 Tyr^{198}, which is fully dependent on Src and partially dependent on PKC and Akt1/2. Moreover, ATP release is mediated via PANX1 channels after ITAM coupled receptor signaling induced by collagen. PAR4 peptide increases phosphorylation of PANX1 Tyr^{198}, fully dependent on SFKs and partially dependent on PKC. Platelet activation with of PAR4 peptide leads to ATP release via PANX1 channels in platelets. CRP = Collagen-related peptide, PAR4 peptide = Protease-activated receptor 4 peptide, PKC = Protein Kinase B, ATP = Adenosintriphosphat, PANX1 = Pannexin 1 [Figure modified from Metz, Elvers, IJMS 2022].

In ECs, PANX1 Tyr^{198} served as an activation marker, which was shown by increased levels of phosphorylation after time dependent TNFα stimulation [92]. The same study showed that application of the SFK inhibiting compound PP2 completely abolished PANX1 Tyr^{198} phosphorylation, which was not the case after pre-incubation of the inactive analogue PP3, underlining the importance of SFKs in PANX1 Tyr^{198} phosphorylation. In the present study, PP2 application resulted in abolished PANX1 Tyr^{198} phosphorylation following all agonists tested, which is is in line with the previous study from Lohman *et al.,* 2015 [185]. Here, reduced phosphorylation of PANX1 at Tyr^{198} was observed after PP2 application even in unstimulated, resting platelets, suggesting autophosphorylation of PANX1 channels. PANX1 activity was confirmed even at physiological extracellular Ca^{2+} concentrations [186], supporting the previously hypothesis autophosphorylation of PANX1 channels in platelets. Autophosphorylation of PANX1 at Tyr^{198} in

platelets might be suitable to maintain intra and extracellular ion hemostasis for e.g., ATP even in a physiological environment. Additionally, collagen induced platelet activation causes the highest fold increase in PANX1 Tyr^{198} phosphorylation, suggesting that GPVI is the central receptor for PANX1 activation. The present study confirmed for the first time that a genetic deletion of GPVI in murine platelets results in significantly decreased PANX1 Tyr^{198} phosphorylation levels upon collagen induced platelet activation compared to unstimulated platelets. Platelet activation with ADP and PAR4 peptide did not alter phosphorylation levels of platelet PANX1 at Tyr^{198} between platelets from WT and *Gp6*$^{-/-}$ mice. These data concludes that PANX1 channels are a target of the GPVI receptor since activation with collagen induces PANX1 phosphorylation at Tyr^{198}, which is completetly abolished in GPVI deficient platelets. These results are in line with a study from Molica and coworkers who already suggested PANX1 as a downstream target of GPVI mediated signaling [80, 82].

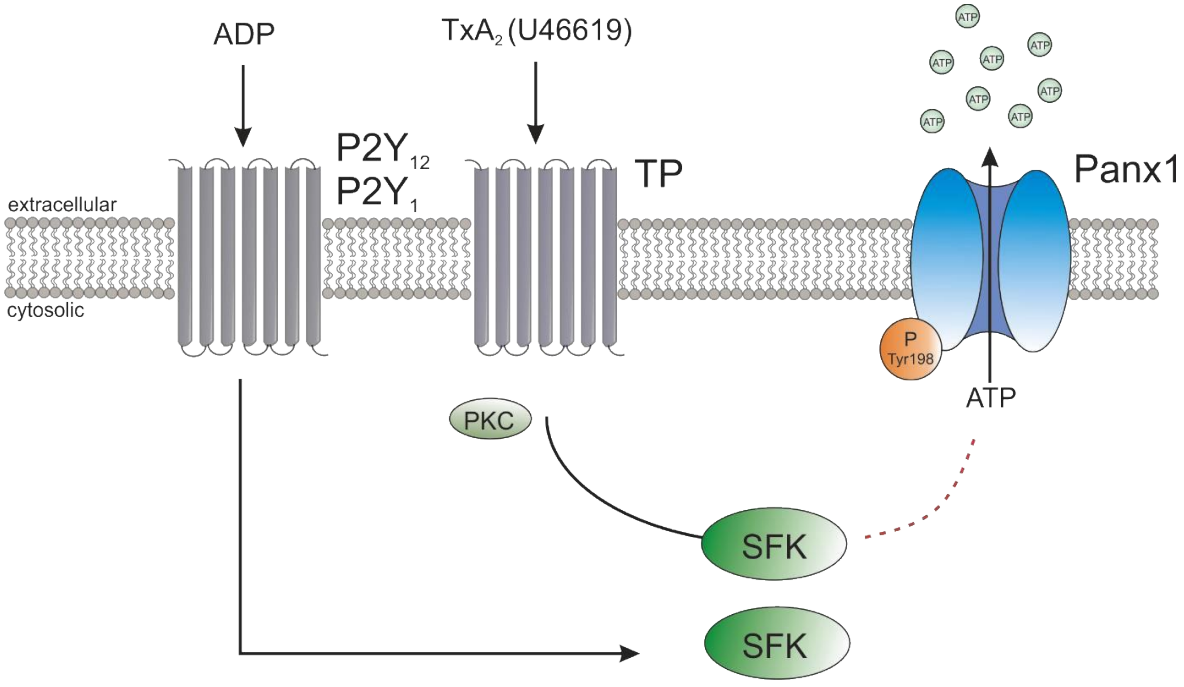

Figure 52: Increased PANX1 Tyr^{198} phosphorylation after platelet activation with the the TxA_2 analogue U46619 but not with ADP. U46619 induced platelet activation leads to phosphorylation of PANX1 Tyr^{198}, which is fully dependent on SFKs and partially dependent on PKC. Additionally, ATP release mediated via PANX1 channels after platelet activation with U46 was observed in human but not in murine platelets. Platelet activation with ADP does not lead to increased phosphorylation levels of PANX1 Tyr^{198} and PANX1 mediated ATP release either in murine or human platelets. ADP = Adenosine diphosphate, U46619 (U46) = Thromboxane A_2 analogue, PKC = Protein Kinase B, SFKs = Src Family Kinases, ATP = Adenosintriphosphat, PANX1 = Pannexin 1 [Figure modified from Metz, Elvers, IJMS 2022].

On the other hand, platelet activation with ADP leads to increased phosphorylation levels of PANX1 at Tyr^{308} in human platelets. Differences between phosphorylation patterns of PANX1 Tyr^{198} and Tyr^{308} in response to various tested platelet agonists suggest different regulatory PANX1 activation mechanisms. In general, PANX1 channels are known to consist of different phosphorylation sites, however, previous studies focused on PANX1 at Tyr^{308}. In the neuronal system, phosphorylation of PANX1 at Tyr^{308} depends on SFKs as central regulators in PANX1 activation [187]. Since neurons and platelets consist of similar characteristics concerning subcellular organization and protein content [188], PANX1 Tyr^{308} phosphorylation in platelets might depend on SFKs as well. One study indicates that the phosphorylation site Tyr^{308} at the C-terminus of PANX1 contains a consensus sequence (YEEI), which corresponds to the predicated ones in SFKs [149], indicating that SFKs are key regulators of PANX1 Tyr^{308} phosphorylation. To date, the literature about PANX1 Tyr^{308} phosphorylation in platelets is very rare; one study pointed to enhanced phosphorylation of PANX1 at Tyr^{308} after collagen induced platelet activation using immunohistochemistry stainings [82]. The authors detected reduced phosphorylation of PANX1 at Tyr^{308} that after inhibition of SFKs as measured by reduced fluorescence intensity. The authors conclude that PANX1 Tyr^{308} represents the Src kinase phosphorylation site and SFKs as key regulators in PANX1 activation upon collagen induced platelet activation [82]. These data on phosphorylation of PANX1 at Tyr^{308} after collagen induced platelet activation are in line with the Western blot analysis from chapter 4.4.1, because platelet activation with high doses of CRP resulted in reduced PANX1 Tyr^{308} phosphorylation after inhibition of SFKs by PP2. Platelet activation induced by low doses of CRP does not depend on SFKs since and this low concentration does not even significantly increase phosphorylation of PANX1 at Tyr^{308}. Beside collagen induced platelet activation, high doses of PAR4 peptide and all tested concentrations of ADP and U46619 induced PANX1 phosphorylation at Tyr^{308}, which is not controlled by SFKs. To date, no data exists about the phosphorylation of PANX1 in platelets using classical platelet agonists in addition to collagen [82]. Taken together, the presented results suggest, that phosphorylation at PANX1 Tyr^{308} might be regulated via different yet unknown kinases in response to GPCR and TP receptor mediated signaling in platelets.

Beside the role of SFKs, it was already discussed that PANX1 consists of phosphorylation sites, which might be potentially regulated by PKC [149-151, 189]. However, the literature is currently ambiguous concerning the involvement of PKC in PANX1 mediated phosphorylation sites [190]. The results of this dissertation provides first evidence for a role for PKC in the phosphorylation of PANX1 at Tyr^{198} in response to ITAM coupled and TP receptor mediated signaling. PKC is involved in the phosphorylation of PANX1 at Tyr^{308} only in response to platelet activation with a

high dose of U46619. The literature underlines an involvement of PKC in platelet mediated TxA_2 synthesis by activation of the mitogen-activated protein kinase-kinase (MEK), extracellular-signal regulated kinase (ERK) and the p38 MAPK signaling pathway [191]. Interestingly, TxA_2 reinforces collagen mediated platelet activation via GPVI mediated signaling leading to amplification of Ca^{2+} influx in platelets [21]. However, positive feedback mechanisms by TxA_2 in collagen induced platelet activation might be a potential reason for the involvement of PKC in PANX1 phosphorylation.

Since the here analyzed kinases are not the central mediators of ADP induced PANX1 Tyr^{308} phosphorylation, the involvement of Akt (PKB) was analyzed because Akt was shown to contribute to ADP induced platelet signaling processes [153]. The results of this thesis display no crucial role for the serine–threonine kinase PKB in PANX1 phosphorylation at Tyr^{198} and Tyr^{308}, except for GPVI mediated signaling induced by low doses of CRP. Since no additional studies are available analyzing the involvement of Akt in PANX1 Tyr^{198} phosphorylation and the results of this thesis showing no major role for PKB in PANX1 phosphorylation, it is conclusive that Akt is not a central regulator in PANX1 phosphorylation and probably only reinforces platelet-signaling cascades. For further investigations, the role of PKA in PANX1 mediated phosphorylation might be of great interest, since PKA was shown to modulate PANX1 phosphorylation in a model of PANX1 activation by mechanical stretch [192]. As already discussed in chapter 5.2, PANX1 channels are mechanosensitive, therefore PKA might be a regulator of platelet PANX1 activation via phosphorylation.

Beside phosphorylation of PANX1 at either Tyr^{198} or Tyr^{308}, platelet activation mainly with ADP led to a proteolytically cleavage of PANX1, which was found in human platelet releasates. The detected cleaved PANX1 fragment had a size of 19 kDa, which is in line with the already reported cleaved fragment from PANX1 channels in macrophages [193]. In apoptotic cells it was shown that cleavage of the C-terminal part of PANX1 channels leads to irreversible opening of the channel [194]. This cellular process was mediated mainly via caspase 3, an indicator of an apoptotic cell status [195]. Interestingly, first data indicated that caspase 3 mediated PANX1 cleavage must not necessarily be associated with cell apoptosis as shown by altered cell morphology if C-terminal PANX1 cleavage might occur directly via caspase 3 [194]. Nevertheless, platelet activation with ADP leads to PANX1 activation as shown by increased PANX1 phosphorylation at Tyr^{308}, which is mediated via to date unknown intracellular signaling mechanisms. Shedding of PANX1 channels indicates a regulatory role for PANX1 activation as already shown for GPVI and GPIb receptor shedding at the platelet surface, which is mediated by ADAM family metalloproteinases [196]. These results give a first hint that ADP induced platelet

activation might also lead to an irreversible opened state of the PANX1 channel, which might not necessarily be associated with platelet apoptosis. Irreversible opening of PANX1 channels mediated by C-terminal cleavage was shown to function as find-me signal for immune cells [197], however this might also play a role for platelets. For future research, it is interesting to investigate, if platelet PANX1 shedding is associated with platelet apoptosis by analyses of active caspase 3 and with platelet-inflammatory cell interactions.

NMDA receptors were shown to activate PANX1 channels by phosphorylation of Tyr^{308} during neurotoxicity in neurons [187]. In detail, this study showed a constitutive interaction of NMDAR and PANX1 even before neuronal NMDA activation, which was mediated via Src. The results presented here confirm that PANX1 activation in platelets is regulated via SFKs following platelet activation with different agonists, which is in line with the present literature concerning the ITAM receptor coupled signaling pathway [82]. However, the involvement of NMDARs in PANX1 activation might be also important in platelets, supported by the results of reduced Src phosphorylation at Tyr^{416} after collagen induced platelet activation in NMDAR deficient platelets compared to control platelets. NMDAR deficient platelet showed no alterations in PANX1 Tyr^{198} phosphorylation levels in resting conditions as well as after platelet activation with CRP and PAR4 peptide, suggesting no direct impact of NMDA receptors on PANX1 activation in platelets. Further experiments are necessary to investigate, if NMDARs act on PANX1 channels metabotropically via SFKs in platelets as it was shown in the neuronal system [149, 187]. Analysis of phosphorylation levels of PANX1 Tyr^{308} in NMDAR deficient platelets compared to respective controls might help to understand NMDAR and PANX1 interactions in platelets. This might be important since it was shown that inhibition of PANX1 phosphorylation by the NMDAR-Src dependent signaling pathway using the TAT-tagged peptide (TAT-$PANX1_{308}$) resulted in a neuroprotective effect in ischemic stroke in rats [101]. Therefore, it would be of great interest to further analyze the activation mechanism of PANX1 channels in platelets by the NMDAR-Src signaling cascade to provide a basic knowledge for further perspectives e.g., the development of anti-platelet therapies.

5.4 Pannexin 1 channels contribute to inflammatory processes

As described above, the results from this study provide strong evidence for a crucial role of platelet PANX1 channels for platelet activation in hemostasis and thrombosis. Therefore, the next aim of my studies was to investigate a potential role of PANX1 in platelet mediated inflammation. Recent studies demonstrate that ATP release via PANX1 channels modulate inflammatory processes by

the recruitment of immune cells to sides of inflammation [77, 79, 92]. These findings are now accomplished by new data from this study strongly suggesting that platelet PANX1 channels are involved in these processes because the number of platelet-neutrophil aggregates was reduced in whole blood from *Panx1 fl/fl PF4-Cre*$^+$ mice compared to respective controls after application of TNFα and LPS *in vitro*. *In vivo*, a reduced number of platelet-neutrophil aggregates was detected in the cicurlation of *Panx1 fl/fl PF4-Cre*$^+$ mice compared to *Panx1 fl/fl PF4-Cre*$^-$ mice after PPE, a crutical parameter in the progression of AAA [198]. In line with these results, a reduced number of infiltrated neutrophils and platelets in aortic tissue were observed in *Panx1 fl/fl PF4-Cre*$^+$ mice. In other cells of the vasculature, PANX1 is known to be responsible for the recruitment of immune cells during inflammation [77, 185], which accounts for platelets in the development of AAA as well. The formation of platelet-neutrophil aggregates is known to be partially mediated via receptor interactions of platelet P-selectin and CD40L with PSGL-1, CD40 and Mac-1 (Integrin $\alpha_M\beta_2$, CD11b/CD18) on leukocytes [199-201]. In this context, platelet P-selectin plays a particularly important role, since this receptor mediates the first interactions between leukocytes and activated platelets [11]. However, no increase in platelet P-selectin exposure after agonist stimulation was measured on the platelet surface after PPE surgery in *Panx1 fl/fl PF4-Cre*$^+$ mice compared to controls. Therefore, the obtained results might be due to a cross talk between activated neutrophils by TNFα or LPS [202] which might further amplify the activation of platelet PANX1 channels, since platelets alone are not activated by the inflammatory stimulants as measured by binding of JON/A to activated integrin $\alpha_{IIb}\beta_3$. Until today, it is controversial discussed if TNFα or LPS are able to induce platelet activation *in vitro* without further stimulus [203, 204]. However, the here presented results do not confirm a role of TNFα as a primary platelet agonist. Moreover, stimulation of TNFα alone does not lead to the phosphorylation of platelet PANX1 at Tyr^{198} in human platelets confirming that TNFα alone does not amplify the activation of the platelet PANX1 channel. In comparison with ECs, TNFα treatment was shown to enhance phosphorylation levels of PANX1 at Tyr^{198}, which were reduced when SFKs were inhibited by PP2 [185] confirming Src family kinases as the central kinases in PANX1 regulation also during activation of the inflammasome in ECs.

At sites of inflammation, platelet-EC interactions are essential to mediate stable platelet adhesion by integrin $\alpha_{IIb}\beta_3$ and integrin $\alpha_V\beta_3$ on the endothelium. Adherence of platelets on ECs facilitates inflammation and the recruitment of immune cells to sites of inflammation [57]. IL-6, produced from inflammatory ECs, contributes to inflammatory processes, while dysregulation of IL-6 has been linked to inflammatory and malignant diseases [205, 206]. Patients, suffering from AAA were shown to have enhanced IL-6 plasma levels [107]. A previous study in astrocytes reports that

PANX1 is responsible for IL-6 release [207], but platelets do not store IL-6 under physiological conditions [156]. Therefore, it might be possible that the platelet PANX1 channel induce endothelial IL-6 release contributing to inflammatory diseases. However, platelet PANX1 channel does not contribute to platelet-induced IL-6 release from ECs *in vitro* because enhanced IL-6 release after incubation of ECs with the supernatant of activated platelets has been observed with both, platelets form *Panx1* knock-out and control mice.

Beside acute inflammatory responses, PANX1 channels have also been found to contribute to chronic inflammation as present in AAA [131, 132]. This studes are in line with the observation of significant enhanced PANX1 plasma levels in human patients suffering from AAA compared to aged-matched controls. Since PANX1 is ubiquitously expressed in the vasculature [208], PANX1 protein detected in the plasma might originally come from other cells such as ECs, leukocytes or RBCs. Until now it is unclear, if PANX1 can be proteolytically cleaved from the plasma membrane, however endogenous PANX1 levels were detected via ELISA. The literature discussed a regulatory role for PANX1 activation by caspase dependent cleavage of the C-terminus during apoptosis, leading to a constitutive opened stage of the channel [197]. Increased PANX1 plasma levels might be a regulatory mechanism as well since clinical studies of male patients displayed increased PANX1 expression levels in aortic tissue [131]. One study found enhanced serum PANX1 levels in patients with traumatic brain injury and conclude that serum PANX1 might serve as a prognostic biomarker for this disease [209]. Further studies are needed to determine, if PANX1 plasma levels in patients might serve as a possible biomarker for the detection of AAA. To date, the role of platelets in the development AAA is not entirely clear. Preliminary data from our laboratory showed that platelets from AAA patients are in a pre-activated state because threshold concentrations of different platelet agonists already induce platelets activation in AAA patienets but not in aged-matched controls [210]. The altered platelet activation state in AAA patients might be the reason for enhanced PANX1 protein found in releasates of platelets from patients suffering from AAA compared to aged-matched controls which accounts for enhanced PANX1 activation and enhanced PANX1 shedding. However, PANX1 Tyr^{198} phosphorylation was decreased upon platelet activation with CRP compared to aged-matched controls. Therefore, it is tempting to speculate that CRP triggered PANX1 Tyr^{198} phosphorylation occurs more rapidly in AAA patients compared to aged-matched controls because of altered platelet physiology. This might lead to accelerated proteolytic cleavage of PANX1 channels which might explain increased PANX1 proteins levels in platelet releasates of AAA patients compared to aged-matched controls. As already mentioned above, the platelet glycoproteins GPIb and GPVI can be shedded from the platelet surface, which is mediated by ADAM family metalloproteinases displaying a marker for

enhanced GPIb and/or GPVI activation [196]. One previous study from Kaxai *et al.* displayed an upregulated ADAM-17 expression in the endothelium of mice in an Ang II-induced murine AAA model [211], suspects that PANX1 might be potentially cleaved by ADAM family metalloproteinases as well. Additionally, the release of MPs is a characteristic feature in the progression of AAA [122, 123]. It was previously shown that inhibition of human PANX1 channels with Prb prevents platelet-derived microparticle (PMP) release *in vitro* [212]. Interestingly, in a model of rheumatoid arthritis, GPVI was identified as a key initiator of PMP formation [213] representing the central receptor in PANX1 activation on platelets. For further perspectives, it might be of great interest to analyze, if altered platelet PANX1 channel activation or PANX1 shedding in AAA patients correlates with enhanced PMP release compared with platelets from aged-matched controls. In addition, it would be important to perform ATP release measurements with platelets from AAA patients and aged-matched controls in response to collagen induced platelet activation to determine potential correlation of PANX1 mediated ATP release in AAA pathology.

To further study the influence of platelet specific PANX1 channels in the development of AAA, the murine PPE model was used, as this is one of the most used experimental models to study the progression of AAA development [214, 215]. Analysis of mice with an EC specific PANX1 knock-out underwent PPE surgery and displayed reduced dilation of the aortic wall (final outcome) compared to control mice [131, 132]. Application of 1.1 mg/kg body weight of the PANX1 inhibitor Prb to mice that underwent PPE surgery significantly reduced AAA size compared to the aortic dilatation from control mice [131]. Nevertheless, it must keep in mind that PANX1 is ubiquitously expressed in the vascular system, therefore Prb treatment systemically acts on PANX1 channels thus blocking the channel on other blood cells or ECs. Beside the impact of PANX1 in the pathogenesis of AAA, recent studies demonstrate that platelets play a critical role in the progression of AAA e.g. by the release of inflammatory cytokines and soluble mediators [139]. Inhibition of ADP induced platelet aggregation by a compound named AZD6140 in a rat aneurysmal model displayed reduced aortic dilatation [127]. Mice, treated with the $P2Y_{12}$ receptor inhibitor clopidogrel showed reduced AAA formation about 47% in an Ang II-induced murine AAA model [128]. Moreover, platelet depletion in C57BL/6J mice that underwent PPE surgery also displayed reduced AAA formation of about 25% compared to non-depleted C57BL/6J mice 10 days after surgery confirming a prominent role of platelets in the pathology of AAA (Wagenhäuser et al., manuscript in preparation). However, platelet restricted PANX1 deletion does not influence the size of the final dilatation of the aortic wall at day 28 post-PPE surgery. This may be due to the fact that the murine AAA model shows weaknesses compared to the

progression of human AAAs, since in most cases no ILT is formed [118]. Previous studies hypothesized that the ILT leads to altered platelet function by wall shear stress [216], e.g. pre-activation of platelets [210], which cannot be mimicked by the murine PPE model [217]. Since PANX1 channels influence thrombus formation as shown by flow chamber experiments, another murine AAA model might be important to provide more insights into the role of platelet PANX1 channels in the pathogenesis of AAAs. For further investigations, the ePPE (External Periadventitial Elastase application) model might be one option, because an ILT is formed and the surgery method is not as error-prone in case of high mortality rates as reported for the classical PPE model [110, 218].

In addition, high mortality rates were observed in platelet PANX1 deficient mice after PPE surgery. In fact, the mortality of the *Panx1 fl/fl PF4-Cre*$^{+}$ mice was 62.5% compared to the *Panx1 fl/fl PF4-Cre*$^{-}$ mice where 20% of the animals did not survive until day 28 after PPE surgery. The literature reports high mortality rates for a successful PPE surgery, because the procedure itself is known to be difficult, because of surgical handling and instrumental set-ups [110]. It is noticeable that most of the animals died within the first day after surgery, probably due to bleeding and/or thrombosis. The surgeons referred to increased bleeding complications of *Panx1 fl/fl PF4-Cre*$^{+}$ animals compared to control animals during PPE surgery which has not been validated by experimental trials. As already discussed in chapter 5.2, Molica and colleagues showed that *Panx1 fl/fl PF4-Cre*$^{+}$ mice have a prolonged tail bleeding time compared to *Panx1 fl/fl PF4-Cre*$^{-}$ mice *in vivo* [82]. Moreover, the same study confirmed a role of platelet PANX1 in arterial thrombosis since the time to arterial occlusion was enhanced by trend in platelet PANX1 deficient mice in a $FeCl_3$-injured mesenteric arteries experiments *in vivo* [82]. Nevertheless, the shear rate in mouse aorta is much higher (2,500s^{-1}) than in mesenteric arteries (1,200 - 1,700s^{-1}) of male mice [219-221]. An increased shear rate alters the initial platelet activation mechanisms and it is known that at pathological shear conditions only the GPIb receptor complex is responsible for platelet adhesion and aggregation [222, 223]. Therefore, a role for platelet PANX1 channels in the regulation and activation of GPIb might explain the effects although the GPIb levels at the surface of unstimulated platelets does not differ between PANX1 deficient and WT platelets during AAA development. Therefore, future analysis might focus on vWF/Botronectin measurements using flow cytometric analysis, which can display a potential dysregulation of GPIb in PANX1 deficient platelets compared to control platelets [224]. Additionally, PANX1 channels are activated via mechanical stimulation [179], therefore a loss of platelet PANX1 channels might account for the observed bleeding disorders during surgery.

After PPE surgery, different time points were analyzed regarding alterations in blood cell counts, expression of platelet surface receptors, platelet activation and the formation of platelet-immune cell aggregates. The acute inflammatory response from the PPE surgery was shown by a significantly increased number of WBCs at day 3 within both groups of *Panx1 fl/fl PF4 Cre*$^{-}$ and *Panx1 fl/fl PF4 Cre*$^{+}$ mice compared to native mice. The acute inflammatory phase transitions into a chronic phase from 7 to 28 days after PPE surgery, which is represented by a continued elevated number of WBCs compared to basal levels. In line, the remodeling of the aortic wall starts after 10 to 14 days post PPE surgery [158], which is accompanied by the infiltration of leukocytes at sites of inflammation [217]. The number of RBCs enhances within the *Panx1 fl/fl PF4 Cre*$^{-}$ mice group by trend only 3 days post PPE surgery, which may be due to the acute surgical intervention. 14 days post PPE surgery WT mice display higher circulating levels of RBCs in the blood stream compared to *Panx1 fl/fl PF4 Cre*$^{+}$ mice, which might be the case due to enhanced erythropoiesis in these mice. Interestingly, at the same time point after PPE surgery higher numbers of platelets were observed in WT compared to PANX1 deficient mice, while platelet size was not different at this timepoint after PPE surgery.

Since platelets are also associated with the process of erythropoiesis e.g. by the hematopoietic transcription factor GATA-1 [225], increased RBC cell counts are indicative of enhanced blood cell generation. This is in line with the fact, that inflammation causes increased proteolytical cleavage of RBCs, by the adherence of RBCs to sites of inflammation on ECs [226], which can potentially count for enhanced erythropoiesis. After 28 days of PPE infusion, platelet size was significantly enhanced in platelets from PANX1 deficient compared to platelets from WT control mice. Newly formed young platelets, which are known as proplatelets, are larger in size, have a different cell shape, contain more mRNA and are more reactive than older platelets [227, 228]. One study displayed that proplatelets can be even 100 times larger than adult platelets, which was found in pulmonary vessels [229], assuming that increased MPV indicates enhanced platelet turnover and enhanced megakaryopoiesis. Therefore, the increased MPV in platelets of *Panx1 fl/fl PF4 Cre*$^{+}$ mice, might be associated with increased generation of new platelets, which, however, was not confirmed by increased platelet counts in the circulation of *Panx1 fl/fl PF4 Cre*$^{+}$. Further investigations might be of great interest to analyze the platelet turn-over in experimental AAA which can be measured via determination of platelet reticulocytes (RNA containing platelets) and glycoprotein desialylation state [231]. Additionally, histological staining of megakaryocytes in organ slices (spleen, bone marrow) would be useful to investigate the megakaryopoiesis in bone marrow and spleen of both genotypes at day 14 and 28 post-PPE.

Overall the results of the present thesis indicate a cruitcal role of PANX1 channels with the inflammatory response by alteration of platelet-neutrophil conjugets, which potentially accounts for a reduced number of infiltrating immune cells in the aortic tissue in *Panx1 fl/fl PF4 Cre*$^{+}$ mice. In human patients, which suffer from AAA, elevated PANX1 protein has been detected in platelet releasates after platelet stimulation and in the plasma isolated from AAA patients compared to aged-matched controls. These results indicate enhanced proteolytically cleavage of PANX1, suggesting that soluble PANX1 might serve as a potential biomarker for AAA.

5.5 Pannexin 1 as a potential anti-thrombotic and anti-inflammatory target for cardiovascular diseases?

The results of this thesis implicate a potential role for platelet PANX1 channels in arterial thrombosis, which has already been described in earlier studies [81, 82]. Moreover, platelet specific PANX1 knock-out mice have prolonged tail bleeding times compared to respective controls *in vivo* suggesting a role for PANX1 in hemostasis [82]. PANX1 might serve as a potential therapeutic target against arterial thrombosis because reduced thrombus formation has been detected in murine knock-out and human inhibitory experiments at low and intermediate arterial shear rates. Since PANX1 is also involved in hemostasis, therefore its role and efficacy as a therapeutic target must be verified with regard to bleeding complications in patients. The PANX1 inhibitors Prb and Cbx are already FDA approved drugs used against gouty arthritis and tracheal ulcers, respectively [232, 233]. However, it is questioning if these drugs might serve as an anti-platelet therapy against arterial thrombosis since no data exists if patients treated with Prb and Cbx suffer from bleeding complications. As already discussed before, Prb and Cbx are not specific inhibitors for PANX1 channels, because they affect also other channels such as gap junction proteins or anion transporters [167]. Therefore, undesired secondary effects must be considered during the evaluation of Prb or Cbx as potential anti-thrombotic compounds. Since both inhibiting compounds are used in clinical trials since many years, safety profiles are standardized. As an alternative approach, PANX1 inhibiting peptides might be a potential solution for patients. However, the recently developed inhibiting peptide against the EL1 of PANX1 channels (^{10}PANX1 peptide; WRQAAFVDSY) [76] seems to be the best choice. Preliminary experiments from our laboratory investigating thrombus formation in the presence of a scrambled peptide version of the ^{10}PANX1 peptide detected reduced thrombus formation particually within the scrambled peptide group, which is an indication of its non-specificity (Data not shown). Additionally, a recent study revealed low serum stability of the ^{10}PANX1 peptide [27], which is not

a suitable option as a therapeutic target [82]. Additionally, a newly developed PANX1 inhibiting target was developed from Molica and colleagues, which showed specific inhibitory effects *in vivo* [82]. This compound seems to be promising; however, further research is necessary to investigate the potential of PANX1 as therapeutic target and its side effects for safety approaches.

Beside the role of PANX1 in arterial thrombosis, the work of this thesis identified an involvement of platelet PANX1 in the inflammatory response of AAA. Using the approved murine AAA model PPE, it has been shown that platelet PANX1 channels do not modulate the dilatation of the aortic wall. However, a potential role for platelet PANX1 was figured out including platelet activation as well as the recruitment of immune cells as measured by platelet-neutrophil aggregate formation after PPE infusion in mice. However, the results from the AAA studies in *Panx1 fl/fl PF4-Cre*$^{+}$ mice suggests that PANX1 only affects inflammation but not aortic remodeling that might be not sufficient to induce alterations in the dilatation of the aorta compared to control mice. Thus, it is tempting to speculate if a therapeutic intervention against platelet PANX1 might induce any beneficial effects for AAA patients. Moreover, the results from PPE operated *Panx1 fl/fl PF4-Cre*$^{+}$ animals showed an increased mortality rate shortly after surgery compared to control mice. This might be due to the role of PANX1 in hemostasis as already shown by elevated bleeding times in *Panx1* knock-out mice [82] that might be causative for the formation of hemorrhages when PANX1 is blocked or deleted in experimental mice with AAA. Therefore, it would be of great interest to perform further studies on the function of platelet PANX1 channels under high shear conditions as found in the aorta [219]. Platelet specific *Panx1* deletion in mice led to increased time to time to respiratory arrest in a venous thromboembolism (VTE) model, 2-fold enhanced tail bleeding time while $FeCl_3$-induced thrombosis in mesenteric arteries was only enhanced by trend [82]. Up to date it is not clear whether PANX1 plays a role at high shear conditions. For this purpose, it would be interesting to study thrombus formation in the murine *in vivo* model of mechanical injury of the abdominal aorta [234] in *Panx1 fl/fl PF4-Cre* mice.

5.6 Concluding remarks and future perspectives

Taken together, the results of this thesis reveal a crucial role for platelet PANX1 channels in hemostasis and thrombosis *in vitro* and *in vivo*. Moreover, the results display that platelet PANX1 contributes to inflammatory processes e.g. in the development of AAA. In the present work, the GPVI-Src signaling axes was identified as one of the major regulators of platelet PANX1 channel activation by phosphorylation of the tyrosine residues Tyr^{198} and Tyr^{308}. Thus, PANX1 is a downstream target of GPVI. Moreover, PANX1 deficent as well as pharmacological inhibition of PANX1 in murine and human platelets, respectively, resulted in reduced thrombus formation on a collagen coated matrix at arterial shear rates. Consequently, PANX1 channels might serve as a novel therapeutic target against arterial thrombosis. Therefore, it is beneficial that the PANX1 inhibiting compounds Prb and Cbx are already FDA approved drugs used against gouty arthritis and tracheal ulcers, respectively [232, 233].

Additionally, this study investigated for the first time the role of platelet PANX1 in inflammatory processes following the progression of AAA. Therefore, *Panx1 fl/fl PF4-Cre*$^{+}$ and *Panx1 fl/fl PF4-Cre*$^{-}$ mice underwent PPE perfusion, a well established mouse model to study the formation and progression of AAA *in vivo*. The results displayed a role for platelet PANX1 in platelet activation and platelet-induced inflammation. However, PANX1 deficiency restricted to platelets led to a significant higher mortality rate early after PPE infusion demonstrating for the first time that PANX1 is an important mediator of hemostasis to prevent hemorrhage formation after surgery. In contrast, previous studies have shown that a genetic deletion of GPVI on the platelet surface leads to fewer thrombotic events without accelerating bleeding [235]. The results of the present study undelines GPVI as a central pathway to activate PANX1 channels in platelets. As genetic deletion of PANX1 or pharmacological PANX1 inhibition altered thrombus formation *ex vivo* and increased tail bleeding time *in vivo* [82], another, as yet unknown, signaling pathway must contribute to PANX1 activation, because *Gp6*$^{-/-}$ mice did not show an enhanced bleeding phenotype. The drug Revacept prevents platelet adhesion by blocking GPVI binding to collagen, which has already been shown to be effective in a phase II clinical trial [236]. Thus, GPVI would be an interesting potential target to prevent the development of AAAs. However, further studies are useful to investigate the role of GPVI in the progression of AAAs. For this purpose, it would first be mandatory to study *Gp6*$^{-/-}$ and control mice within the PPE model as a first experimental approach. However, further studies are needed to determine whether the modulation of platelet GPVI-PANX1 signaling axes could represent a novel therapeutic strategy/biomarker for the treatment/ diagnosis of CVDs and especially for AAA.

6 References

1. Kehrel, B., *Blood platelets: biochemistry and physiology.* Hamostaseologie, 2003. **23**(4): p. 149-158.
2. Schmitt, A., et al., *Of mice and men: comparison of the ultrastructure of megakaryocytes and platelets.* Experimental hematology, 2001. **29**(11): p. 1295-1302.
3. Sandilos, J.K., et al., *Pannexin 1, an ATP release channel, is activated by caspase cleavage of its pore-associated C-terminal autoinhibitory region.* Journal of Biological Chemistry, 2012. **287**(14): p. 11303-11311.
4. Zucker-Franklin, D. and C.S. Philipp, *Platelet production in the pulmonary capillary bed: new ultrastructural evidence for an old concept.* The American journal of pathology, 2000. **157**(1): p. 69-74.
5. Italiano Jr, J. and R. Shivdasani, *Megakaryocytes and beyond: the birth of platelets.* Journal of Thrombosis and Haemostasis, 2003. **1**(6): p. 1174-1182.
6. Selvadurai, M.V. and J.R. Hamilton, *Structure and function of the open canalicular system–the platelet's specialized internal membrane network.* Platelets, 2018. **29**(4): p. 319-325.
7. Angénieux, C., et al., *Time-dependent decay of mRNA and ribosomal RNA during platelet aging and its correlation with translation activity.* PloS one, 2016. **11**(1): p. e0148064.
8. George, J.N., *Platelets.* Lancet, 2000. **355**(9214): p. 1531-9.
9. Quach, M.E., W. Chen, and R. Li, *Mechanisms of platelet clearance and translation to improve platelet storage.* Blood, The Journal of the American Society of Hematology, 2018. **131**(14): p. 1512-1521.
10. Leslie, M., *Beyond clotting: the powers of platelets*. 2010, American Association for the Advancement of Science.
11. Smyth, S., et al., *Platelet functions beyond hemostasis.* Journal of Thrombosis and Haemostasis, 2009. **7**(11): p. 1759-1766.
12. Kaczmarek, E., et al., *Identification and characterization of CD39/vascular ATP diphosphohydrolase.* Journal of Biological Chemistry, 1996. **271**(51): p. 33116-33122.
13. Allard, B., et al., *The ectonucleotidases CD 39 and CD 73: novel checkpoint inhibitor targets.* Immunological reviews, 2017. **276**(1): p. 121-144.
14. Radziwon-Balicka, A., et al., *Differential eNOS-signalling by platelet subpopulations regulates adhesion and aggregation.* Cardiovascular research, 2017. **113**(14): p. 1719-1731.
15. Wu, K.K. and J.-Y. Liou, *Cellular and molecular biology of prostacyclin synthase.* Biochemical and biophysical research communications, 2005. **338**(1): p. 45-52.
16. Suslova, T.E., et al., *Platelet hemostasis in patients with metabolic syndrome and type 2 diabetes mellitus: cGMP-and NO-dependent mechanisms in the insulin-mediated platelet aggregation.* Frontiers in Physiology, 2015. **5**: p. 501.
17. Varga-Szabo, D., I. Pleines, and B. Nieswandt, *Cell adhesion mechanisms in platelets.* Arteriosclerosis, thrombosis, and vascular biology, 2008. **28**(3): p. 403-412.
18. Jurk, K. and B. Kehrel, *Platelets: physiology and biochemistry Semin Thromb Hemost 31: 381–392.* Find this article online, 2005.
19. Clemetson, J.M., et al., *The platelet collagen receptor glycoprotein VI is a member of the immunoglobulin superfamily closely related to FcαR and the natural killer receptors.* Journal of Biological Chemistry, 1999. **274**(41): p. 29019-29024.
20. Watson, S.P. and J. Gibbins, *Collagen receptor signalling in platelets: extending the role of the ITAM.* Immunology today, 1998. **19**(6): p. 260-264.
21. Nieswandt, B. and S.P. Watson, *Platelet-collagen interaction: is GPVI the central receptor?* Blood, 2003. **102**(2): p. 449-461.

22. Offermanns, S., *Activation of platelet function through G protein–coupled receptors.* Circulation research, 2006. **99**(12): p. 1293-1304.
23. Metz, L.M. and M. Elvers, *Pannexin-1 Activation by Phosphorylation Is Crucial for Platelet Aggregation and Thrombus Formation.* International Journal of Molecular Sciences, 2022. **23**(9): p. 5059.
24. Bennett, J.S., *Structure and function of the platelet integrin alphaIIbbeta3.* The Journal of clinical investigation, 2005. **115**(12): p. 3363-3369.
25. Chatterjee, M., et al., *Molecular Drivers of Platelet Activation: Unraveling Novel Targets for Anti-Thrombotic and Anti-Thrombo-Inflammatory Therapy.* International Journal of Molecular Sciences, 2020. **21**(21): p. 7906.
26. Varga-Szabo, D., I. Pleines, and B. Nieswandt, *Cell adhesion mechanisms in platelets.* Arterioscler Thromb Vasc Biol, 2008. **28**(3): p. 403-12.
27. Wencel-Drake, J.D., et al., *Localization of internal pools of membrane glycoproteins involved in platelet adhesive responses.* The American journal of pathology, 1986. **124**(2): p. 324.
28. Fox, J., *Transmembrane signaling across the platelet integrin glycoprotein IIb-IIIa.* Annals of the New York Academy of Sciences, 1994. **714**: p. 75-87.
29. Nieswandt, B., D. Varga-Szabo, and M. Elvers, *Integrins in platelet activation.* J Thromb Haemost, 2009. **7 Suppl 1**: p. 206-9.
30. Law, D.A., et al., *Integrin cytoplasmic tyrosine motif is required for outside-in alphaIIbbeta3 signalling and platelet function.* Nature, 1999. **401**(6755): p. 808-11.
31. Salsmann, A., et al., *A new functional role of the fibrinogen RGD motif as the molecular switch that selectively triggers integrin alphaIIbbeta3-dependent RhoA activation during cell spreading.* J Biol Chem, 2005. **280**(39): p. 33610-9.
32. Hechler, B. and C. Gachet, *Purinergic receptors in thrombosis and inflammation.* Arteriosclerosis, thrombosis, and vascular biology, 2015. **35**(11): p. 2307-2315.
33. Fabre, J.-E., et al., *Decreased platelet aggregation, increased bleeding time and resistance to thromboembolism in P2Y 1-deficient mice.* Nature medicine, 1999. **5**(10): p. 1199-1202.
34. Sangkuhl, K., et al., *Platelet aggregation pathway.* Pharmacogenetics and genomics, 2011. **21**(8): p. 516-521.
35. Mangin, P., et al., *The P2Y1 receptor plays an essential role in the platelet shape change induced by collagen when TxA2 formation is prevented.* Journal of Thrombosis and Haemostasis, 2004. **2**(6): p. 969-977.
36. Varga-Szabo, D., A. Braun, and B. Nieswandt, *Calcium signaling in platelets.* J Thromb Haemost, 2009. **7**(7): p. 1057-66.
37. Hathaway, D.R. and R.S. Adelstein, *Human platelet myosin light chain kinase requires the calcium-binding protein calmodulin for activity.* Proceedings of the National Academy of Sciences, 1979. **76**(4): p. 1653-1657.
38. T J Rink, a. and S.O. Sage, *Calcium Signaling in Human Platelets.* Annual Review of Physiology, 1990. **52**(1): p. 431-449.
39. Lian, L., et al., *The relative role of PLCbeta and PI3Kgamma in platelet activation.* Blood, 2005. **106**(1): p. 110-7.
40. Suzuki-Inoue, K., et al., *Murine GPVI stimulates weak integrin activation in PLCgamma2-/- platelets: involvement of PLCgamma1 and PI3-kinase.* Blood, 2003. **102**(4): p. 1367-73.
41. Parekh, A.B. and J.W. Putney Jr, *Store-operated calcium channels.* Physiological reviews, 2005. **85**(2): p. 757-810.
42. ROSADO, J.A. and S.O. SAGE, *Coupling between inositol 1, 4, 5-trisphosphate receptors and human transient receptor potential channel 1 when intracellular Ca2+ stores are depleted.* Biochemical Journal, 2000. **350**(3): p. 631-635.

43. Cavallini, L., M. Coassin, and A. Alexandre, *Two classes of agonist-sensitive Ca2+ stores in platelets, as identified by their differential sensitivity to 2,5-di-(tert-butyl)-1,4-benzohydroquinone and thapsigargin.* Biochem J, 1995. **310 (Pt 2)**(Pt 2): p. 449-52.
44. Dahlbäck, B., *Blood coagulation and its regulation by anticoagulant pathways: genetic pathogenesis of bleeding and thrombotic diseases.* Journal of internal medicine, 2005. **257**(3): p. 209-223.
45. Gale, A.J., *Continuing education course# 2: current understanding of hemostasis.* Toxicologic pathology, 2011. **39**(1): p. 273-280.
46. Quinn, M., D. Fitzgerald, and D. Cox, *Platelet function: assessment, diagnosis, and treatment*. 2007: Springer Science & Business Media.
47. Shapiro, M.J., et al., *Protease-activated receptors 1 and 4 are shut off with distinct kinetics after activation by thrombin.* J Biol Chem, 2000. **275**(33): p. 25216-21.
48. Kahn, M.L., et al., *A dual thrombin receptor system for platelet activation.* Nature, 1998. **394**(6694): p. 690-4.
49. Dachary-Prigent, J., et al., *Annexin V as a probe of aminophospholipid exposure and platelet membrane vesiculation: a flow cytometry study showing a role for free sulfhydryl groups.* Blood, 1993. **81**(10): p. 2554-65.
50. Dale, G.L., et al., *Stimulated platelets use serotonin to enhance their retention of procoagulant proteins on the cell surface.* Nature, 2002. **415**(6868): p. 175-9.
51. Schreuder, M., P.H. Reitsma, and M.H.A. Bos, *Blood coagulation factor Va's key interactive residues and regions for prothrombinase assembly and prothrombin binding.* J Thromb Haemost, 2019. **17**(8): p. 1229-1239.
52. Gale, A.J., *Continuing education course #2: current understanding of hemostasis.* Toxicol Pathol, 2011. **39**(1): p. 273-80.
53. Kruithof, E.K. and S. Dunoyer-Geindre, *Human tissue-type plasminogen activator.* Thromb Haemost, 2014. **112**(2): p. 243-54.
54. Collen, D. and B. Wiman, *Fast-acting plasmin inhibitor in human plasma.* Blood, 1978. **51**(4): p. 563-9.
55. Bonfanti, R., et al., *PADGEM (GMP140) is a component of Weibel-Palade bodies of human endothelial cells.* Blood, 1989. **73**(5): p. 1109-1112.
56. McEver, R.P., et al., *GMP-140, a platelet alpha-granule membrane protein, is also synthesized by vascular endothelial cells and is localized in Weibel-Palade bodies.* The Journal of clinical investigation, 1989. **84**(1): p. 92-99.
57. Nording, H.M., P. Seizer, and H.F. Langer, *Platelets in inflammation and atherogenesis.* Frontiers in immunology, 2015. **6**: p. 98.
58. Gawaz, M., et al., *Transient platelet interaction induces MCP-1 production by endothelial cells via IκB kinase complex activation.* Thrombosis and haemostasis, 2002. **88**(08): p. 307-314.
59. Lu, B., et al., *Abnormalities in monocyte recruitment and cytokine expression in monocyte chemoattractant protein 1–deficient mice.* The Journal of experimental medicine, 1998. **187**(4): p. 601-608.
60. Gawaz, M., et al., *Platelets induce alterations of chemotactic and adhesive properties of endothelial cells mediated through an interleukin-1-dependent mechanism. Implications for atherogenesis.* Atherosclerosis, 2000. **148**(1): p. 75-85.
61. May, A.E., et al., *Engagement of glycoprotein IIb/IIIa (αIIbβ3) on platelets upregulates CD40L and triggers CD40L-dependent matrix degradation by endothelial cells.* Circulation, 2002. **106**(16): p. 2111-2117.
62. Asfaha, S., et al., *Mice that express human interleukin-8 have increased mobilization of immature myeloid cells, which exacerbates inflammation and accelerates colon carcinogenesis.* Gastroenterology, 2013. **144**(1): p. 155-166.
63. McEver, R.P., *Selectins: initiators of leucocyte adhesion and signalling at the vascular wall.* Cardiovascular research, 2015. **107**(3): p. 331-339.

64. Manfredi, A.A., et al., *The neutrophil's choice: phagocytose vs make neutrophil extracellular traps.* Frontiers in immunology, 2018. **9**: p. 288.
65. Finsterbusch, M., et al., *Measuring and interpreting platelet-leukocyte aggregates.* Platelets, 2018. **29**(7): p. 677-685.
66. Panchina, Y., et al., *A ubiquitous family of putative gap junction molecules.* Current biology, 2000. **10**(13): p. R473-R474.
67. Yen, M.R. and M.H. Saier Jr, *Gap junctional proteins of animals: the innexin/pannexin superfamily.* Progress in biophysics and molecular biology, 2007. **94**(1-2): p. 5-14.
68. Bruzzone, R., et al., *Pannexins, a family of gap junction proteins expressed in brain.* Proceedings of the national academy of sciences, 2003. **100**(23): p. 13644-13649.
69. Penuela, S., et al., *Pannexin channels and their links to human disease.* Biochemical Journal, 2014. **461**(3): p. 371-381.
70. Bao, L., S. Locovei, and G. Dahl, *Pannexin membrane channels are mechanosensitive conduits for ATP.* FEBS letters, 2004. **572**(1-3): p. 65-68.
71. Iglesias, R., et al., *Pannexin 1: the molecular substrate of astrocyte "hemichannels".* Journal of Neuroscience, 2009. **29**(21): p. 7092-7097.
72. Boassa, D., et al., *Pannexin 1 channels contain a glycosylation site that targets the hexamer to the plasma membrane.* Journal of Biological Chemistry, 2007. **282**(43): p. 31733-31743.
73. Boassa, D., et al., *Trafficking dynamics of glycosylated Pannexin 1proteins.* Cell communication & adhesion, 2008. **15**(1-2): p. 119-132.
74. Sosinsky, G.E., et al., *Pannexin channels are not gap junction hemichannels.* Channels, 2011. **5**(3): p. 193-197.
75. Locovei, S., L. Bao, and G. Dahl, *Pannexin 1in erythrocytes: function without a gap.* Proceedings of the National Academy of Sciences, 2006. **103**(20): p. 7655-7659.
76. Pelegrin, P. and A. Surprenant, *Pannexin-1 mediates large pore formation and interleukin-1beta release by the ATP-gated P2X7 receptor.* Embo j, 2006. **25**(21): p. 5071-82.
77. Adamson, S.E. and N. Leitinger, *The role of Pannexin 1in the induction and resolution of inflammation.* FEBS Letters, 2014. **588**(8): p. 1416-1422.
78. Marcus, A.J., et al., *The endothelial cell ecto-ADPase responsible for inhibition of platelet function is CD39.* The Journal of clinical investigation, 1997. **99**(6): p. 1351-1360.
79. Seo, J.H., M.S. Dalal, and J.E. Contreras, *Pannexin-1 Channels as Mediators of Neuroinflammation.* Int J Mol Sci, 2021. **22**(10).
80. Molica, F., et al., *Functional role of a polymorphism in the Pannexin 1gene in collageninduced platelet aggregation.* Thrombosis and haemostasis, 2015. **114**(08): p. 325-336.
81. Taylor, K., et al., *Amplification of human platelet activation by surface pannexin-1 channels.* Journal of Thrombosis and Haemostasis, 2014. **12**(6): p. 987-998.
82. Molica, F., et al., *Selective inhibition of Panx1 channels decreases hemostasis and thrombosis in vivo.* Thrombosis research, 2019. **183**: p. 56-62.
83. Wang, J., D.G. Jackson, and G. Dahl, *The food dye FD&C Blue No. 1 is a selective inhibitor of the ATP release channel Panx1.* Journal of General Physiology, 2013. **141**(5): p. 649-656.
84. Bhaskaracharya, A., et al., *Probenecid blocks human P2X7 receptor-induced dye uptake via a pannexin-1 independent mechanism.* PloS one, 2014. **9**(3): p. e93058.
85. Iglesias, R., D.C. Spray, and E. Scemes, *Mefloquine blockade of Pannexin 1currents: resolution of a conflict.* Cell communication & adhesion, 2009. **16**(5-6): p. 131-137.
86. Michalski, K. and T. Kawate, *Carbenoxolone inhibits Pannexin 1 channels through interactions in the first extracellular loop.* Journal of General Physiology, 2016. **147**(2): p. 165-174.
87. Willebrords, J., et al., *Inhibitors of connexin and pannexin channels as potential therapeutics.* Pharmacology & Therapeutics, 2017. **180**: p. 144-160.

88. Sagar, G.V. and D. Larson, *Carbenoxolone inhibits junctional transfer and upregulates Connexin43 expression by a protein kinase A-dependent pathway.* Journal of cellular biochemistry, 2006. **98**(6): p. 1543-1551.
89. COUILLIN, I., A. GOMBAULT, and L. Baron, *ATP release and purinergic signaling in NLRP3 inflammasome activation.* Frontiers in immunology, 2013. **3**: p. 414.
90. Corriden, R. and P.A. Insel, *New insights regarding the regulation of chemotaxis by nucleotides, adenosine, and their receptors.* Purinergic signalling, 2012. **8**(3): p. 587-598.
91. Scheckenbach, K.E., et al., *Connexin channel-dependent signaling pathways in inflammation.* J Vasc Res, 2011. **48**(2): p. 91-103.
92. Lohman, A.W., et al., *Pannexin 1 channels regulate leukocyte emigration through the venous endothelium during acute inflammation.* Nature Communications, 2015. **6**(1): p. 7965.
93. Chekeni, F.B., et al., *Pannexin 1 channels mediate 'find-me' signal release and membrane permeability during apoptosis.* Nature, 2010. **467**(7317): p. 863-7.
94. Gombault, A., L. Baron, and I. Couillin, *ATP release and purinergic signaling in NLRP3 inflammasome activation.* Front Immunol, 2012. **3**: p. 414.
95. Negoro, H., et al., *Pannexin 1involvement in bladder dysfunction in a multiple sclerosis model.* Sci Rep, 2013. **3**: p. 2152.
96. Sofoluwe, A., et al., *ATP amplifies NADPH-dependent and-independent neutrophil extracellular trap formation.* Scientific reports, 2019. **9**(1): p. 1-11.
97. Li, W., et al., *Carbenoxolone blocks endotoxin-induced protein kinase R (PKR) activation and high mobility group box 1 (HMGB1) release.* Mol Med, 2013. **19**(1): p. 203-11.
98. Seo, J.H., et al., *Myeloid Pannexin-1 mediates acute leukocyte infiltration and leads to worse outcomes after brain trauma.* J Neuroinflammation, 2020. **17**(1): p. 245.
99. Smallwood, L., et al., *Polymorphisms of the matrix metalloproteinase 9 gene and abdominal aortic aneurysm.* The British journal of surgery, 2008. **95**(10): p. 1239-1244.
100. Li, S., I. Bjelobaba, and S.S. Stojilkovic, *Interactions of Pannexin 1 channels with purinergic and NMDA receptor channels.* Biochim Biophys Acta Biomembr, 2018. **1860**(1): p. 166-173.
101. Weilinger, N.L., et al., *Metabotropic NMDA receptor signaling couples Src family kinases to pannexin-1 during excitotoxicity.* Nature neuroscience, 2016. **19**(3): p. 432-442.
102. Hellenthal, F.A., et al., *Biomarkers of abdominal aortic aneurysm progression. Part 2: inflammation.* Nature Reviews Cardiology, 2009. **6**(8): p. 543-552.
103. Sampson, U.K., et al., *Estimation of global and regional incidence and prevalence of abdominal aortic aneurysms 1990 to 2010.* Global heart, 2014. **9**(1): p. 159-170.
104. Johnston, K.W., et al., *Suggested standards for reporting on arterial aneurysms.* Journal of vascular surgery, 1991. **13**(3): p. 452-458.
105. Sakalihasan, N., R. Limet, and O.D. Defawe, *Abdominal aortic aneurysm.* The Lancet, 2005. **365**(9470): p. 1577-1589.
106. Sakalihasan, N., et al., *Abdominal aortic aneurysms.* Nature reviews Disease primers, 2018. **4**(1): p. 1-22.
107. Juvonen, J., et al., *Elevated circulating levels of inflammatory cytokines in patients with abdominal aortic aneurysm.* Arteriosclerosis, thrombosis, and vascular biology, 1997. **17**(11): p. 2843-2847.
108. Defawe, O.D., et al., *TIMP-2 and PAI-1 mRNA levels are lower in aneurysmal as compared to athero-occlusive abdominal aortas.* Cardiovascular research, 2003. **60**(1): p. 205-213.
109. Aziz, F. and H. Kuivaniemi, *Role of matrix metalloproteinase inhibitors in preventing abdominal aortic aneurysm.* Annals of vascular surgery, 2007. **21**(3): p. 392-401.
110. Busch, A., et al., *Four Surgical Modifications to the Classic Elastase Perfusion Aneurysm Model Enable Haemodynamic Alterations and Extended Elastase Perfusion.* Eur J Vasc Endovasc Surg, 2018. **56**(1): p. 102-109.

111. Grøndal, N., R. Søgaard, and J.S. Lindholt, *Baseline prevalence of abdominal aortic aneurysm, peripheral arterial disease and hypertension in men aged 65–74 years from a population screening study (VIVA trial).* Journal of British Surgery, 2015. **102**(8): p. 902-906.
112. Vardulaki, K., et al., *Quantifying the risks of hypertension, age, sex and smoking in patients with abdominal aortic aneurysm.* Journal of British Surgery, 2000. **87**(2): p. 195-200.
113. Lindholt, J.S., et al., *Systemic levels of cotinine and elastase, but not pulmonary function, are associated with the progression of small abdominal aortic aneurysms.* European journal of vascular and endovascular surgery, 2003. **26**(4): p. 418-422.
114. Chaikof, E.L., et al., *The Society for Vascular Surgery practice guidelines on the care of patients with an abdominal aortic aneurysm.* Journal of vascular surgery, 2018. **67**(1): p. 2-77. e2.
115. Wanhainen, A., et al., *Editor's choice–European Society for Vascular Surgery (ESVS) 2019 clinical practice guidelines on the management of abdominal aorto-iliac artery aneurysms.* European Journal of Vascular and Endovascular Surgery, 2019. **57**(1): p. 8-93.
116. Ullery, B.W., R.L. Hallett, and D. Fleischmann, *Epidemiology and contemporary management of abdominal aortic aneurysms.* Abdominal Radiology, 2018. **43**(5): p. 1032-1043.
117. Sakalihasan, N., et al., *Abdominal aortic aneurysms.* Nat Rev Dis Primers, 2018. **4**(1): p. 34.
118. Zhu, C., et al., *Intraluminal Thrombus Predicts Rapid Growth of Abdominal Aortic Aneurysms.* Radiology, 2020. **294**(3): p. 707-713.
119. Harter, L.P., et al., *Ultrasonic evaluation of abdominal aortic thrombus.* Journal of Ultrasound in Medicine, 1982. **1**(8): p. 315-318.
120. Kavanagh, E.G., et al., *The biaxial mechanical behaviour of abdominal aortic aneurysm intraluminal thrombus: classification of morphology and the determination of layer and region specific properties.* Journal of biomechanics, 2014. **47**(6): p. 1430-1437.
121. Wilson, J.S., et al., *Biochemomechanics of intraluminal thrombus in abdominal aortic aneurysms.* Journal of biomechanical engineering, 2013. **135**(2).
122. Adolph, R., et al., *Cellular content and permeability of intraluminal thrombus in abdominal aortic aneurysm.* Journal of vascular surgery, 1997. **25**(5): p. 916-926.
123. Touat, Z., et al., *Renewal of mural thrombus releases plasma markers and is involved in aortic abdominal aneurysm evolution.* The American journal of pathology, 2006. **168**(3): p. 1022-1030.
124. Kazi, M., et al., *Influence of intraluminal thrombus on structural and cellular composition of abdominal aortic aneurysm wall.* Journal of vascular surgery, 2003. **38**(6): p. 1283-1292.
125. Khan, J.A., et al., *Intraluminal thrombus has a selective influence on matrix metalloproteinases and their inhibitors (tissue inhibitors of matrix metalloproteinases) in the wall of abdominal aortic aneurysms.* Annals of vascular surgery, 2012. **26**(3): p. 322-329.
126. Weyrich, A., et al., *Platelets in atherothrombosis: new and evolving roles.* Current pharmaceutical design, 2007. **13**(16): p. 1685-1691.
127. Dai, J., et al., *Effect of blocking platelet activation with AZD6140 on development of abdominal aortic aneurysm in a rat aneurysmal model.* Journal of vascular surgery, 2009. **49**(3): p. 719-727.
128. Liu, O., et al., *Clopidogrel, a Platelet P2Y12 Receptor Inhibitor, Reduces Vascular Inflammation and Angiotensin II Induced-Abdominal Aortic Aneurysm Progression.* PLOS ONE, 2012. **7**(12): p. e51707.
129. Kamp, T.J., et al., *Myocardial infarction, aortic dissection, and thrombolytic therapy.* American heart journal, 1994. **128**(6): p. 1234-1237.

130. Kantelhardt, S.R., et al., *Recurrent Aortic Dissection in Marfan's Syndrome: Possible Effects of Anticoagulation: Finalist, Cardiology in ReviewFellowship/Residency Clinical Case Contest.* Cardiology in review, 2003. **11**(4): p. 240-243.
131. Spinosa, M., et al., *Abstract 16283: Inhibition of Pannexin-1 Channels Attenuates Vascular Inflammation and Aortic Aneurysm Formation.* Circulation, 2018. **138**(Suppl_1): p. A16283-A16283.
132. Sharma, A.K., et al., *Abstract 16658: Pannexin-1 Channels on Endothelial Cells Modulates Aortic Aneurysm Formation.* Circulation, 2016. **134**(suppl_1): p. A16658-A16658.
133. Pyo, R., et al., *Targeted gene disruption of matrix metalloproteinase-9 (gelatinase B) suppresses development of experimental abdominal aortic aneurysms.* The Journal of clinical investigation, 2000. **105**(11): p. 1641-1649.
134. Pyo, R., et al., *Targeted gene disruption of matrix metalloproteinase-9 (gelatinase B) suppresses development of experimental abdominal aortic aneurysms.* J Clin Invest, 2000. **105**(11): p. 1641-9.
135. Busch, A., et al., *Extra- and Intraluminal Elastase Induce Morphologically Distinct Abdominal Aortic Aneurysms in Mice and Thus Represent Specific Subtypes of Human Disease.* J Vasc Res, 2016. **53**(1-2): p. 49-57.
136. Angiolillo, D.J., et al., *Antiplatelet drug response variability and the role of platelet function testing: A practical guide for interventional cardiologists.* Catheterization and Cardiovascular Interventions, 2009. **73**(1): p. 1-14.
137. Kumar, A. and J. Kao, *Platelet resistance to antiplatelet drugs.* Recent Patents on Cardiovascular Drug Discovery (Discontinued), 2009. **4**(2): p. 98-108.
138. Gum, P.A., et al., *Profile and prevalence of aspirin resistance in patients with cardiovascular disease.* The American Journal of Cardiology, 2001. **88**(3): p. 230-235.
139. Owens, A.P., et al., *Platelet Inhibitors Reduce Rupture in a Mouse Model of Established Abdominal Aortic Aneurysm.* Arteriosclerosis, Thrombosis, and Vascular Biology, 2015. **35**(9): p. 2032-2041.
140. Morton, L.F., et al., *Integrin α2β1-independent activation of platelets by simple collagen-like peptides: collagen tertiary (triple-helical) and quaternary (polymeric) structures are sufficient alone for α2β1-independent platelet reactivity.* Biochemical Journal, 1995. **306**(2): p. 337-344.
141. Xu, W.-f., et al., *Cloning and characterization of human protease-activated receptor 4.* Proceedings of the National Academy of Sciences, 1998. **95**(12): p. 6642-6646.
142. Klatt, C., et al., *Platelet-RBC interaction mediated by FasL/FasR induces procoagulant activity important for thrombosis.* The Journal of clinical investigation, 2018. **128**(9): p. 3906-3925.
143. Woehrle, T., et al., *Pannexin-1 hemichannel-mediated ATP release together with P2X1 and P2X4 receptors regulate T-cell activation at the immune synapse.* Blood, 2010. **116**(18): p. 3475-84.
144. Schlessinger, J., *Cell signaling by receptor tyrosine kinases.* Cell, 2000. **103**(2): p. 211-25.
145. Reddy, E.C. and M.L. Rand, *Procoagulant phosphatidylserine-exposing platelets in vitro and in vivo.* Frontiers in cardiovascular medicine, 2020. **7**: p. 15.
146. Dale, G.L., et al., *Stimulated platelets use serotonin to enhance their retention of procoagulant proteins on the cell surface.* Nature, 2002. **415**(6868): p. 175-179.
147. Dale, G.L., *Coated-platelets: an emerging component of the procoagulant response.* J Thromb Haemost, 2005. **3**(10): p. 2185-92.
148. Chiu, Y.-H., et al., *Revisiting multimodal activation and channel properties of Pannexin 1.* Journal of General Physiology, 2017. **150**(1): p. 19-39.
149. Weilinger, N.L., P.L. Tang, and R.J. Thompson, *Anoxia-induced NMDA receptor activation opens pannexin channels via Src family kinases.* Journal of Neuroscience, 2012. **32**(36): p. 12579-12588.

150. Barbe, M.T., H. Monyer, and R. Bruzzone, *Cell-cell communication beyond connexins: the pannexin channels.* Physiology, 2006. **21**(2): p. 103-114.
151. DeLalio, L.J., et al., *Constitutive SRC-mediated phosphorylation of pannexin 1at tyrosine 198 occurs at the plasma membrane.* Journal of Biological Chemistry, 2019. **294**(17): p. 6940-6956.
152. Chen, M.L., et al., *Crosstalk between activated and inactivated c-Src in hepatocellular carcinoma.* Dis Markers, 2011. **30**(6): p. 325-33.
153. Woulfe, D.S., *Akt signaling in platelets and thrombosis.* Expert review of hematology, 2010. **3**(1): p. 81-91.
154. Jacinto, E., et al., *Mammalian TOR complex 2 controls the actin cytoskeleton and is rapamycin insensitive.* Nature cell biology, 2004. **6**(11): p. 1122-1128.
155. Marin, V., et al., *The IL-6-Soluble IL-6Rα Autocrine Loop of Endothelial Activation as an Intermediate Between Acute and Chronic Inflammation: an Experimental Model Involving Thrombin.* The Journal of Immunology, 2001. **167**(6): p. 3435-3442.
156. Heddle, N.M., *Cytokines in Platelet Concentrates.* Hematology, 1997. **2**(6): p. 473-484.
157. Koval, M., et al., *Pannexin 1as a driver of inflammation and ischemia–reperfusion injury.* Purinergic Signalling, 2021.
158. Bhamidipati, C.M., et al., *Development of a novel murine model of aortic aneurysms using peri-adventitial elastase.* Surgery, 2012. **152**(2): p. 238-246.
159. Cohen, J.R., et al., *Role of the neutrophil in abdominal aortic aneurysm development.* Cardiovasc Surg, 1993. **1**(4): p. 373-6.
160. Klopf, J., et al., *Neutrophils as Regulators and Biomarkers of Cardiovascular Inflammation in the Context of Abdominal Aortic Aneurysms.* Biomedicines, 2021. **9**(9): p. 1236.
161. Yuan, Z., et al., *Abdominal Aortic Aneurysm: Roles of Inflammatory Cells.* Front Immunol, 2020. **11**: p. 609161.
162. Daugherty, A., L.A. Cassis, and H. Lu, *Complex pathologies of angiotensin II-induced abdominal aortic aneurysms.* J Zhejiang Univ Sci B, 2011. **12**(8): p. 624-8.
163. Patrono, C., *Aspirin as an antiplatelet drug.* New England Journal of Medicine, 1994. **330**(18): p. 1287-1294.
164. Thachil, J., *Antiplatelet therapy - a summary for the general physicians.* Clinical medicine (London, England), 2016. **16**(2): p. 152-160.
165. Angiolillo, D.J., *The evolution of antiplatelet therapy in the treatment of acute coronary syndromes.* Drugs, 2012. **72**(16): p. 2087-2116.
166. Cunningham, R.F., Z.H. Israili, and P.G. Dayton, *Clinical pharmacokinetics of probenecid.* Clin Pharmacokinet, 1981. **6**(2): p. 135-51.
167. Kirk Allen, T., *Pannexin-1 and other anion channels in platelets and megakaryocytes*. 2015.
168. Balkenhol, J., et al., *Comparison of the central human and mouse platelet signaling cascade by systems biological analysis.* BMC Genomics, 2020. **21**(1): p. 897.
169. Gayle, R.B., et al., *Inhibition of platelet function by recombinant soluble ecto-ADPase/CD39.* The Journal of clinical investigation, 1998. **101**(9): p. 1851-1859.
170. Campbell, W., et al., *Anti-platelet activity of beta-adrenergic antagonists: inhibition of thromboxane synthesis and platelet aggregation in patients receiving long-term propranolol treatment.* The Lancet, 1981. **318**(8260-8261): p. 1382-1384.
171. Flaumenhaft, R. and A. Sharda, *19 - Platelet Secretion*, in *Platelets (Fourth Edition)*, A.D. Michelson, Editor. 2019, Academic Press. p. 349-370.
172. Nurden, A.T. and P. Nurden, *Congenital platelet disorders and understanding of platelet function.* British journal of haematology, 2014. **165**(2): p. 165-178.
173. Lannan, K.L., R.P. Phipps, and R.J. White, *Thrombosis, platelets, microparticles and PAH: more than a clot.* Drug Discovery Today, 2014. **19**(8): p. 1230-1235.
174. Lohman, A. and B. Isakson, *Differentiating connexin hemichannels and pannexin channels in cellular ATP release.* FEBS letters, 2014. **588**.

175. Fong, K.P., et al., *Directly Activating the Integrin αIIbβ3 Initiates Outside-In Signaling by Causing αIIbβ3 Clustering.* Journal of Biological Chemistry, 2016. **291**(22): p. 11706-11716.
176. Faraday, N., et al., *Leukocytes can enhance platelet-mediated aggregation and thromboxane release via interaction of P-selectin glycoprotein ligand 1 with P-selectin.* Anesthesiology, 2001. **94**(1): p. 145-51.
177. Hörmann, H., *Die Rolle des extrazellulären Matrixproteins Biglykan in der Thrombozytenadhäsion und arteriellen Thrombusbildung*. 2020, Universitäts-und Landesbibliothek der Heinrich-Heine-Universität Düsseldorf.
178. Hanstein, R., et al., *Promises and pitfalls of a Pannexin 1transgenic mouse line.* Frontiers in pharmacology, 2013. **4**: p. 61-61.
179. Whyte-Fagundes, P. and G. Zoidl, *Mechanisms of Pannexin 1channel gating and regulation.* Biochimica et Biophysica Acta (BBA) - Biomembranes, 2018. **1860**(1): p. 65-71.
180. Hechler, B., et al., *A role of the fast ATP-gated P2X1 cation channel in thrombosis of small arteries in vivo.* J Exp Med, 2003. **198**(4): p. 661-7.
181. Bakker, D., et al., *Comparison of Velocity Profiles for Different Flow Chamber Designs Used in Studies of Microbial Adhesion to Surfaces.* Applied and environmental microbiology, 2003. **69**: p. 6280-7.
182. Davis, M.J., et al., *Regulation of ion channels by protein tyrosine phosphorylation.* American Journal of Physiology-Heart and Circulatory Physiology, 2001. **281**(5): p. H1835-H1862.
183. Levitan, I.B., *Modulation of ion channels by protein phosphorylation and dephosphorylation.* Annu Rev Physiol, 1994. **56**: p. 193-212.
184. Park, K.-S., et al., *Potassium Channel Phosphorylation in Excitable Cells: Providing Dynamic Functional Variability to a Diverse Family of Ion Channels.* Physiology, 2008. **23**(1): p. 49-57.
185. Lohman, A.W., et al., *Pannexin 1 channels regulate leukocyte emigration through the venous endothelium during acute inflammation.* Nature communications, 2015. **6**(1): p. 1-12.
186. Barbe, M.T., H. Monyer, and R. Bruzzone, *Cell-cell communication beyond connexins: the pannexin channels.* Physiology (Bethesda), 2006. **21**: p. 103-14.
187. Weilinger, N.L., et al., *Metabotropic NMDA receptor signaling couples Src family kinases to pannexin-1 during excitotoxicity.* Nature Neuroscience, 2016. **19**(3): p. 432-442.
188. Canobbio, I., *Blood platelets: Circulating mirrors of neurons?* Research and practice in thrombosis and haemostasis, 2019. **3**(4): p. 564-565.
189. Penuela, S., et al., *Pannexin 1and pannexin 3 are glycoproteins that exhibit many distinct characteristics from the connexin family of gap junction proteins.* J Cell Sci, 2007. **120**(Pt 21): p. 3772-83.
190. Taylor, K.a., G. Little, and J.M. Gibbins, *Mind the gap: connexins and pannexins in platelet function.* Platelets, 2021. **32**(7): p. 888-894.
191. Yacoub, D., et al., *Essential role of protein kinase C delta in platelet signaling, alpha IIb beta 3 activation, and thromboxane A2 release.* J Biol Chem, 2006. **281**(40): p. 30024-35.
192. López, X., et al., *Stretch-Induced Activation of Pannexin 1 channels Can Be Prevented by PKA-Dependent Phosphorylation.* International journal of molecular sciences, 2020. **21**(23): p. 9180.
193. Chen, K.W., B. Demarco, and P. Broz, *Pannexin-1 promotes NLRP3 activation during apoptosis but is dispensable for canonical or noncanonical inflammasome activation.* Eur J Immunol, 2020. **50**(2): p. 170-177.
194. Sandilos, J.K., et al., *Pannexin 1, an ATP release channel, is activated by caspase cleavage of its pore-associated C-terminal autoinhibitory region.* The Journal of biological chemistry, 2012. **287**(14): p. 11303-11311.

195. Perrotta, P.L., C.L. Perrotta, and E.L. Snyder, *Apoptotic activity in stored human platelets.* Transfusion, 2003. **43**(4): p. 526-535.
196. Gardiner, E.E., et al., *Controlled shedding of platelet glycoprotein (GP)VI and GPIb-IX-V by ADAM family metalloproteinases.* J Thromb Haemost, 2007. **5**(7): p. 1530-7.
197. Chekeni, F.B., et al., *Pannexin 1 channels mediate 'find-me'signal release and membrane permeability during apoptosis.* Nature, 2010. **467**(7317): p. 863-867.
198. Klopf, J., et al., *Neutrophils as Regulators and Biomarkers of Cardiovascular Inflammation in the Context of Abdominal Aortic Aneurysms.* Biomedicines, 2021. **9**(9).
199. Haselmayer, P., et al., *TREM-1 ligand expression on platelets enhances neutrophil activation.* Blood, The Journal of the American Society of Hematology, 2007. **110**(3): p. 1029-1035.
200. Kurose, I., et al., *Molecular determinants of reperfusion-induced leukocyte adhesion and vascular protein leakage.* Circulation Research, 1994. **74**(2): p. 336-343.
201. Lievens, D., et al., *Platelet CD40L mediates thrombotic and inflammatory processes in atherosclerosis.* Blood, The Journal of the American Society of Hematology, 2010. **116**(20): p. 4317-4327.
202. Jersmann, H.P., D.A. Rathjen, and A. Ferrante, *Enhancement of lipopolysaccharide-induced neutrophil oxygen radical production by tumor necrosis factor alpha.* Infection and immunity, 1998. **66**(4): p. 1744-1747.
203. Jayachandran, M., et al., *In vivo effects of lipopolysaccharide and TLR4 on platelet production and activity: implications for thrombotic risk.* Journal of Applied Physiology, 2007. **102**(1): p. 429-433.
204. Cambien, B., et al., *Antithrombotic activity of TNF-α.* The Journal of Clinical Investigation, 2003. **112**(10): p. 1589-1596.
205. *Interleukin-6 Production by Endothelial Cells via Stimulation of Protease-Activated Receptors Is Amplified by Endotoxin and Tumor Necrosis Factor-α.* Journal of Interferon & Cytokine Research, 2001. **21**(4): p. 231-240.
206. Su, H., C.-T. Lei, and C. Zhang, *Interleukin-6 Signaling Pathway and Its Role in Kidney Disease: An Update.* Frontiers in Immunology, 2017. **8**(405).
207. Wei, L., et al., *Effect of pannexin-1 on the release of glutamate and cytokines in astrocytes.* Journal of Clinical Neuroscience, 2016. **23**: p. 135-141.
208. Billaud, M., J.K. Sandilos, and B.E. Isakson, *Pannexin 1in the regulation of vascular tone.* Trends in cardiovascular medicine, 2012. **22**(3): p. 68-72.
209. Ni, B.-K., et al., *Evaluation of serum pannexin-1 as a prognostic biomarker for traumatic brain injury.* Clinica Chimica Acta, 2019. **488**: p. 159-164.
210. Jürgen, K., *Platelet and red blood cell interaction–Unraveling of interaction molecules during cell-cell contact*. 2021.
211. Kawai, T., et al., *Vascular ADAM17 (a Disintegrin and Metalloproteinase Domain 17) Is Required for Angiotensin II/β-Aminopropionitrile–Induced Abdominal Aortic Aneurysm.* Hypertension, 2017. **70**(5): p. 959-963.
212. Wei, H., *Mechanisms of microparticle release from human platelets*. 2020, University of Cambridge.
213. Boilard, E., et al., *Platelets Amplify Inflammation in Arthritis via Collagen-Dependent Microparticle Production.* Science, 2010. **327**(5965): p. 580-583.
214. Lysgaard Poulsen, J., J. Stubbe, and J.S. Lindholt, *Animal Models Used to Explore Abdominal Aortic Aneurysms: A Systematic Review.* Eur J Vasc Endovasc Surg, 2016. **52**(4): p. 487-499.
215. Azuma, J., et al., *Creation of murine experimental abdominal aortic aneurysms with elastase.* J Vis Exp, 2009(29).
216. Hansen, K.B., A. Arzani, and S.C. Shadden, *Mechanical platelet activation potential in abdominal aortic aneurysms.* Journal of biomechanical engineering, 2015. **137**(4): p. 041005-041005.

217. Busch, A., et al., *Translating mouse models of abdominal aortic aneurysm to the translational needs of vascular surgery.* JVS-vascular science, 2021. **2**: p. 219-234.
218. Lu, G., et al., *A novel chronic advanced stage abdominal aortic aneurysm murine model.* J Vasc Surg, 2017. **66**(1): p. 232-242.e4.
219. Panteleev, M.A., et al., *Wall shear rates in human and mouse arteries: Standardization of hemodynamics for in vitro blood flow assays: Communication from the ISTH SSC subcommittee on biorheology.* Journal of Thrombosis and Haemostasis, 2021. **19**(2): p. 588-595.
220. Greve, J.M., et al., *Allometric scaling of wall shear stress from mice to humans: quantification using cine phase-contrast MRI and computational fluid dynamics.* American Journal of Physiology-Heart and Circulatory Physiology, 2006. **291**(4): p. H1700-H1708.
221. Falati, S., et al., *Real-time in vivo imaging of platelets, tissue factor and fibrin during arterial thrombus formation in the mouse.* Nature medicine, 2002. **8**(10): p. 1175-1180.
222. Clemetson, K.J., *Platelet GPIb-V-IX Complex.* Thromb Haemost, 1997. **78**(07): p. 266-270.
223. NIESWANDT, B., I. PLEINES, and M. BENDER, *Platelet adhesion and activation mechanisms in arterial thrombosis and ischaemic stroke.* Journal of Thrombosis and Haemostasis, 2011. **9**(s1): p. 92-104.
224. Liu, J., et al., *Botrocetin/VWF-induced signaling through GPIb-IX-V produces TxA2 in an alphaIIbbeta3- and aggregation-independent manner.* Blood, 2005. **106**(8): p. 2750-6.
225. Shivdasani, R.A., et al., *A lineage-selective knockout establishes the critical role of transcription factor GATA-1 in megakaryocyte growth and platelet development.* The EMBO Journal, 1997. **16**(13): p. 3965-3973.
226. Straat, M., et al., *Red Blood Cell Clearance in Inflammation.* Transfusion Medicine and Hemotherapy, 2012. **39**(5): p. 353-360.
227. Behnke, O. and A. Forer, *From megakaryocytes to platelets: platelet morphogenesis takes place in the bloodstream.* European Journal of Haematology, 1998. **60**(S61): p. 3-23.
228. Armstrong, P.C., et al., *Newly Formed Reticulated Platelets Undermine Pharmacokinetically Short-Lived Antiplatelet Therapies.* Arteriosclerosis, Thrombosis, and Vascular Biology, 2017. **37**(5): p. 949-956.
229. Thon, J.N., et al., *Microtubule and cortical forces determine platelet size during vascular platelet production.* Nature communications, 2012. **3**(1): p. 1-9.
230. Korniluk, A., et al., *Mean Platelet Volume (MPV): New Perspectives for an Old Marker in the Course and Prognosis of Inflammatory Conditions.* Mediators of Inflammation, 2019. **2019**: p. 9213074.
231. Salvagno, G.L., et al., *Evaluation of platelet turnover by flow cytometry.* Platelets, 2006. **17**(3): p. 170-7.
232. Cunningham, R., Z. Israili, and P. Dayton, *Clinical pharmacokinetics of probenecid.* Clinical pharmacokinetics, 1981. **6**(2): p. 135-151.
233. Doll, R., I. Hill, and C. Hutton, *Treatment of gastric ulcer with carbenoxolone sodium and oestrogens.* Gut, 1965. **6**(1): p. 19.
234. BENDER, M., I. HAGEDORN, and B. NIESWANDT, *Genetic and antibody-induced glycoprotein VI deficiency equally protects mice from mechanically and FeCl3-induced thrombosis.* Journal of Thrombosis and Haemostasis, 2011. **9**(7): p. 1423-1426.
235. Andrews, R.K., J.F. Arthur, and E.E. Gardiner, *Targeting GPVI as a novel antithrombotic strategy.* Journal of blood medicine, 2014. **5**: p. 59-68.
236. Schüpke, S., et al., *Revacept, a Novel Inhibitor of Platelet Adhesion, in Patients Undergoing Elective PCI-Design and Rationale of the Randomized ISAR-PLASTER Trial.* Thromb Haemost, 2019. **119**(9): p. 1539-1545.

7 Appendix

7.1 Unshown Data

7.1.1 Platelet second wave mediators do not induce tyrosine phosphorylation

In Figure 19, it was shown that PANX1 defiecent platelets showed reduced tyrosine phosphorylation after high stimulation with PAR4 peptide. To determine whether the second wave mediators ADP and U46619 also induce tyrosine phosphorylation, Western blot analyses were performed. The data indicate that ADP and U46 alone do not induce tyrosine phosphorylation after platelet activation with all concentrations tested. In addition, no alterations between both genotypes were observed.

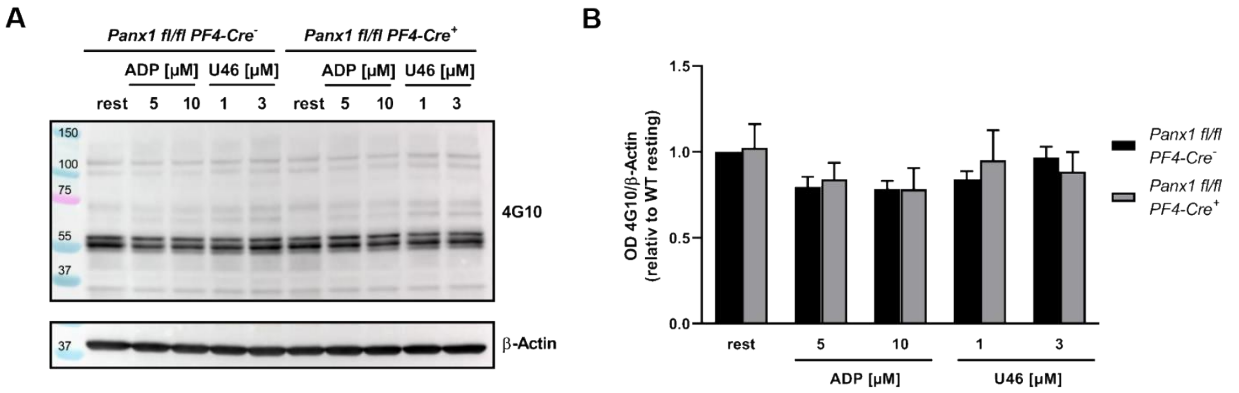

Figure 53: The second wave mediators ADP and U46119 do not induce tyrosine phosphorylation in murine platelets. (A) Representative image and (B) quantification of tyrosine phosphorylation (4G10) via Western blot analysis from isolated platelets from *Panx1 fl/fl Pf4-Cre*$^{+}$ and *Panx1 fl/fl Pf4-Cre*$^{-}$ mice activated with 5 and 10 µM ADP and 1 and 3 µM U46119 (n = 4). Statistical analyses were performed using a two-way ANOVA followed by a Sidak's multiple comparisons post-hoc test. Bar graphs indicate mean values ± SEM, Rest = Resting, ADP = Adenosine diphosphate, U46 (U46619) = Thromboxane A_2 analogue, Panx1 = Pannexin 1, OD = Optical density.

7.1.2 Aggregation and adhesion after pharmacological inhibition of pannexin 1without inhibition of second-wave activation upon collagen stimulation

Chapter 4.2.3 displays that PANX1 deficient platelets show a reduction in aggregation responses upon collagen stimulation under inhibition of platelet second wave activation by apyrase (0.04 U/mL). To analyze, if aggregation responses from *Panx1 fl/fl PF4-Cre*$^{-}$ and *Panx1 fl/fl PF4-Cre*$^{+}$ mice differ also without inhibition of platelet second wave activation, similar experiments were performed without apyrase.

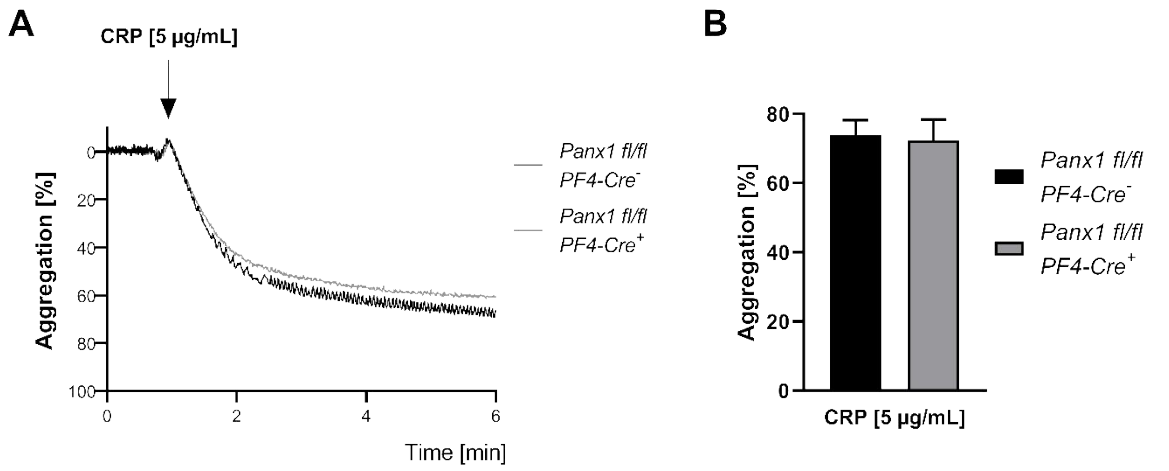

Figure 54: Aggregation is not altered in PANX1 deficient platelets in response to platelet activation with 5 µg/mL CRP compared to respective control platelets without platelet second wave inhibition by apyrase. Isolated platelets from *Panx1 fl/fl PF4-Cre*$^{-}$ and *Panx1 fl/fl PF4-Cre*$^{+}$ mice were stimulated with 5 µg/mL CRP and aggregation responses were measured by light transmission aggregometry for 6 min. Representative curves of aggregation-responses of platelet activation with (A) 5 µg/mL CRP. (B) Graph displays results of the maximal detected aggregation responses (n (WT) = 3, n (KO) = 3). Statistical analyses were performed using an unpaired student's t-test. Bar graphs indicate mean values ± SEM. CRP = collagen-related peptide, WT = Wild type, KO = Knock-out.

Aggregation responses from *Panx1 fl/fl PF4-Cre*$^{-}$ and *Panx1 fl/fl PF4-Cre*$^{+}$ mice in response to 5 µg/mL CRP without apyrase do not differ between predicted genotypes as shown in Figure 54. As a translational approach, human platelets were pre-treated with or without the PANX1 inhibiting compounds Cbx and Prb. Aggregation responses were analyzed upon high dose collagen induced platelet activation. The results indicate no differences between platelets pre-treated with Prb compared to controls (Figure 55 A, B). Application of 50 µM Cbx to human platelets resulted in reduced aggregation responses upon 5 µg/mL CRP stimulation (Figure 55 A, B $p = 0.011$). Additionally, adhesion experiments were performed to study the adhesion of platelets with or without Prb pre-treatment on collagen for 20 min as an extracellular matrix protein. The results do not show alterations between Prb treated platelets and controls regarding their adhesion behavior on a collagen coated matrix (Figure 55 E).

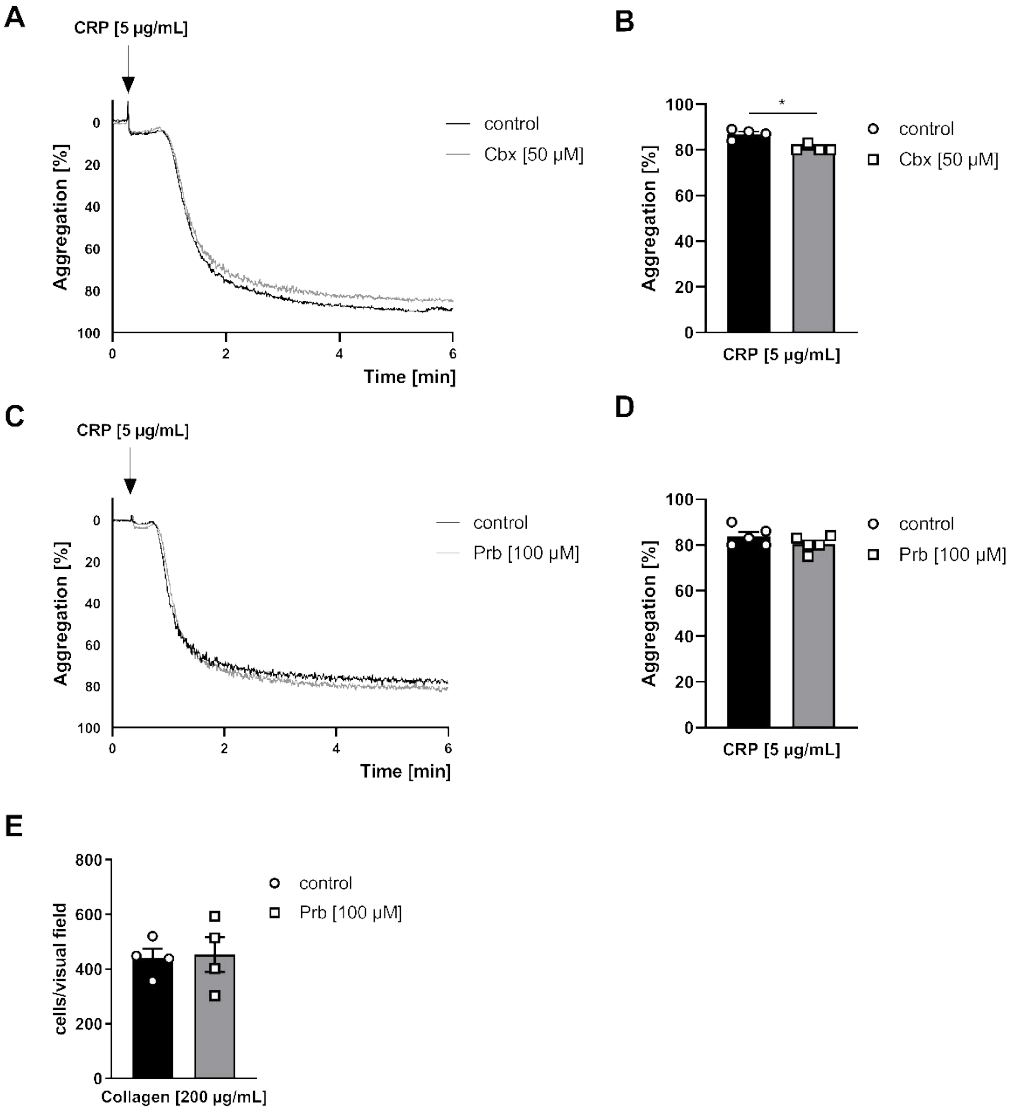

Figure 55: Inhibition of PANX1 by Carbenoxolone (Cbx) but not Probenecid (Prb) leads to reduced platelet aggregation upon high dose collagen stimulation. (A, B) Isolated platelets were preincubated with or without 50 µM Cbx and stimulated with 5 µg/mL CRP and aggregation responses were measured by light transmission aggregometry for 6 min. Representative curves of aggregation-responses of platelet activation with (A) 5 µg/mL CRP. (B) Graph displays results of the maximal detected aggregation responses (n (control) = 4, n (Cbx) = 4). (C, D) Isolated platelets were preincubated with or without 100 µM Prb and stimulated with 5 µg/mL CRP and aggregation responses were measured by light transmission aggregometry for 6 min. Representative curves of aggregation-responses of platelet activation with (C) 5 µg/mL CRP. (D) Graph displays results of the maximal detected aggregation responses (n (control) = 5, n (Prb) = 5). (E) Isolated platelets were preincubated with or without 100 µM Prb and platelet adhesion was studied for 20 min on a collagen [200 µg/mL] coated matrices (n (control) = 4, n (Prb) = 4). Statistical analyses were performed using a two-tailed paired student's t-test. Bar graphs indicate mean values ± SEM, *p < 0.05. CRP = Collagen-related peptide, Prb = Probenecid, Cbx = Carbenoxolone.

7.1.3 ATP release and ROS generation is tendency enhanced without inhibition of platelet second wave activation

Chapter 4.1 displayed a functional role of PANX1 in non-vascular ATP release by inhibition of second wave platelet activation with apyrase (0.04 U/mL). Since the collagen induced platelet activation is the main PANX1 activator, the role of PANX1 was investigated without second wave platelet inhibition. Therefore, ATP release measurements were performed via a bioluminescence assay in response to different concentrations of CRP using PANX1 deficient and control platelets.

The data shows that ATP release is significantly reduced at platelet resting conditions ($p = 0.0014$), however platelet activation with 1 µg/mL CRP significantly ($p = 0.048$) and 5 µg/mL CRP tendency ($p = 0.062$) increases ATP release in PANX1 deficient platelet compared to their respective controls (Figure 56). Additionally, ROS generation was measured upon platelet activation with 5 µg/mL CRP as well as under resting conditions. Figure 56 B displayed that platelet activation with 5 µg/mL CRP tendency enhances ROS-generation in PANX1 deficient platelets ($p = 0.06$).

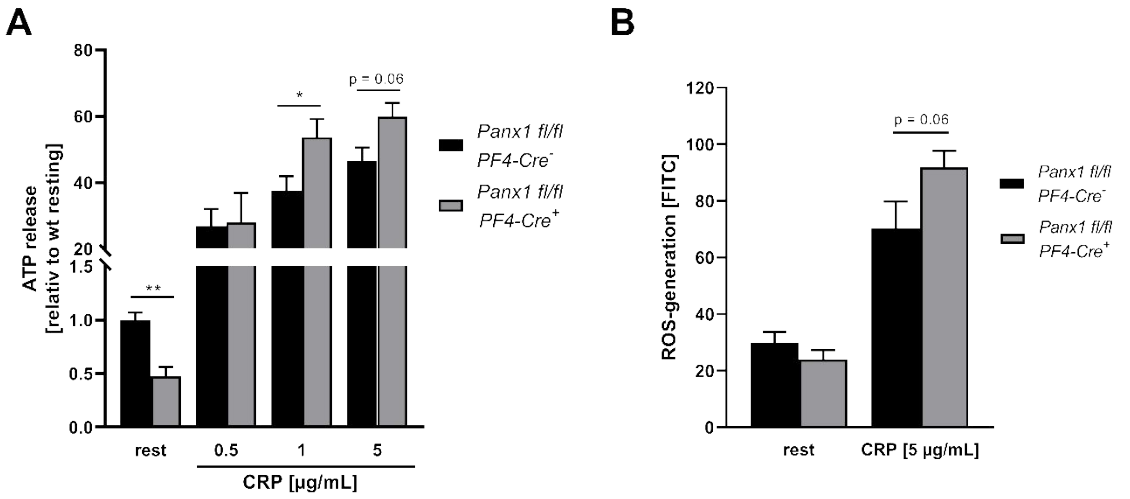

Figure 56: PANX1 deficient platelets show reduced ATP in a resting state, which enhances upon high dose collagen stimulation compared to respective control platelets. (A) ATP release measurements were performed via a bioluminescence assay in response to indicated concentrations of CRP using platelets from *Panx1 fl/fl PF4-Cre*$^-$ and *Panx1 fl/fl PF4-Cre*$^+$ mice (n (WT = 5-7, n (KO) = 6). (B) ROS generation was measured upon platelet activation with 5 µg/mL CRP as well as under resting conditions by the cell-permeable dye DCF-DA [FITC] (n (WT) = 4, n (KO) = 4). Statistical analyses were performed using a two-way ANOVA followed by a Sidak's multiple comparisons post-hoc test. Bar graphs indicate mean values ± SEM, *$p < 0.05$ and **$p < 0.01$. Rest = Resting, CRP = Collagen-related peptide, ROS = Reactive oxygen species, DCF-DA = 2′,7′-Dichlorofluorescindiacetat, KO = Knock-out, WT = Wild type.

7.1.4 Inhibition of pannexin 1 channels on RBCs does not alter thrombus formation *ex vivo*

Chapter 4.2.4 displayed a functional role of PANX1 channels on arterial thrombosis. At a shear rate of 1000s^{-1}, pharmacological inhibition of PANX1 in human whole blood by Prb resulted in reduced surface coverage and thrombus volume in a thrombus formation assay *ex vivo* (Figure 23). Recently our working group identified a critical role for RBCs in thrombus formation [142]. PANX1 channels are expressed on RBCs as well, therefore we aim investigating the influence of PANX1 channels on RBCs on thrombus formation. Therefore, isolated RBCs were treated with 100 µM Prb and reconstructed with platelets in plasma (2 x 10^5 platelets/µL and 4 x 10^6 RBCs/µL) and perfused over a collagen coated matrix at 1000s^{-1}. Isolated RBCs reconstructed with platelets in plasma served as a control. Surface coverage in percent and thrombus volume by the MFI were analyzed.

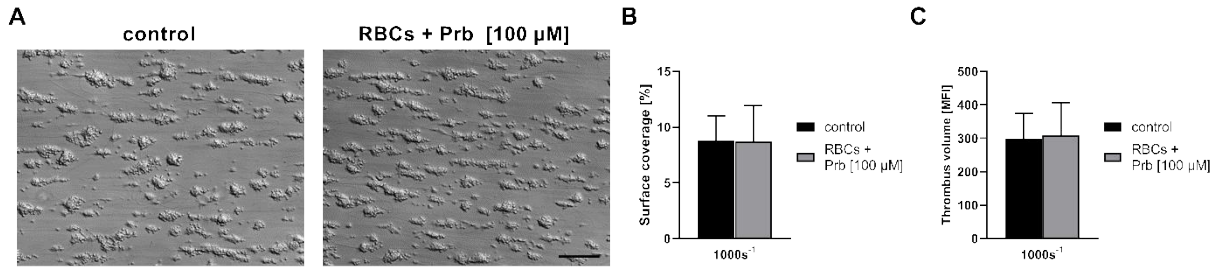

Figure 57: Pharmacological inhibition of PANX1 channels on RBCs does not alter thrombus formation at an arterial shear rate of 1000s^{-1} *ex vivo*. RBCs, plts and plasma were isolated from human whole blood and RBCs were pretreated with or without 100 µM Prb. Cells were reconstructed to human physiological blood conditions and perfused over a collagen coated matrices ex vivo at 1000s^{-1} (n (control) =5, n (RBC Prb) = 5). (A) Representative BF images of flow chamber experiments with (right) or without (left) inhibition of PANX1 channels on RBCs. Scale bar represent 100 µM. (B) Analysis of surface coverage [%] and (C) thrombus formation [MFI]. Statistical analyses were performed using an unpaired student's t-test. Bar graphs indicate mean values ± SEM. Prb = Probenecid, MFI = Mean fluorescence intensity, RBCs = Red blood cells, Plts = Platelets, BF = Bright field.

Inhibition of PANX1 channels on RBCs by 100 µM Prb does not influence thrombus formation investigated in a human thrombus formation assay at an intermediate arterial shear rate of 1000s^{-1} (Figure 57). In detail, surface coverage (Figure 57 B) as well as thrombus volume (Figure 57 C) were not altered under these experimental conditions. These results indicate a role for platelet PANX1 channels but not erythrocyte PANX1 channels in thrombus formation at intermediate arterial shear rates *ex vivo*.

7.1.5 Level of significances in aortic dilatation after PPE surgery

Table 3: Level of significances within genotypes compared to respective baseline size

Days post-PPE surgery	*Panx1 fl/fl PF4-Cre$^-$ mice*	*Panx1 fl/fl PF4-Cre$^+$ mice*
3	**; 0.0014	*; 0.021
7	***; < 0.0001	***; < 0.0001
14	***; < 0.0001	***; < 0.0001
21	***; < 0.0001	***; < 0.0001
28	***; < 0.0001	***; < 0.0001

7.1.6 Level of significances of blood cell counts after PPE surgery

7.1.6.1 WBC count

Table 4: Level of significances of WBCs within genotypes compared to WBC cell count at day 0 during PPE surgery

Days post-PPE surgery	*Panx1 fl/fl PF4-Cre$^-$ mice*	*Panx1 fl/fl PF4-Cre$^+$ mice*
3	***; < 0.0001	***; < 0.0001
7	***; < 0.0006	**; < 0.0024
14	***; < 0.0005	**; < 0.003
28	***; < 0.0001	***; < 0.0004

7.1.6.2 RBC count

Table 5: Level of significances of RBCs within genotypes compared to RBC cell count at day 0 during PPE surgery

Days post-PPE surgery	*Panx1 fl/fl PF4-Cre$^-$ mice*	*Panx1 fl/fl PF4-Cre$^+$ mice*
3	ns; 0.0537	ns; 0.6371
7	ns; 0.9942	ns; 0.9976
14	ns; 0.7015	ns; 0.9962
28	ns; 0.9905	ns; 0.9881

7.1.6.3 Platelet count

Table 6: Level of significances of platelets within genotypes compared to platelet cell count at day 0 during PPE surgery

Days post-PPE surgery	*Panx1 fl/fl PF4-Cre$^-$ mice*	*Panx1 fl/fl PF4-Cre$^+$ mice*
3	ns; 0.7093	ns; 0.9511
7	ns; 0.9744	ns; 0.9024
14	ns; 0.1102	ns; 0.7253
28	ns; 0.9972	ns; 0.0969

7.1.6.4 Platelet MPV

Table 7: Level of significances of platelet MPV within genotypes compared to platelet MPV at day 0 during PPE surgery

Days post-PPE surgery	*Panx1 fl/fl PF4-Cre$^-$ mice*	*Panx1 fl/fl PF4-Cre$^+$ mice*
3	***; 0.0008	ns; 0.3958
7	***; < 0.0001	ns; 0.0654
14	**; 0.0014	ns; 0.2570
28	*; 0.0301	ns; 0.7731

7.1.7 Level of significances in platelet-neutrophil aggregate formation

7.1.7.1 Platelet-neutrophil aggregates (resting)

Table 8: Level of significances within predicted genotypes compared to respective baseline values (Platelet resting)

Days post-PPE surgery	Agonist	*Panx1 fl/fl PF4-Cre$^-$ mice*	*Panx1 fl/fl PF4-Cre$^+$ mice*
3	resting	ns; 0.1256	ns; 0.3985
7	resting	ns; 0.2114	ns; 0.1634
14	resting	**; 0.0023	ns; 0.5074
28	resting	ns; 0.7225	ns; 0.3202

7.1.7.2 Platelet-neutrophil aggregates (CRP 5 µg/mL)

Table 9: Level of significances within predicted genotypes compared to respective baseline values (CRP 5 µg/mL)

Days post-PPE surgery	Agonist	*Panx1 fl/fl PF4-Cre$^-$ mice*	*Panx1 fl/fl PF4-Cre$^+$ mice*
3	CRP (5 µg/mL)	***; < 0.0001	***; 0.0003
7	CRP (5 µg/mL)	***; < 0.0001	***; < 0.0001
14	CRP (5 µg/mL)	*; 0.0202	ns; 0.2514
28	CRP (5 µg/mL)	**; 0.0032	**; 0.0023

7.1.7.3 Platelet-neutrophil aggregates (Thrombin 0.1 U/mL)

Table 10: Level of significances within predicted genotypes compared to respective baseline values (Thrombin 0.1 U/mL)

Days post-PPE surgery	Agonist	*Panx1 fl/fl PF4-Cre$^-$ mice*	*Panx1 fl/fl PF4-Cre$^+$ mice*
3	Thrombin (0.1 U/mL)	***; < 0.0001	***; < 0.0001
7	Thrombin (0.1 U/mL)	***; 0.0003	*; 0.0378
14	Thrombin (0.1 U/mL)	**; 0.0049	**; 0.0049
28	Thrombin (0.1 U/mL)	***; 0.0002	**; 0.0018

7.1.8 IF staining of murine aortic walls after PPE surgery

7.1.8.1 Corresponding images for Ly6G staining

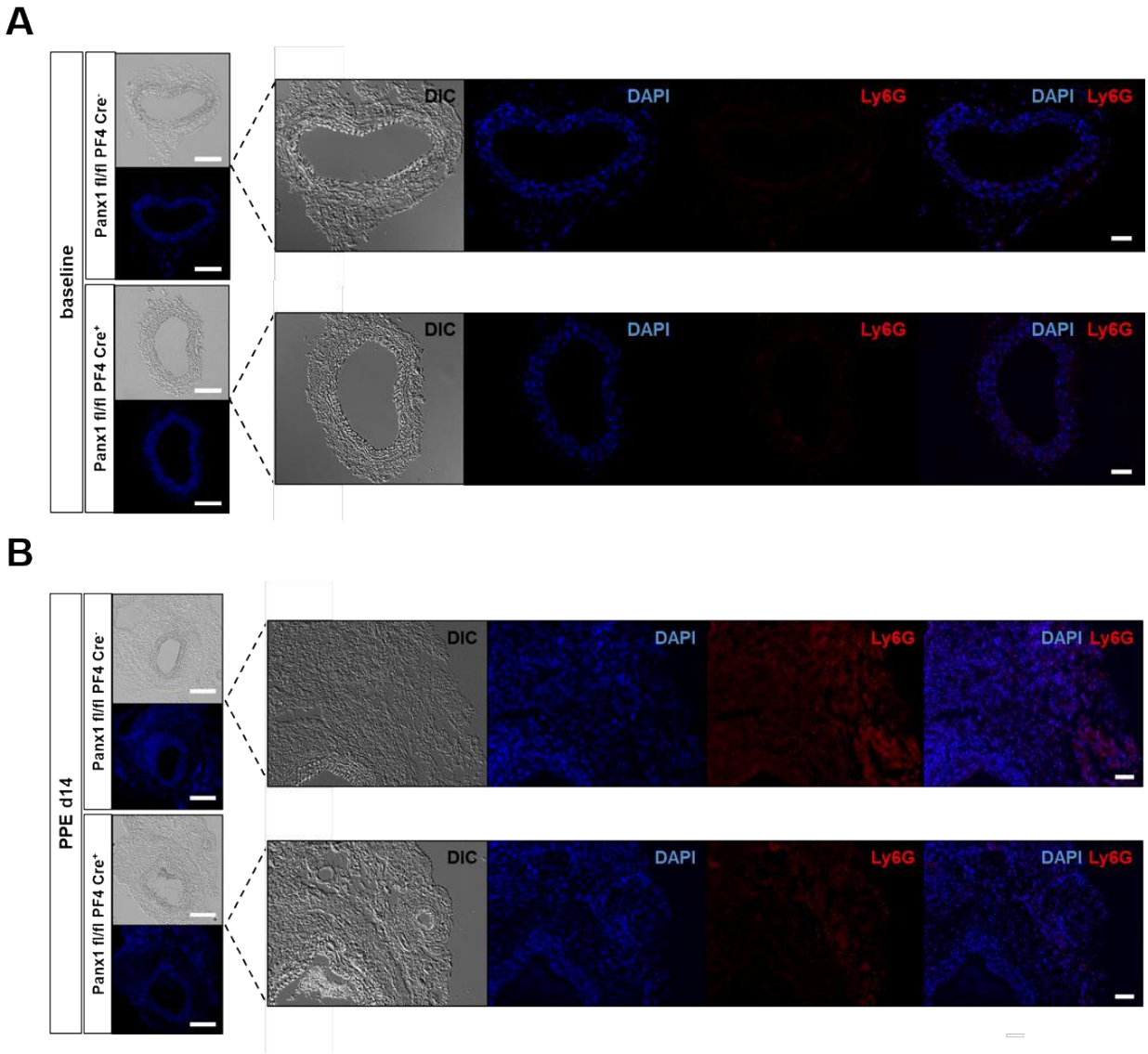

Figure 58: Representative images of neutrophil infiltration during PPE surgery. Aortic sections from murine tissues from *Panx1 fl/fl PF4-Cre*$^{-}$ and *Panx1 fl/fl PF4-Cre*$^{+}$ mice were analyzed regarding neutrophil infiltration (A) before (Baseline) and (B) 14 days after PPE surgery. Neutrophils were visualized using the neutrophil specific marker (Ly6G-Cy5 in red), while cell nuclei were stained with DAPI (blue). (Left) Representative overview images of aortic sections in DIC and DAPI. Scale bars represents 200 µM. (Right) Single channel images of DIC, DAPI, Ly6G and merged (DAPI and Ly6G) according to Figure 49. Scale bar represents 50 µM D = Day, PPE = Porcine Pancreatic Elastase, Panx1 = Pannexin 1, d = Days, DIC = Differential Interference Contrast.

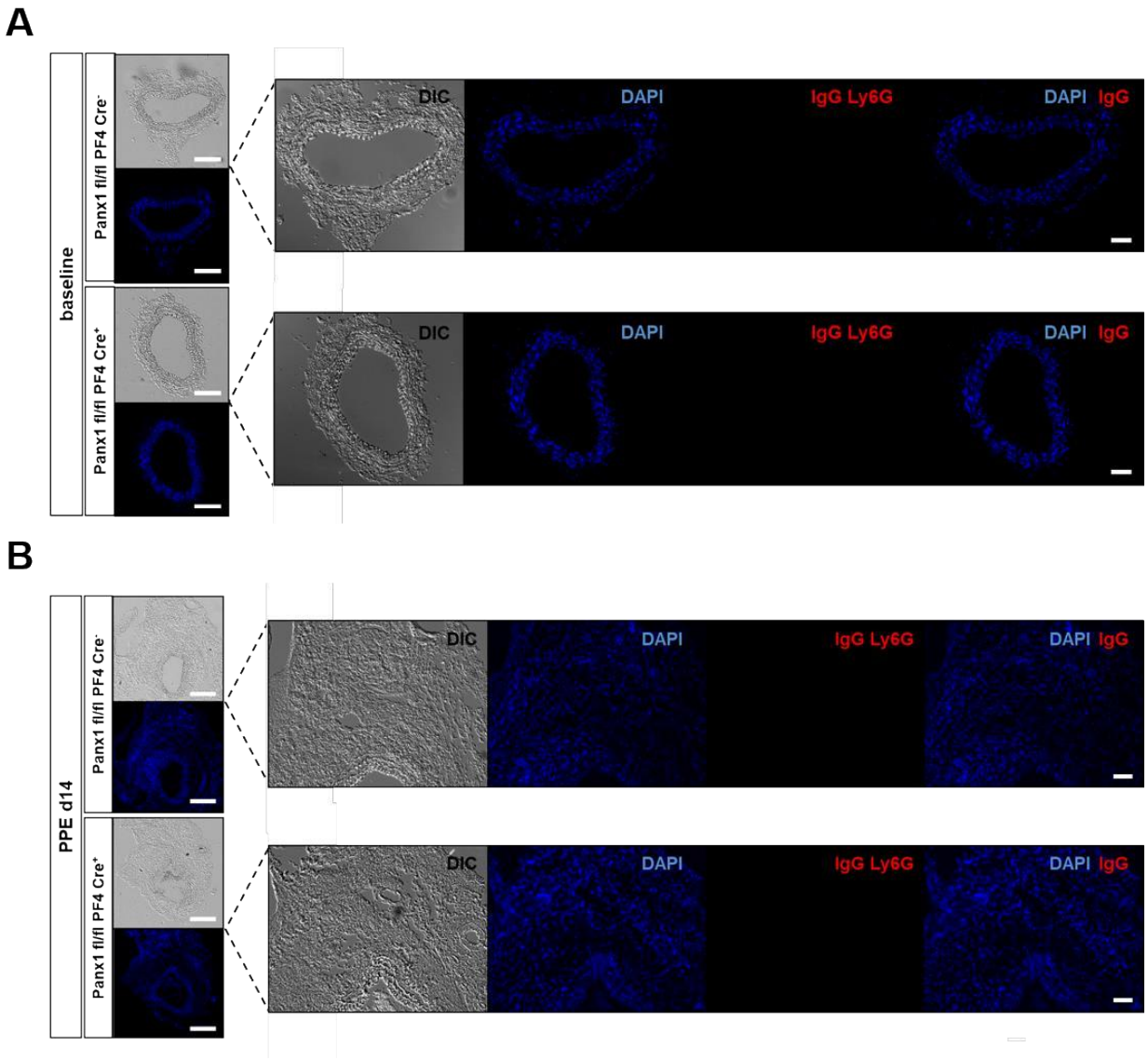

Figure 59: Representative images of control staining for neutrophil infiltration during PPE surgery. Aortic sections from murine tissues from *Panx1 fl/fl PF4-Cre*$^{-}$ and *Panx1 fl/fl PF4-Cre*$^{+}$ mice were stained with IgG control for Ly6G (neutrophils) (A) before (Baseline) and (B) 14 days after PPE surgery. IgG control for Ly6G were visualized in red (IgG-Cy5), while cell nuclei were stained with DAPI (blue). (Left) Representative overview images of aortic sections in DIC and DAPI. Scale bars represents 200 µM. (Right) Single channel images of DIC, DAPI, Ly6G and merged (DAPI and Ly6G) according to Figure 58. Scale bar represents 50 µM D = Day, PPE = Porcine Pancreatic Elastase, Panx1 = Pannexin 1, d = Days, DIC = Differential Interference Contrast.

7.1.8.2 Corresponding images for GPIb staining

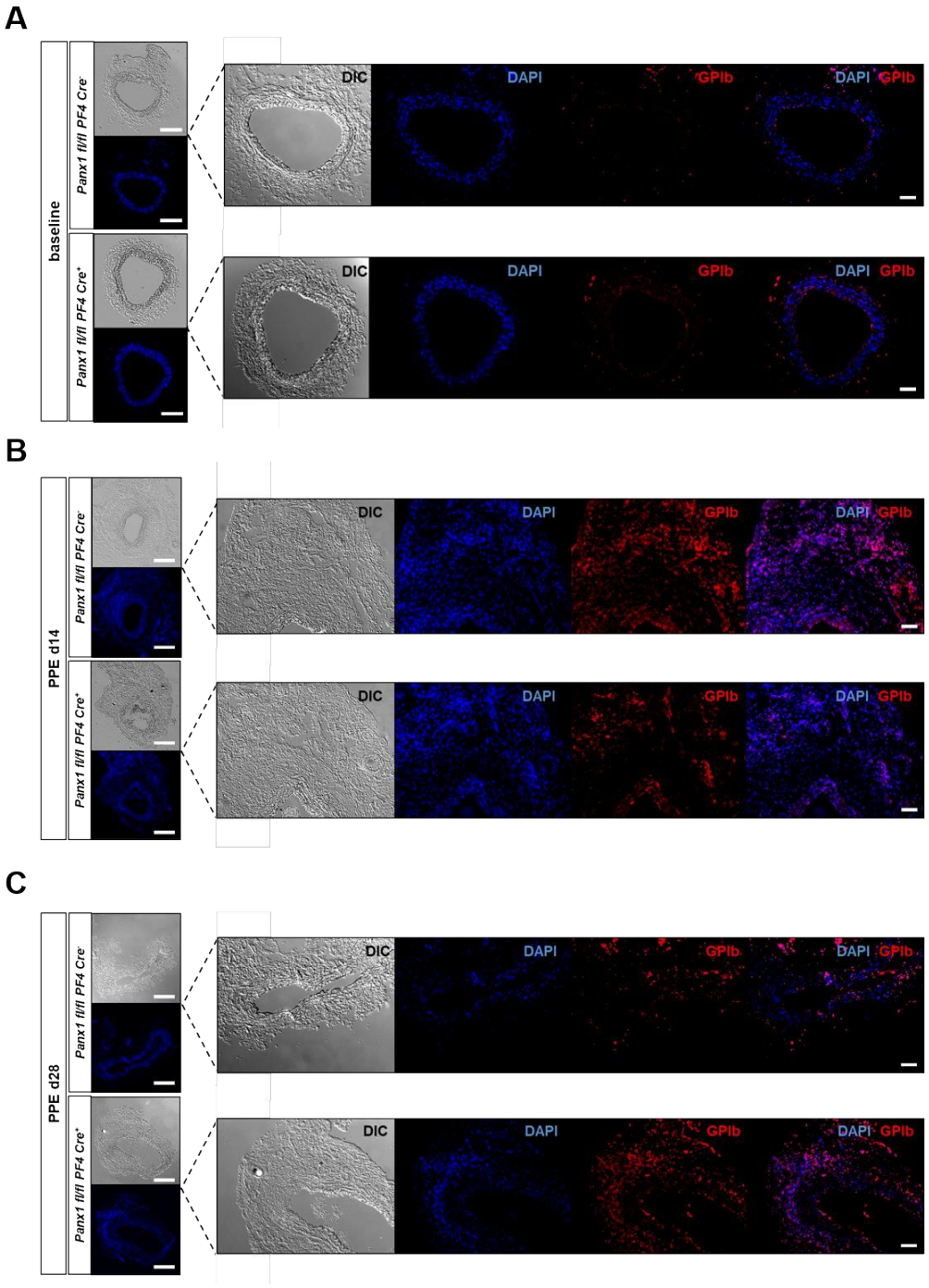

Figure 60: Representative images of platelet migration in aortic tissue 14 and 28 days after PPE surgery. Aortic sections from murine tissues from *Panx1 fl/fl PF4-Cre*$^{-}$ and *Panx1 fl/fl PF4-Cre*$^{+}$ mice were analyzed regarding platelet migration (A) before (Baseline), (B) 14 days and (C) 28 days after PPE surgery. Platelets were stained with the platelet specific marker (GPIB-Cy5 in red), while cell nuclei were stained with DAPI (blue). (Left) Representative overview images of aortic sections in DIC and DAPI. Scale bars represents 200 µM. (Right) Single channel images of DIC, DAPI, GPIb and merged (DAPI and GPIb) according to Figure 50. Scale bar represents 50 µM D = Day, PPE = Porcine Pancreatic Elastase, Panx1 = Pannexin 1, d = Days, DIC = Differential Interference Contrast.

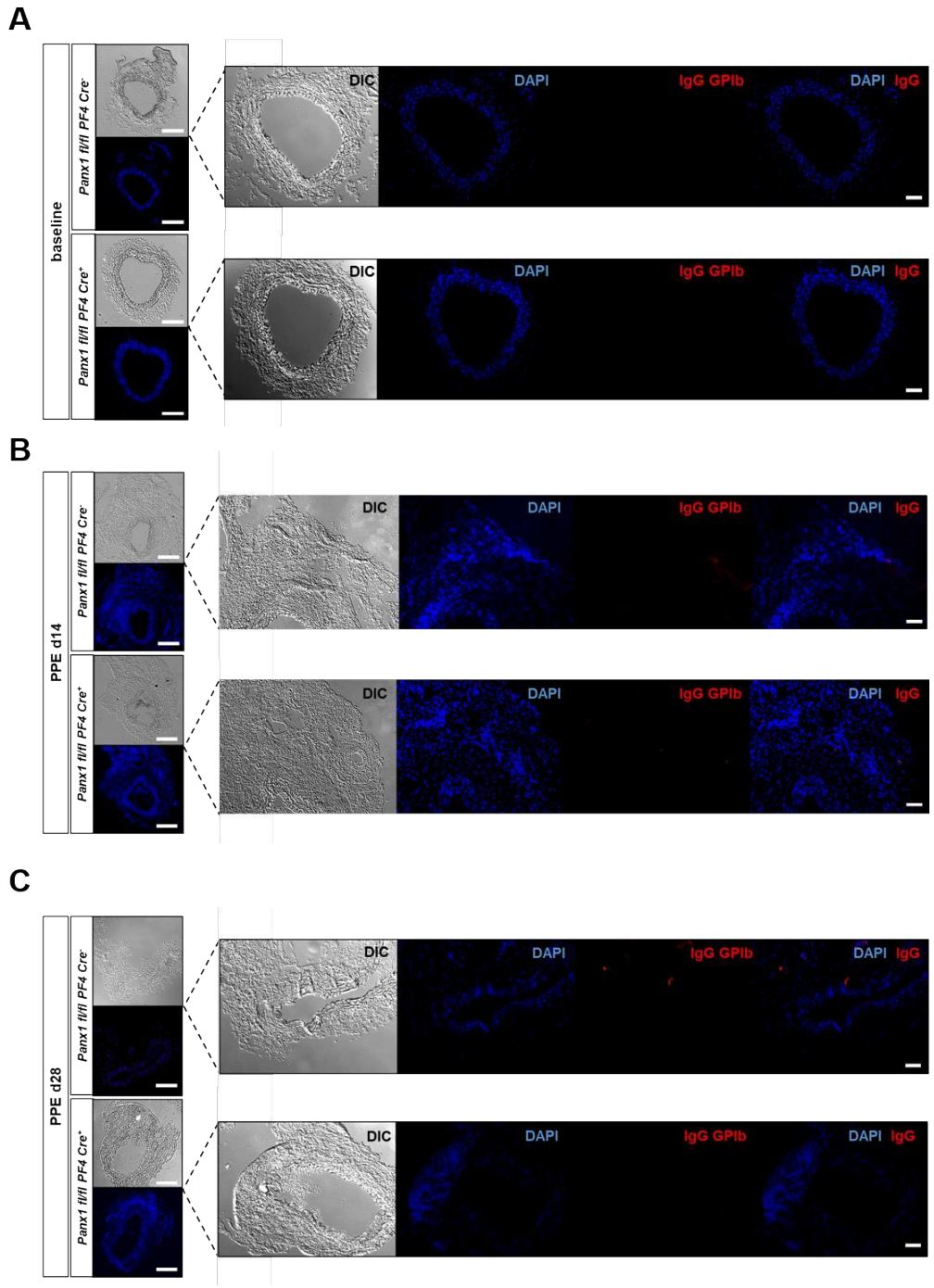

Figure 61: Representative images of control staining for platelet migration during PPE surgery. Aortic sections from murine tissues from *Panx1 fl/fl PF4-Cre*$^{-}$ and *Panx1 fl/fl PF4-Cre*$^{+}$ mice were stained with IgG control for GPIb (Platelets) (A) before (Baseline), (B) 14 days and (C) 28 days after PPE surgery. IgG control for GPIb were stained in red (IgG-Cy5), while cell nuclei were stained with DAPI (blue). (Left) Representative overview images of aortic sections in DIC and DAPI. Scale bars represents 200 µM. (Right) Single channel images of DIC, DAPI, GPIb and merged (DAPI and GPIb) according to Figure 60. Scale bar represents 50 µM D = Day, PPE = Porcine Pancreatic Elastase, Panx1 = Pannexin 1, d = Days, DIC = Differential Interference Contrast.

7.2 List of publications

2022 **Metz, Lisa Maria**, and Margitta Elvers. "Pannexin-1 Activation by Phosphorylation Is Crucial for Platelet Aggregation and Thrombus Formation." *International Journal of Molecular Sciences* 23.9 (2022): 5059. https://doi.org/10.3390/ijms23095059

Some results of this thesis have already been published as cited in the figure ledgends as *Metz, Elvers, IJMS 2022.*

2020 Chatterjee, M.; Ehrenberg, A.; Toska, L.M.; **Metz, L.M**.; Klier, M.; Krueger, I.; Reusswig, F.; Elvers, M. Molecular Drivers of Platelet Activation: Unraveling Novel Targets for Anti-Thrombotic and Anti-Thrombo-Inflammatory Therapy. *Int. J. Mol. Sci.* 2020, *21*, 7906. https://doi.org/10.3390/ijms21217906

7.3 List of conferences

02/2021 Online presentation at the 65th annual meeting from the GTH (Society for Thrombosis and Hemostasis) in Lausanne, Switzerland

07/2020 Online poster presentation at the ISTH (International society for Thrombosis and Hemostasis) in Milan, Italy

02/2020 Poster presentation at 64th annual meeting from the GTH (Society for Thrombosis and Hemostasis) in Bremen, Germany

12/2018 Poster presentation at „Autumn school" organized by the IRTG1902 (HHU) and UVA in Charlottesville, USA

7.4 Acknowledgement/Danksagung

Zunächst möchte ich Frau Prof. Dr. Margitta Elvers danken, die es mir ermöglicht hat diese lehrreiche Dissertation in ihrer Arbeitsgruppe anfertigen zu dürfen. Außerdem möchte ich mich bedanken für ihre Ratschläge sowie ihre Zeit für die Korrektur dieser Arbeit.

Ein weiterer großer Dank gilt Herr Prof. Dr. Christoph Fahlke für die Übernahme des Erstgutachtens.

Besonders bedanken möchte ich mich bei allen aktuellen als auch ehemaligen Mitarbeitern der AG für die Unterstützung und die angenehme Arbeitsatmosphäre. So ein tolles Team mit großem Rückhalt habe ich selten erlebt ☺ Ein besonderer Dank gilt an Martina, die mit ihrer guten Laune mich immer ermutigt hat weiterzumachen. Außerdem möchte ich auch Laura und Friedrich besonders erwähnen. Danke für euren guten Ratschläge, spannenden Diskussionen hinsichtlich meiner experimentellen Planungen und lustigen Kaffeepausen. Ein weiterer Dank gilt Lili für die Korrektur meiner Arbeit!

Ein weiterer riesiger Dank gilt all meinen lieben Freunden. Besonders erwähnen möchte ich meine großartigen Freundinnen Lari, Brata, Ali, Anna und Bettina! Ohne euch wäre das alles nicht möglich gewesen. Danke, dass ihr auch in schweren Phasen für mich da seid, mich immer motiviert und unterstützt.

Von Herzen danke ich auch meiner Familie und besonders meinem Freund Philipp für die großartige Unterstützung und Rückhalt während meines gesamten Studiums! Danke, dass ihr immer an mich glaubt und hinter mir steht, egal was passiert ☺

7.5 Declaration/Eidesstattliche Erklärung

Metz, Lisa Maria — Name, Vorname

2113377 — Matrikelnummer

Ich versichere hiermit an Eides Statt, dass ich die vorliegende Dissertation mit dem Titel:

"The role of the platelet pannexin 1 channel in thrombosis, hemostasis and the development of abdominal aortic aneurysms"

selbstständig und ohne unzulässige fremde Hilfe erbracht habe. Ich habe keine anderen als die angegebenen Quellen und Hilfsmittel benutzt. Für den Fall. dass die Arbeit zusätzlich auf einem Datenträger eingereicht wird erkläre ich, dass die schriftliche und die elektronische Form vollständig übereinstimmen. Die Arbeit hat in gleicher oder ähnlicher Form noch keiner Prüfungsbehörde vorgelegen.

Ort, Datum

Unterschrift

Belehrung

§ 156 StGB: Falsche Versicherung an Eides Statt

Wer vor einer zur Abnahme einer Versicherung an Eides Statt zuständigen Behörde eine solche Versicherung falsch abgibt oder unter Berufung auf eine solche Versicherung falsch aussagt. wird mit Freiheitsstrafe bis zu drei Jahren oder mit Geldstrafe bestraft.

§ 161 StGB: Fahrlässiger Falscheid; fahrlässige falsche Versicherung an Eides Statt

(1) Wenn eine der in den §§ 154 bis 156 bezeichneten Handlungen aus Fahrlässigkeit begangen worden ist. so tritt Freiheitsstrafe bis zu einem Jahr oder Geldstrafe ein.

(2) Straflosigkeit tritt ein. wenn der Täter die falsche Angabe rechtzeitig berichtigt. Die Vorschriften des § 158 Abs. 2 und 3 gelten entsprechend.

Die vorstehende Belehrung habe ich zur Kenntnis genommen:

Ort, Datum

Unterschrift